EXPERIMENTAL PROGRAM FOR FIBER REINFORCED POLYMER RETROFIT OF REINFORCED CONCRETE DIAPHRAGMS

Hunter G. Hutton

Thesis submitted to the faculty of the Virginia Polytechnic Institute and State University
in partial fulfillment of the requirements for the degree of

Master of Science
In
Civil Engineering

Eric J. Jacques, Chair
Matthew R. Eatherton, Co-Chair
Carin L. Roberts-Wollmann
Scott Case

August 11, 2023
Blacksburg, VA

Keywords: reinforced concrete diaphragm, retrofit, FRP

EXPERIMENTAL PROGRAM FOR FIBER REINFORCED POLYMER RETROFIT OF REINFORCED CONCRETE DIAPHRAGMS

Hunter G. Hutton

ABSTRACT

Lateral forces generated by wind, earthquakes, and other horizontal loads are transmitted from the floor diaphragms to the columns and walls that comprise the vertical lateral force resisting system in a building. Strengthening of the diaphragms in older reinforced concrete buildings may be necessary for several reasons, including to enhance seismic performance, address inadequate strength or stiffness, provide missing or incomplete load paths, improve inadequate shear transfer/connection capacity, and to accommodate changes in the use and occupancy of the structure. Engineers are currently using externally bonded fiber reinforced polymer (FRP) composites to retrofit deficient diaphragms. However, this application is beyond the scope of current FRP-related design documents, including ACI PRC-440.2R-17 "Guide for the Design and Construction of Externally bonded FRP Systems for Strengthening Concrete Structures". The lack of consensus around design recommendations for FRP strengthening of diaphragms is problematic and creates uncertainty about which approaches are proven and what are best practice.

This thesis summarizes the results from an experimental research program designed to investigate the shear behavior of reinforced concrete diaphragms strengthened using externally bonded FRP. Six one-half scale reinforced concrete cantilever diaphragms were tested in shear to evaluate the influence of FRP material, density, spacing, orientation, and intermediate anchorage configuration on the performance of diaphragm strengthening. The specimens were designed to represent the diaphragm shear zone adjacent to a shear wall in a concrete building. The tests were performed using a reverse cyclic displacement protocol representative of earthquake actions. The tests included a baseline unretrofitted concrete specimen, followed by five retrofitted specimens with different configurations of externally bonded FRP. Each retrofitted specimen was designed to maintain a similar FRP axial stiffness while varying the FRP retrofit parameters.

The results demonstrated that externally bonded FRP retrofitting improved both the shear strength and stiffness of the strengthened test specimens. All the retrofitted specimens experienced an FRP debonding failure initiated by intermediate shear cracks with the field of the diaphragm, occurring after yielding of the internal steel rebar. The results highlighted that the overall behavior of the specimens was influenced by the way the retrofit schemes were proportioned and detailed. For example, the application of FRP parallel to the direction of applied shear was found to be most effective at increasing the diaphragm strength. Conversely, the application of FRP perpendicular to the applied shear was found to increase the diaphragm ductility. In addition, the shear strength contribution of externally bonded FRP was significantly influenced by the retrofit surface coverage. Compared with narrow strips of high-density fabric, retrofits detailed with less dense fabric spread uniformly over the surface exhibited superior performance due to better control of the shear cracks. Furthermore, no meaningful difference in performance was observed between diaphragms strengthened with glass and carbon FRP composites, provided the retrofits were proportioned to achieve comparable levels of stiffness. This finding suggests that either type of fabric may be suitable for diaphragm strengthening. Finally, the use of overstrength intermediate FRP anchors did not noticeably affect the FRP shear strength contribution. However, the presence of intermediate anchors led to localized failures that concentrated inelastic diaphragm response between anchor locations, resulting in a significant reduction in diaphragm deformation capacity.

The test results were used to develop design recommendations for shear strengthening existing concrete diaphragms using externally bonded FRP. The recommendations included guidance on how to establish the effective FRP design strain and the nominal shear strength contribution of the FRP, both of which tended to be conservative and underestimated the actual behavior observed during the experiments. The recommendations also address the use of intermediate and end FRP anchors, limitations on the clear spacing between sheets, and other factors pertinent to retrofit design.

EXPERIMENTAL PROGRAM FOR FIBER REINFORCED POLYMER RETROFIT OF REINFORCED CONCRETE DIAPHRAGMS

Hunter G. Hutton

GENERAL AUDIENCE ABSTRACT

The floor diaphragm in a reinforced concrete building transmits lateral forces generated by wind, earthquakes, and other horizontal loads to the building's vertical lateral force resisting system. Diaphragms in older reinforced concrete buildings are often retrofitted to meet seismic demands. Retrofitting deficient diaphragms increases infrastructure sustainability by promoting reuse and reconfiguration of existing buildings while mitigating structural deficiencies. Using externally bonded fiber reinforced polymer (FRP) composites is a common strengthening technique often used without supporting guidance or test data. An industry need for diaphragm retrofit provisions, coupled with a substantial lack of data clearly indicates a need for experimental testing of diaphragm elements strengthened with externally bonded FRP.

This thesis summarizes the results from an experimental research program designed to investigate the shear behavior of reinforced concrete diaphragms strengthened using externally bonded FRP. Six reinforced concrete diaphragm specimens were tested to study how variations in FRP material, density, spacing, orientation, and anchorage configuration impacted the performance of the retrofit. One specimen served as a control while the five other specimens were retrofitted with various configurations of FRP. The control specimen experienced a diagonal tension shear failure while each FRP strengthened specimen exhibited an FRP debonding failure, which was initiated by intermediate shear cracks occurring within the field of the diaphragm. The experimental results were analyzed to understand how the FRP retrofits affected the strength, stiffness, ductility, and energy dissipation of each specimen. It was concluded that externally bonded FRP improves the seismic performance of a building by increasing the in-plane shear strength of the diaphragm. Existing design provisions were evaluated and compared to the experimental findings. Design recommendations were formed based on the observed affect of the test variables.

Acknowledgments

This material is based on work supported by the Concrete Research Council of the American Concrete Institute Foundation, Simpson Strong-Tie, Structural Technologies, Fyfe, and GeoTree Solutions. In-kind funding was provided by Simpson Strong-Tie, Structural Technologies, Fyfe, and Banker Steel. This material is also based upon work supported by the National Science Foundation (NSF) under Grant No. CMMI-2050030. Any opinions, findings, conclusions, or recommendations expressed in this material are those of the author(s) and do not necessarily reflect the views of the NSF of other sponsors. This research would not have been possible without the support these organizations.

I am very thankful for the continual guidance from Dr. Jacques and Dr. Eatherton who served as my advisors throughout the project. The input from Dr. Roberts-Wollmann and Dr. Case also contributed to the success of this research. Ryan Stevens's initial designs for the specimen and testing setup was crucial to kickstart this project. The guidance and recommendations made by the project's advisory panel were also invaluable to the success of the study. The advisory panel included Aniket Borwankar, Tarek Alkhrdaji, Scott Arnold, John Hepfinger, John Hooper, Kent Harries, and Enrique del Rey Castillo. The assistance of Dr. Mokarem, Brett Framer, and Garrett Blankenship in the lab was vital during construction. I also greatly appreciate the work done by my undergraduate research assistants including Ray Bodnar, Grace Whitesell, Thomas Bracy, and Quinton Moyer. Furthermore, I am extremely thankful to have received additional support from my friends/research colleagues including Zachary Coleman, Colson Brandetsas, Chris Jackson, and Pratiksha Dhakal.

I am very grateful to have received the Charles Via M.S. Fellowship from Virginia Tech and the Robert F. Mast Memorial Fellowship from the American Concrete Institute Foundation. These awards provided financial stability during my studies.

Table of Contents

Chapter 1. Introduction

1.1. General

The role of the horizontal lateral force resisting system (hLFRS) in a building is to transmit lateral loads to the vertical lateral force resisting system (vLFRS). In reinforced concrete structures, the hLFRS is comprised of diaphragm shear zones, chords, and collectors. The chords are designed to resist flexure due to lateral loading, while the diaphragm shear zones are designed to ensure these lateral loads are transferred to the collectors. Finally, the collectors are designed to transfer the lateral loads into the vLFRS. Figure 1.1 illustrates the role of the hLFRS in a typical reinforced concrete building.

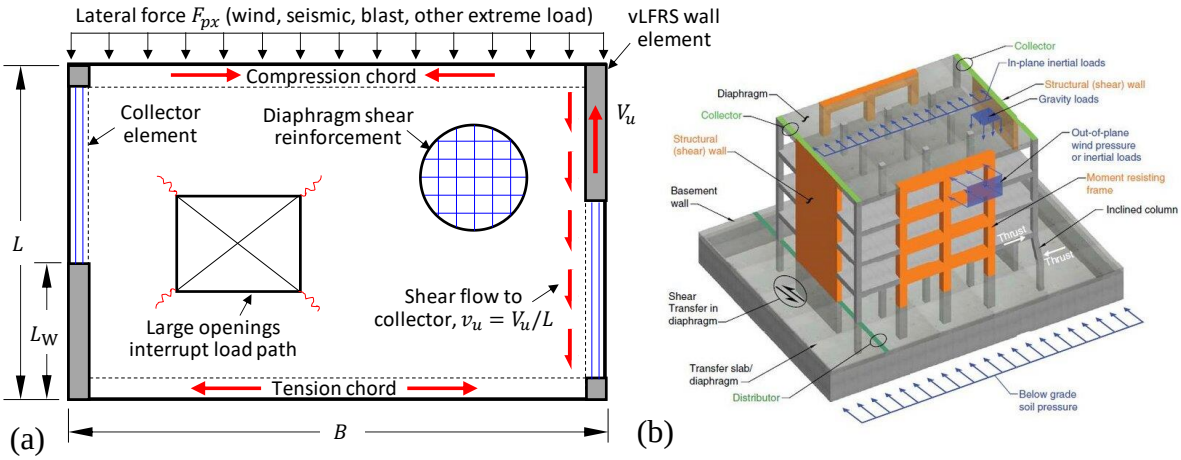

Figure 1.1. Reinforced Concrete hLFRS: (a) Components of the hLFRS; (b) Schematic of the Lateral Force Resisting System in a Typical Concrete Building (ACI 2019).

1.2. Motivation

Reinforced concrete hLFRS often require retrofit when elements of the vLFRS are relocated due to renovations, when there are new penetrations cut in the slab, or in older buildings when deficiencies in the hLFRS load path, strength, or ductility are discovered. Interviews with engineers who have experience strengthening older buildings indicated that typical deficiencies in reinforced concrete hLFRS include: (i) low strength concrete with compressive strengths less than 3000 psi; (ii) thin slab depths that do not meet current code requirements;

(iii) Grade 40 reinforcing steel; and (iv) reinforcement ratios/spacings that do not meet code requirements. Some reinforced concrete hLFRS retrofits rely on providing increased slab thickness and encasement of existing components to improve the seismic performance (FEMA 2006). However, engineers struggle with these interventions since they are expensive, disruptive, and add considerable mass to the building, which in turn increases seismic demands and may require strengthening the gravity system and/or vLFRS.

Alternatively, FRP composites may be used as a retrofit technique for diaphragm strengthening. Techniques involve bonding a FRP composite system to the existing concrete surface to add additional tension strength to the system. Externally bonded FRP is a proven and commercially viable construction technology widely used for mitigating earthquake vulnerabilities and corrosion-related issues in slabs, moment frames, and shear walls (ACI 2017). Yet, the use of FRP to address hLFRS deficiencies is outside the scope of current FRP-related design documents (del Rey Castillo et al. 2019). The lack of consensus-based design recommendations for FRP strengthening of deficient hLFRS is problematic and creates uncertainty about which approaches are proven and what is best practice. Despite these issues, a number of FRP strengthening projects on concrete hLFRS have been completed over the past decade to address deficiencies related to chords, collectors, and in-plane diaphragm shear strength in hospitals, schools, government, and private sector buildings, both in the United States and abroad (Rosenboom and Kehoe 2009; Arnold et al. 2011; Ellsworth 2013; Aegion 2016; MacFarlane and Gold 2016; Rosenboom et al. 2017; Ormeno et al. 2019).

The completion of the aforementioned projects indicates a clear industry need for viable FRP strengthening techniques as cost-effective alternatives to traditional strengthening. However, ACI PRC-440.2R-17 (2017) which is the American Concrete Institute's Guide for the *Design and Construction of Externally Bonded FRP Systems for Strengthening Concrete Structures* does not cover FRP strengthening of hLFRS due to a lack of available test data (Harries and Witt 2019). This lack of guidance is problematic because ACI PRC-440 (2017) is the current state-of-the-art document being used for strengthening concrete structures with FRP. Most other components covered by ACI PRC-440 (2017) can be tested at full or near full scale, while full-scale FRP-strengthened hLFRS tests are not feasible for most testing programs (Erickson 2019). Members of ACI Subcommittee 440.0F have been aware of the

deficiency within ACI 440 (2017), but they have been unable to develop new guidance due to the lack of available data.

As a result of a lack of data related to FRP strengthening of hLFRS, designers have relied on test data of FRP strengthened shear walls to justify diaphragm strengthening (FEMA 2006). However, this approach may be inappropriate because shear walls have significantly different geometry, stress states, and failure modes. Diaphragms are often much thinner with ratios of thickness to plan dimension substantially smaller than shear walls. Shear walls are often prismatic and act as cantilever beams with well-defined axial force, bending and shear at the base (ACI 1992), whereas diaphragms have many reaction points by the vLFRS with openings and reentrant corners making the stress states highly indeterminate and complex. Flexural hinging at the base is the preferred failure mode for shear walls which is not applicable to hLFRS because they are likely to experience diaphragm shear failure, loss of shear transfer at the perimeter, or axial failure of a collector.

1.3. Objectives & Scope

The overall objective of this research project was to investigate the performance of reinforced concrete diaphragms retrofitted using externally bonded FRP. To achieve this objective, a large-scale experimental test setup was devised, and reinforced concrete test specimens were specifically designed to exhibit a shear failure that would allow for FRP shear strengthening in subsequent specimens. A total of six specimens were tested, with one serving as the unretrofitted control and the remaining five strengthened with various configurations of externally bonded FRP systems. Strain and strength limits for diaphragm strengthening were explored as a function of FRP material, density, and spacing. The effectiveness of end anchorage versus intermediate anchorage on FRP bond performance was also investigated. Furthermore, parallel versus perpendicular orientation of FRP plies with respect to the direction of applied shear force was studied. The experimental results were compared to design calculations from ACI PRC-440.2R (2017) in order to validate and expand upon existing guidelines. The experiments focused on diaphragm shear strengthening due to the critical lack of design guidance and test data. This research contributed to increased infrastructure sustainability by facilitating reuse and reconfiguration of existing buildings to satisfy changing occupant needs

while also mitigating structural deficiencies to produce resilient behavior during natural hazards.

The scope of this research program was as follows:

1. Reviewed previous research into the use of fiber reinforced polymers for retrofitting reinforced concrete diaphragms to establish the state-of-the-art-practice and identify research gaps.

2. Conducted experimental testing of six, 4 in. thick, 10 ft × 8.5 ft cantilever diaphragms. One specimen served as an unretrofitted control while the five remaining specimens were strengthened with various arrangements of externally bonded FRP. The five retrofit configurations varied FRP material, ply width, ply spacing, ply orientation, and anchorage. To understand specimen behavior including stiffness, strength, ductility, debonding, anchor failure, and FRP strain level, each test utilized ten string potentiometers, two laser displacement transducers, and sixteen to twenty-two strain gauges.

3. Analyzed test data to understand how variations in FRP material, ply width, ply spacing, ply orientation, and anchorage effected stiffness, strength, FRP strain, ductility, and energy dissipation.

4. Evaluated existing ACI PRC-440.2R specifications relating to shear strengthening of diaphragms with FRP to identify any issues and knowledge gaps in the existing specifications and propose revisions.

1.4. Thesis Organization

Chapter 1 presents an overview of the project and research objectives. Chapter 2 summarizes relevant literature pertaining to the retrofit of reinforced concrete diaphragms with externally bonded FRP. Chapter 3 presents specimen details and methods involved to complete the experimental study. Chapter 4 provides the test results from the six specimens. Chapter 5 includes an analysis of the testing results. Chapter 6 evaluates the impact of the variables within the testing matrix, and Chapter 7 provides conclusions and design recommendations.

Additional design calculations, design drawings, experimental measurements, FRP data sheets, crack maps, and detailed corrections are provided in the Appendices.

Chapter 2. Literature Review

2.1. Overview

Limited literature is available regarding in-plane shear strengthening of reinforced concrete diaphragms with externally bonded FRP. Nonetheless, this chapter summarizes the current state of design guidelines, a review of prior research involving FRP strengthening of reinforced concrete diaphragms, and a discussion of example buildings where FRP has been applied to improved diaphragm action.

2.2. Current Strengthening Guidelines

ACI PRC-440.2R-17 (2017) is the American Concrete Institute's Guide for the *Design and Construction of Externally Bonded FRP Systems for Strengthening Concrete Structures*. Shear strengthening of reinforced concrete members is presented in Chapter 11; however, the guidance within this chapter is primarily focused on reinforced concrete beams and columns. Due to this focus, the recommended retrofit schemes, including complete wrapping, three-sided U-wrapping, and a two-sided installation, do not apply to reinforced concrete diaphragms that are most typically strengthened on one side only (Dhakal et al. 2022). Nevertheless, due to the lack of specific guidelines the guidance within Chapter 11 of ACI PRC-440.2R (2017) is used to design and proportion strengthening schemes for shear deficient reinforced concrete diaphragms (Ormeno et al. 2019). To determine the shear strength of a reinforced concrete member strengthened with FRP, Eq. (1) can be used.

$$V_n = V_c + V_s + \Psi_f V_f \tag{1}$$

where: V_n is the nominal shear strength (lbs); V_c is the nominal shear strength provided by concrete (lbs); V_s is the nominal shear strength provided by steel (lbs.); Ψ_f is the FRP strength reduction factor that accounts for bond reliability; and V_f is the nominal shear strength provided by FRP (lbs). This expression assumes that the peak concrete shear strength, reinforcement yielding, and debonding or rupture of FRP occur simultaneously.

The nominal shear strength provided by concrete, V_c, can be calculated with Eq. (2) adopted from Chapter 12 of ACI 318 (2019).

$$V_c = A_{cv} 2\lambda \sqrt{f_c'} \tag{2}$$

where: V_c is the nominal shear strength provided by concrete (lbs); A_{cv} is the gross concrete section for diaphragms (in.^{2}); λ is the lightweight concrete modification factor; and f_c' is the concrete compressive strength (psi).

The nominal shear strength provided by reinforcing steel, V_s, can be calculated with Eq. (3) and is also adopted from Chapter 12 of ACI 318 (2019).

$$V_s = A_{cv} \rho_t f_y \tag{3}$$

where: V_s is the nominal shear strength provided by steel (lbs); A_{cv} is the gross concrete section for diaphragms (in.^{2}); ρ_t is the ratio of distributed reinforcement oriented parallel to in-plane shear; and f_y is the reinforcement yield strength (psi). The contribution of reinforcement oriented perpendicular to the in-plane shear is typically ignored for design purposes.

The nominal shear strength provided by FRP, V_f, can be calculated with Eq. (4).

$$V_f = \frac{A_{fv} f_{fe} (sin\alpha + cos\alpha) d_{fv}}{s_f} \tag{4}$$

where: V_f is the nominal shear strength provided by FRP (lbs); A_{fv} is the area of FRP shear reinforcement (in.^{2}); f_{fe} is the effective stress in FRP (psi); α is the angle of application of primary FRP reinforcement relative to the longitudinal axis of the member (deg); d_{fv} is the effective depth of FRP shear reinforcement (in.); and s_f is the center-to-center spacing of FRP strips (in.).

The effective stress of FRP used in Eq. (4) can be determined with Eq. (5) which is dependent on an effective strain. Chapter 11 of ACI PRC-440.2R (2017) explains the effective strain is significant because externally applied FRP typically debonds from the concrete surface prior to reaching the FRP material's ultimate strain.

$$f_{fe} = E_f \varepsilon_{fe} \tag{5}$$

where: f_{fe} is the effective stress in FRP (psi); E_f is the tensile modulus of elasticity of FRP (psi); and ε_{fe} is the effective strain in FRP (in./in.).

Two equations for determining the effective FRP strain are presented in Chapter 11 of ACI PRC-440.2R (2017). Equation 11.4.1.1 is intended for completely wrapped members while Equation 11.4.1.2 is intended for bonded U-wraps or bonded face plies. Both equations were developed for unanchored FRP retrofits on beams and impose an effective strain limitation of 0.4%. While neither equation may be appliable for diaphragm retrofits, the project's advisory panel indicated that engineers are using the equation for U-wraps/bonded face plies for diaphragm retrofit design. This equation was calibrated from FRP pull-tests which could be similar to tension forces experienced by FRP sheets installed on reinforced concrete diaphragms for shear reinforcement (Khalifa et al. 1998). The effective FRP strain for U-wraps/bonded face plies can be determined with Eq. (6).

$$\varepsilon_{fe} = \kappa_v \varepsilon_{fu} \leq 0.004 \tag{6}$$

where: ε_{fe} is the effective strain in FRP (in./in.); κ_v is the bond-dependent coefficient for shear; and ε_{fu} is the rupture strain of FRP (in./in.).

The bond-dependent coefficient for shear, κ_v, can be calculated with Eq. (7) and is dependent on the active bond length, L_e, the concrete modification factor, k_1, and the wrapping scheme modification factor, k_2. Each of these variables can be determined with equations (8), (9), and (10) respectively.

$$\kappa_v = \frac{k_1 k_2 L_e}{468 \varepsilon_{fu}} \tag{7}$$

where: κ_v is the bond-dependent coefficient for shear; k_1 is the concrete modification factor; k_2 is the wrapping scheme modification factor; L_e is the active bond length (in.); and ε_{fu} is the rupture strain of FRP (in./in.).

$$L_e = \frac{2500}{(nt_f E_f)^{0.58}} \tag{8}$$

where: L_e is the active bond length (in.); n is the number of FRP plies; t_f is the thickness of one FRP ply (in.); and E_f is the tensile modulus of elasticity of FRP (psi).

$$k_1 = \left(\frac{f_c'}{4000}\right)^{2/3} \tag{9}$$

where: k_1 is the concrete modification factor; and f_c' is the concrete compressive strength (psi).

$$k_2 = \frac{d_{fv} - L_e}{d_{fv}} \text{ (U} - \text{wraps)} \tag{10}$$

$$k_2 = \frac{d_{fv} - 2L_e}{d_{fv}} \text{(two sides bonded)}$$

where: k_2 is the retrofit scheme modification factor; d_{fv} is the effective depth of FRP shear reinforcement (in.); and L_e is the active bond length (in.).

Dhakal et al. (2022) reported that a panel of academic and industry professionals recommended a design strain ε_{fe} no greater than 0.15% to prevent intermediate crack induced debonding, limit the loss of aggregate interlock contributing to the concrete shear strength, and limit the reinforcing steel strain to control crack widths (Dhakal et al. 2022). However, no data is available to support this limit. Therefore, one major desired outcome of this study is to determine an effective FRP design strain for FRP strengthened reinforced concrete diaphragms.

Chapter 11 of ACI PRC-440.2R (2017) also discusses the need for further research to investigate the spacing of FRP strips. The spacing of FRP is an important parameter that is intended to control cracking. Wider FRP strip spacing tends to increase diagonal concrete crack formations in the clear spacing between strips (Khalifa et al. 1998). Currently, the only limitation is for FRP to adhere to the internal steel shear reinforcement spacing limitations defined in Chapter 18 of ACI 318 (2019) which limits the spacing of reinforcement in floor and roof systems to 18 in. Furthermore, a reinforcement limit is defined within Chapter 11

which is presented as Eq. (11). This requirement is intended to limit the shear strength provided by reinforcing steel and FRP in order to prevent diagonal crushing of concrete struts.

$$V_s + V_f \leq 8\sqrt{f_c'}\, b_w d \tag{11}$$

where: V_s is the nominal shear strength provided by steel (lbs); V_f is the nominal shear strength provided by FRP (lbs); f_c' is the compressive strength of concrete (psi); b_w is the web width (in.); and d is the distance from the extreme compression fiber to the centroid of the tension reinforcement (in.).

Chapter 13 of ACI PRC-440.2R (2017) includes guidance for seismic strengthening; however, reinforced concrete diaphragms are not mentioned. Nonetheless, provisions are included for shear wall strengthening. Eq. (12) from Chapter 13 provides the nominal shear strength of FRP for a one-to-two-sided retrofit. This equation is frequently used for diaphragm retrofits. Ormeno et al. (2019) explained that because no explicit diaphragm strengthening guidelines exist, the design equations intended for beams, slabs, and walls are often adopted for diaphragm strengthening in practice (Ormeno et al. 2019).

$$V_f = 2t_f \varepsilon_{fe} E_f d_{fv} \text{ (two} - \text{sided retrofit)} \tag{12}$$

$$V_f = 0.75 t_f \varepsilon_{fe} E_f d_{fv} \text{ (one} - \text{sided retrofit)}$$

where: V_f is the nominal shear strength provided by FRP (lbs); t_f is the nominal thickness of one ply of FRP reinforcement (in.); ε_{fe} is the effective strain in FRP (in./in.); E_f is the tensile modulus of elasticity of FRP (psi); d_{fv} is the effective depth of the shear wall (in.); and the constant represents the number of sides retrofitted with FRP; however, it is conservatively reduced to 0.75 for one sided retrofits.

2.3. Diaphragm Tests

Aryan et al. (2022) performed a series of five tests involving reinforced concrete diaphragms subjected to cyclic, three-point bending, in-plane shear load. One specimen served as an unretrofitted control while the four others were strengthened with various configurations of externally bonded FRP. The four retrofits varied FRP material, FRP ply width, and the number

of sides to which the FRP was applied. The testing setup used in the study is shown in Figure 2.1.

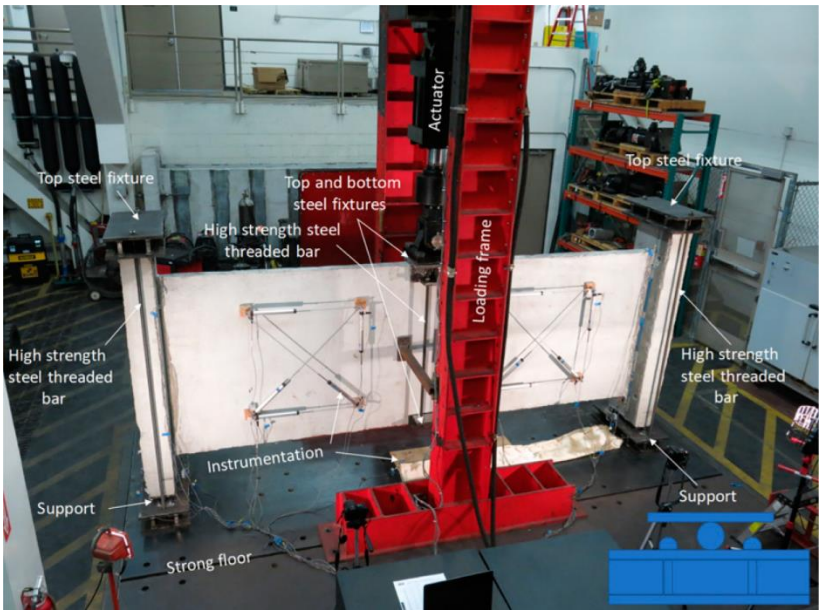

Figure 2.1. Testing Setup Used by Aryan et al. (Aryan et al. 2022).

The control specimen (Specimen 3-0 in Figure 2.2) was reported to have failed due to concrete diagonal shear cracking. The three specimens strengthened on only one side failed due to FRP debonding followed by concrete diagonal shear cracking. The authors noted that the specimen strengthened on both sides (Specimen 3-G-2) locally failed due to concrete crushing at the load application point. The experimental results showed that each strengthened specimen experienced an increase in shear capacity, initial stiffness, and energy dissipation. The shear capacity and stiffness improvements are shown in Figure 2.2 which compares each specimen's load-deflection envelope curve. The CFRP strengthened specimens (Specimens 3-H-1 and 3-H2-1) and GFRP strengthened specimens (Specimens 3-G-1 and 3-G-2) both showed an increase in ductility up to 93% and 36%, respectively. The authors also reported that the steel reinforcement strains corresponding to the one-sided retrofits were reduced by about 50% when compared to the control specimen. Moreover, the CFRP and GFRP strains were limited to 0.5% and 0.75% prior to debonding, respectively. The authors also compared the experimental results to the theoretical shear capacity using the shear wall retrofit equations presented previously as Eq. (12). This analysis showed that the predicted strength values were 14 to 33 percent less than the experimental values. It should also be noted that none of the FRP

sheets were anchored on any of the retrofitted specimens. Instead, the FRP sheets were wrapped at the edges through the diaphragm thickness, a condition which provides excellent mechanical anchorage to the FRP. The authors realized that the ends of a diaphragm are not often accessible in practice; therefore, they recommend future research on FRP anchorage systems (Aryan et al. 2022).

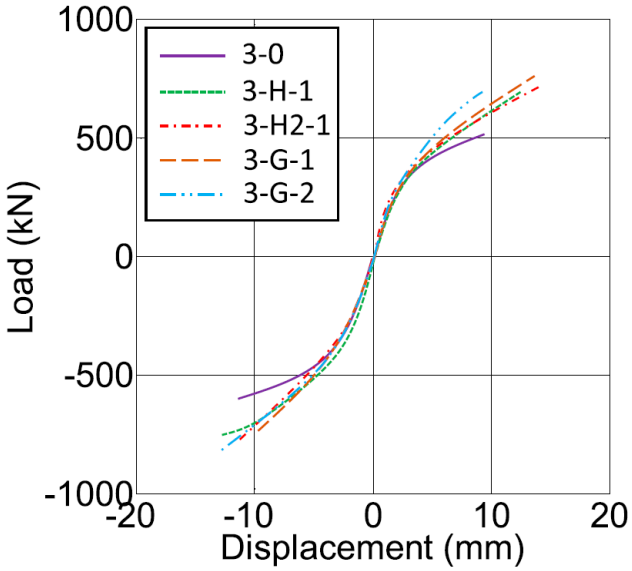

Figure 2.2. Load Deflection Envelopes (Aryan et al. 2022).

A study carried out by Nakashima et al. (1981) involved in-plane loading of unstrengthened reinforced concrete diaphragms. The test specimens were intended to represent an interior floor panel supported by a shear wall on one side and by columns on the other. Full scale specimens were not feasible; therefore, a scale ratio of 1:4.5 was utilized. The testing setup was novel because it allowed two specimens to be constructed and cast at the same time. The specimens were isolated from each other by a central panel that allowed each specimen to be tested independently. Each specimen also received in-plane load via five evenly spaced studs. A dimensioned plan and elevation view of the specimen configuration is shown in Figure 2.3.

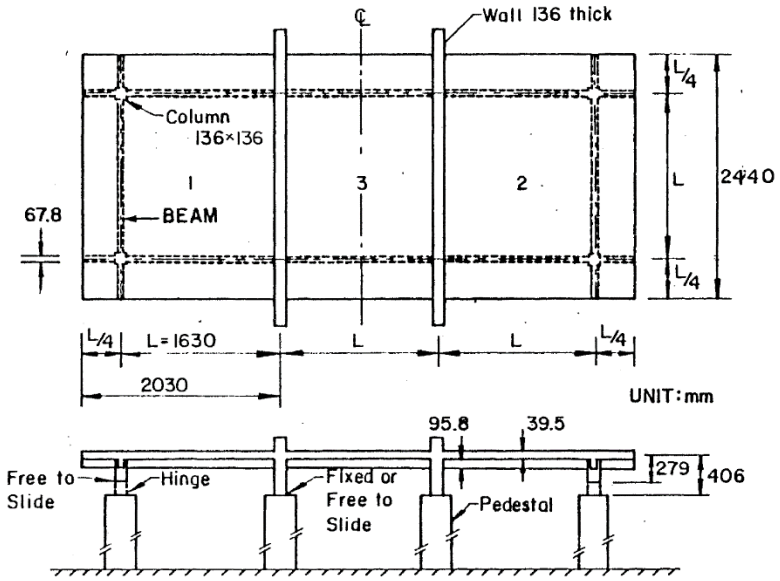

Figure 2.3. Nakashima et al.'s Specimen Details (Nakashima et al. 1981).

From the experimental testing of six specimens, the authors reported that cyclic loading reduced the in-plane capacity of the specimens up to 25%, and applying service gravity loads reduced the in-plane capacity by about 15%. However, the researchers also reported that the effect of cyclic loading or combined in-plane and gravity loading on ductility was negligible. Furthermore, the authors noted that the opening and closing of the major crack controlled the deflection once the ultimate load had been exceeded. The failure of the specimen was associated with rupturing of reinforcing steel at the major crack. The authors also analytically concluded that the in-plane capacity of reinforced concrete diaphragms is controlled by a flexural or shear failure. The shear failure is described as a diagonal crack that separates a triangular section from the rest of the diaphragm (Nakashima et al. 1981).

2.4. Building Diaphragms Strengthened with FRP

Del Rey Castillo et al. (2019) reported on two existing projects that involved strengthening of reinforced concrete diaphragms with FRP. One project involved a building in Auckland, New Zealand where the hollowcore precast floor system was proven to have inadequate tension capacity due to lateral loading scenarios. To remedy the deficiency, FRP strips were applied in both orthogonal directions. Additional FRP strips were installed along the perimeter which was anchored with FRP anchors. The other project was focused on another deficient hollowcore floor system within a building in Wellington, New Zealand. To strengthen the

tension capacity of this diaphragm, FRP strips were again installed in both orthogonal directions. FRP strips were also installed along the perimeter; however, this retrofit utilized embedded steel plates that were anchored to the bond beam instead of FRP anchors. A plan view of this retrofit is illustrated in Figure 2.4. The authors concluded that the common approach to increase diaphragm capacity with FRP involves installing an orthogonal grid of FRP strips paired with perimeter strips that are anchored to the existing boundary element. However, the authors emphasize that there is no research data to justify this common retrofit approach or any anchorage types. Furthermore, the authors point out that no design guidance currently exists for diaphragm strengthening in ACI PRC-440 (2017), CNR-DT200 (2013), or fib bulletin 14 (2001) (del Rey Castillo et al. 2019).

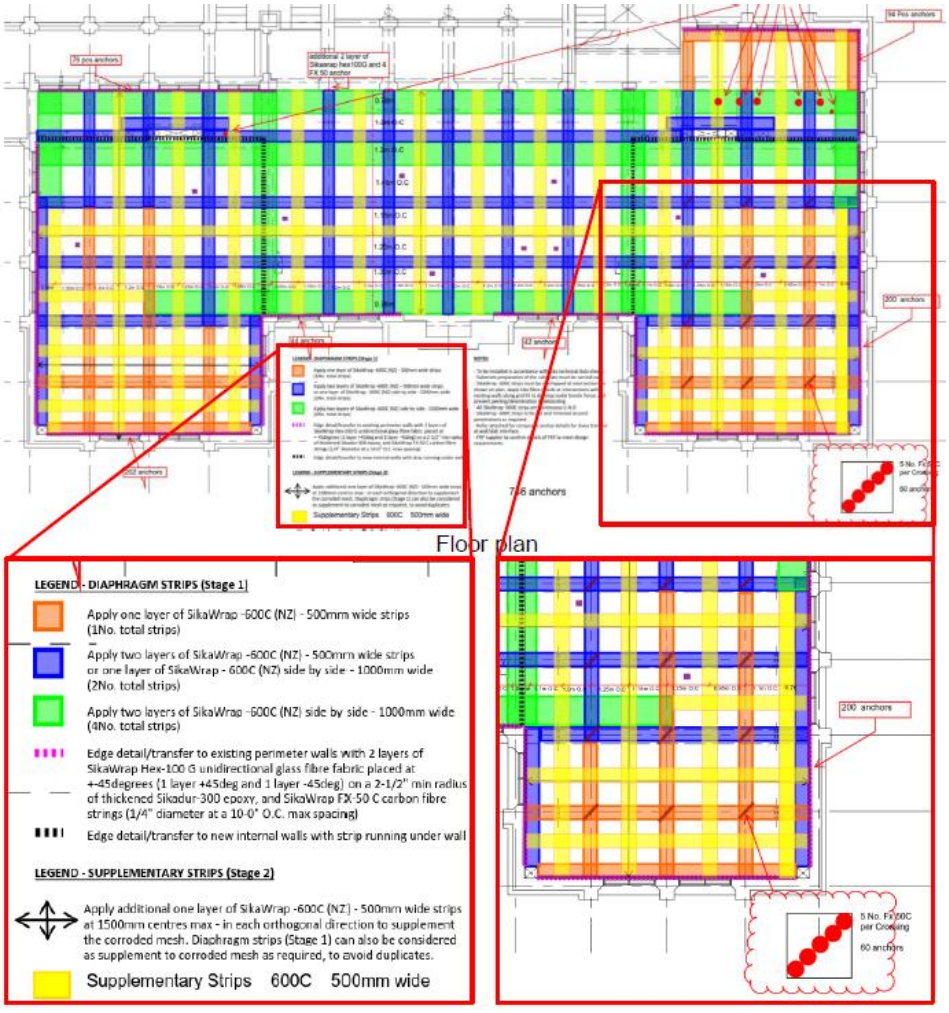

Figure 2.4. FRP Plan Schematic (Del Rey Castillo et al. 2019).

Ormeno et al. (2019) conducted in-situ shear-tear tests on FRP strips installed in the Wellington, New Zealand building previously mentioned. These tests were conducted by applying an in-plane tensile load to one end of an externally bonded FRP sheet to determine the tensile capacity of the bonded system. While the authors recognized that no strengthening procedure currently exists, the test results were compared to effective tensile strain and bond length predictions. The authors reported that the in-situ tensile strains were 1.5 times greater than what was predicted using ACI PRC-440.2R. Additionally, it was noted that higher tensile strengths could be developed if the FRP was bonded beyond the calculated development length using ACI PRC-440.2R. Ultimately, the authors concluded that specific guidelines need to be developed for FRP diaphragm retrofits including specific equations for calculating the tensile capacify of FRP (Ormeno et al. 2019).

2.5. Summary of Literature Review

This literature review demonstrates a clear need for experimental testing focused on FRP strengthened diaphragms. While common retrofit practices are being used, very little research and no design guidelines currently exist to support these practices. The experimental study described in this thesis aims to close several of the critical knowledge gaps pertaining to diaphragm shear strengthening and use the results to draft preliminary design recommendations.

Chapter 3. Experimental Program

3.1. Overview

This experimental program consisted of six cantilever reinforced concrete diaphragm tests. One specimen served as an unretrofitted control while the five remaining specimens were strengthened with various arrangements of externally bonded FRP and FRP anchorages. This chapter provides an overview of the test matrix and retrofit schemes studied, specimen details, configuration of the test setup, testing procedure, instrumentation, and construction sequence.

3.2. Test Matrix

Isometric views of the cantilever diaphragm specimen are presented in Figure 3.1. The diaphragm spanned 8 ft 6 in. (102 in.) from the shear wall boundary and measured 10 ft (120 in.) in depth. Two 10 in. wide chord beams and one 12 in. wide edge beam extended 6 in. below the underside of the 4 in. thick slab. See Section 3.3 for more specimen details.

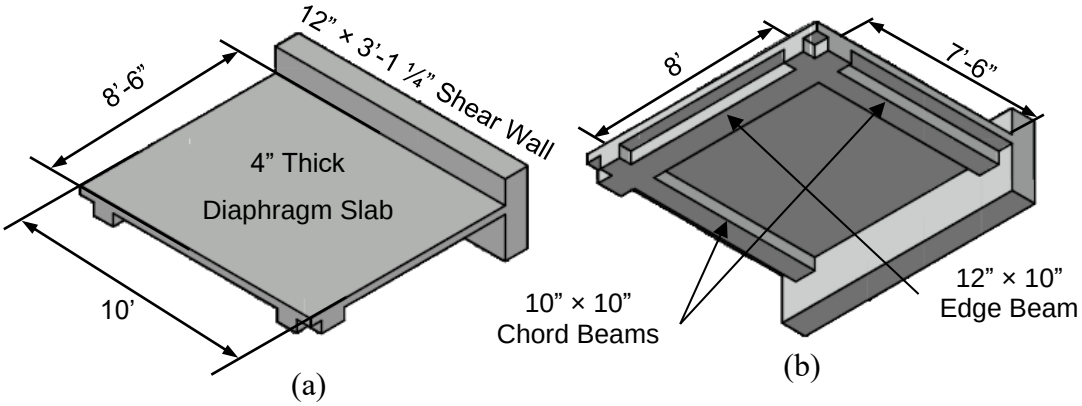

Figure 3.1. Isometric Views of the Diaphragm Specimen: (a) Top View; (b) Bottom View.

The test matrix, shown in Table 3.1, consisted of six cantilever diaphragm specimens. One specimen, CD1, served as the unretrofitted control, while the five remaining specimens, CD2-6, were retrofitted with various arrangements of externally bonded FRP.

Table 3.1. Retrofit Testing Matrix.

		FRP Ply Configuration					FRP Anchor Configuration			Design
Specimen ID	**FRP Material**	**Composite Modulus, E_f (ksi)**	**Thickness, t_f (in.)**	**Width, w_f (in.)**	**Spacing, s_f (in.)**	**Orientation, α (deg.)**	**Layout**	**Diameter (in.)**	**Anchors Per Sheet**	**Axial Stiffness, K_f (kips/in./in.)**
CD1	N/A	N/A	N/A	N/A	N/A	N/A	N/A	N/A	N/A	N/A
CD2	VWrap C100HM, CFRP	16700	0.02	12.0	24	0	End Only	0.5	2	4008
CD3	Tyfo SCH-11UP, CFRP	13900	0.02	14.5	23.2	0	Intermed. +End	0.75	4	4031
CD4	Tyfo SEH-51A, GFRP	3730	0.05	21.0	21	0	End Only	0.5	4	3917
CD5	VWrap C200HM, CFRP	14240	0.04	7.0	25.7	0	End Only	0.75	2	3987
CD6	VWrap C100HM, CFRP	16700	0.02	12.0	24	90	Intermed. +End	0.75	4	4008

One important consideration in the retrofit design process was the actuator's load capacity of 330 kips. This load capacity dictated a design strength limit to ensure each specimen could be tested to failure. The control specimen was designed to fail in shear at approximately half of the actuator's capacity. Furthermore, each retrofitted specimen was designed to incorporate four FRP sheets with an individual ply stiffness, K_f, of approximately 4000 kips/in./in. The individual ply stiffness was calculated with Eq. (13). Each retrofit was also designed to target a reinforcement limit where the shear strength contribution of steel and FRP (assuming an FRP design strain of 0.4%) was limited to 5 to 7 times $\sqrt{f_c'}\, b_w d$.

$$K_f = E_f t_f w_f \tag{13}$$

where: K_f the stiffness of one FRP ply in units of kips per longitudinal strain (kips/in./in.); E_f is the average FRP composite tensile modulus reported by the manufacturer (ksi); t_f is the FRP ply thickness reported by the manufacturer (in.); and w_f is the width of the FRP sheet (in.). The relevant values for each specimen are provided in Table 3.1.

Each retrofitted specimen utilized FRP anchors installed at the ends of the sheets to delay debonding. The end anchors for Specimen CD2 were sized based on recommendations of the project's advisory panel, resulting in an anchor diameter required to develop half of the tensile strength of the FRP sheet being anchored. The remaining retrofitted specimens, CD3-CD6, utilized anchors sized to satisfy an overstrength factor of 1.5 times the area required to develop the tensile strength of the FRP sheet being anchored. Specimens CD3 and CD6 also included equivalently sized intermediate anchors to investigate any improvement to bond and strain development resulting from anchors placed within the shear transfer region. This was expected to simulate typical field retrofits which involve applying FRP in the parallel and perpendicular directions while also providing intermediately spaced FRP anchors.

According to members of the project's advisory panel, typical field retrofits commonly utilize a 20-oz/yd^2, 24-inch wide, unidirectional CFRP fabric. As each specimen was designed to represent a half scale diaphragm, the retrofits were also specified as half scale. Consequently, Specimen CD2 was designed with a 10-oz/yd^2, 12-in wide, unidirectional CFRP fabric. Specimens CD3 to CD6 varied FRP material, width, thickness, spacing, and/or orientation while maintaining a similar ply stiffness as the first retrofitted specimen. For practicality, the layout of FRP was designed to be in the parallel or perpendicular direction of the applied shear to cross the expected diagonal tension crack in the field of the diaphragm. The following provides a detailed description of each of the specimens.

3.2.1 CD1: Unretrofitted Control Diaphragm

Specimen CD1 was designed to study the shear capacity of a reinforced concrete diaphragm and serve as the control specimen. The specimen was designed so that diaphragm shear would be the controlling limit state. Flexure, concrete crushing, and direct shear at the slab-to-shear wall interface were designed to be stronger than the diaphragm shear strength. However, due to poor concrete consolidation within the edge beam, this specimen was strengthened to avoid a premature direct shear failure near the load application points. This involved the installation of one, 12 in. wide, 10 ft long, ±45° bidirectional 18-oz/yd^2 CFRP sheet directly adjacent to the loading channel. Additionally, six, 30 in. × 12 in., ±45° 18-oz/yd^2 bidirectional CFRP sheets were installed between each loading point. This strengthening configuration was anchored with a total of twelve $\emptyset 1/2$ in. CFRP anchors with a 60-degree, 12-inch-long splay,

embedded at an average depth of 4 in. The strengthening layout of Specimen CD1 is shown in Figure 3.2. A photograph of this specimen is shown in Figure 3.8(a).

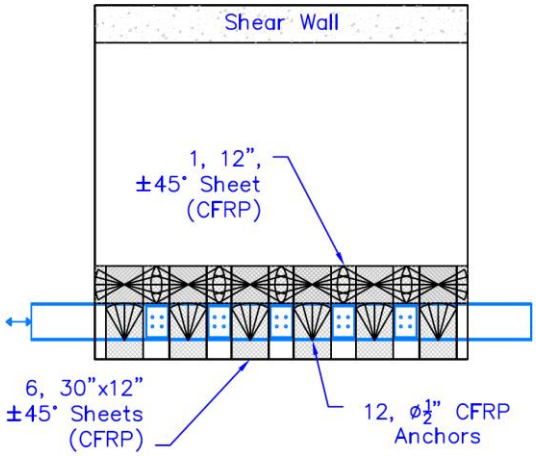

Figure 3.2. Strengthening of Specimen CD1.

3.2.2 CD2: Baseline CFRP Retrofit with End Anchors

The first, most simple retrofit corresponds to Specimen CD2 which was intended to study a typical half-scale CFRP strengthening scheme that covers approximately 50% of the diaphragm. A 9.7-oz/yd^2, 12-inch wide, unidirectional CFRP fabric (Simpson Strong-Tie 2022a), spaced at 24 in. was selected for the retrofit of CD2. A $\emptyset 1/2$ in. CFRP anchor with a 60-degree, 12-inch-long splay was embedded at an average depth of 4 in. at both ends of each CFRP strip. The anchors were installed 5.5 in. from each end of the diaphragm to avoid the reinforcing steel within the specimen's chord beams when drilling the anchor holes. Like Specimen CD1, poor concrete consolidation within the edge beam warranted additional strengthening to prevent a premature direct shear failure. The additional strengthening included the installation of six, 30 in. × 12 in., ±45° bidirectional CFRP sheets between each loading point. The retrofit layout of Specimen CD2 is shown in Figure 3.3(a), and the anchor details are shown in Figure 3.3(b). This specimen is also shown in Figure 3.8(b).

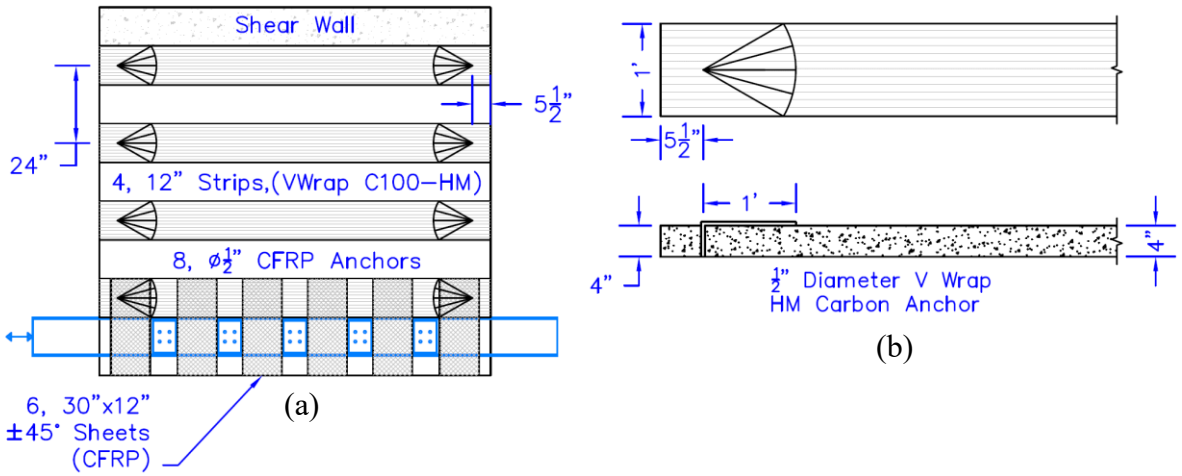

Figure 3.3. Retrofit of Specimen CD2: (a) Plan View of Retrofit; (b) Anchor Details.

3.2.3 CD3: Baseline CFRP Retrofit with Intermediate Anchors

Specimen CD3 was intended to study the potential benefit of providing intermediate anchors within the field of the diaphragm. It was expected that these intermediate anchors would delay intermediate crack-induced debonding of the FRP and consequently allow a greater FRP strain prior to debonding. This specimen's retrofit was composed of a 11.6-oz/yd^2, 14.5-inch wide, unidirectional CFRP fabric (Fyfe 2022a), spaced at 23.2 in. Specimen CD3 was equivalent to Specimen CD2 with two additional intermediate anchors provided on each sheet. The intermediate anchors were spaced 38.5 in. from each end anchor. This spacing was selected to avoid the diaphragm reinforcing steel when drilling anchor holes and resulted in a non-uniform anchor layout. All anchors were upsized to $\emptyset 3/4$ in. to satisfy an overstrength factor of 1.5 times the area required to develop the tensile strength of the FRP sheet being anchored. This overstrength factor came from the experience and recommendations of the project's advisory panel and was used for all remaining specimens. Additionally, the anchor embedment depth was reduced to 3 in. to avoid concrete blowouts during drilling. Each anchor fan was 14.5 in. long with a 60-degree splay. The retrofit layout of Specimen CD3 is shown in Figure 3.4(a), and the anchor details are shown in Figure 3.4(b). A photograph of this specimen is shown in Figure 3.8(c).

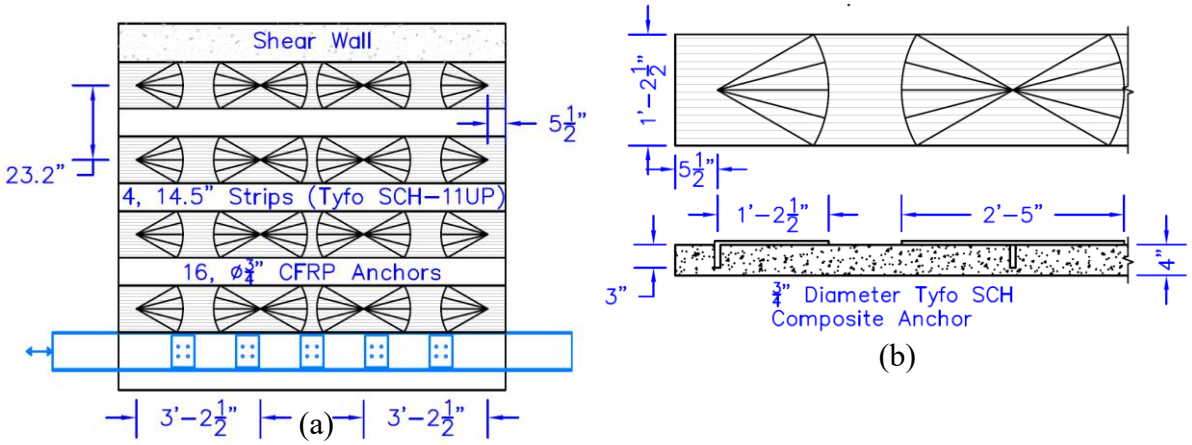

Figure 3.4. Retrofit of Specimen CD3: (a) Plan View of Retrofit; (b) Anchor Details.

3.2.4 CD4: Full Coverage, Low Modulus, GFRP Retrofit with End Anchors

The purpose of Specimen CD4 was to investigate the effect of laminate axial stiffness by providing a 27-oz/yd^2, 21-inch wide, unidirectional GFRP fabric (Fyfe 2022b), spaced at 21 in. This retrofit maintained an equivalent axial stiffness of Specimen CD2 while utilizing a fabric with a lower modulus and greater surface coverage. While this retrofit would require more surface preparation than the others, it was expected that the cracks in the diagram would be more uniformly restrained, resulting in improved overall load-deflection and FRP bond behavior. Two $\emptyset 1/2$ in. CFRP anchors with a 60-degree, 12-inch-long splay were embedded at an average depth of 3 in. at both ends of each GFRP sheet. This anchorage configuration was expected to perform better than one $\emptyset 3/4$ in. anchor while maintaining the same area of one $\emptyset 3/4$ in. anchor, thus providing an anchor overstrength factor of 1.5. The retrofit layout of Specimen CD4 is shown in Figure 3.5(a), and the anchor details are shown in Figure 3.5(b). A photograph of this specimen is shown in Figure 3.8(d).

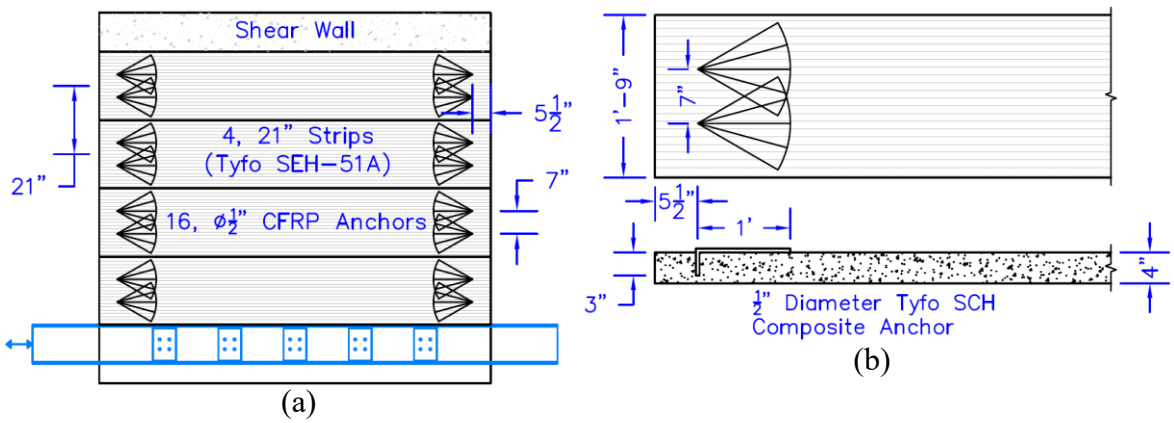

Figure 3.5. Retrofit of Specimen CD4: (a) Plan View of Retrofit; (b) Anchor Details.

3.2.5 CD5: Narrow Coverage, High Modulus, CFRP Retrofit with End Anchors

Specimen CD5 was intended to study the effect of laminate axial stiffness by maintaining an equivalent ply stiffness of Specimen CD2 while utilizing a fabric with a higher modulus and less surface coverage. The retrofit was composed of a 17.7-oz/yd^2, 7-inch wide, unidirectional CFRP fabric (Simpson Strong-Tie 2022b), spaced at 25.7 in. A Ø3/4 in. CFRP anchor was provided at both ends of each CFRP strip. Each anchor fan was splayed 12 in. in length and embedded at a depth of 3 in. The wide clear spacing between strips was expected to cause more severe cracking in the field of the diaphragm and allow a spacing limitation to be determined. While this retrofit presented constructability challenges related to the use of narrow FRP strips, it also provided the advantage of reduced surface preparation. The retrofit layout of Specimen CD5 is shown in Figure 3.6(a), and the anchor details are shown in Figure 3.6(b). A photograph of this specimen is shown in Figure 3.8(e).

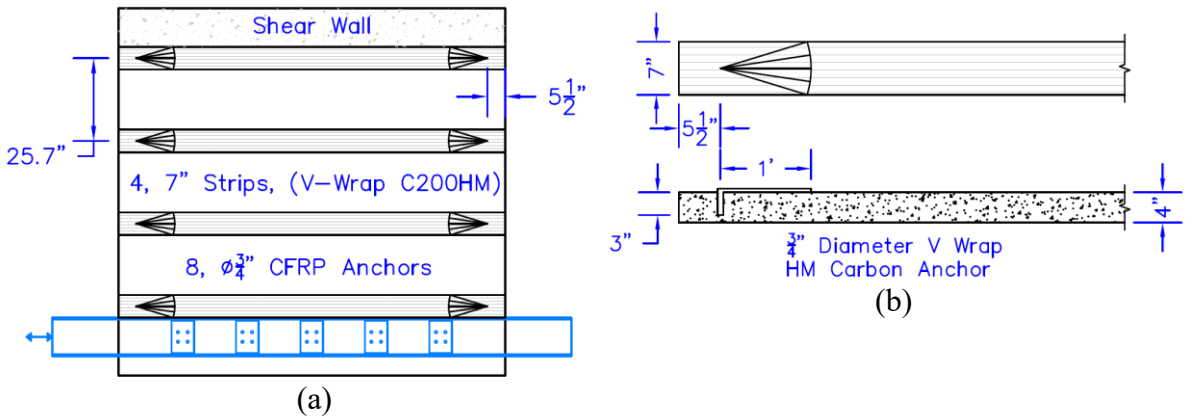

Figure 3.6. Retrofit of Specimen CD5: (a) Plan View of Retrofit; (b) Anchor Details.

3.2.6 CD6: Baseline CFRP Retrofit Installed Perpendicular to Load

The motivation behind Specimen CD6 was to study the effect of FRP installed perpendicular to the direction of applied shear force. Like Specimen CD3, a 9.7-oz/yd^2, 12-inch wide, unidirectional CFRP fabric (Simpson Strong-Tie 2022a), spaced at 24 in. was selected for this retrofit. A $\emptyset 3/4$ in. CFRP anchor was provided at both ends of each CFRP strip along with two intermediate anchors spaced at 26 in. Each anchor fan was splayed 12 in. in length and embedded at a depth of 3 in. Installing the strips perpendicular to the applied shear was expected to be a less effective strengthening strategy as opposed to a parallel retrofit. The retrofit layout of Specimen CD6 is shown in Figure 3.7(a), and the anchor details are shown in Figure 3.7(b). A photograph of this specimen is shown in Figure 3.8(f).

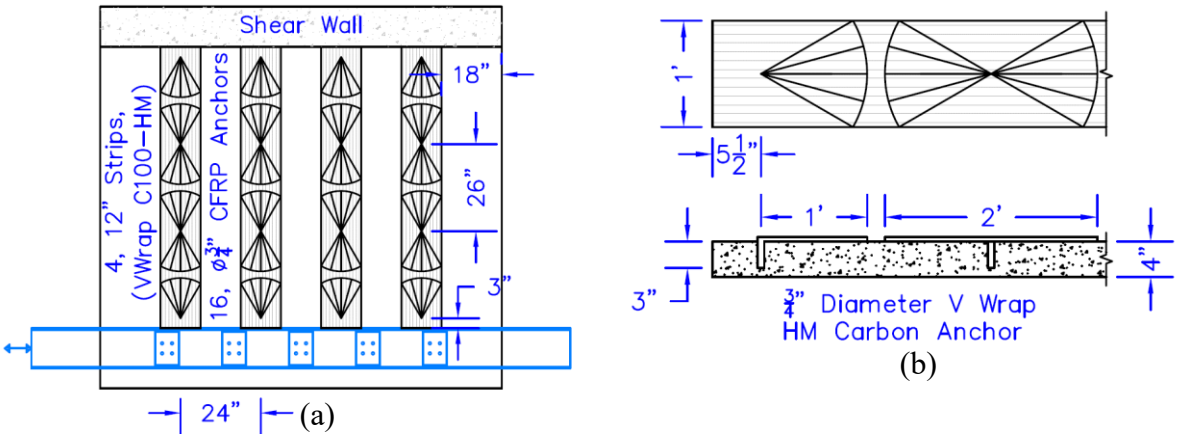

Figure 3.7. Retrofit of Specimen CD6: (a) Plan View of Retrofit (b) Anchor Details.

Figure 3.8. Photos of Strengthened Specimens: (a) Specimen CD1; (b) Specimen CD2; (c) Specimen CD3; (d) Specimen CD4; (e) Specimen CD5; (f) Specimen CD6.

3.3. Reinforced Concrete Specimen Details

Figure 3.9 presents a plan view of the diaphragm specimen along with a cross sectional view of the chord beams, edge beam, and shear wall. Each specimen consisted of a 10 ft × 8.5 ft cantilever diaphragm with an adjacent 12 in. thick, integrally cast shear wall. Each

diaphragm specimen was a four-inch-thick, two-way flat slab with beams that was intended to be approximately half-scale relative to a typical building. Each specimen incorporated two chord beams and one edge beam. The reinforced concrete specimens were designed to simulate a deficient diaphragm shear zone in a hLFRS adjacent to a shear wall. This configuration enabled the research to focus on mechanisms of shear resistance within the diaphragm zone as well as shear transfer between the slab and vLFRS. The complete set of detailed drawings for the specimen are included in Appendix A.

The slab reinforcement shown in Figure 3.9(a) consisted of two mats of orthogonal D5 deformed steel wire bars spaced at 12 in. center-to-center in each direction with $1/2$ in. cover. The D5 deformed bars are geometrically equivalent to No. 2 deformed bars; however, it should be noted that these bars have a higher strength and lower ductility in comparison to typical ASTM A615 reinforcing steel (see Section 3.8.2 for material properties). This slab reinforcement was selected based on the minimum reinforcing steel requirements, $0.0018A_g$, in ACI 318 for shrinkage and temperature reinforcement. The deformed wires were hooked to provide suitable anchorage into the shear wall segment and at the slab edges.

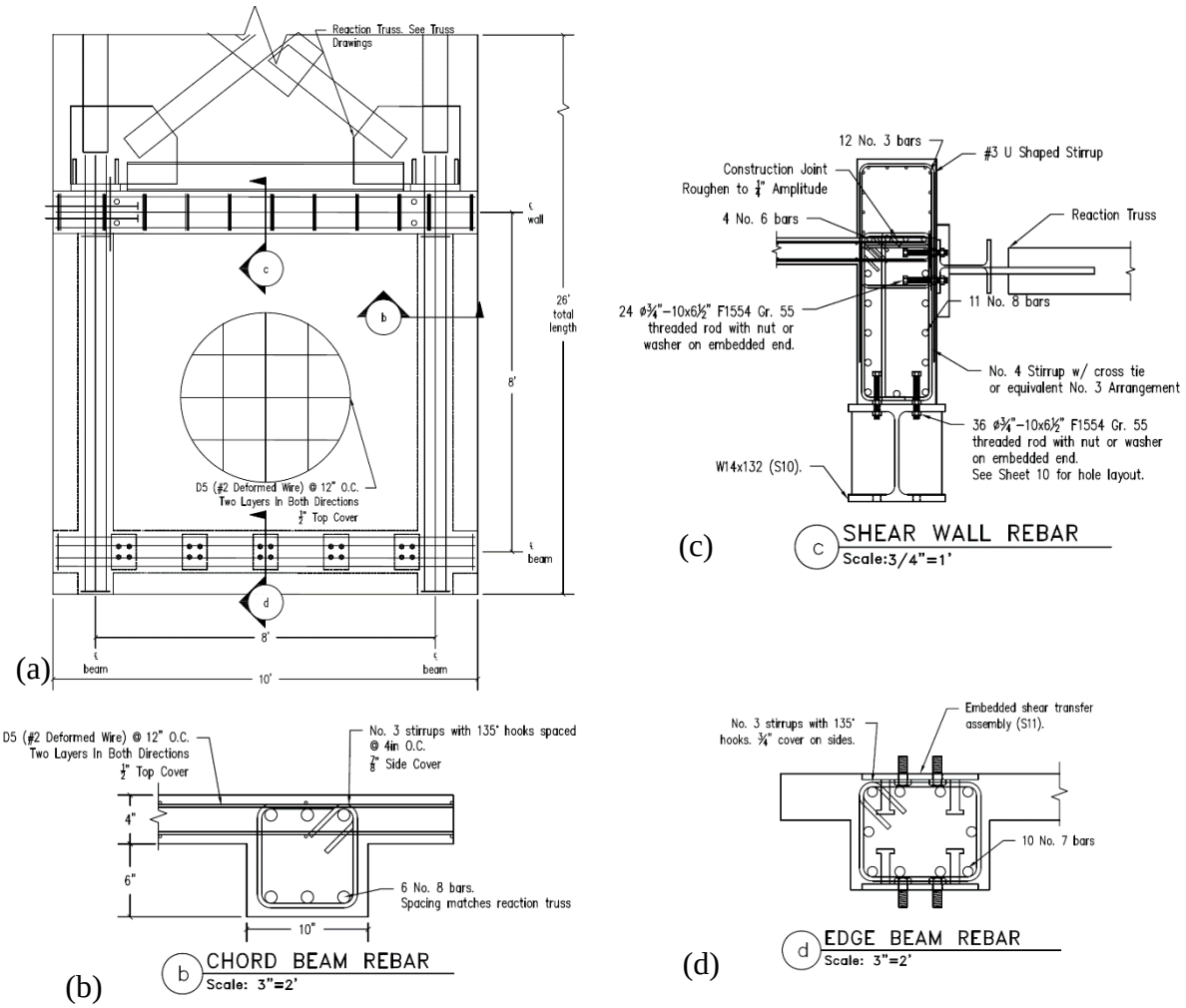

Figure 3.9. Test Specimen Construction Details: (a) Plan View of the Diaphragm; (b) Chord Beam Reinforcing; (c) Shear Wall Segment Reinforcing; (d) Edge Beam Reinforcing with Embedded Shear Transfer Assemblies.

The chord beams were 10 in. wide and extended 6 in. below the underside of the slab with 8 ft center-to-center spacing. The flexural chord beam reinforcement, shown in Figure 3.9(b), was designed to remain elastic up to the maximum capacity of the actuator and consisted of 6 ea. No. 8 bars enclosed by No. 3 stirrups spaced at 4 in.

Each diaphragm specimen was cast integrally with a 12 in. thick shear wall segment that had a cross-section of 37.25 in. ×12 in. (D×W). The shear wall reinforcement, shown in Figure 3.9(c), was overdesigned to able to withstand a reaction of 660 kips. The primary chord beam reinforcement extended through the shear wall segment and was fixed to the truss using rebar couplers. The rebar couplers were installed on the chord reinforcement on each side of the truss bearing plates to be able to develop tension / compression under cyclic load reversals.

In plane shear resistance at the truss / shear wall interface was developed using a total of 24 ea. $\emptyset 3/4$ in. shear studs. Additional in-plane horizontal and overturning resistance of the shear wall segments was provided by a series of $\emptyset 1 - 3/8$ in. threaded rod tie downs.

The edge beam was 12 in. wide and extended 6 in. below the underside of the slab with 8 ft center-to-center spacing with the adjacent shear wall. The reinforcement within the edge beam consisted of 10 ea. No. 7 bars enclosed by No. 3 stirrups spaced at 4 in. The edge beam also included ten embedded shear transfer assemblies shown in Figure 3.9(d). Each shear transfer assembly consisted of a 10 in. × 7 in. × $1/2$ in. steel plate with four, $\emptyset 3/4$ in. headed shear studs welded to each plate.

3.4. Description of Test Setup

The experimental test setup shown in Figure 3.10 incorporated two cantilever diaphragm specimens connected in the middle with a steel truss. This configuration was used because it allowed for the casting of two specimens simultaneously and produced reactions into the strong floor that were parallel to the strong axis of the strong floor beams. The test setup was developed based on Nakashima et al.'s (1981) experimental program. The free end of each cantilever diaphragm was supported with rollers mounted on concrete pedestals which restrained out-of-plane translation. To transfer loads into the specimen as uniformly as possible, in-plane load was applied to the slab through two, MC12×31 loading channels bolted to the ten shear transfer assemblies embedded in the edge beam. Each shear transfer assembly applied the actuator load to the specimen via four $\emptyset 3/4$ in. headed shear studs. Additionally, uplift was restrained at two locations. Figure 3.11(a) shows how the actuator head was restrained from vertical translation, and Figure 3.11(b) details how the free end of the loading channels were restrained from vertical translation. The shear wall segment of each diaphragm was cast on a W12×132 bearing beam through 32 ea. $\emptyset 3/4$ in. shear studs. In-plane horizontal and overturning resistance of the shear wall segments was provided by a W24×87 reaction block. The design calculations for the test setup are provided in Appendix B.

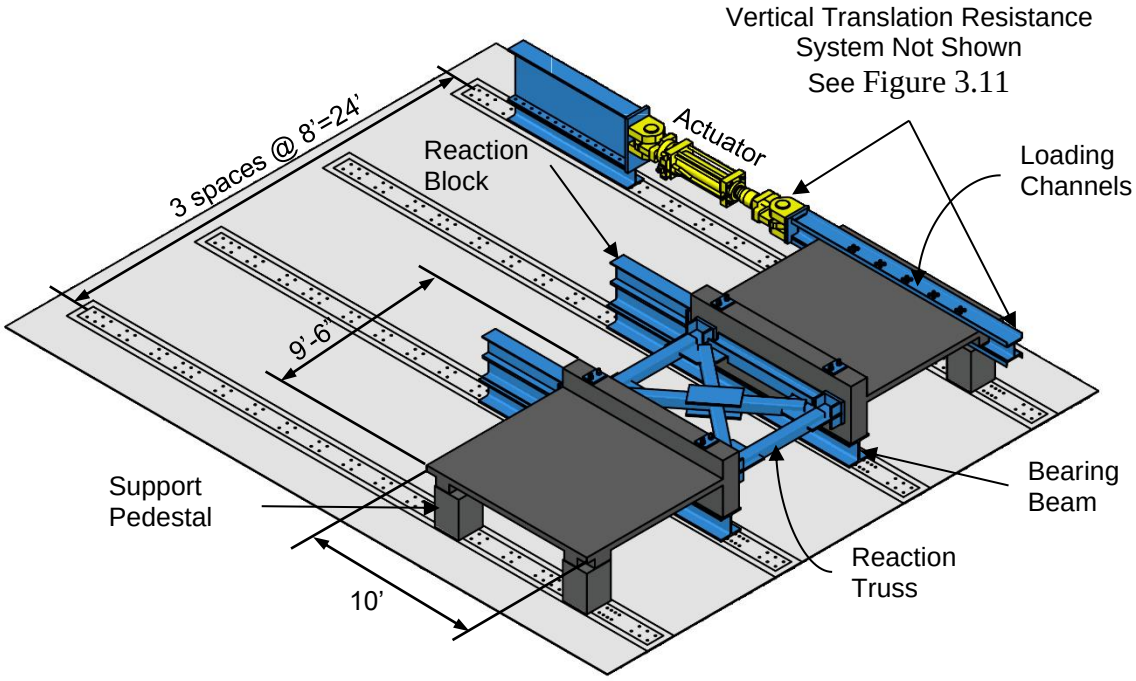

Figure 3.10. Schematic Illustration of the Test Setup.

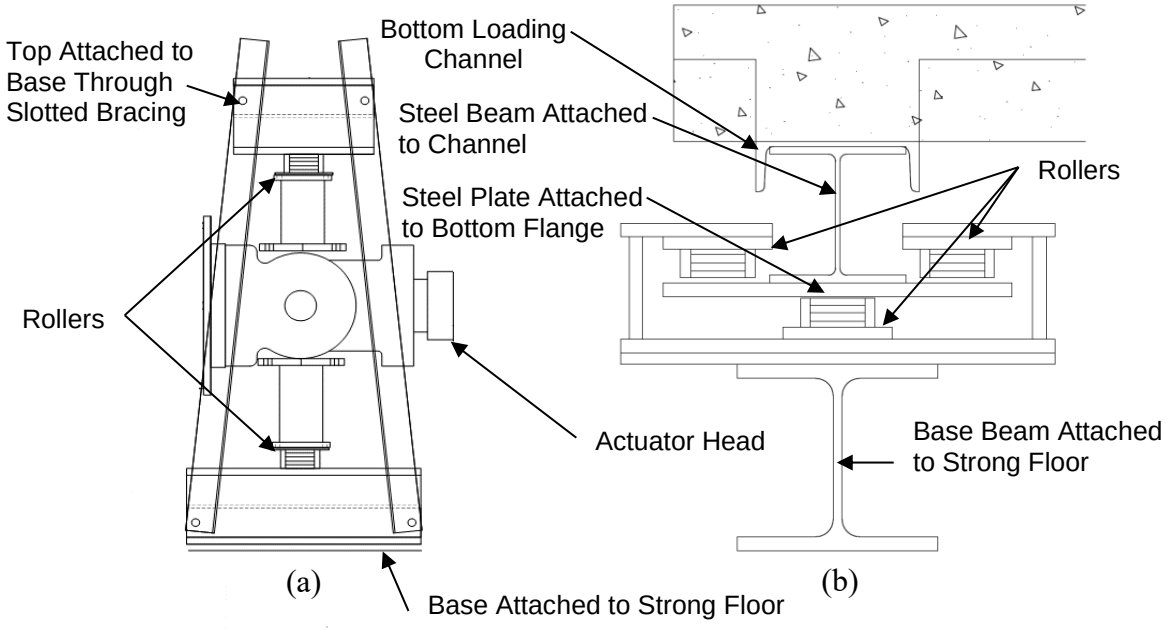

Figure 3.11. Vertical Translation Resistance Systems: (a) Actuator Vertical Translation Resistance System (Avellaneda-Ramirez 2021); (b) Loading Channel Vertical Translation Resistance System.

Figure 3.12 shows an excerpt of the reaction truss drawings. The reaction truss, reactions blocks, and bearing beams were reusable, which helped lower the per-test experimental cost. Furthermore, experimental time was accelerated in this configuration because two

specimens were cast at once and tested sequentially. The complete set of detailed reaction truss drawings and design calculations are provided in Appendix C and D respectively.

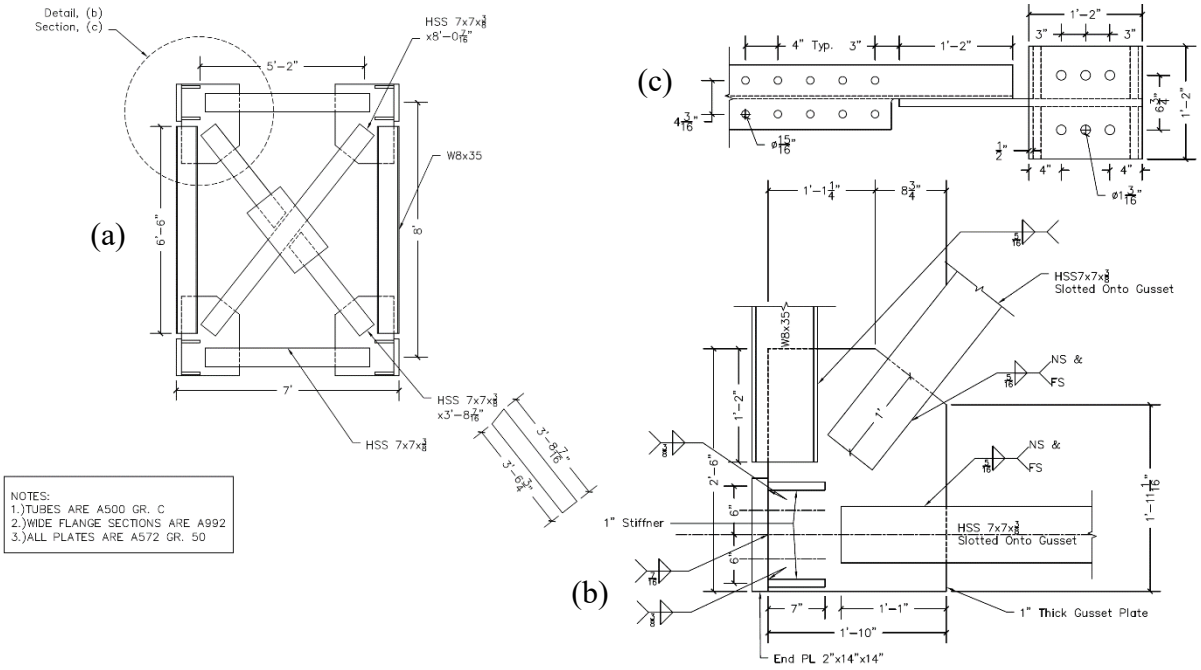

Figure 3.12. Details of Reactions Truss: (a) Plan View of Truss; (b) Corner Connection Plan Detail; (c) Corner Connection Section Detail.

3.5. Test Procedure and Loading Program

The diaphragm specimens were tested using a 330-kip actuator that transferred load to the specimen through the loading channels. The reversed cyclic displacement protocol imposed on each specimen is provided in Table 3.2. This protocol followed the quasi-static cyclic testing guidelines in FEMA 461 (2007). Per these guidelines, there were two cycles at each displacement step and the displacement increased 40% from one step to the next. Specimen CD2 was tested first and as shown in Table 3.2, for all subsequent specimens, some displacement steps were eliminated and some rates were increased. Positive displacements were associated with extension of the actuator, and negative displacements were associated with retraction of the actuator. Tests were stopped after reaching displacements of 2.178 in. to prevent damage to the equipment or the test setup.

Table 3.2. Loading Protocols.

Loading Protocol V1 (CD2)				Loading Protocol V2 (CD1,3,4,5,6)			
Step	Displace-ment (in.)	Number of Cycles	Rate (in./min)	Step	Displace-ment (in.)	Number of Cycles	Rate (in./min)
1	0.010	2	0.050	1	0.038	2	0.061
2	0.014	2	0.050	2	0.054	2	0.086
3	0.020	2	0.050	3	0.075	2	0.120
4	0.027	2	0.050	4	0.105	2	0.169
5	0.038	2	0.050	5	0.148	2	0.236
6	0.054	2	0.050	6	0.207	2	0.331
7	0.075	2	0.060	7	0.289	2	0.463
8	0.105	2	0.084	8	0.405	2	0.648
9	0.148	2	0.118	9	0.567	2	0.907
10	0.207	2	0.165	10	0.794	2	1.270
11	0.289	2	0.231	11	1.111	2	1.778
12	0.405	2	0.324	12	1.556	2	2.000
13	0.567	2	0.454	13	2.178	2	2.000
14	0.794	2	0.635	-	-	-	-
15	1.111	2	0.889	-	-	-	-
16	1.556	2	1.245	-	-	-	-
17	2.178	2	1.742	-	-	-	-

3.6. Instrumentation

Each test utilized sixteen strain gauges, ten string potentiometers, two laser displacement transducers, four time-lapse cameras, and a digital image correlation (DIC) system. Each retrofitted specimen also included an additional six strain gauges distributed along the FRP laminates (locations shown in Chapter 4). Figure 3.13 displays the instrumentation layout used with each test setup. The first two specimens, CD1 and CD2, had several deviations in the instrumentation layout. String potentiometers SP-TN and SP-TS were attached to the reaction truss during testing of Specimens CD1 and CD2. Both instruments were fixed to a ground support for all other specimens. Additionally, string potentiometer SP-SW was in plane with the actuator during testing of Specimen CD2. This instrument was relocated to the underside of the diaphragm to measure the displacement at the exterior face of the edge beam for all other specimens. The distances between the mounting points of each string potentiometer were measured prior to each test and are documented in Appendix E.

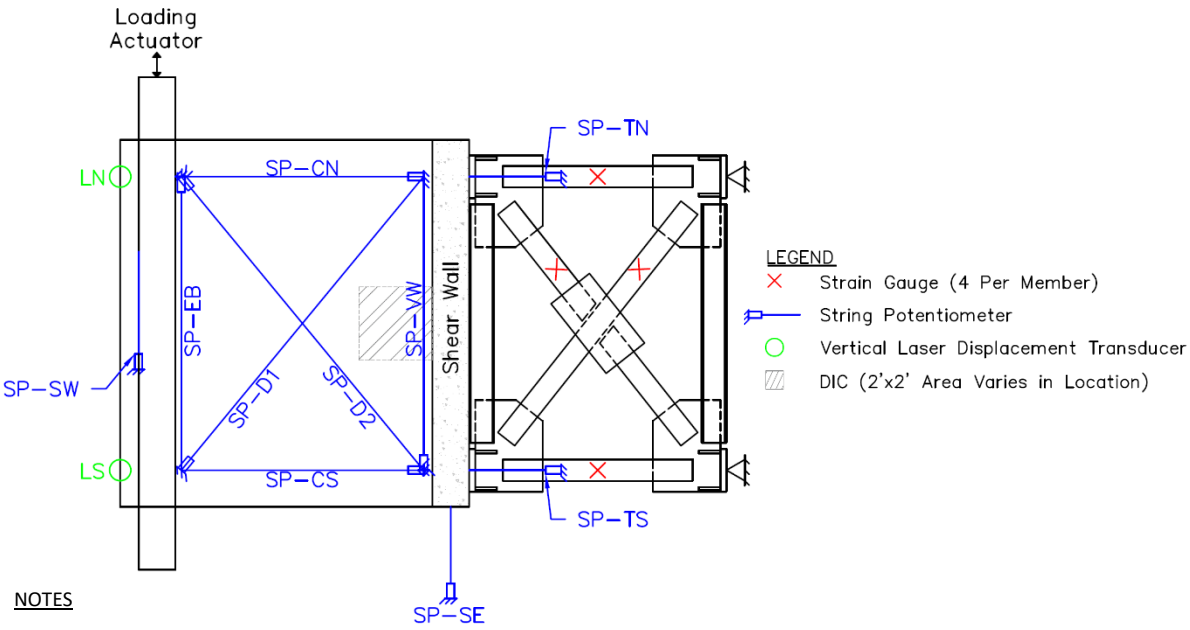

Figure 3.13. Instrumentation Plan.

Sixteen strain gauges were distributed onto the reaction truss where each HSS member included 1 strain gauge per side. For each diagonal and chord member, the four strain measurements were averaged together to eliminate the effect of bending in either direction and obtain an average axial strain. These strain measurements allowed the load distribution to be compared against the anticipated load pattern. The experimental forces were found to generally agree with the truss design forces (see Appendix F). To measure the FRP strain level for the retrofitted specimens, the two interior FRP laminates were instrumented with three strain gauges each. The precise locations of the FRP strain gauges are presented in Chapter 4. The resistance and gauge length of the strain gauges was 120Ω and 5 mm respectively.

Each specimen was instrumented with ten string potentiometers to measure displacement under loading. Six of the string potentiometers including SP-CN, SP-CS, SP-D1, SP-D2, SP-VW, and SP-EB were used to determine the shear angle of the slab inside the beams, hereafter referred to as the local shear angle, γ_L. Using the Law of Cosines, a shear angle at each corner of the slab inside the beams was calculated. The four resulting shear angles were

averaged together to determine the local shear angle. The necessary equations required to determine the local shear angle are provided as Eq. (14).

$$\gamma_{L1} = \gamma_{01} - \cos^{-1}\frac{(C_0 + \Delta D2)^2 - (A_0 + \Delta CN)^2 - (B_0 + \Delta EB)^2}{-2 \cdot (A_0 + \Delta CN) \cdot (B_0 + \Delta EB)} \tag{14}$$

$$\gamma_{L2} = \gamma_{02} - \cos^{-1}\frac{(C_0 + \Delta D2)^2 - (D_0 + \Delta CS)^2 - (E_0 + \Delta \mathrm{VW})^2}{-2 \cdot (D_0 + \Delta \mathrm{CS}) \cdot (E_0 + \Delta \mathrm{VW})}$$

$$\gamma_{L3} = \gamma_{03} - \cos^{-1}\frac{(F_0 + \Delta D1)^2 - (A_0 + \Delta CN)^2 - (E_0 + \Delta \mathrm{VW})^2}{-2 \cdot (A_0 + \Delta CN) \cdot (E_0 + \Delta \mathrm{VW})}$$

$$\gamma_{L4} = \gamma_{04} - \cos^{-1}\frac{(F_0 + \Delta D1)^2 - (D_0 + \Delta CS)^2 - (B_0 + \Delta \mathrm{EB})^2}{-2 \cdot (D_0 + \Delta CS) \cdot (B_0 + \Delta \mathrm{EB})}$$

$$\gamma_L = \frac{\gamma_{L1} + \gamma_{L2} + (-\gamma_{L3}) + (-\gamma_{L4})}{4}$$

where: A_0 is the initial distance between the mounting rods of SP-CN and SP-EB; B_0 is the initial distance between the mounting rods of SP-EB and SP-D1; C_0 is the initial distance between the mounting rods of SP-D2 and SP-CS; D_0 is the initial distance between the mounting rods of SP-CS and SP-D1; E_0 is the initial distance between the mounting rods of SP-VW and SP-CN; F_0 is the initial distance between the mounting rods of SP-D1 and SP-CN; ΔCN is the recorded displacement from SP-CN; ΔEB is the recorded displacement from SP-EB; $\Delta D2$ is the recorded displacement from SP-D2; ΔCS is the recorded displacement from SP-CS; $\Delta \mathrm{VW}$ is the recorded displacement from SP-VW; $\Delta D1$ is the recorded displacement from SP-D1; γ_{L1} is the shear angle calculated with sensors SP-CN, SP-EB, and SP-D2; γ_{01} is the initial angle formed by the mounting rods of sensors SP-CN, SP-EB, and SP-D2; γ_{L2} is the shear angle calculated with sensors SP-CS, SP-VW, and SP-D2; γ_{02} is the initial angle formed by the mounting rods of sensors SP-CS, SP-VW, and SP-D2; γ_{L3} is the shear angle calculated with sensors SP-CN, SP-VW, and SP-D1; γ_{03} is the initial angle formed by the mounting rods of sensors SP-CN, SP-VW, and SP-D1; γ_{L4} is the shear angle calculated with sensors SP-CS, SP-EB, and SP-D1; γ_{04} is the initial angle formed by the mounting rods of sensors SP-CS, SP-EB, and SP-D1; and γ_L is the local shear angle.

Four string potentiometers outside the chord and edge beams including SP-SE, SP-SW, SP-TN, and SP-TS were used to determine a shear angle hereafter referred to as the global shear angle, γ_G. Equation (15) was used to calculate the global shear angle. Figure 3.14(a) illustrates the local shear angle of a specimen while Figure 3.14(b) presents the global shear angle. The local shear angle was considered to best represent the shear behavior of the diaphragm slab; however, the string potentiometers used for this measurement were unreliable after peak load due to the movement and damage of the mounting rods after concrete cracking in their vicinity. The global shear angle was beneficial because it could be calculated for the entire duration of testing but also included the deformation of the flexural chords and edge beam.

$$\gamma_G = \frac{\Delta SE - \Delta SW}{A} - \frac{\Delta TN - \Delta TS}{B} \tag{15}$$

where: γ_G is the global shear angle; ΔSE is the recorded displacement from sensor SP-SE; ΔSW is the recorded displacement from sensor SP-SW; ΔTN is the recorded displacement from sensor SP-TN; ΔTS is the recorded displacement from sensor SP-TS; A is the distance between sensors SP-SW and SP-SE; and B is the distance between sensors SP-TN and SP-TS.

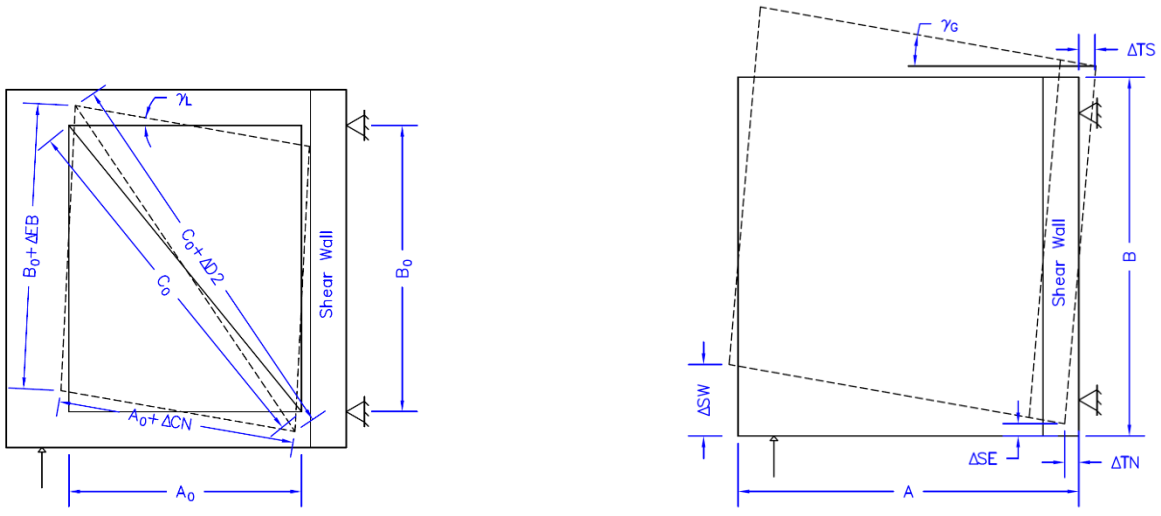

Figure 3.14. Shear Angle Illustration: (a) Local Shear Angle; (b) Global Shear Angle.

3.7. Construction of Test Specimens

The construction of the test specimens began by building wooden formwork. Formwork details are provided in Appendix G. Plywood panels supported by 2×4's were leveled to the elevation of the bottom of the specimen's monolithic beams. These panels were supported by a series of double 2×6 girders that were elevated by a series of braced 4×4's with adjustable shoring jacks. A photo of the shoring system is provided as Figure 3.15(a). The depth of the specimen's beams were then formed using 2×6 and plywood panels. Finally, the edge of the slab was formed using a 4 in. piece of plywood that was braced with 2×4's. The shear wall forms also consisted of plywood panels supported by 2×4 studs and whalers with tension ties. The formwork built was intended to be reused for all specimens; therefore, it was covered with a thin, 2 mm sheet of plastic to prevent damage during formwork stripping operations.

Rebar cages for the shear wall, chord beams, and edge beam were also tied during this time. These cages were tied outside of the formwork for efficiency and later placed into the formwork. The shear wall cages were first placed into the forms. Figure 3.15(b) provides a photo of the reaction truss and shear wall cages in place. Next, the chord cages were woven through the shear wall cages and into the reaction truss where couplers were placed on both sides of each piece of coupled rebar. Once these cages were in place, the free ends were hoisted approximately 6 in. in the air with an overhead crane and woven together with the edge beam cage. This system of rebar was then lowered to its resting place. The top plates belonging to the embedded shear assembly were then suspended with a series of 10 in. × 7 in. plywood panels connected to two overhead 2×6's. The 2×6's spanned across the depth of the specimen and bolted to each free end of the bottom, cast in place channel. To complete the rebar arrangement, the bottom and then top mat of slab reinforcement was spaced and tied. Figure 3.15(c) shows a pair of specimens ready to be cast.

For each placement, one concrete truck delivered concrete to the lab. Two specimens were cast at a time; however, each set of specimens involved two separate concrete placements. The initial placement involved placing both diaphragms and both shear walls to the top slab elevation. From the truck, concrete was placed into a hopper that was flown to the formwork using an overhead crane. The formwork was filled from the shear wall over to the cantilever edge. Each beam and shear wall were consolidated using a submersion vibrator, and a vibratory

screed was used on the surface of the diaphragm field. Once the concrete was finished, it was covered with 6 mm plastic for moisture curing. Additionally, the tops of the shear walls were intermediately raked with a piece of No. 3 rebar to establish a construction joint with a roughened surface.

The secondary placement simply involved extending each shear wall 12 in. above the slab elevation. To prepare for this placement, the construction joint was cleaned and vacuumed of any loose aggregate or debris. Next, the longitudinal rebar was tied to the exposed U-stirrups, and formwork consisting of plywood panels and 2×4 studs was erected. The formwork also utilized six tension ties to resist outward lateral pressure. Prior to the concrete arriving, the shear wall surface was dampened with water using a spray bottle. The concrete was again placed with an overhead crane and hopper and consolidated using a submersion vibrator. The surface was trowel finished and covered with 6mm plastic for moisture curing. Figure 3.15(d) provides a photo of the cured specimens.

After a minimum of seven days of moisture curing, the surface of each specimen was prepared for FRP installation. In accordance with the bond critical application guidelines of ACI PRC-440.2R (2017), the diaphragm surface was ground with a concrete diamond angle grinder to achieve a surface profile no less than Concrete Surface Profile (CSP) 3. A photo of the concrete surface after grinding is shown as Figure 3.15(e). Once the surface was ground, the locations of each FRP sheet and anchor were measured and marked. Next, the anchors holes were drilled to the appropriate depth using a concrete hammer drill. After drilling, the anchor holes were cleaned by simultaneously blowing debris from the hole using compressed air while vacuuming the loose particles. Finally, the diaphragm surface was swept and blown off with an air compressor.

The externally bonded FRP was installed once the concrete had cured for at least 14 days. This process started by priming the concrete surface with the manufacturers suggested amount of resin. Resin thickened with fumed silica was then uniformly applied to the primed areas to fill voids and smooth the concrete surface. Additionally, each anchor hole was primed using the thickened resin. The FRP sheets, which were cut and prepared prior to installation, were then hand saturated with resin. The sheets were then transported and placed at the appropriate locations on each specimen. To work each sheet into place and remove excess epoxy

and air bubbles, a plastic drywall trowel was run across the surface of the FRP. Once the sheets were installed, a small incision was made at the location of each anchor hole with a razor blade. The fiber anchors were then hand saturated with resin. To install the anchors, the dowel was first inserted into the hole, and then the fan was splayed to the appropriate dimensions. To complete the installation, thickened resin was uniformly distributed on top of each FRP sheet and anchor. Any anchor holes not completely filled were topped off with thickened resin. Figure 3.15(f) shows a completed externally bonded FRP installation.

Figure 3.15. Photos of Construction Progression: (a) Shoring Erection; (b) Reaction Truss in Position; (c) Specimens Ready to Cast; (d) Specimens Cured; (e) Surface Grinded; (f) Externally Bonded FRP System Installed.

3.8. Material Properties

3.8.1 Concrete

The diaphragms were constructed and cast in three separate pairs. Each pair of specimens was specified to have a 28-day compression strength of 3500 psi using $3/8$ in. crushed limestone aggregate and a slump of 6 in. The compressive strength f_c', splitting tensile strength f_{sp}, and modulus of elasticity E_c for each of the diaphragms at the time of testing is summarized in Table 3.3. Each value is representative of an average of at least two concrete cylinders.

Concrete test cylinders were prepared according to ASTM C31 (2022). Compression tests were conducted following ASTM C39 (2021). Additionally, splitting tensile tests were conducted in accordance with ASTM C496 (2017), and the elastic modulus was determined following ASTM C469 (2022).

Table 3.3. Concrete Material Properties at the Time of Testing.

Specimen	**6"×12" Compressive Strength, f_c' (psi)**	**4"×8" Compressive Strength, f_c' (psi)**	**Splitting Tensile Strength, f_{sp} (psi)**	**Modulus of Elasticity, E_c (×10^6 psi)**
CD1	4760	4320	445	3.55
CD2	4570	4340	400	3.38
CD3	3670	3610	370	3.23
CD4				
CD5	3950	4250	410	3.53
CD6	4470	4500	420	3.64

3.8.2 Reinforcing Steel

The reinforcement within the field of the diaphragm consisted of Grade 75, D5 deformed wire. Following ASTM A370 (2022), coupon tests were conducted to obtain the stress-strain behavior and yield strength of the D5 deformed wire. The stress-strain relationship of the diaphragm reinforcement, obtained from three coupon tests, is shown in Figure 3.16.

All other reinforcing steel used to construct the shear wall, chord beams, and edge beam consisted of Grade 60, A615 rebar. The material properties for these bars were not established because they were designed to remain elastic during testing.

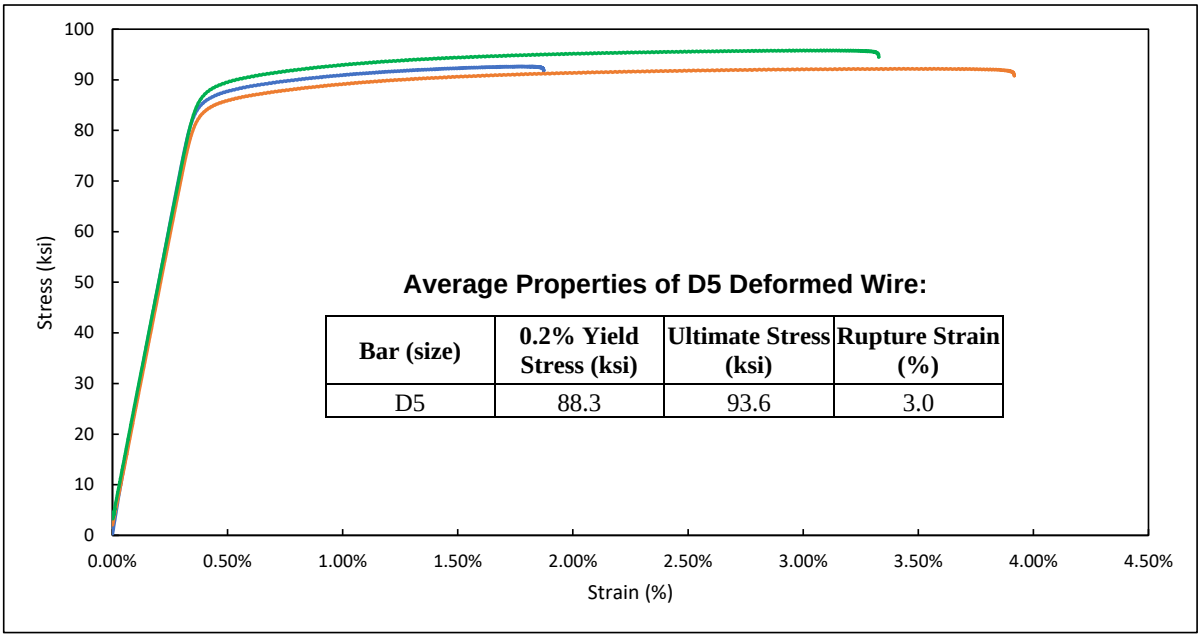

Figure 3.16. Stress-Strain Relationship of D5 Coupons.

3.8.3 Externally Bonded FRP

As shown in the retrofit test matrix in Table 3.1, four different types of FRP systems from two manufacturers were used. Specimen CD2 was strengthened with Simpson Strong-Tie and Structural Technology's V-Wrap C100HM. Specimen CD3 was strengthened with Fyfe's Tyfo-SCH-11UP. Specimen CD4 was strengthened with Fyfe's Tyfo-SEH-51A. Specimen CD5 was strengthened with Simpson Strong-Tie and Structural Technology's V-Wrap C200HM. Finally, Specimen CD6 was strengthened with Simpson Strong-Tie and Structural Technology's V-Wrap C100HM. The average dry fiber and cured composite properties reported by the manufacturer for these materials is summarized in Table 3.4. It should be noted that the average composite properties of the Tyfo-SEH-51A system were not reported by the manufacturer; therefore, Table 3.4 provides the manufacturer's reported design values for this material only. The manufacturer's technical data sheets for each composite system are provided in Appendix H.

The mechanical properties of the FRP composites were established with rectangular FRP coupons 12 in. long and 1 in. wide cut from two ply FRP witness panels which were prepared on the day of each diaphragm retrofit. Two inch long, emery cloth strips were later bonded to the ends of each coupon specimen using Loctite gel. These strips were intended to prevent a failure in the grip region during testing. Three FRP coupons representative of each

FRP material underwent tensile testing in accordance with ASTM D3039 (2008). The cured laminate material properties obtained from these coupons is compared to the manufactured reported material properties in Table 3.4. Additionally, the stress-strain relationship of each FRP coupon is included in Figure 3.17.

Table 3.4. Manufactured Reported and Experimental Average FRP Properties.

Material	**V-Wrap C100HM (CFRP) (Simpson Strong-Tie 2022a)**			**Tyfo-SCH-11UP (CFRP) (Fyfe 2022a)**		
Origin	Manufacturer		Experimental	Manufacturer		Experimental
Type	Dry Fiber	Composite	Composite	Dry Fiber	Composite	Composite
Tensile Strength (ksi)	790	216	225	550	143	167
Tensile Modulus (ksi)	42000	16700	13474	33400	13900	11804
Ultimate Elongation (%)	1.9	1.3	1.6	1.7	1.0	1.4
Thickness (in.)	-	0.02	0.02	-	0.02	0.03
Material	**Tyfo-SEH-51A (GFRP) (Fyfe 2022b)**			**V-Wrap C200HM (CFRP) (Simpson Strong-Tie 2022b)**		
Origin	Manufacturer(1)		Experimental	Manufacturer		Experimental
Type	Dry Fiber	Composite	Composite	Dry Fiber	Composite	Composite
Tensile Strength (ksi)	470	66	106	790	180	105
Tensile Modulus (ksi)	10500	3730	4596	42000	14240	9224
Ultimate Elongation (%)	4.5	1.8	2.4	1.9	1.27	1.14
Thickness (in.)	-	0.05	0.04	-	0.04	0.07

(1): Manufacturer's properties shown for Tyfo-SEH-51A are design values. Average values not published on Fyfe's technical data sheet.

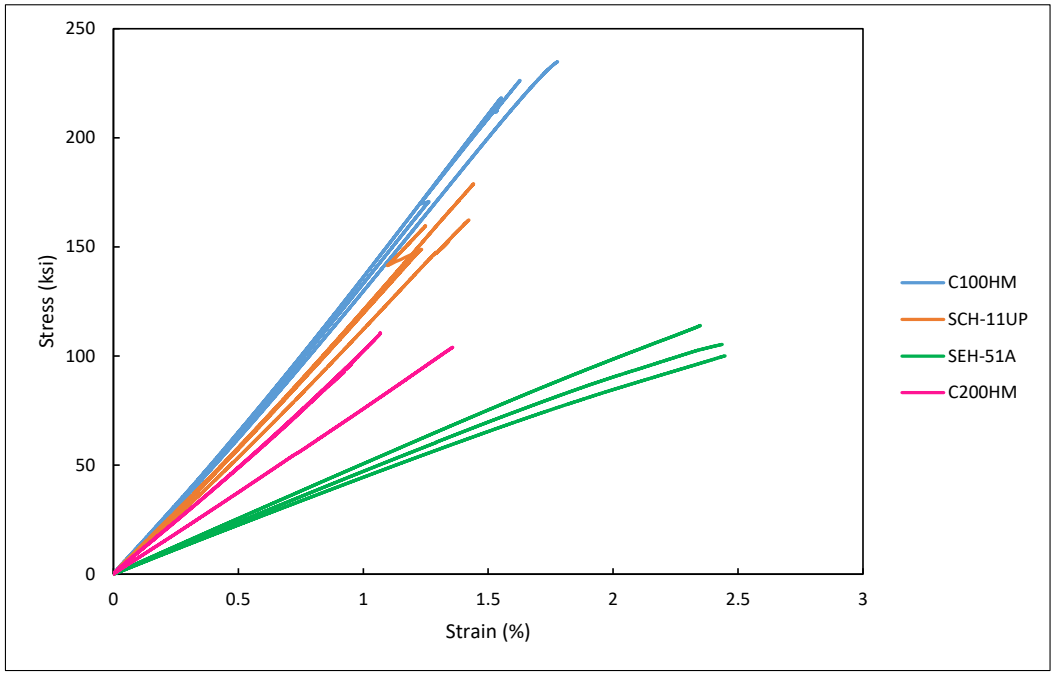

Figure 3.17. Stress-Strain Relationship of FRP Coupons.

3.8.4 FRP Anchors

Each strengthened specimen utilized a carbon fiber anchor system; however, the manufacturer and diameter varied. Specimen CD2 was anchored with Simpson Strong-Tie and Structural Technology's Ø1/2 in. CSS V-Wrap HMCA. Specimen CD3 was anchored with Fyfe's Ø3/4 in. Tyfo SCH Composite Anchor. Specimen CD4 was anchored with Fyfe's Ø1/2 in. Tyfo SCH Composite Anchor. Specimens CD5 and CD6 were both anchored with Simpson Strong-Tie and Structural Technology's Ø3/4 in. CSS V-Wrap HMCA. The dry fiber and cured composite properties reported by the manufacturer for these anchors is summarized in Table 3.5. The manufacturer's technical data sheets for each anchor system are provided in Appendix H.

Table 3.5. Manufacturer Reported FRP Anchor Properties.

Material	**CSS V-Wrap HMCA (Simpson Strong-Tie 2022)**		**Tyfo SCH Composite Anchor (Fyfe 2022)**	
Type	Dry Fiber	Composite	Dry Fiber	Composite
Tensile Strength (ksi)	790	165	620	110
Tensile Modulus (x 10^6 psi)	42	15	36	-
Ultimate Elongation (%)	1.9	1.1	1.7	-

Chapter 4. Experimental Results

4.1. General

The experimental results obtained from testing six reinforced concrete diaphragms are presented in this chapter. The five specimens retrofitted with various configurations of FRP were studied to determine any enhancement in strength, ductility, or serviceability. For applicable specimens, the complete set of crack maps are provided in Appendix I. For each specimen, the predicted shear strength contributions of concrete, reinforcing steel, and FRP are provided in Table 4.1. The shear strength provided by concrete was calculated with Eq. (2) using the respective 6 in. × 12 in. compressive strengths from Table 3.3, and the shear strength provided by the reinforcing steel was calculated with Eq. (3) using the experimental yield stress of 88.3 ksi. Assuming an effective FRP strain of 0.4% and an effective depth of 120 in., the shear strength provided by FRP was calculated with Eq. (4) using the ply configuration variables from Table 3.1. These predicted strength values are provided in each respective hysteric plot of applied load versus local and global shear angle within this chapter.

Table 4.1. Predicted Shear Strength Components

Specimen	**Concrete Shear Strength, V_c (kip)**	**Steel Shear Strength, V_s (kip)**	**FRP Shear Strength, V_f (kip)**	**Diaphragm Shear Strength, $V_c + V_s + V_f$ (kip)**
CD1	66	78	-	144
CD2	65	78	80	223
CD3	58	78	83	220
CD4	58	78	90	226
CD5	60	78	74	213
CD6	64	78	80	222

Various failure mechanisms including diagonal tension cracking, rebar rupture, FRP debonding, FRP rupture, anchor pullout, and anchor rupture are discussed within this chapter. Examples of each of these typical failure modes is shown in Figure 4.1.

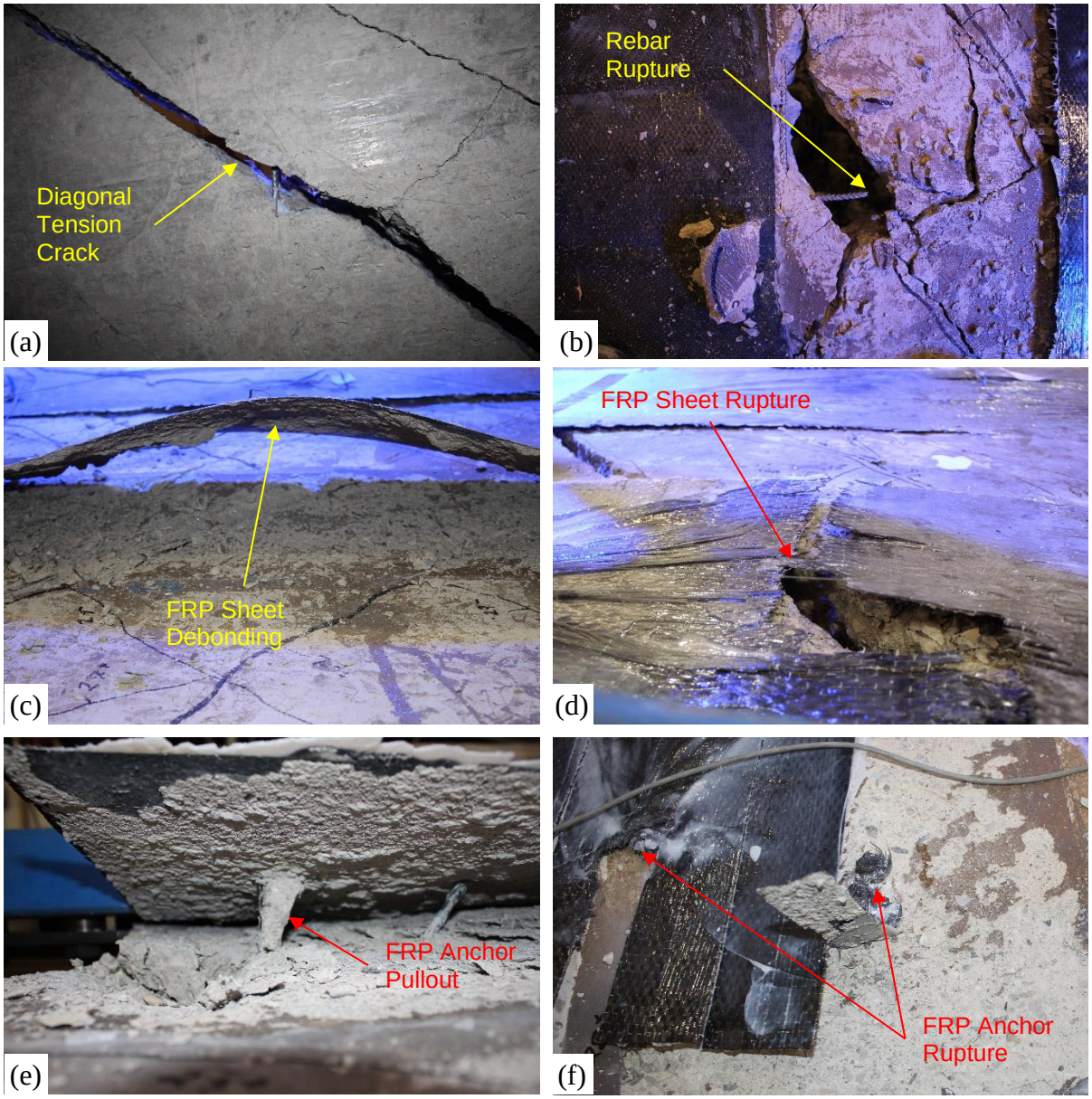

Figure 4.1. Typical Failure Modes: (a) Diagonal Tension Crack; (b) Rebar Rupture; (c) FRP Debonding; (d) FRP Rupture; (e) Anchor Pullout; (f) Anchor Rupture.

4.2. Specimen CD1

Specimen CD1 was tested to observe the performance and failure mode of reinforced concrete diaphragms in high seismic zones. Additionally, this specimen served as a baseline for comparison with the five FRP retrofitted specimens. The baseline specimen reached a peak load of 203 kips before failing due to diagonal tension shear followed by reinforcing steel rupture. At the peak load, the local shear angle was measured as 0.0044 radians while the

global shear angle was measured as 0.0049 radians. The hysteric plots of applied load versus local and global shear angle are provided as Figure 4.2(a) and Figure 4.2(b) respectively. The points labeled A through F on each of these plots correspond to the photos in Figure 4.3(a) through Figure 4.3(f). The global shear angle values corresponding to this specimen represent a correction that was needed to account for string potentiometers SP-TN and SP-TS being mounted to the reaction truss which was not rigid during testing. The correction is detailed in Appendix J.

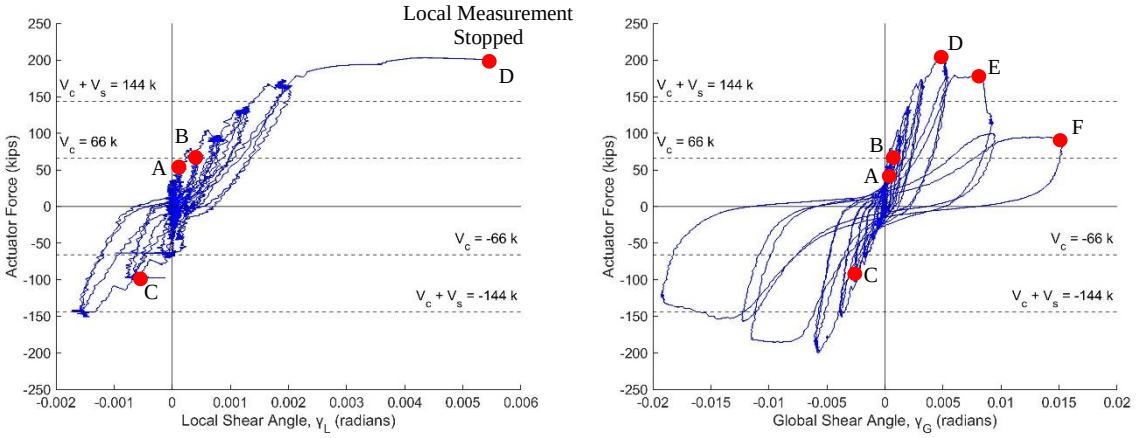

(a) (b)

Figure 4.2. Hysteretic Shear Angle Response of Specimen CD1: (a) Local Shear Angle; (b) Global Shear Angle.

Cracks were marked and measured throughout the test, and maps were prepared to document each crack and associated width at cycles 11, 16, and 21. The first observation of cracking was made during the positive portion of cycle 11 corresponding to a load of 52 kips. Figure 4.3(a) shows the condition of the specimen as this point. Only one crack was visible which resembled a combined flexural-shear crack with a width 0.15 mm. Diagonal tension cracking began during the positive portion of cycle 14 corresponding to a load of 67 kips. Figure 4.3(b) shows the state of the specimen at this point of testing. While more diagonal tension cracks propagated in the positive loading direction with average widths of 0.3 to 0.5 mm, diagonal tension cracks in the negative loading direction did not appear until cycle 17 corresponding to a load of -98 kips. This trend of crack development indicated asymmetry in the rigidity of the test setup. The condition of the specimen at this point of the test is shown in Figure 4.3(c). The specimen reached its peak capacity of 203 kips during cycle 19, and its corresponding condition is shown in Figure 4.3(d). Imminent failure was observed at a load of

approximately 175 kips when the primary diagonal tension crack widened disproportionally to other cracks. The state of the specimen at this point during testing is shown in Figure 4.3(e). The crack widening then resulted in rebar necking and rupture as the load increased. Figure 4.4 shows the extent of cracking at cycle 21 which corresponds to an applied displacement of 1.111 in. The final state of the specimen corresponding to a residual load of 93 kips is shown in Figure 4.3(f).

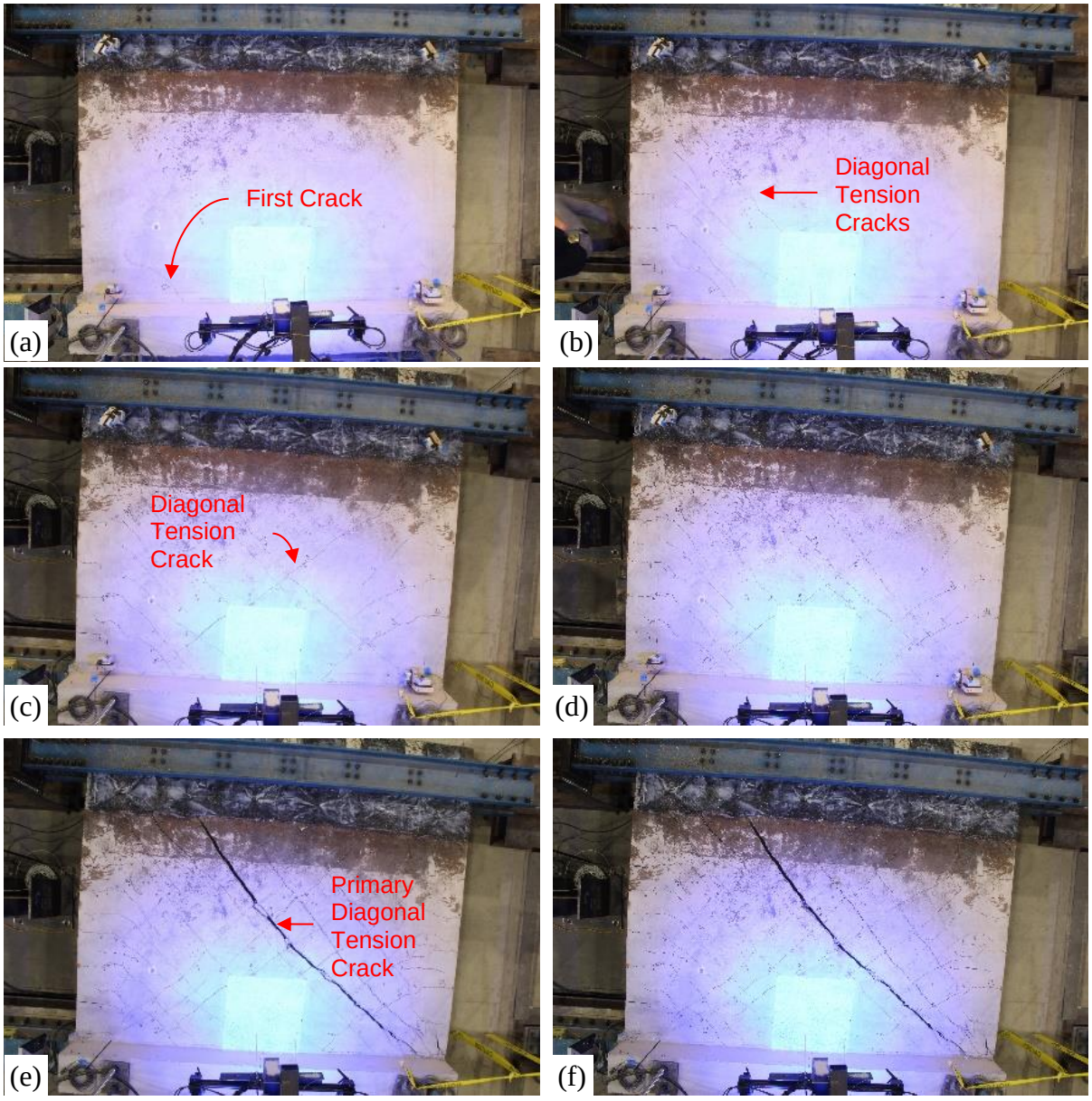

Figure 4.3. Failure Progression of Specimen CD1: (a) Initial Cracking at 52 kips; (b) First Diagonal Tension Cracking at 67 kips; (c) Diagonal Tension Cracking at -98 kips; (d) Condition at Peak Load of 203 kips; (e) Dilation of Primary Diagonal Tension Crack at 175 kips; (f) Final Condition of Failed Specimen at 93 kips.

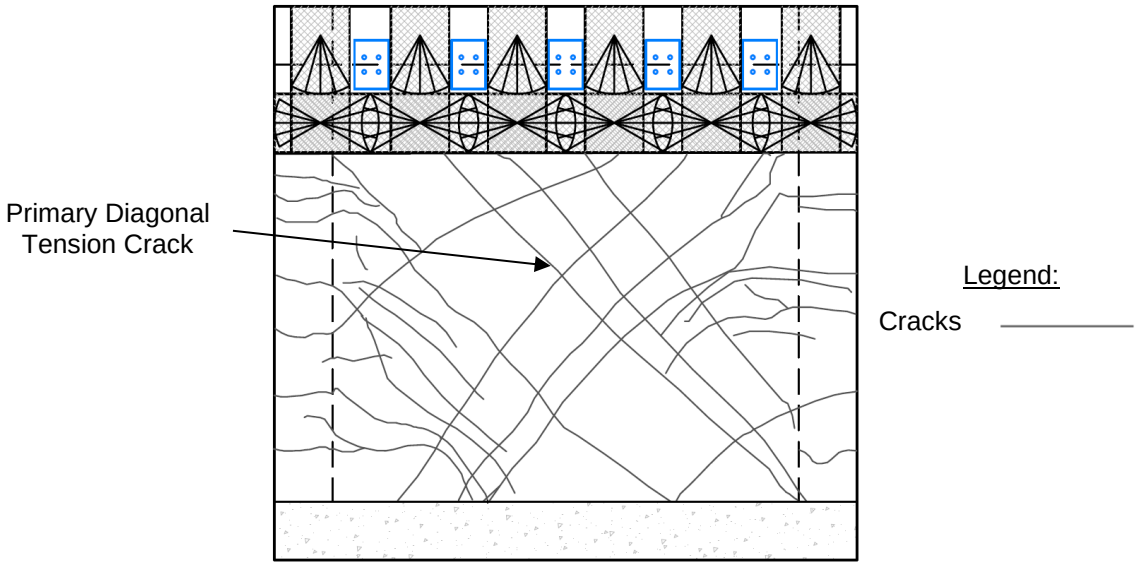

Figure 4.4. Extent of Damage of Specimen CD1 at Cycle 21 (1.111 in. Displacement).

4.3. Specimen CD2

Specimen CD2 was tested to observe the performance and failure mode of a reinforced concrete diaphragm strengthened with CFRP covering approximately 50% of the surface with end anchorage only. The specimen reached a peak load of 280 kips before failing due to intermediate crack induced FRP debonding and anchor rupture followed by diagonal tension shear and reinforcing steel rupture. At the peak load, the local shear angle was measured as 0.00378 radians while the global shear angle was approximated as 0.00691 radians. The hysteric plots of applied load versus local and global shear angle are provided in Figure 4.5(a) and Figure 4.5(b) respectively. The points labeled A through F on each of these plots correspond to the photos in Figure 4.8(a) through Figure 4.8(f). The global shear angle values corresponding to this specimen represent an approximate correction that was necessary due to concrete cracking and spalling at the mounting location of string potentiometers SP-SW and SP-SE. The correction is a function of the actuator displacement and is detailed in Appendix J. For this reason, the global shear angle measurements for this specimen should be used carefully.

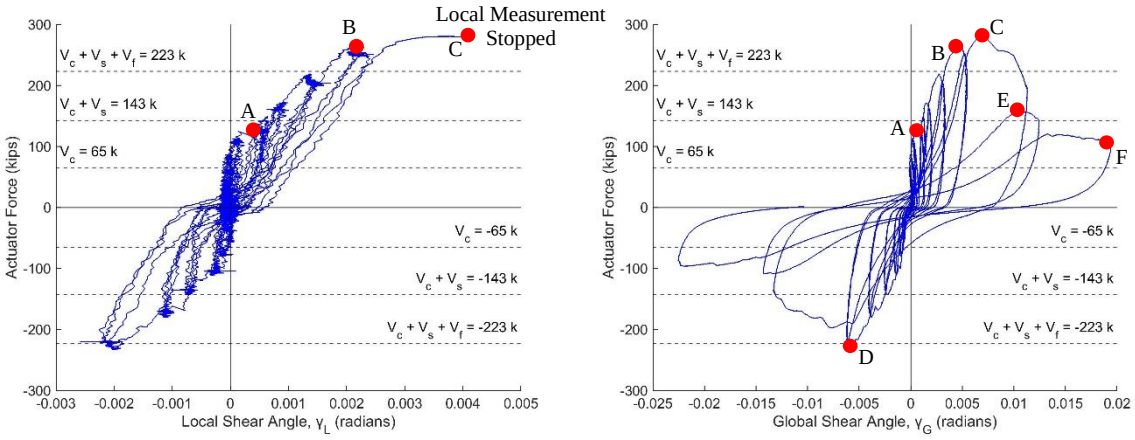

Figure 4.5. Hysteretic Shear Angle Response of Specimen CD2: (a) Local Shear Angle; (b) Global Shear Angle.

The FRP strain behavior recorded from the FRP strain gauges, such as the plot of actuator force versus FRP strain shown in Figure 4.6, is not intuitive upon first inspection. Therefore, the following discussion is provided for better understanding. The strain gauges installed on the FRP captured variable data that was highly dependent on the location of the gauge and cracks in the specimen. Figure 4.6 provides a typical FRP strain gauge response curve which is labeled with four key points. Point I shows the initial elastic response prior to a crack forming near the strain gauge. The strain then increases at Point II when a crack forms and engages the FRP sheet where the strain gauge was installed. The strain behavior then typically follows a cyclic pattern until peak load is reached at Point III. The termination of the curve at Point IV represents the maximum strain recorded by the gauge.

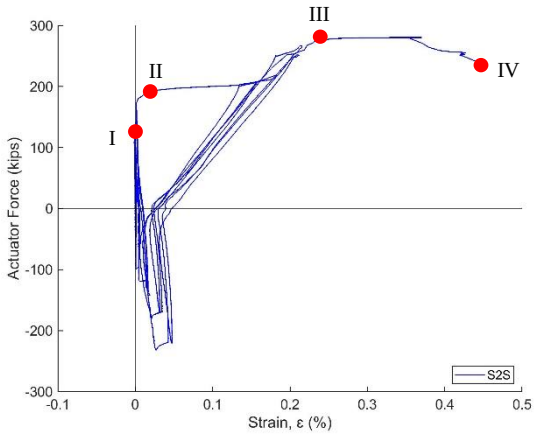

Figure 4.6. Typical FRP Strain Walk Through

The strain measurements associated with FRP sheets S2 and S3 are provided in Figure 4.7(a) and Figure 4.7(b) respectively. Three strain gauges were installed on both FRP sheets; however, strain gauge S3N was not functional during testing. Figure 4.7(c) presents the location and label of each FRP sheet and strain gauge. Cracks in the diaphragm were observed to transverse the FRP sheets near the locations of gauges S2M, S2S, and S3M. The FRP strains measured at these locations when peak load occurred were 0.32%, 0.37%, and 0.30%, respectively. At peak load, the FRP strains measured with gauges S2N and S3S, which were not located near a crack, were 0.02% and 0.01%, respectively.

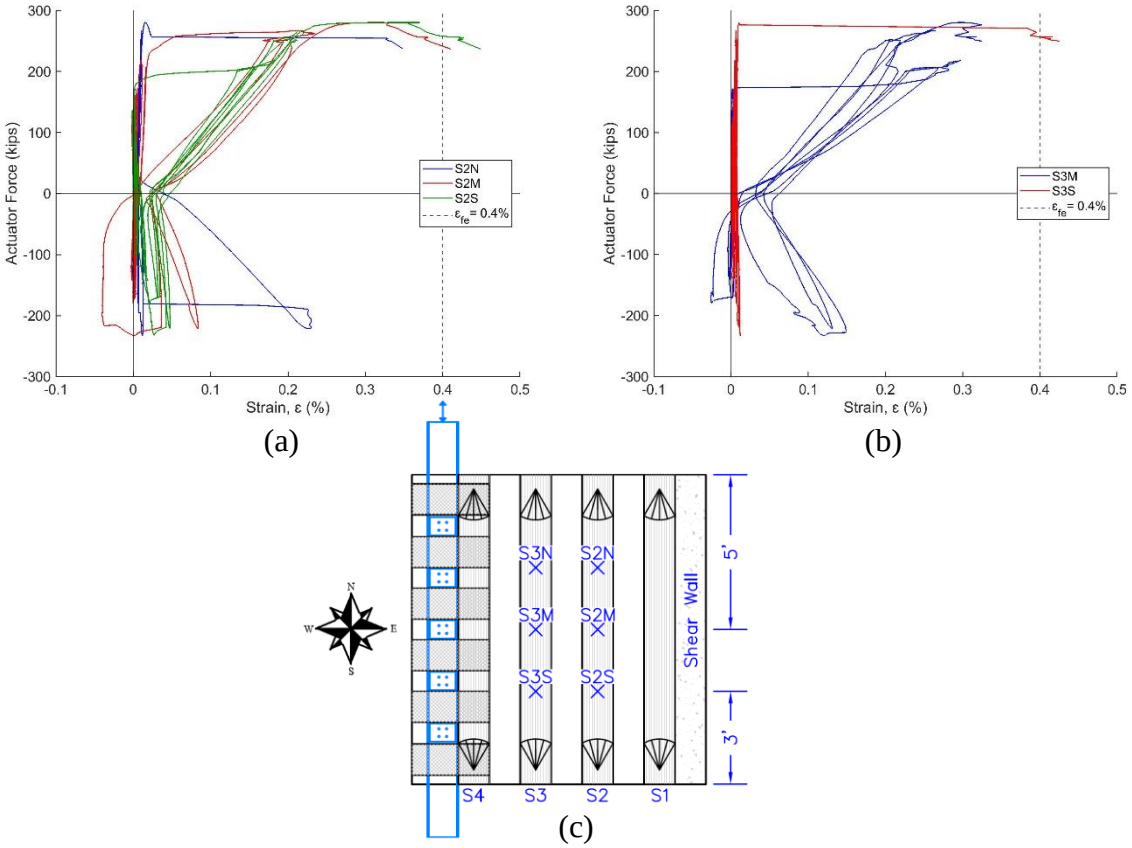

Figure 4.7. FRP Strain Response of Specimen CD2: (a) Strain Response of Sheet S2; (b) Strain Response of Sheet S3; (c) Strain Gauge Layout.

Although cracks were marked on the concrete surface throughout the test, the crack locations and associated widths were not mapped and recorded. The first observation of cracking between FRP sheets was made during the positive portion of cycle 23 corresponding to a load of 125 kips. Figure 4.8(a) shows the condition of the specimen at this point of testing. Diagonal tension cracks continued to form causing FRP sheets S3 and S4 to experience local

edge debonding during the positive portion of cycle 29 corresponding to a load of 266 kips. Figure 4.8(b) shows the state of the specimen at this point of the test. Figure 4.9 was created based on overhead photos and demonstrates the approximate extent of cracking and debonding at cycle 29 which corresponds to an applied displacement of 1.111 in. The specimen reached its peak capacity of 280 kips during the positive portion of cycle 31, and its corresponding condition is shown in Figure 4.8(c). At the peak load, FRP sheets S2 and S3 debonded approximately 75% along each respective sheet's length. Sheet S2 remained engaged due to both end anchors maintaining integrity; however, sheet S3 lost full capacity due to the south end anchor rupturing. Furthermore, during the negative portion of cycle 31 (corresponding to a load of -233 kips), the south end anchor of sheet S4 pulled out and both end anchors of sheet S1 resisted end peeling. The condition of the specimen at this point is shown in Figure 4.8(d). After the majority of debonding had occurred, the specimen began to predominately fail due to diagonal tension shear during the positive portion of cycle 32 corresponding to a load of 159 kips. The state of the specimen at this point of the test is shown in Figure 4.8(e). Finally, the primary diagonal tension crack widened and rebar began to rupture during the positive portion of cycle 33 corresponding to a load of 111 kips. The final condition of the specimen is shown in Figure 4.8(f).

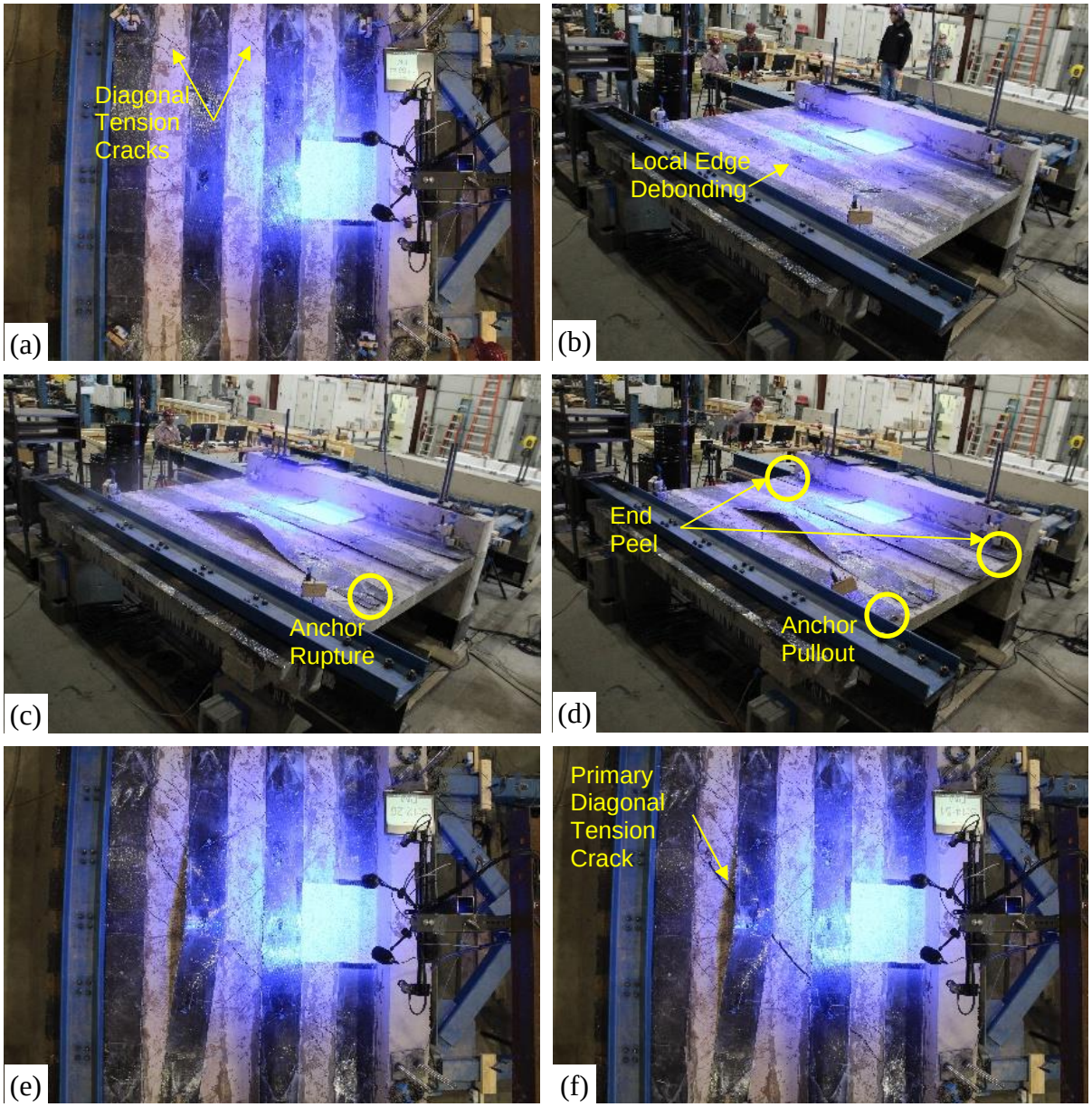

Figure 4.8. Failure Progression of Specimen CD2: (a) First Diagonal Tension Cracks at 125 kips; (b) Localized Edge Debonding of Sheet S3 at 266 kips; (c) Anchor Rupture and Debonding of Sheet S3 at 280 kips; (d) Anchor Pullout and End Peeling at -233 kips; (e) Condition After Debonding at 159 kips; (f) Final Condition of Failed Specimen at 111 kips.

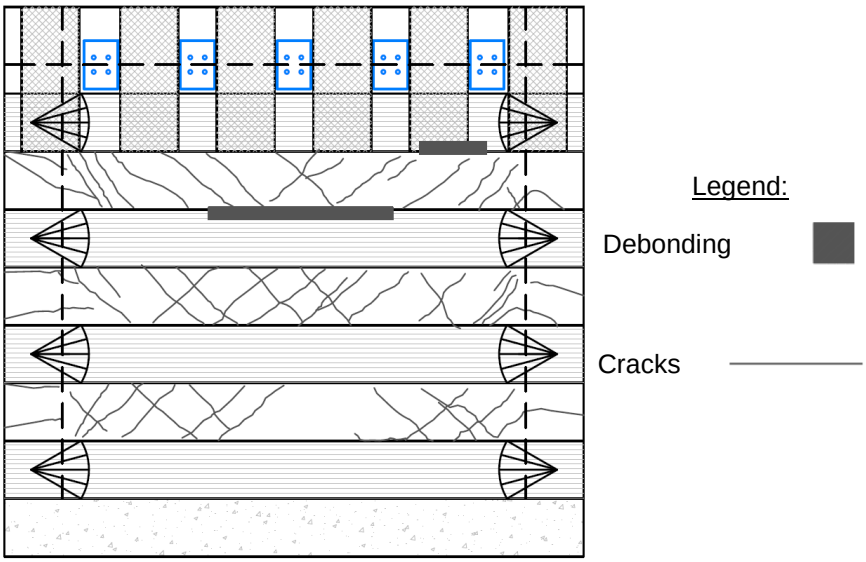

Figure 4.9. Approximate Extent of Damage of Specimen CD2 at Cycle 29 (1.111 in. Displacement).

4.4. Specimen CD3

Specimen CD3 was tested to observe the performance and failure mode of a reinforced concrete diaphragm strengthened with a CFRP retrofit scheme equivalent to specimen CD2 paired with intermediate anchors. The specimen reached a peak load of 259 kips before failing due to FRP rupture, intermediate crack induced FRP debonding, and anchor pullout followed by diagonal tension shear and reinforcing steel rupture. At the peak load, the local shear angle was measured as 0.00231 radians while the global shear angle was measured as 0.00326 radians. The hysteric plots of applied load versus local and global shear angle are provided as Figure 4.10(a) and Figure 4.10(b) respectively. The points labeled A through F on each of these plots correspond to the photos in Figure 4.12(a) through Figure 4.12(f).

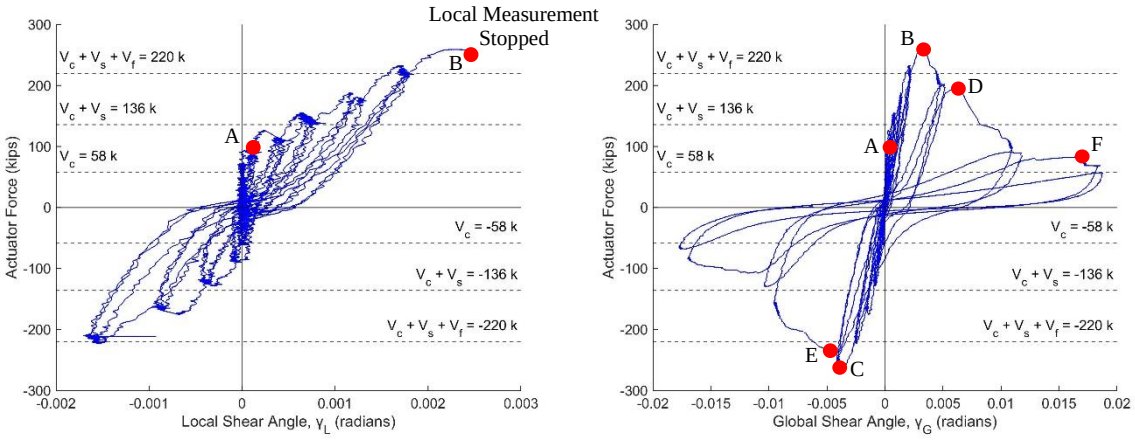

Figure 4.10. Hysteretic Shear Angle Response of Specimen CD3: (a) Local Shear Angle; (b) Global Shear Angle.

The strain measurements associated with FRP sheets S2 and S3 are provided in Figure 4.11(a) and Figure 4.11(b) respectively. Three strain gauges were installed on both FRP sheets; however, strain gauge S3S malfunctioned shortly after the specimen reached its peak capacity. Figure 4.11(c) presents the location and label of each FRP sheet and strain gauge. Cracks in the diaphragm were observed to transverse the FRP sheets near the locations of gauges S2M, S2S, S3N, and S3M. The FRP strains measured at these locations when peak load occurred were 0.45%, 0.27%, 0.34%, and 0.35%, respectively. At peak load, the FRP strains measured with gauges S2N and S3S, which were not located near a crack, were 0.17% and 0.04%, respectively.

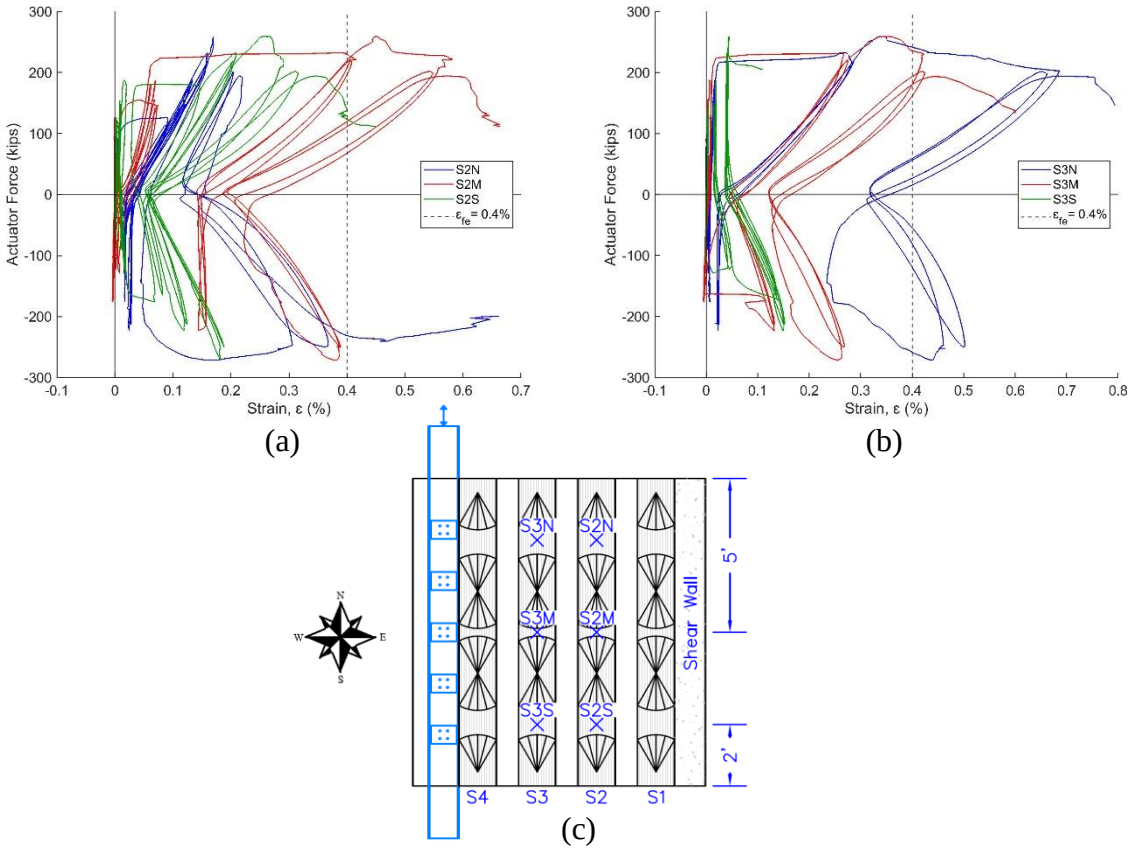

Figure 4.11. FRP Strain Response of Specimen CD3: (a) Strain Response of Sheet S2; (b) Strain Response of Sheet S3; (c) Strain Gauge Layout.

Cracks were marked and measured throughout the test, and maps were prepared to document each crack and associated width at cycles 11, 16, and 21. The first observation of cracking between FRP sheets was made during the positive portion of cycle 11 corresponding to a load of 91 kips. Figure 4.12(a) shows the condition of the specimen at this point of the test. Only one crack was visible with a measured width of 0.1 mm. Diagonal tension cracks, with average widths of 0.3 mm to 0.75 mm, continued to form causing FRP sheets S1, S2, and S3 to experience local edge debonding during the positive portion of cycle 15 corresponding to a load of 144 kips. The specimen reached its peak capacity of 259 kips during the positive portion of cycle 21, and its corresponding condition is shown in Figure 4.12(b). At the peak load, FRP sheets S2 and S3 centrally debonded approximately 75% of each sheet's respective length. Both sheets remained engaged due to anchor action; however, sheet S4 ruptured in the area between the North end anchor and adjacent intermediate anchor. Furthermore, during the negative portion of cycle 21 (corresponding to a load of -271 kips), the south end of sheet S4

experienced end peeling. The state of the specimen at this point of testing is shown in Figure 4.12(c). Cracks widths measured up to 2 mm after the rupture and debonding had occurred. Figure 4.13 depicts the extent of cracking, debonding, and sheet rupture at cycle 21 which corresponds to an applied displacement of 1.111 in. The exaggerated crack openings allowed the reinforcing steel to elongate and rupture during the positive portion of cycle 23 corresponding to a load of 192 kips. Figure 4.12(d) shows the condition of the specimen during this point of the test. During this cycle, the south ends of sheets S2 and S3 also experienced end peeling. The end peeling continued to occur during the negative portion of cycle 23 corresponding to a load of -240 kips. Figure 4.12(e) shows the state of the specimen at this point of testing. Both North ends of sheets S1 and S2 experienced end peeling. Prior to the positive portion of cycle 25 (corresponding to a load of 82 kips), end peeling was restrained by the end anchors; however, sheets S2 and S3 completely debonded once anchor pullout occurred during cycle 25. The debonded condition is shown in Figure 4.12(f). During cycle 25, sheet S2's North end anchor and adjacent intermediate anchor pulled out while sheet S3's South end anchor and adjacent intermediate end anchor pulled out.

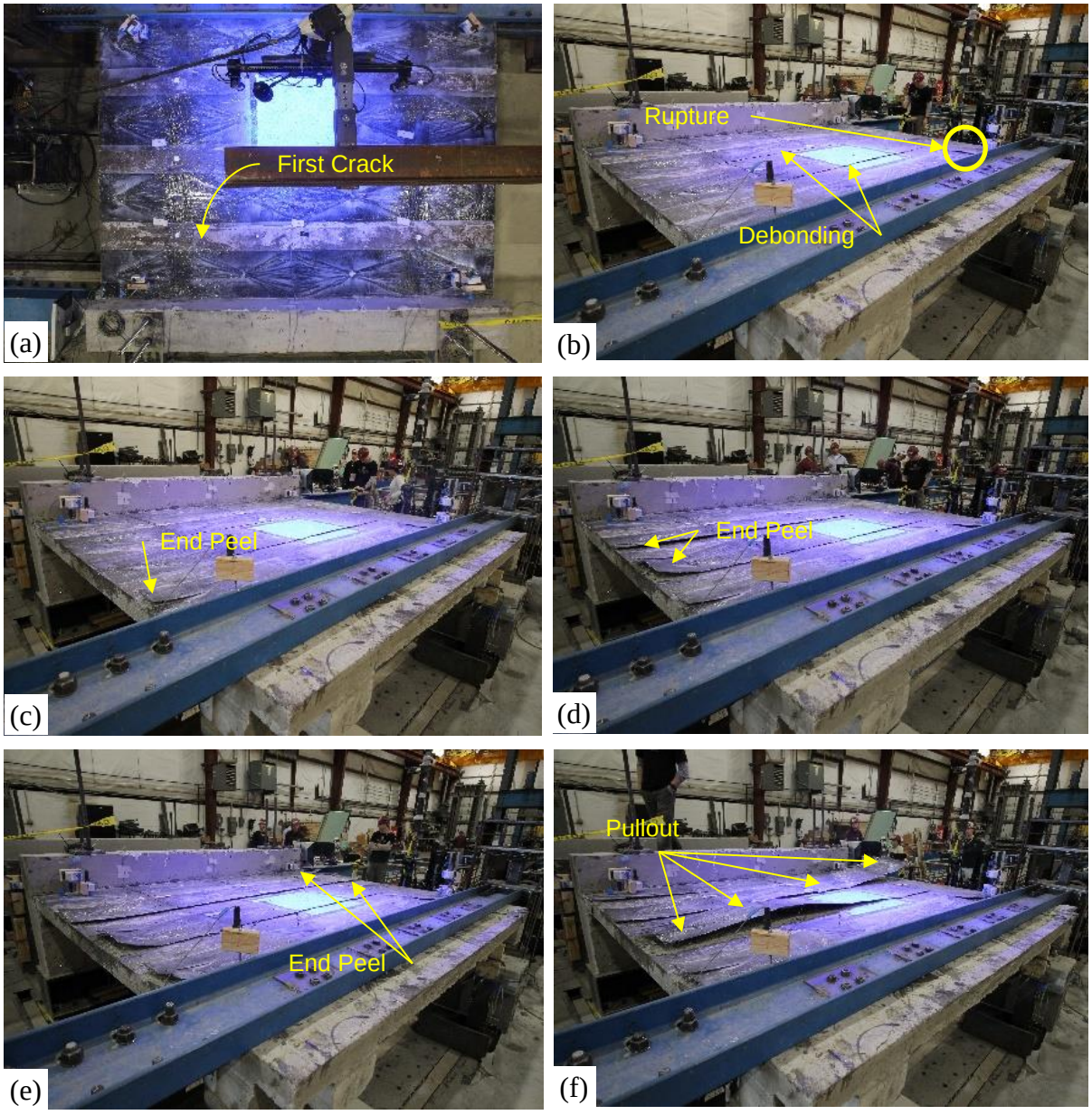

Figure 4.12. Failure Progression of Specimen CD3: (a) First Diagonal Tension Cracks at 91 kips; (b) FRP Rupture and Debonding at 259 kips; (c) South End Peeling of Sheet S4 at -271 kips; (d) South End Peeling of Sheets S2 and S3 at 192 kips; (e) North End Peeling of Sheets S1 and S2 at -240 kips; (f) Anchor Pullout of Sheets S2 and S3 at 82 kips.

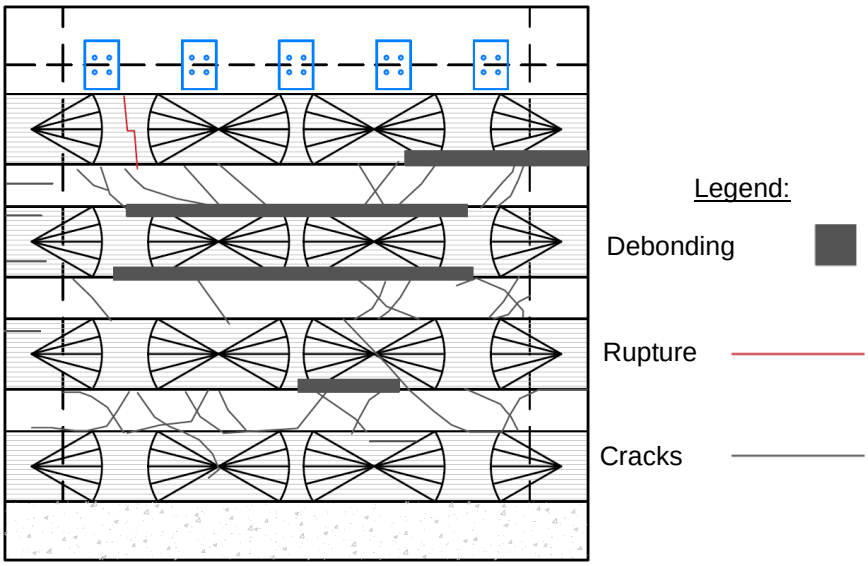

Figure 4.13. Extent of Damage of Specimen CD3 at Cycle 21 (1.111 in. Displacement).

4.5. Specimen CD4

Specimen CD4 was tested to observe the performance and failure mode of a reinforced concrete diaphragm strengthened with GFRP covering 100% of the surface with end anchorage only. The specimen reached a peak load of 263 kips before failing due to intermediate crack induced FRP debonding, anchor rupture, and anchor pullout followed by diagonal tension shear and reinforcing steel rupture. At the peak load, the local shear angle was measured as 0.00195 radians while the global shear angle was measured as 0.00409 radians. The hysteric plots of applied load versus local and global shear angle are provided as Figure 4.14(a) and Figure 4.14(b) respectively. The points labeled A through F on each of these plots correspond to the photos in Figure 4.16(a) through Figure 4.16(f).

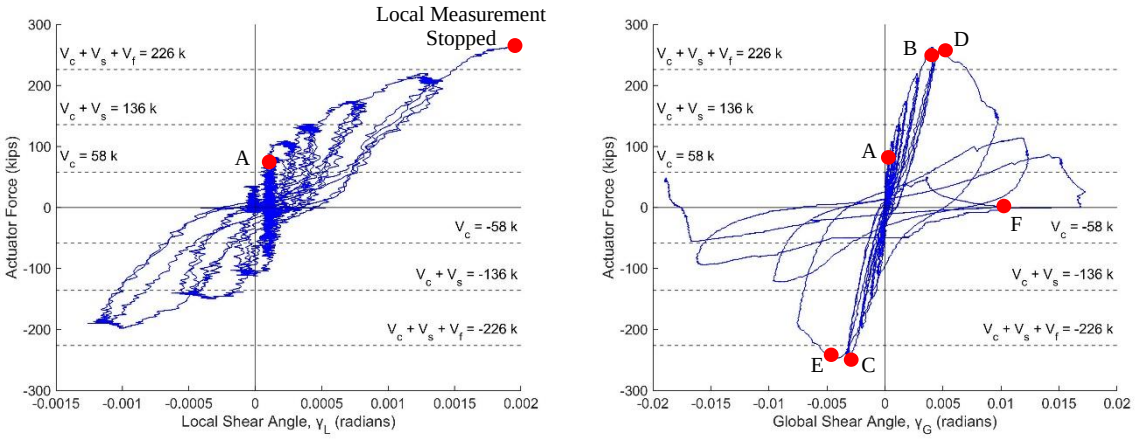

Figure 4.14. Hysteretic Shear Angle Response of Specimen CD4: (a) Local Shear Angle; (b) Global Shear Angle.

The strain measurements associated with FRP sheets S2 and S3 are provided in Figure 4.15(a) and Figure 4.15(b) respectively. Three strain gauges were installed on both FRP sheets. Figure 4.15(c) presents the location and label of each FRP sheet and strain gauge. Cracks in the diaphragm were observed to transverse the FRP sheets near the locations of gauges S2M, S2S, S3N, S3M, and S3S. The FRP strains measured at these locations when peak load occurred were 0.27%, 0.32%, 0.45%, 0.23%, and 0.47%, respectively. At peak load, the FRP strain measured with gauge S2N, which was not located near a crack, was 0.08%.

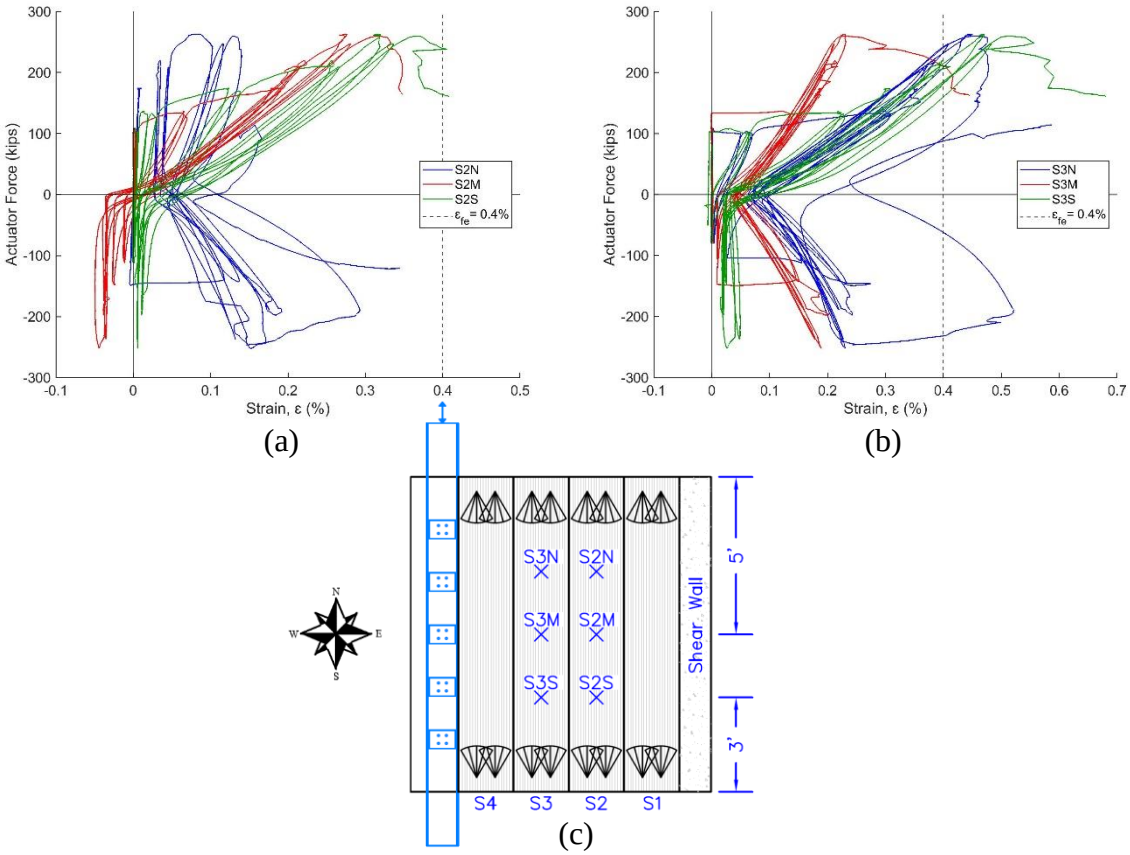

Figure 4.15. FRP Strain Response of Specimen CD4: (a) Strain Response of Sheet S2; (b) Strain Response of Sheet S3; (c) Strain Gauge Layout.

Cracks were marked and measured throughout the test, and maps were prepared to document each crack and associated width at cycles 11, 16, and 21. It should be noted that the cracks were mapped from the underside of this specimen due to the FRP covering the entire top surface. The first observation of cracking was made during the positive portion of cycle 11 corresponding to a load of 83 kips. Figure 4.16(a) shows the condition of the specimen at this point of testing. Only one crack was visible with a measured width of 0.2 mm. Additional diagonal tension cracks, with average widths of 0.3 mm to 0.5 mm, were documented through cycle 16. The specimen reached its peak capacity during cycle 21, corresponding to a load of 263 kips, with average crack widths ranging from 0.2 mm to 0.75 mm. Figure 4.17 shows the extent of cracking and debonding at cycle 21 which corresponds to an applied displacement of 1.111 in. During the positive portion of cycle 22 (corresponding to a load of 247 kips), the edge of FRP sheet S4 debonded along its entire length while the edge of sheet S2 centrally debonded approximately 25% of its length. Figure 4.16(b) shows the state of the specimen at

this point of the test. Furthermore, the south end of sheet S4 began to experience end peeling during the negative portion of cycle 22 corresponding to a load of -236 kips. The condition of the specimen at this point of the test is shown in Figure 4.16(c). During the positive portion of cycle 23 (corresponding to a load of 260 kips), the south end anchor groups of sheets S4 and S3 both failed as the sheets fully debonded approximately 50% along their lengths. The state of the specimen at this point of the test is shown in Figure 4.16(d). One anchor in each group ruptured while the other pulled out. Additionally, sheet S2's edge debonding propagated to the south end anchor group causing partial anchor pullout. As shown in Figure 4.16(e), the negative portion of cycle 23 (corresponding to a load of -247 kips) caused the debonding of sheets S4, S3, and S2 to propagate towards the north end anchor groups. Sheets S4 and S3 lost full capacity while sheet S2 remained engaged due to anchor action. Diagonal tension shear then began to dominate the failure. The widest diagonal tension cracks exceeded 2 mm in width which allowed the reinforcing steel to elongate and rupture. The final state of the specimen, corresponding to a load of 1 kip, is shown in Figure 4.16(f).

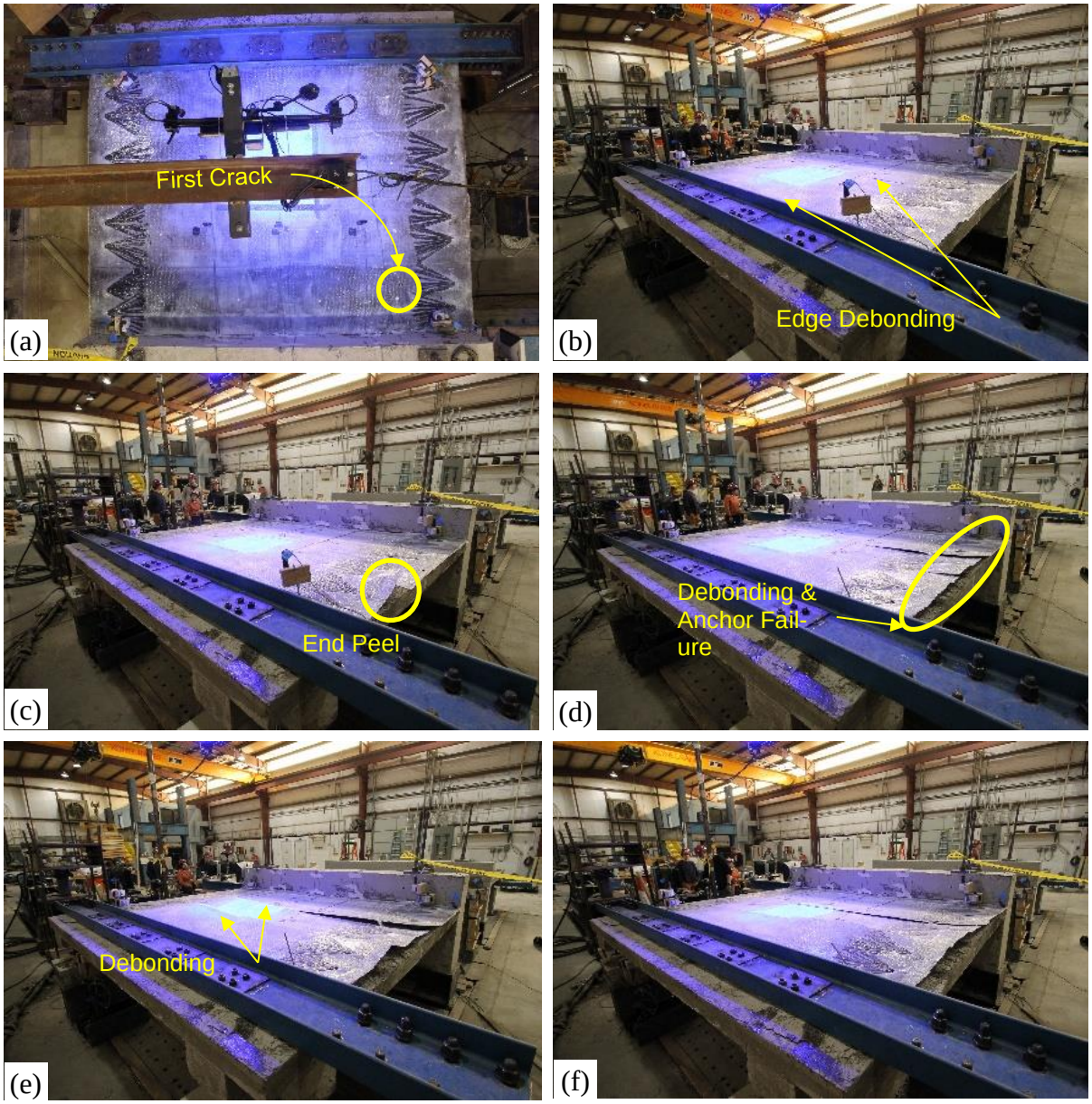

Figure 4.16. Failure Progression of Specimen CD4: (a) First Crack at 83 kips; (b) Edge Debonding of Sheet S4 at 247 kips; (c) End Peeling of Sheet S4 at -236 kips; (d) Debonding and Anchor Failures of Sheets S4, S3, and S2 at 260 kips; (e) Debonding Propagating Northward at -247 kips; (f) Final Condition of Failed Specimen at 1 kip.

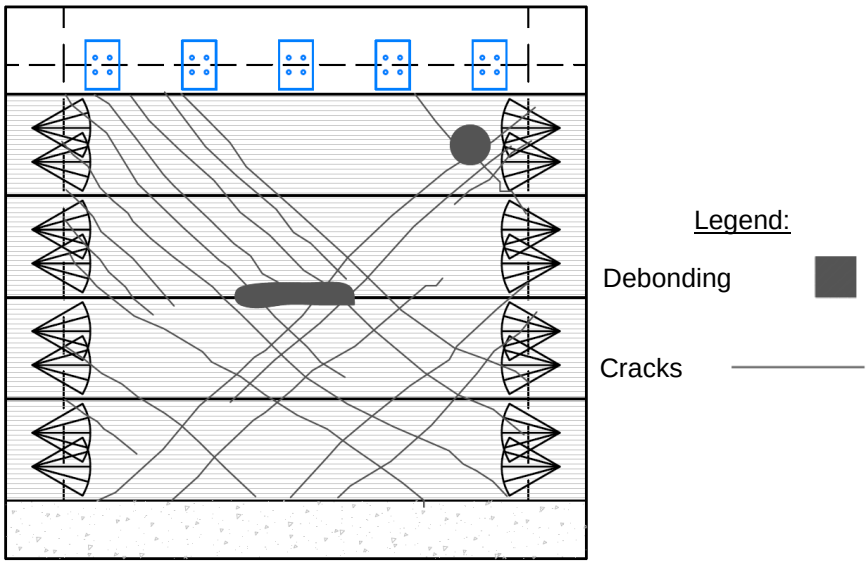

Figure 4.17. Extent of Damage of Specimen CD4 at Cycle 21 (1.111 in. Displacement).

4.6. Specimen CD5

Specimen CD5 was tested to observe the performance and failure mode of a reinforced concrete diaphragm strengthened with GFRP covering approximately 30% of the surface with end anchorage only. The specimen reached a peak load of 240 kips before failing due to intermediate crack induced FRP debonding and anchor pullout followed by diagonal tension shear and reinforcing steel rupture. At the peak load, the local shear angle was measured as 0.00267 radians while the global shear angle was measured as 0.00428 radians. The hysteric plots of applied load versus local and global shear angle are provided as Figure 4.18(a) and Figure 4.18(b) respectively. The points labeled A through F on each of these plots correspond to the photos in Figure 4.20(a) through Figure 4.20(f).

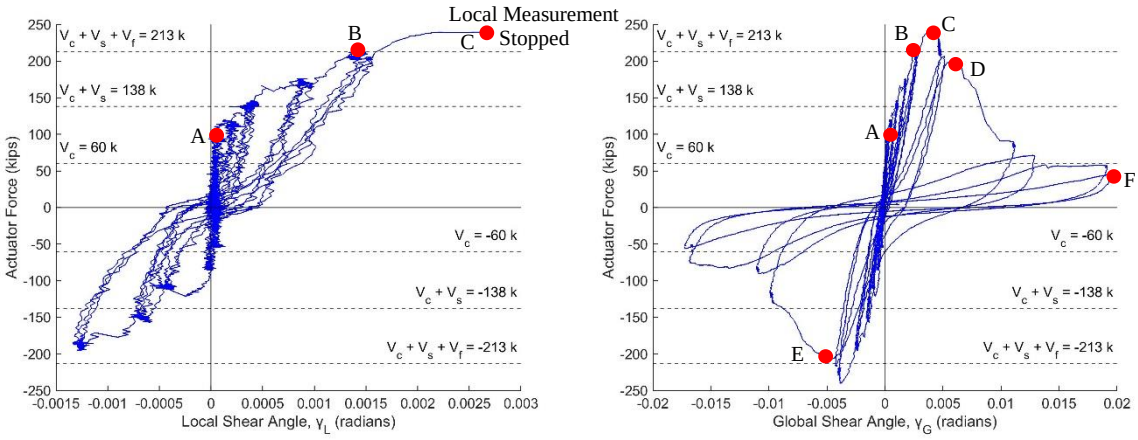

(a) (b)

Figure 4.18. Hysteretic Shear Angle Response of Specimen CD5: (a) Local Shear Angle; (b) Global Shear Angle.

The strain measurements associated with FRP sheets S2 and S3 are provided in Figure 4.19(a) and Figure 4.19(b) respectively. Three strain gauges were installed on both FRP sheets; however, strain gauge S2M malfunctioned prior to the specimen reaching its peak capacity. Figure 4.19(c) presents the location and label of each FRP sheet and strain gauge. Cracks in the diaphragm were observed to transverse the FRP sheets near the locations of gauges S2S, S3N, and S3M. The FRP strains measured at these locations when peak load occurred were 0.27%, 0.25%, and 0.36%, respectively. At peak load, the FRP strains measured with gauges S2N and S3S, which were not located near a crack, were 0.14% and 0.03%, respectively.

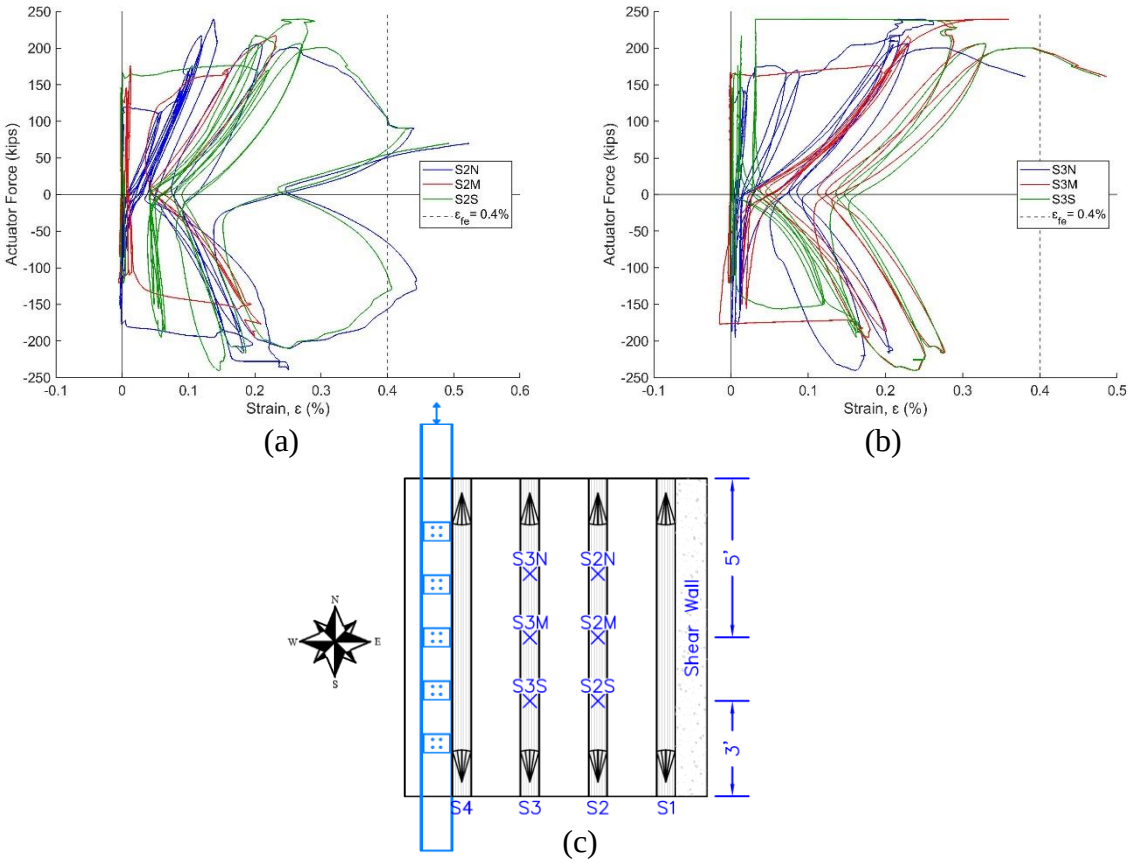

Figure 4.19. FRP Strain Response of Specimen CD5: (a) Strain Response of Sheet S2; (b) Strain Response of Sheet S3; (c) Strain Gauge Layout.

Cracks were marked and measured throughout the test, and maps were prepared to document each crack and associated width at cycles 11, 16, and 21. The first observation of cracking was made during the positive portion of cycle 11 corresponding to a load of 96 kips. Figure 4.20(a) shows the condition of the specimen at this point of testing. Only two cracks were visible with measured widths of 0.15 mm. Additional diagonal tension cracks, with average widths of 0.1 mm to 0.5 mm, were documented through cycle 16. The diagonal tension cracks continued to form and cause central edge debonding of FRP sheet S2 during the positive portion of cycle 19 corresponding to a load of 217 kips. Figure 4.20(b) shows the state of the specimen at this point of the test. The specimen reached its peak capacity during cycle 21, corresponding to a load of 240 kips, with average crack widths ranging from 0.1 mm to 1.25 mm. At the peak load, sheet S3 experienced central edge debonding while sheet S4 underwent edge debonding near the North end anchor. The corresponding condition of the specimen at peak load is shown in Figure 4.20(c). Figure 4.21 demonstrates the extent of cracking and

debonding at cycle 21 which corresponds to an applied displacement of 1.111 in. During the positive portion of cycle 23 (corresponding to a load of 200 kips), sheets S2 and S3 centrally debonded along approximately 75% of their lengths, sheet S4's North end anchor pulled out, and sheet S3 underwent end peeling at the North end anchor. The specimen's primary diagonal tension crack also widened which allowed rebar to begin to elongate and rupture. Figure 4.20(d) shows the condition of the specimen during this point of the test. Furthermore, during the negative portion of cycle 23 (corresponding to a load of -210 kips) the North end anchor of sheet S3 partially pulled out and another diagonal tension crack widened. Figure 4.20(e) shows the state of the specimen at this point of testing. Diagonal tension shear then began to dominate the failure allowing more rebar to elongate and rupture. The final state of the failed specimen, corresponding to a load of 44 kips, is shown in Figure 4.20(f).

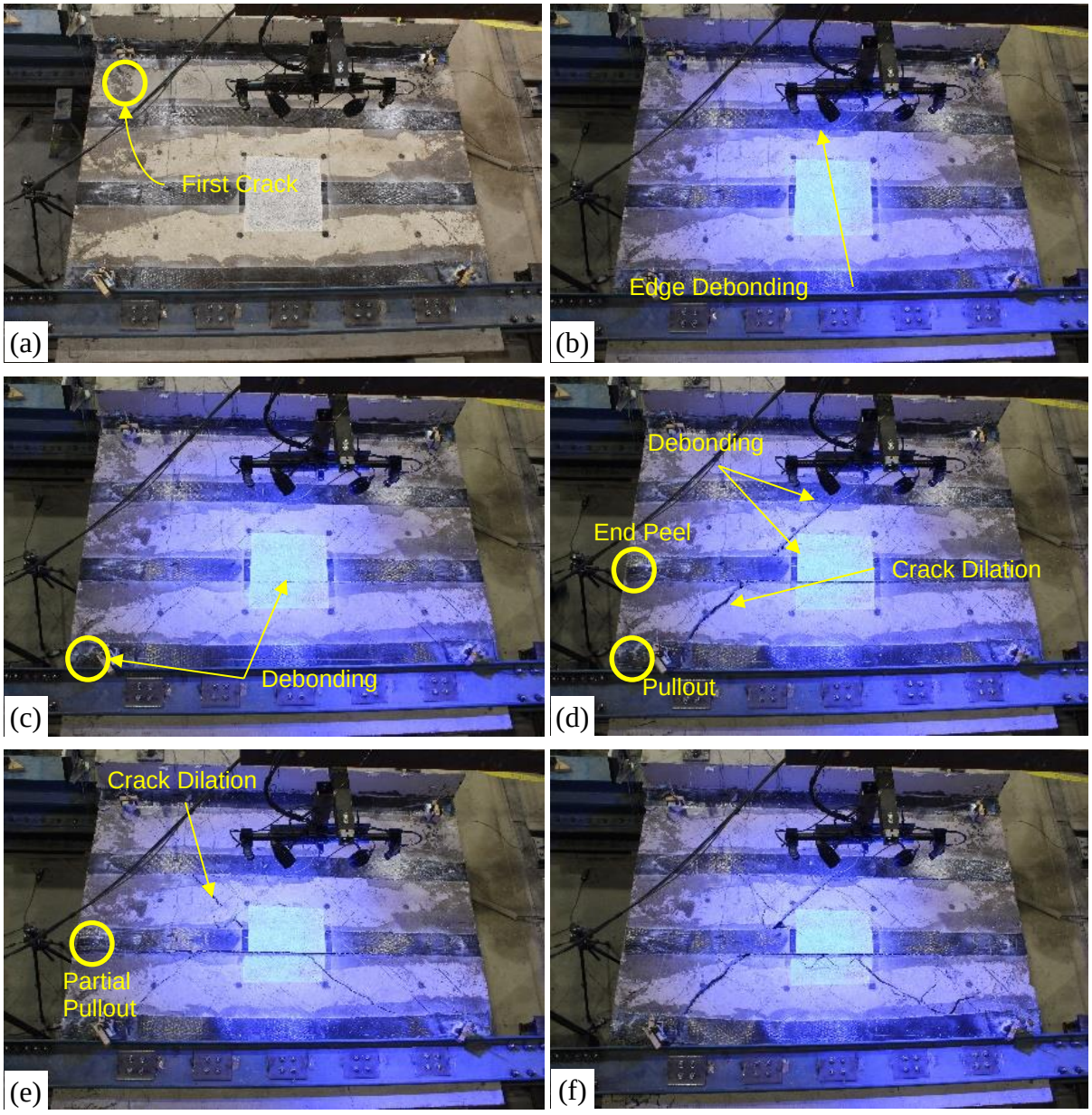

Figure 4.20. Failure Progression of Specimen CD5: (a) First Crack at 96 kips; (b) Central Edge Debonding of Sheet S2 at 217 kips; (c) Debonding of Sheets S3 and S4 at 240 kips; (d) Crack Dilation at 200 kips; (e) Mirrored Crack Dilation at -210 kips; (f) Final Condition of Failed Specimen at 44 kips.

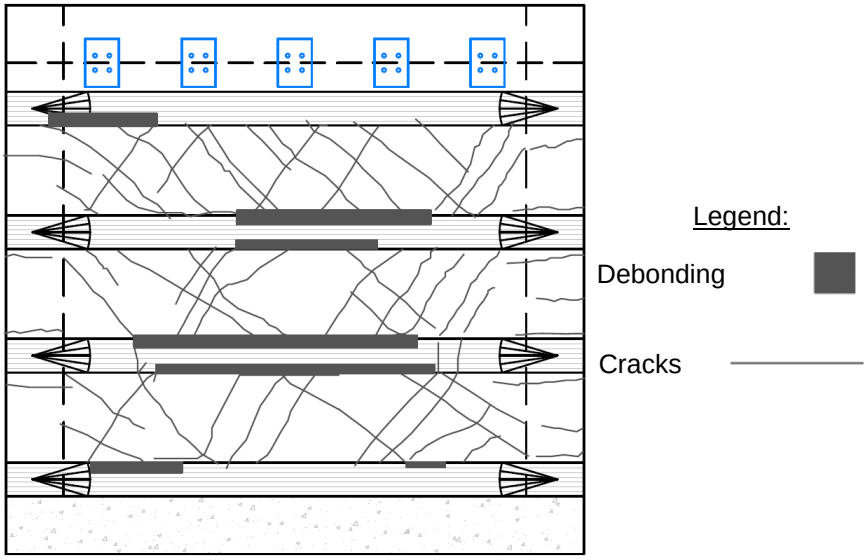

Figure 4.21. Extent of Damage of Specimen CD5 at Cycle 21 (1.111 in. Displacement).

4.7. Specimen CD6

Specimen CD6 was tested to observe the performance and failure mode of a reinforced concrete diaphragm strengthened with CFRP installed perpendicular to the direction of applied shear force. Other than FRP orientation, the retrofit scheme for CD6 was nominally the same as that of CD3. The specimen reached a peak load of 250 kips before failing due to intermediate crack induced FRP debonding and anchor pullout followed by diagonal tension shear and reinforcing steel rupture. At the peak load, the local shear angle was measured as 0.00271 radians while the global shear angle was measured as 0.00364 radians. The hysteric plots of applied load versus local and global shear angle are provided as Figure 4.22(a) and Figure 4.22(b) respectively. The points labeled A through F on each of these plots correspond to the photos in Figure 4.24(a) through Figure 4.24(f).

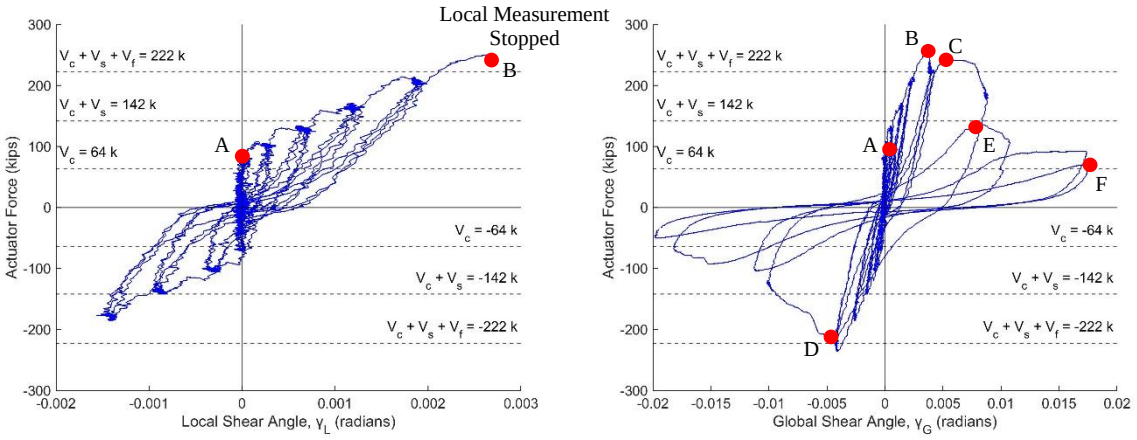

Figure 4.22. Hysteretic Shear Angle Response of Specimen CD6: (a) Local Shear Angle; (b) Global Shear Angle.

The strain measurements associated with FRP sheets S2 and S3 are provided in Figure 4.23(a) and Figure 4.23(b) respectively. Three strain gauges were installed on both FRP sheets. Figure 4.23(c) presents the location and label of each FRP sheet and strain gauge. Cracks in the diaphragm were observed to transverse the FRP sheets near the locations of gauges S2N, S2M, S3M, and S3S. The FRP strains measured at these locations when peak load occurred were 0.38%, 0.48%, 0.32%, and 0.46%, respectively. At peak load, the FRP strains measured with gauges S2S and S3N, which were not located near a crack, were 0.04% and 0.09%, respectively.

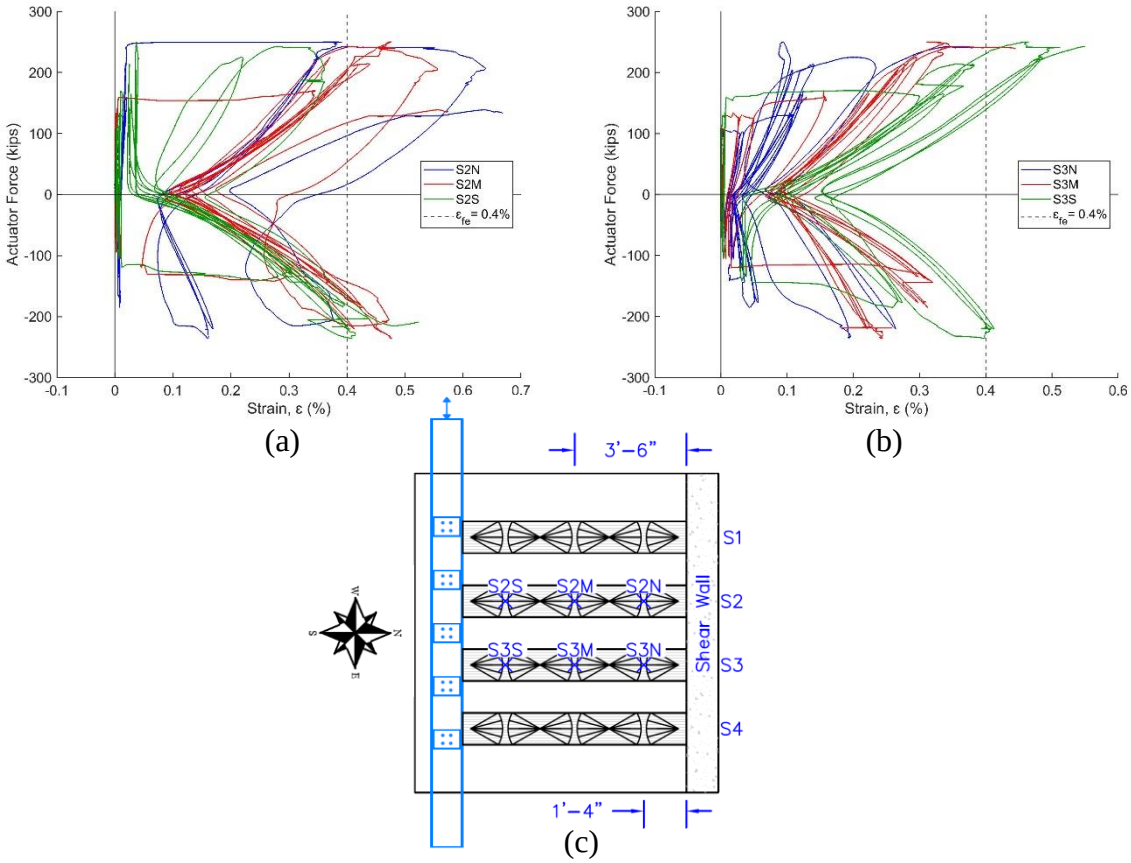

Figure 4.23. FRP Strain Response of Specimen CD6: (a) Strain Response of Sheet S2; (b) Strain Response of Sheet S3; (c) Strain Gauge Layout.

Cracks were marked and measured throughout the test, and maps were prepared to document each crack and associated width at cycles 11, 16, and 21. The first observation of cracking was made during the positive portion of cycle 11 corresponding to a load of 84 kips. Figure 4.24(a) shows the condition of the specimen at this point of testing. Only two cracks were visible with measured widths of 0.1 mm and 0.15 mm. Additional diagonal tension cracks, with average widths of 0.15 mm to 0.4 mm, were documented through cycle 16. The specimen reached its peak capacity of 250 kips during the positive portion of cycle 21, and its corresponding condition is shown in Figure 4.24(b). At the peak load, diagonal tension cracks continued to form and cause sheets S2 and S3 to experience centralized debonding along approximately 75% of their lengths. Localized areas of edge debonding were also documented on sheets S1 and S4. The average crack widths ranged from 0.2 mm to 2 mm during this cycle. Figure 4.25 depicts the extent of cracking and debonding at cycle 21 which corresponds to an applied displacement of 1.111 in. During the positive portion of cycle 23 (corresponding to a

load of 242 kips), sheet S2's South end anchor and adjacent intermediate anchor pulled out while the South end of sheet S1 and the North end of sheet S3 both experienced edge debonding. The specimen's primary diagonal tension crack also widened which allowed rebar to begin to elongate and rupture. Figure 4.24(c) shows the state of the specimen at this point of the test. Furthermore, during the negative portion of cycle 23 (corresponding to a load of -214 kips), the South end of sheet S4 and the North end of sheet S1 experienced edge debonding. Another diagonal tension crack also widened curing this cycle which is shown Figure 4.24(d). Sheet S3's North end anchor and adjacent intermediate anchor then pulled out during the positive portion of cycle 24 corresponding to a load of 138 kips. The condition of the specimen during this point of testing is shown in Figure 4.24(e). Diagonal tension shear then began to dominate the failure allowing more rebar to elongate and rupture. The final state of the failed specimen, corresponding to a load of 71 kips, is shown in Figure 4.24(f).

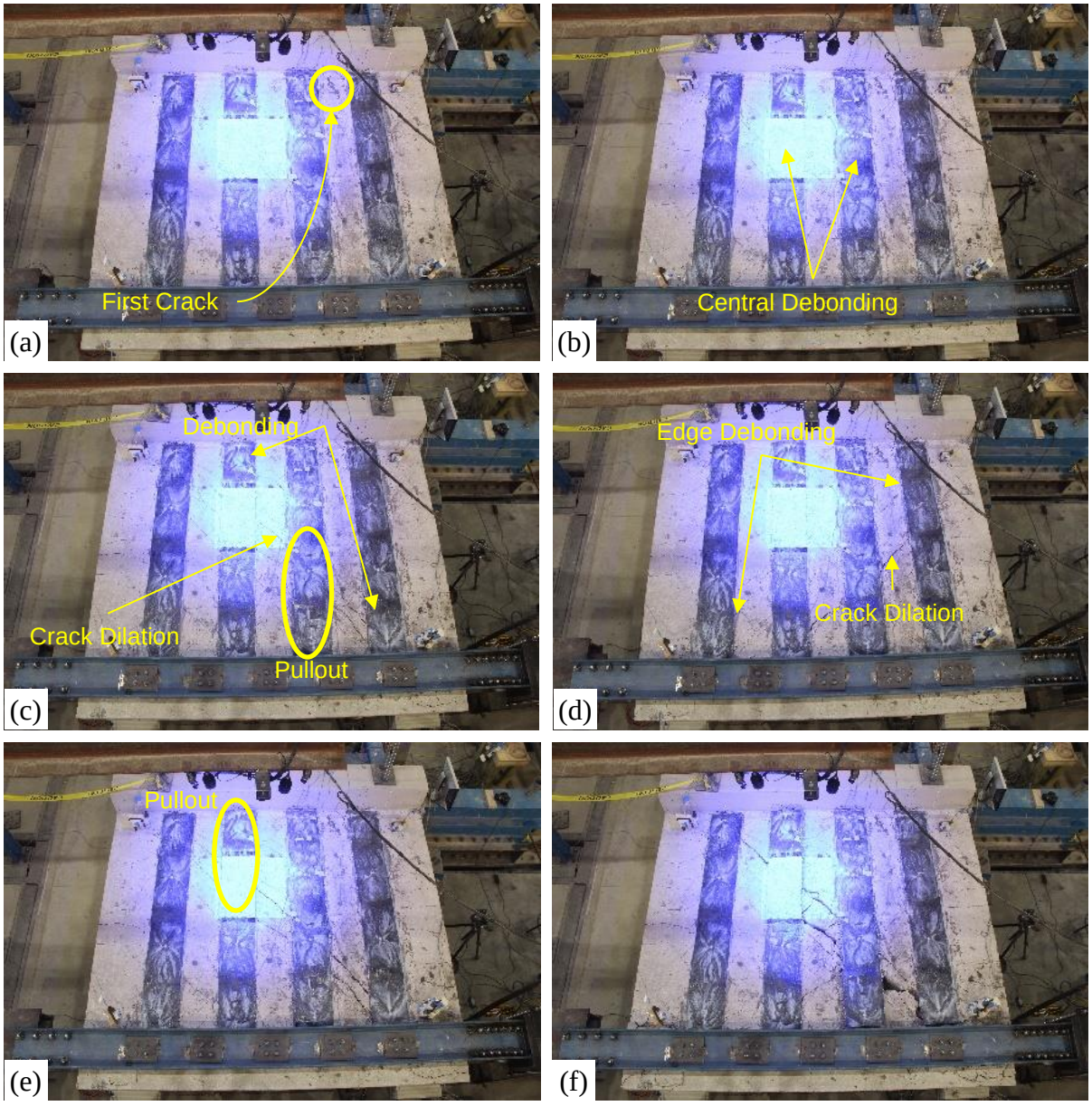

Figure 4.24. Failure Progression of Specimen CD6: (a) First Crack at 84 kips; (b) Debonding of Sheets S2 and S3 at 250 kips; (c) Crack Dilation at 242 kips; (d) Mirrored Crack Dilation at -214 kips; (e) Pullout of Sheet 3 Anchors at 138 kips; (f) Final Condition of Failed Specimen at 71 kips.

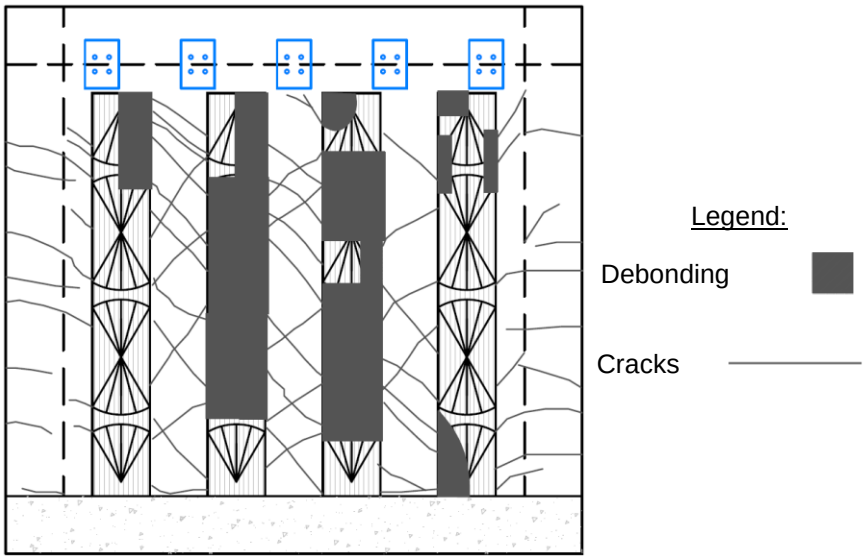

Figure 4.25. Extent of Damage of Specimen CD6 at Cycle 21 (1.111 in. Displacement).

Chapter 5. Analysis of Results

5.1. Overview

The experimental results obtained from diaphragm testing are utilized in this chapter to analyze strength, FRP strain, stiffness, ductility, and energy dissipation of each specimen.

5.2. Global Envelope Comparisons

Each global envelope curve provided in Figure 5.1 serves to simplify the hysteric global behavior of each specimen into a single curve. The envelope curves were not derived from local behavior because the local shear angle measurements were unable to capture post peak deformation.

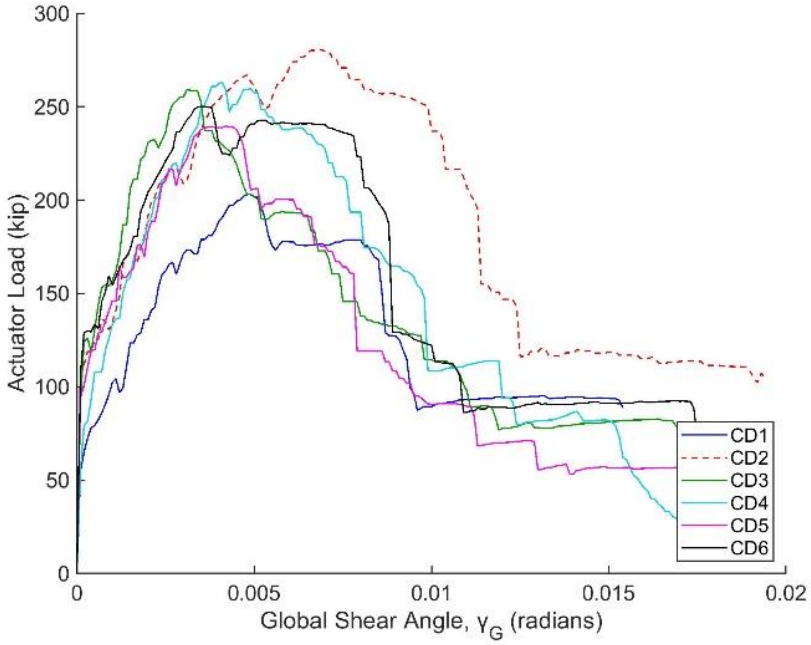

Figure 5.1. Global Envelope Curves.

Comparing the global envelope curves in Figure 5.1 shows that all specimens were initially very stiff. This implied that externally bonded FRP did not impact the behavior of a reinforced concrete diaphragm prior to cracking of concrete. Specimen CD1, the unretrofitted control, first cracked due to a load of 52 kips. The average load to cause cracking in the retro-fitted specimens was 96 kips which is an 85% relative increase in cracking strength compared

to Specimen CD1. After cracking, a drop in stiffness was experienced by all specimens. The post cracking stiffness of each retrofitted specimen appeared very similar likely because each retrofit incorporated four FRP sheets with an individual ply stiffness of approximately 4000 kips/in/in.

Specimen CD1 failed in diagonal tension shear and reached a peak load of 203 kips. The failure mode of each retrofitted specimen involved intermediate crack induced FRP debonding caused by diagonal tension cracking. End anchors typically served to resist complete debonding but eventually failed due to pullout or rupture. Specimen CD3 was unique because it experienced FRP sheet rupture likely due to the stress concentrations caused by the intermediate anchors. The peak load of each retrofitted specimen ranged from 240 kips (Specimen CD5) to 280 kips (Specimen CD6). On average, the retrofitted specimens reached a peak load of 258 kips which is a 27% relative increase compared to specimen CD1. This trend demonstrates that FRP strengthening can significantly increase the load capacity of reinforced concrete diaphragms. While the peak load capacity of the retrofitted specimens was similar, small differences could be attributed to variations in the concrete strength at the time of testing.

As will be discussed in the following section, a more detailed analysis was conducted to investigate the influence of varying retrofit parameters on strengthened diaphragm behavior.

5.3. Diaphragm Shear Strength

The overall strength of the cantilever diaphragm specimens was a result of the superposition of several behaviors. These included the shear strength provided by the concrete, reinforcing steel, and externally bonded FRP, along with the strength generated by the moment frame formed by the heavily reinforced chord and edge beams positioned around the perimeter of the specimens. Taking into account the relative proportion of these behaviors was crucial for determining the specific contribution of externally bonded FRP to the overall shear strength of the diaphragms. The following section describes an analysis to decompose the peak strength of the diaphragms into contributions of concrete and steel, externally bonded FRP, and the additional strength provided by frame action.

5.3.1 Contribution of Frame Action to Diaphragm Strength

The chords and edge beam were believed to interact and provide frame like action that increased the in-plane shear strength of each specimen. To account for the frame action, a frame stiffness was first calculated for each specimen using Eq. (16). This equation represents a simplified frame model consisting of two, fixed columns subjected to a lateral point load as shown in Figure 5.2(a). The simplified frame model assumes that the edge beam was effectively rigid which is consistent with the observed deformed configuration of each specimen up to peak load.

$$K_{Frame} = 2 \cdot \frac{12 E_c I_e}{h^3} \tag{16}$$

where: K_{Frame} is the frame stiffness (k/in.); E_c is the experimental modulus of elasticity of concrete (ksi); I_e is the effective moment of inertia of the chord beams (in.^{4}); and h is the length of one chord beam from the face of the shear wall to the free end of the specimen (102 in.).

The equation used to determine the effective moment of inertia, I_e, was adapted from Chapter 4 of ACI 435R (2020) and is provided as Eq. (17).

$$I_e = 0.7 I_g + 0.3 I_{cr} \tag{17}$$

where: I_e is the effective moment of inertia (in.^{4}); I_g is the gross moment of inertia of one 10 in. square chord beam (in.^{4}); and I_{cr} is the cracked moment of inertia of one 10 in. square chord beam calculated using a cracked, transformed sectional analysis (in.^{4}). Table 5.1 summarizes the moments of inertia used to calculate the frame action which vary due to the differences in the specimen's modulus of elasticity of concrete.

Using the calculated frame stiffness, an idealized linear elastic-perfectly plastic strength versus global shear angle relationship was generated for each specimen. The point of plasticity was calculated using Eq. (18). Figure 5.2(b) shows the frame action curve and experimental positive envelope curve of Specimen CD1. Similar analyses were performed for the other diaphragm specimens. A summary of the variables associated with the analysis of

each specimen's frame action and the frame contribution at the shear angle associated with peak load, V_{Frame}, is provided in Table 5.1.

$$V_p = 2 \cdot \frac{2M_n}{h} \tag{18}$$

where: V_p is the plastic shear capacity of the frame (kip); M_n is the moment capacity of one chord beam (in-k); and h is the length of one chord beam from the face of the shear wall to the free end of the specimen (102 in.). The moment capacity M_n of a chord beam was calculated based on a strain compatibility section analysis using Whitney stress block and three, two bar layers of linear-perfectly plastic, No. 8, Grade 60 rebar.

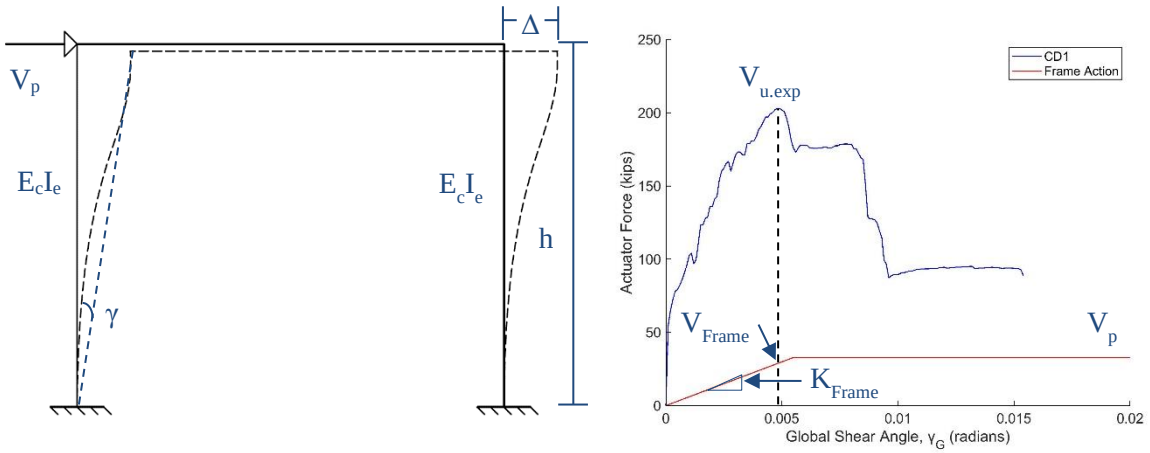

(a) (b)

Figure 5.2. Frame Action: (a) Frame Model; (b) Frame Action Versus Positive Envelope for Specimen CD1.

Table 5.1. Summary of Frame Action.

Specimen	**Cracked Moment of Inertia, I_{cr} (in.^{4})**	**Effective Moment of Inertia, I_e (in.^{4})**	**Frame Stiffness, K_{Frame} (k/in.)**	**Plastic Shear Capacity, V_p (kip)**	**Frame Contribution, V_{Frame} (kip)**	**Global Shear Angle at Peak Load (rad)**
CD1	489	730	58.6	33	30	0.00494
CD2	510	736	56.3	32	32	0.00691
CD3	531	743	54.2	31	18	0.00326
CD4	531	743	54.2	31	23	0.00409
CD5	492	731	58.3	31	25	0.00428
CD6	479	727	59.9	32	22	0.00364

The values of V_{Frame} are used in Eq. (19) to determine the nominal experimental shear strength of each specimen excluding strength attributed to frame action. Section 5.3.3 also uses V_{Frame} to determine the contribution of FRP to the diaphragm shear strength.

$$V_{n,exp} = V_{u,exp} - V_{Frame} \tag{19}$$

where: $V_{n,exp}$ is the nominal experimental shear strength excluding strength attributed to frame action (kip); $V_{u,exp}$ is the positive experimental shear strength (kip); and V_{Frame} is the shear strength from frame action (kip). These values are provided in Table 5.2 for each specimen.

Table 5.2. Summary of Nominal, Experimental Shear Strength.

Specimen	**Experimental Shear Strength, $V_{u,exp}$ (kip)**	**Frame Contribution, V_{Frame} (kip)**	**Nominal Experimental Shear Strength, $V_{n,exp}$ (kip)**
CD1	203	30	173
CD2	280	32	248
CD3	259	18	241
CD4	263	23	240
CD5	240	25	215
CD6	250	22	228

5.3.2 Contribution of Concrete and Steel to Diaphragm Strength

Due to the conservative nature of the shear strength provisions in ACI 318 (2019), the Modified Compression Field Theory (MCFT) was used to calculate the contribution of concrete and reinforcing steel to the shear strength of each diaphragm specimen. Software program Response-2000 version 1.9.6 (Bentz 2001) was used to facilitate the MCFT calculations (Bentz et al. 2006). The following provides a description of the input parameters used in the Response-2000 analysis. It should be noted that all input parameters except the concrete compressive strength remained the same for the analysis of each specimen.

The concrete material properties were defined by entering the respective 6 in. × 12 in. compressive strengths from Table 3.3. The remaining concrete properties were held constant using: a default tension strength of 300 psi; a default peak strain of 0.197%; an aggregate size of 0.39 in.; and a default tension stiffing factor of 1.0. Furthermore, the default concrete base curve, compression softening, and tension stiffening models were left as

"Popovics/Thorenfeldt/Collins", "Collins-Bentz 2011", and "Bentz 1999" respectively. Separate steel material properties were defined for each the diaphragm and chord reinforcement. The diaphragm reinforcement stress-strain properties, shown in Figure 3.16, were defined by entering an elastic modulus of 29008 ksi, a yield strength of 88.3 ksi, a strain at hardening of 0.3%, a strain at peak of 3%, and an ultimate strength of 93.6 ksi. The chord beam reinforcement material properties were defined by entering an elastic modulus of 29008 ksi, a yield strength of 68 ksi, a strain at hardening of 0.7%, a strain at peak of 10%, and an ultimate strength of 75 ksi.

The diaphragm cross sectional dimensions were entered using the user defined concrete cross section option. A screenshot from Response-2000 showing details of the cross section and material properties is provided in Figure 5.3. Each chord beam was assigned six, No. 8 longitudinal bars. Furthermore, ten distributed layers of two, No. 2 longitudinal bars and two layers of No. 2 single-leg transverse bars distributed at a spacing of 12 in. were assigned to represent the diaphragm reinforcement. Additionally, the full member properties were input by entering an overall length of 102 in., selecting a fixed end type of right support, selecting a constant shear analysis, applying a live load of 8.5 kip-ft at 102 in., and maintaining all other default settings.

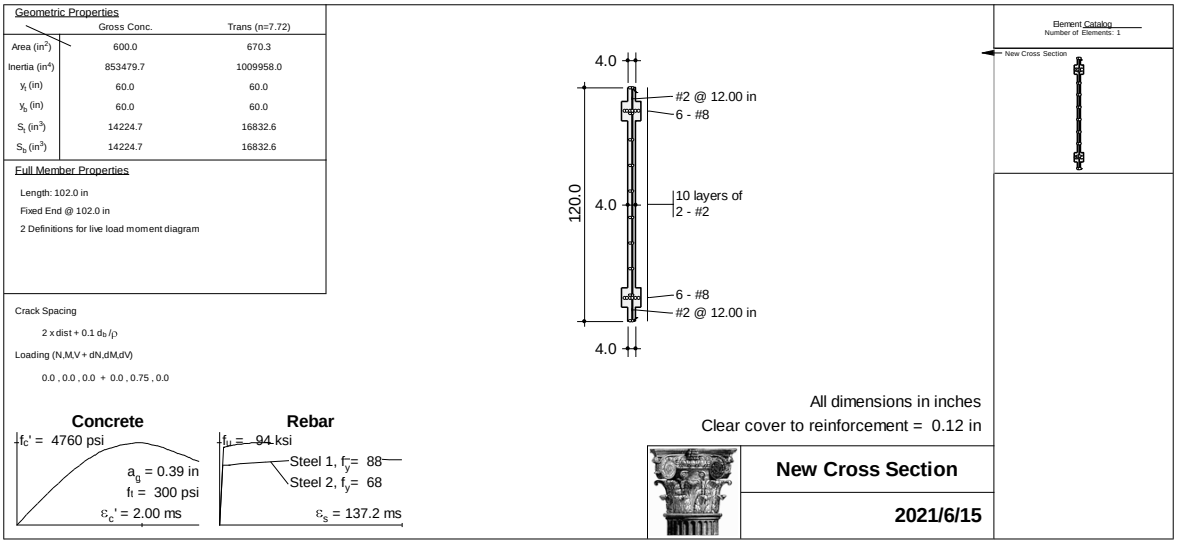

Figure 5.3. Response-2000 Input

The member shear response was computed for each specimen, and the shear strength from concrete and steel was recorded. Figure 5.4 provides an example of the results from a

member analysis generated by Response-2000. The shear strength provided by concrete and reinforcing steel predicted by Response-2000, V_{R2K}, is summarized in Table 5.3 for each of the six diaphragm specimens. The value of V_{R2K} for each specimen was similar (approximately 170 kips) with minor variations due concrete compressive strength differences. The calculated shear strength provided by concrete and reinforcing steel using ACI 318-19 is approximately 144 kips, which is 18% lower than the capacity predicted by MCFT. This significant difference further emphasizes the importance of employing enhanced tools to precisely capture the shear strength of diaphragms. Values of V_{R2K} are used in Section 5.3.3 to determine the contribution of FRP to the diaphragm shear strength.

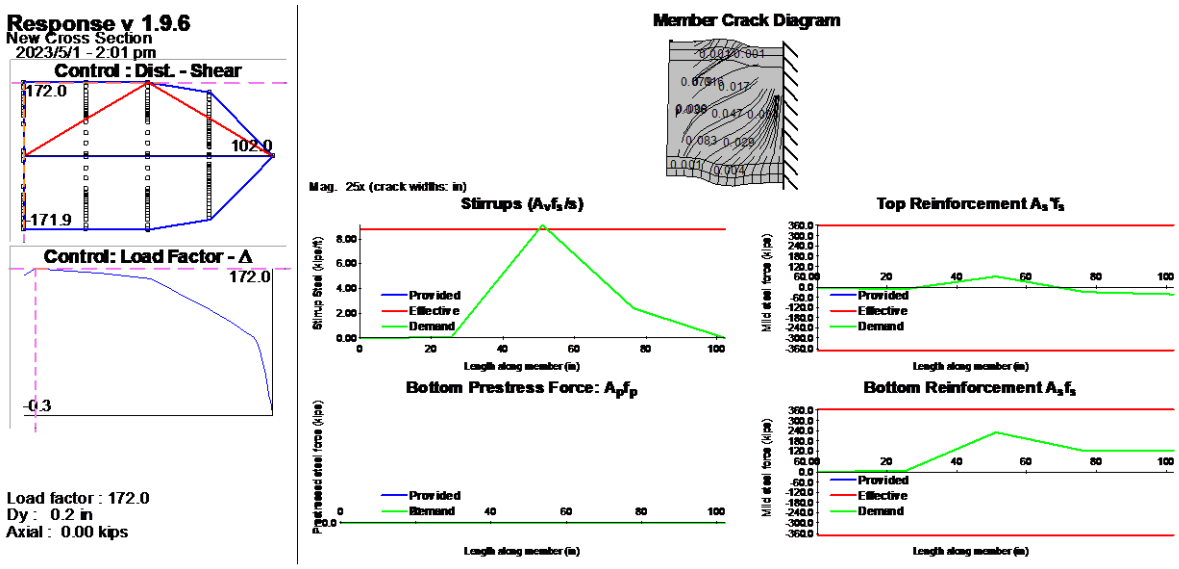

Figure 5.4. Response-2000 Member Output

Table 5.3. Shear Capacities from Response-2000

Specimen	Response-2000 Shear Strength, V_{R2K} (kip)
CD1	172
CD2	171
CD3	162
CD4	162
CD5	166
CD6	170

5.3.3 Contribution of FRP to Diaphragm Shear Strength

The shear strength provided by FRP, $V_{f,exp}$, was computed using Eq. (20). It was determined by subtracting the frame action produced by perimeter beams, V_{Frame} , and the shear strength provided by concrete and reinforcing steel, V_{R2K}, from the peak experimental diaphragm strength, $V_{u,exp}$. The calculation assumed a superposition of behaviors, implying that the peak strengths of all strength components were achieved simultaneously.

$$V_{f,exp} = V_{u,exp} - V_{Frame} - V_{R2K} \tag{20}$$

Table 5.4. Experimental Strength Provided by FRP

Specimen	Experimental Shear Strength, $V_{u,exp}$ (kip)	Frame Contribution, V_{Frame} (kip)	Response-2000 Shear Strength, V_{R2K} (kip)	FRP Shear Strength, $V_{f,exp}$ (kip)
CD1	203	30	172	1
CD2	280	32	171	77
CD3	259	18	162	79
CD4	263	23	162	78
CD5	240	25	166	48
CD6	250	22	170	58

The theoretical shear strength provided by FRP for Specimen CD1 should be 0 kips since this was an unretrofitted specimen. This result was confirmed as Eq. (20) predicted a $V_{f,exp}$ value of 1 kip which validates the calculation process. In terms of strength provided by FRP, the retrofits corresponding to Specimens CD2, CD3, and CD4 were the most effective and similar because the FRP was installed parallel to the direction of loading and was adequately spaced and anchored. Retrofitted Specimens CD5 and CD6 produced the lowest values of $V_{f,exp}$ and were the least effective because of CD5's wide spacing of FRP sheets and CD6's perpendicular sheet orientation. The results of this analysis are used in Section 5.4 to estimate an FRP debonding strain for each specimen.

5.3.4 FRP Reinforcement Limits

The total shear strength provided by reinforcement is taken as the sum of the contribution of the FRP shear reinforcement and the steel shear reinforcement (ACI 2017). As described in Eq. (11), the sum of the shear strengths provided by the reinforcement and concrete

is limited to $8\sqrt{f_c'}\,b_w d$ by ACI PRC-440.2R (2017) to prevent diagonal crushing failures in concrete members. The ultimate strengths of the six diaphragms were normalized to explore how close the diaphragm specimens were to the reinforcement limit $8\sqrt{f_c'}\,b_w d$. First, frame action was deducted from each specimen's global envelope curve. After deducting the assumed frame action described in Section 5.3.1, the resulting force data was divided by $A_{cv}\sqrt{f_c'}$. The gross diaphragm area, A_{cv}, was taken as 480 in^2 and the concrete compressive strength, f_c' (psi), corresponded to the respective 6 in. × 12 in. compressive strength data from Table 3.3. The global normalized envelope curves are provided in Figure 5.5 which also shows the reinforcement limit of $8\sqrt{f_c'}\,b_w d$. The ultimate normalized strength of Specimen CD1 was 5.26 while the retrofitted specimen's ultimate normalized strength ranged from 7.14 to 8.32. The retrofitted specimen's normalized strengths were approximately 1.47 times greater than the unretrofitted control and did not appear to be significantly affected by retrofit configuration. It should be noted that Specimens CD3 and CD4 narrowly exceeded the reinforcement limit and did not experience concrete crushing. The ultimate normalized strength calculated for each specimen is summarized in Table 5.5.

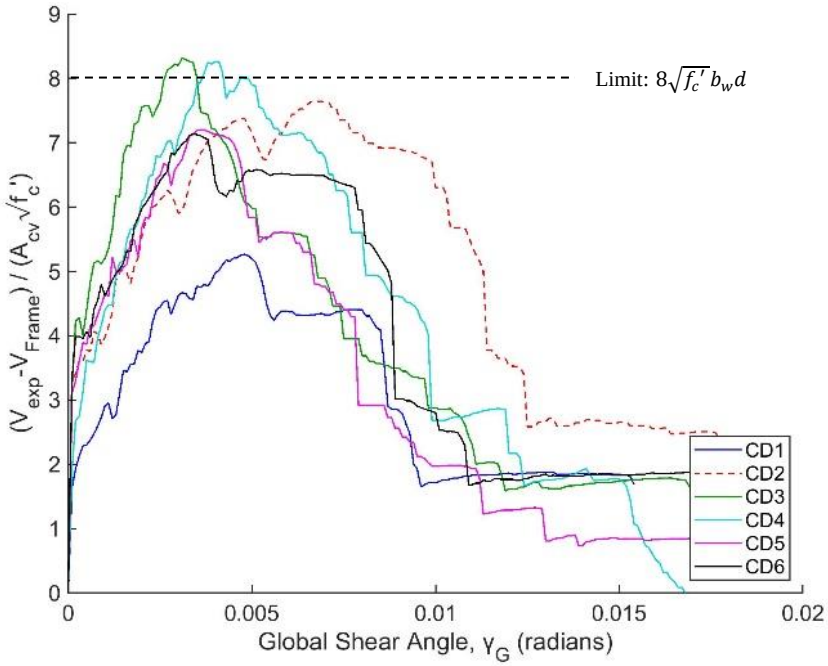

Figure 5.5. Normalized Envelope Curves Excluding Frame Action

Table 5.5. Summary of Ultimate Normalized Strengths

Specimen	Ultimate Normalized Strength, $(V_{u,exp} - V_{Frame})/\left(A_{cv}\sqrt{f_c'}\right)$
CD1	5.26
CD2	7.64
CD3	8.32
CD4	8.26
CD5	7.20
CD6	7.14

5.4. FRP Debonding Strain

A key outcome of this study was to evaluate the applicability of Eq. (6) to reinforced concrete diaphragms by analyzing and comparing the recorded FRP debonding strains with the design strains calculated with the equation. However, the available experimental FRP strain data was constrained due to limitations of the strain gauge's placement and proximity to cracks in the concrete. The FRP strain gauges could only capture the peak strain in the FRP sheet if a crack directly intersected the sheet at the gauge's location. As a result, the strain data may not fully represent the overall behavior of the FRP sheet in areas without crack engagement. To overcome this limitation, the estimated FRP debonding strain, $\varepsilon_{f,exp}$, was derived from the FRP shear contribution, $V_{f,exp}$. Rationale to report the measured experimental FRP debonding strain, $\varepsilon_{f,SG}$, was created, and design strains, $\kappa_v \varepsilon_{fu}$, were calculated with Eq. (6). Finally, the design strains and estimated strains were compared to the measured experimental strains.

5.4.1 Estimated Debonding Strain

Equation (4) was reformulated into Eq. (21) to estimate the FRP debonding strain from the experimental shear strength provided by FRP.

$$\varepsilon_{f,exp} = \frac{V_{f,exp} s_f}{A_{fv} E_f (sin + cos\alpha) d_{fv}} \tag{21}$$

where: $\varepsilon_{f,exp}$ is the estimated FRP debonding strain (in./in.); $V_{f,exp}$ is the experimental shear strength provided by FRP (kips); s_f is the center-to-center spacing of FRP strips (in.), A_{fv} is the area of one FRP strip (in.^{2}); E_f is the tensile modulus of FRP (ksi); α is the angle of

application of primary FRP reinforcement relative to the longitudinal axis of the member (deg); and d_{fv} is the effective depth of FRP (in.).

The effective depth, d_{fv}, used in Eq. (21) for CD2, CD3, CD4, and CD5 was 96 in. which corresponds to the center-to-center distance of the chord beams. This distance was selected because diagonal tension cracking was typically not observed to extend past the centerline of the chord beams. However, the FRP on CD6 was oriented perpendicular to the direction of applied shear load and did not extend past the chord beams. Therefore, an effective depth of 84 in. corresponding to the edge-to-edge distance of exterior sheets was selected for CD6. A summary of the results and variables associated with Eq. (21) are provided in Table 5.6. These strains will be further discussed and compared in Section 5.4.3.

Table 5.6. Estimated FRP Debonding Strain Analysis

Specimen	**Experimental FRP Shear Strength, $V_{f,exp}$ (kip)**	**Area of FRP Sheet, A_{fv} (in.^{2})**	**Spacing of FRP, s_f (in.)**	**Effective Depth, d_{fv} (in.)**	**Orientation, α (deg)**	**FRP Modulus of Elasticity, E_f (ksi)**	**Estimated FRP Debonding Strain, $\varepsilon_{f,exp}$ (%)**
CD1	1	-	-	-	-	-	-
CD2	80	0.24	24	96	0	16700	0.48
CD3	79	0.29	23.2	96	0	13900	0.47
CD4	78	1.05	21	96	0	3730	0.44
CD5	48	0.28	25.7	96	0	14240	0.32
CD6	58	0.24	24	84	90	16700	0.42

5.4.2 Experimental FRP Debonding Strain

The experimental FRP strains represented strain at the locations of the strain gauges and did not necessarily capture the maximum strains anywhere in the FRP sheets. Regardless, the largest FRP strain recorded from any of the strain gauges when the specimen reached its peak capacity may provide useful information about the possible contribution of FRP to shear strength. Due to the strain gauge limitations, the experimental FRP debonding strain, $\varepsilon_{f,SG}$, was assumed to be the maximum recorded strain at the time of peak load, ε_{SGmax}, for Specimens CD2 through CD5. The FRP retrofit of Specimen CD6 was thought to strengthen the specimen in both shear and flexure due to its 90-degree orientation to the applied load.

Consequently, the experimental strain data recorded for Specimen CD6 was assumed to include components contributing to shear and flexure that required decoupling.

To decouple the flexural component from the experimental data for CD6, program Response-2000 was utilized once again. The model previously discussed in Section 5.3.2 was further refined by including rebar with linear elastic material properties to represent each externally bonded FRP sheet. The FRP material model was defined by entering an elastic modulus of 16705 ksi, a yield strength of 182.6 ksi, a strain at hardening of 1.09%, a strain at peak of 1.3%, and an ultimate strength of 216 ksi. This material model was assigned to longitudinal bars located at the centerline of each FRP sheet. These longitudinal bars were assigned an area of 0.24 in^2 which corresponds to the cross-sectional area of each FRP applied to CD6. A sectional response was then generated to obtain the longitudinal strain of the two interior FRP bars at section cut A-A shown in Figure 5.6. Section A-A is located 86 in. from the cantilever end and corresponds to the location where strain gauges S2N and S3N were installed. To determine the peak moment at section A-A, the experimental capacity of 250 kips was multiplied by 86 in. which equates to 21500 kip-in or 1792 kip-ft. A strain profile for this exact moment was not computed by Response-2000; therefore, linear interpolation was utilized with the data corresponding to moments of 1638.5 kip-ft and 1794.3 kip-ft. The resulting strain profile which includes the longitudinal strain at the centerline of sheets S2 and S3 is shown in Figure 5.6.

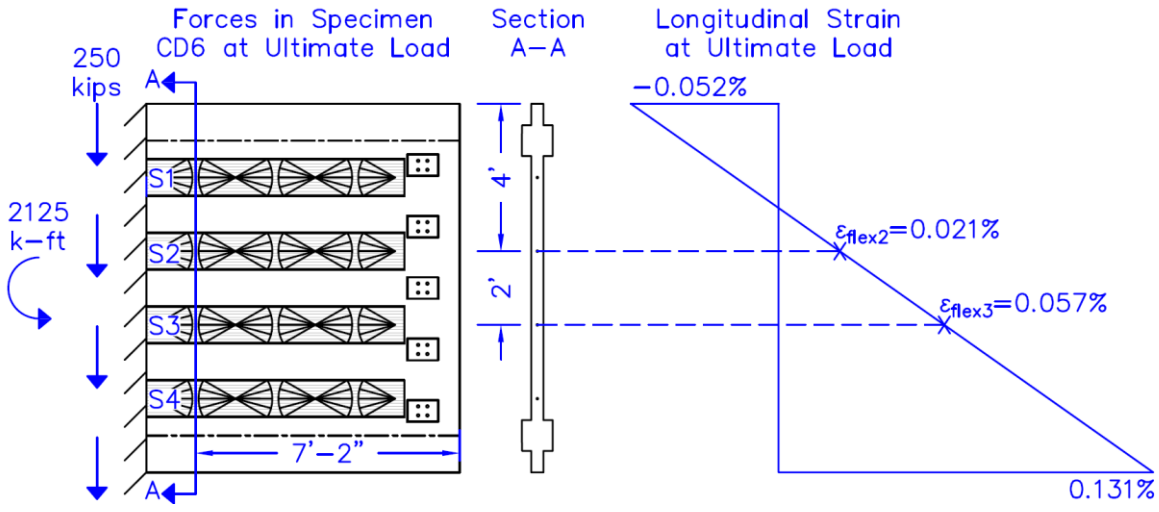

Figure 5.6. Flexural Strain Analysis for CD6

From the longitudinal strain analysis, the flexural component of the experimental FRP strain, ε_{flex}, was assumed to be 0.06%. This flexural component was then subtracted from the maximum recorded strain at peak load, ε_{SGmax}, to obtain the experimental FRP debonding strain, $\varepsilon_{f,SG}$. The strain values described in this section are summarized in Table 5.7 and will be further discussed and compared in Section 5.4.3.

Table 5.7. Experimental FRP Debonding Strain Analysis

Specimen	Max Experimental Strain at Peak Load, ε_{SGmax} (%)	Flexural Strain, ε_{flex} (%)	Experimental FRP Debonding Strain, $\varepsilon_{f,SG}$ (%)
CD2	0.37	-	0.37
CD3	0.45	-	0.45
CD4	0.47	-	0.47
CD5	0.36	-	0.36
CD6	0.48	0.06	0.42

5.4.3 Design Debonding Strain Limit from ACI PRC-440.2R

An FRP debonding design strain was calculated for each retrofitted specimen using the methodology presented in ACI PRC-440 (2017). The resulting calculations utilizing Equations (6) through (10) are summarized in Table 5.8.

Table 5.8. Debonding Design Strain Calculations.

Specimen	Active Bond Length, L_e (in.)	Concrete Modification Factor, k_1	Retrofit Modification Factor, k_2	FRP Rupture Strain, ε_{fu} (%)	Bond Coefficient for Shear, κ_v	Design Strain, $\kappa_v\varepsilon_{fu}$ (%)
CD2	1.56	1.09	0.97	1.3	0.27	0.35
CD3	1.74	0.94	0.96	1	0.34	0.34
CD4	2.19	0.94	0.95	1.8	0.23	0.42
CD5	1.15	0.99	0.98	1.27	0.19	0.24
CD6	1.56	1.08	0.96	1.3	0.27	0.35

Table 5.9 summarizes the calculated design strains and debonding strain values from Sections 5.4.1 and 5.4.2. The experimental FRP debonding strain values, $\varepsilon_{f,SG}$, were reasonably similar to the estimated FRP debonding strain values, $\varepsilon_{f,exp}$. This comparison instilled confidence in the experimental FRP debonding strain values, $\varepsilon_{f,SG}$, which were initially doubted due to the limitations of capturing FRP strain in areas without crack engagement. Therefore, the experimental FRP

debonding strains were assumed to be the known values. Figure 5.7 compares the relative accuracy of the design strains, $\kappa_v \varepsilon_{fu}$, and estimated debonding strains, $\varepsilon_{f,exp}$, to the experimental debonding strains, $\varepsilon_{f,SG}$. In general, both sets of strains reasonably matched the experimental debonding strains. The estimated debonding strain, $\varepsilon_{f,exp}$, of Specimen CD2 is an outlier likely due to an absence of principle cracks near the working strain gauges at the time of peak load. The outlying design strain, $\kappa_v \varepsilon_{fu}$, corresponding to Specimen CD5 indicated that the design calculations are most conservative when using denser FRP fabric. Each calculated design strain value was less than the corresponding experimental debonding strain and the estimated debonding strain. The average ratio of $\kappa_v \varepsilon_{fu}/\varepsilon_{f,SG}$ was noted to be 0.82 with a coefficient of variation (COV) of 0.14. While this implied Eq. (6) is conservative for design purposes, other limit states such as the need to limit crack widths, maintain aggregate interlock, and limit steel yielding may need to be taken into consideration.

Table 5.9. Summary of FRP Strain Analysis

Specimen	**Estimated FRP Debonding Strain, $\varepsilon_{f,exp}$ (%)**	**Experimental FRP Debonding Strain, $\varepsilon_{f,SG}$ (%)**	**Design Strain, $\kappa_v \varepsilon_{fu}$ (%)**	$\kappa_v \varepsilon_{fu}/\varepsilon_{f,SG}$ (%/%)
CD2	0.48	0.37	0.35	0.95
CD3	0.47	0.45	0.34	0.75
CD4	0.44	0.47	0.42	0.90
CD5	0.32	0.36	0.24	0.66
CD6	0.42	0.42	0.35	0.83
			Average	0.82
			COV	0.14

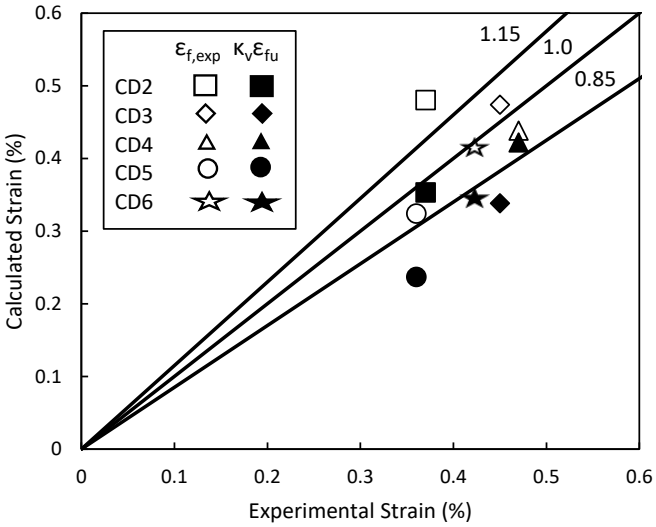

Figure 5.7. Accuracy Comparison of Calculated FRP Strains.

5.5. Diaphragm Stiffness

As can be seen in Figure 5.1, the stiffness of each specimen was initially very high, reflecting high shear rigidity of concrete prior to cracking. However, as cracking occurred, the stiffness of the specimens decreased, with the steel reinforcement and FRP becoming actively engaged and playing a significant role in contributing to the overall stiffness. Consequently, it may not be appropriate to characterize the stiffness of each specimen with just one value. First the initial global stiffness values of the uncracked diaphragm were predicted using mechanics-based equations. Measured global stiffness values were then quantified using the experimental data to determine the effects of FRP strengthening on global stiffness behavior. While diaphragm deformation in Chapter 4 was expressed in terms of rotation in radians, for the sake of convenience, stiffness is being defined here in units of kips per inch (k/in.). To obtain stiffness in units of kips per radian (k/rad), one can multiply the reported stiffness value by the lever arm of the applied load of 90 in. The predicted initial stiffness values were then compared to the experimental stiffness values to determine a modifier for predicting the stiffness of the cracked diaphragm.

5.5.1 Initial Global Stiffness of the Uncracked Diaphragm

Before cracking occurred, the externally bonded FRP and reinforcing steel were assumed to have minimal influence on stiffness. Therefore, the initial global stiffness of the

uncracked diaphragm was predicted considering only the concrete contribution. The process to predict the initial global stiffness of concrete-filled steel deck diaphragms outlined by Avellaneda-Ramirez et al. (2022) was adopted in this study. The total deflection at the free end of the cantilever diaphragm specimens was assumed to consist of bending and shear deformations and was calculated with Eq. (22).

$$\Delta_{tot} = \Delta_b + \Delta_s \tag{22}$$

where: Δ_{tot} is the total deflection of the reinforced concrete diaphragm (in.); Δ_b is the deflection due to bending (in.); and Δ_s is the deflection due to shear (in.).

The bending deflection at the free end of the cantilever diaphragm specimens was calculated with Eq. (23). This equation assumes that the gross concrete section, including the diaphragm and chord beams, resisted bending deformations.

$$\Delta_b = \frac{Va^3}{3E_cI_c} \tag{23}$$

where: Δ_b is the bending deflection of the reinforced concrete diaphragm (in.); V is the applied load (kips); a is the distance from the shear wall face to the centerline of loading (90 in.); E_c is the modulus elasticity of concrete (ksi); and I_c is the gross moment of inertia of the slab and chord beams (in.^{4}). The modulus of elasticity of concrete used in these calculations was obtained from experimental data reported in Table 3.3.

The shear deflection at the free end of the cantilever diaphragm was calculated with Eq. (24). This equation assumes only the 4 in. thick concrete diaphragm field resisted shear.

$$\Delta_s = \frac{Va}{G_cbt_c} \tag{24}$$

where: Δ_s is the shear deflection of the reinforced concrete diaphragm (in.); V is the applied load (kips); a is the distance from the shear wall face to the centerline of loading (90 in.); b is the depth of the diaphragm (120 in.); G_c is the concrete shear modulus (ksi); and t_c is the thickness of the diaphragm field (in.).

The concrete shear modulus was calculated with Eq. (25), and the Poisson's ratio for concrete was assumed as 0.2.

$$G_c = \frac{E_c}{2(1+\nu_c)} \tag{25}$$

where: G_c is the concrete shear modulus (ksi); E_c is the concrete modulus of elasticity (ksi); and ν_c is the assumed Poisson's ratio for concrete.

Finally, the predicted initial stiffness of each uncracked specimen due to a unit load of 100 kips was calculated with Eq. (26). A summary of the predicted initial stiffness calculations is provided in Table 5.10.

$$K_{PI} = \frac{V_{100}}{\Delta_{tot100}} \tag{26}$$

where: K_{PI} is the predicted initial stiffness (k/in.); V_{100} is a unit load of 100 kips; and Δ_{tot100} is the predicted total deflection due to a 100 kip unit load calculated using Eq. (22).

Table 5.10. Predicted Initial Stiffness Results

Specimen	**Unit Load, V_{100} (kip)**	**Concrete Modulus of Elasticity, E_c (ksi)**	**Concrete Shear Modulus, G_c (ksi)**	**Shear Stiffness, $G_c t_c$ (k/in.)**	**Shear Deflection, Δ_s (in.)**	**Bending Deflection, Δ_b (in.)**	**Total Deflection, Δ_{tot100} (in.)**	**Stiffness, K_{PI} (k/in.)**
CD1	100	3550	1479	5917	0.0127	0.0080	0.0207	4832
CD2	100	3380	1408	5633	0.0133	0.0084	0.0217	4600
CD3	100	3230	1346	5383	0.0139	0.0088	0.0227	4396
CD4	100	3230	1346	5383	0.0139	0.0088	0.0227	4396
CD5	100	3530	1471	5883	0.0127	0.0081	0.0208	4805
CD6	100	3640	1517	6067	0.0124	0.0078	0.0202	4954

The experimental initial stiffness, K_{EI}, was intended to be determined from the local shear angle data; however, this method proved unreliable. Prior to cracking, the local shear angle data was within the noise level of the sensors used. Consequently, the local shear angle cycles prior to cracking appeared vertical which implied infinite stiffness as shown in Figure 5.8.

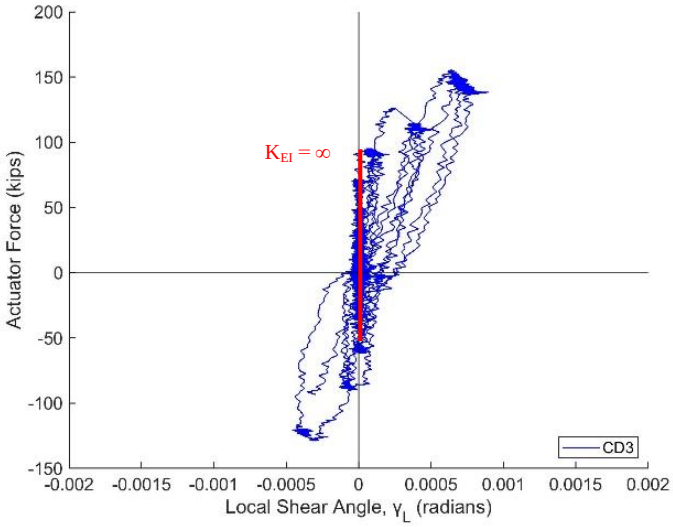

Figure 5.8. Undefined Experimental Initial Stiffness

5.5.2 Global Secant Stiffness

Two secant stiffnesses, K_{SPeak} and $K_{S75\%}$, were determined using the envelope curves of each specimen's global shear angle response. Stiffness K_{SPeak} corresponds to the slope of a secant line intersecting the peak experimental capacity on the envelope curve and is used to study how the FRP shear strength contribution affects stiffness. Additionally, stiffness $K_{S75\%}$ corresponds to the slope of a secant line intersecting the approximate factored experimental capacity on the envelope curve. The factored experimental capacity was assumed to be 75% of the peak experimental load which is consistent with the reduction factor ($\phi = 0.75$) applied to the shear strength of reinforced concrete diaphragms. The secant line of $K_{S75\%}$ was adopted from work done by Priestly and Park (1987) to quantify the ductility of concrete bridge columns under seismic loading and is later used in Section 5.6 to quantify each diaphragm's ductility. A visual example of both secant stiffnesses for Specimen CD1 is provided in Figure 5.9. Furthermore, the experimental stiffness values for each specimen are summarized and compared to the predicted stiffness values in Table 5.11. Each experimental stiffness value was converted from units of kip per radian to kip per inch by dividing by the lever arm of the applied load of 90 in. Values for Specimen CD2 are excluded due to the uncertainty of the global shear angle correction.

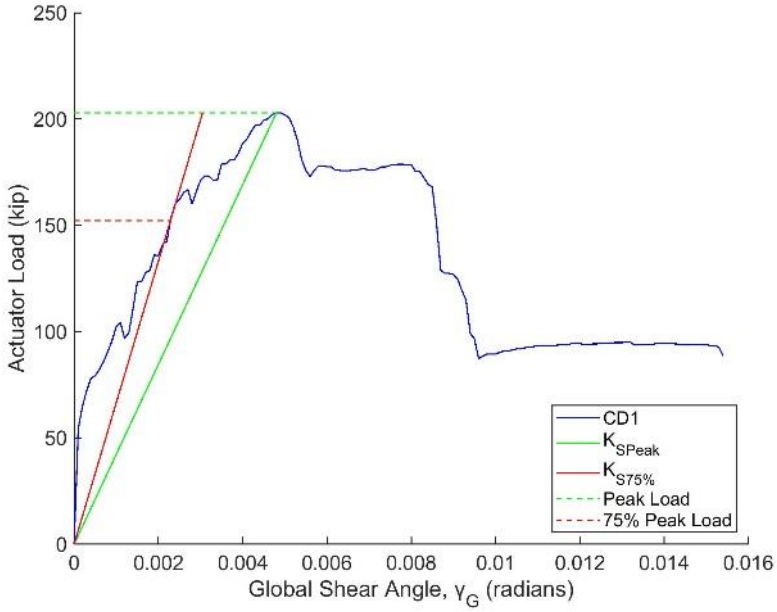

Figure 5.9. Experimental Secant Stiffness

Table 5.11. Summary of Experimental Stiffness Results

Specimen	**Peak Load (kip)**	**Global Shear Angle at Peak Load (rad)**	**Stiff-ness, K_{SPeak} (k/in.)**	K_{SPeak}/K_{PI}	**75% Peak Load (kip)**	**Global Shear Angle at 75% Peak Load (rad)**	**Stiff-ness, $K_{S75\%}$ (k/in.)**	$K_{S75\%}/K_{PI}$
CD1	203	0.00494	457	0.09	152	0.00229	739	0.15
CD3	259	0.00326	883	0.20	194	0.00144	1499	0.34
CD4	263	0.00409	714	0.16	197	0.00217	1010	0.23
CD5	240	0.00428	623	0.13	180	0.00198	1010	0.21
CD6	250	0.00364	763	0.15	188	0.00175	1190	0.24
Average	-	-	-	0.15	-	-	-	0.23

Figure 5.10 shows a trendline which demonstrates as the shear strength provided by FRP increased, the diaphragm's secant stiffness K_{SPeak} increased. The secant stiffness K_{SPeak} of the retrofitted specimens (excluding CD2) increased by an average of 63% in comparison to Specimen CD1. The perpendicular retrofit of Specimen CD6 increased the stiffness of the diaphragm similarly as the parallel retrofits did in comparison to the unretrofitted specimen. The largest secant stiffness value corresponds to Specimen CD3 which is likely due to the intermediate anchors that were incorporated into the retrofit.

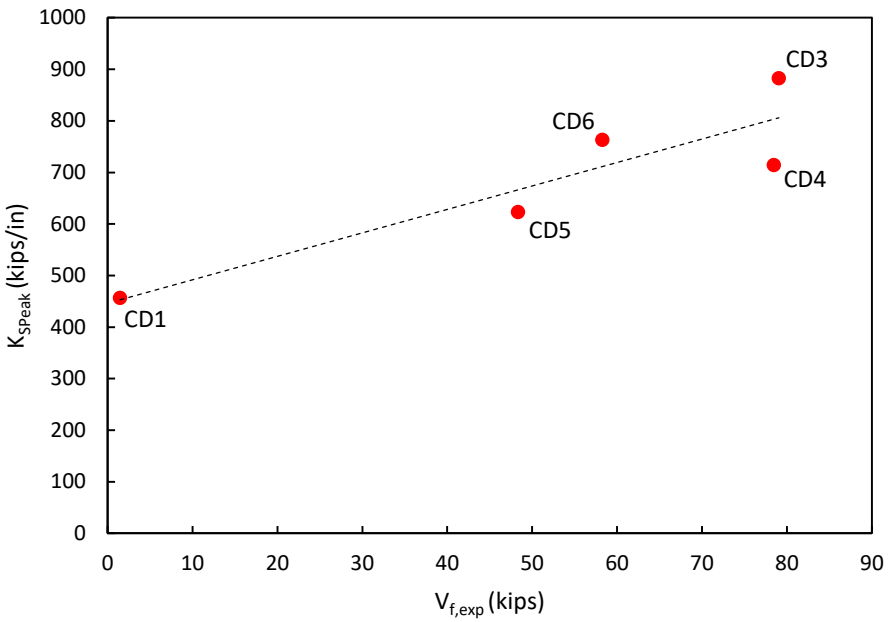

Figure 5.10. Trend Relating FRP Shear Strength Contribution to Stiffness

To compare the predicted initial stiffness to the two secant stiffnesses, ratios of K_{SPeak}/K_{PI} and $K_{S75\%}/K_{PI}$ were calculated and included in Table 5.11. The average of these two ratios was 0.15 and 0.23 respectively. Either average ratio could be used as a modifier in the stiffness prediction methodology described in Section 5.5.1 to estimate the stiffness of the cracked diaphragm. The modifier would need to be applied to I_c in Eq. (23) and bt_c in Eq. (24) to calculate a value that matches the experimental stiffness on average. However, using either average ratio as a modifier would not explicitly separate the effect of FRP on stiffness.

5.6. Diaphragm Ductility and Energy Dissipation

Ductility was quantified to investigate the seismic performance of each specimen. The ductility ratio, μ, was calculated by dividing the critical shear angle, γ_c, by the yielding shear angle, γ_y. The critical shear angle was intended to represent the ultimate deformation capacity of a specimen and was estimated as the post peak global shear angle corresponding to 80% of peak capacity. This estimate of the critical shear angle was adopted from FEMA P695 (2009). Moreover, the yielding shear angle was extrapolated from the secant stiffness, $K_{S75\%}$, where the secant line intersects peak capacity as shown in Figure 5.11. This estimate of the yielding shear angle was adopted from the previously mentioned work completed by Park and Priestly

(1987). The resulting ductility ratio for each specimen excluding CD2 can be found in Table 5.12. Specimen CD2 was not included in this analysis due to the uncertainty of the global shear angle correction. In comparison to the unretrofitted control, only Specimen CD6's perpendicular retrofit showed an increase in ductility. In general, the addition of FRP did not increase the ductility of the specimens; however, the FRP retrofits did not seem to reduce the ductility either. This indicates that factors relating to reinforced concrete diaphragm ductility such as the diaphragm force reduction factor included in the alternate diaphragm design procedure of ASCE 7-22 (2022) could be used for reinforced concrete diaphragms retrofitted with externally bonded FRP.

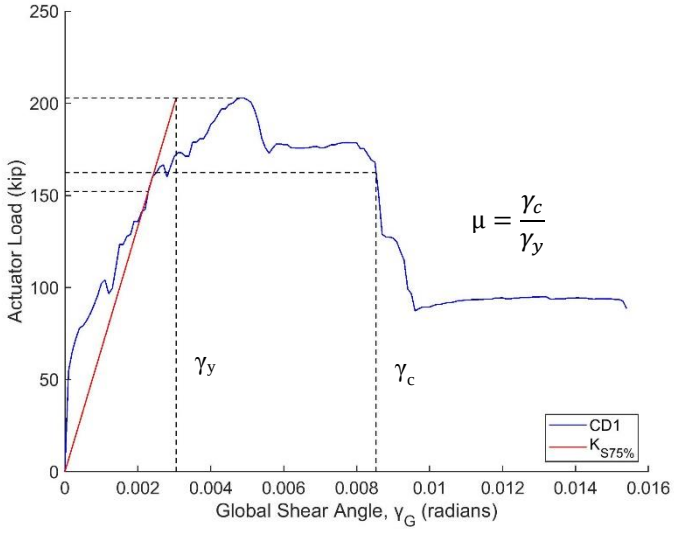

Figure 5.11. Example of Quantifying Ductility for Specimen CD1.

Table 5.12. Summary of Ductility Values

Specimen	**Yielding Shear Angle, γ_y (rad)**	**Critical Shear Angle, γ_c (rad)**	**Ductility Ratio, μ**
CD1	0.00305	0.00853	2.80
CD3	0.00192	0.00470	2.45
CD4	0.00289	0.00755	2.62
CD5	0.00264	0.00637	2.42
CD6	0.00234	0.00846	3.62

To further investigate the ability to deform after peak load, the critical shear angle of each specimen was compared. While the critical shear angle of Specimen CD1 was the highest, the critical shear angles of Specimen CD4 and CD6 were relatively similar. This suggests that

these specimens maintained a similar deformation capacity after peak load in comparison to the unretrofitted specimen. The critical shear angles of Specimen CD3 and CD5 were lower in comparison to Specimen CD1 which demonstrates the deformation capacity after peak load was less than the unretrofitted specimen.

In addition to ductility, energy dissipation was studied to better understand the seismic performance of each specimen. The cumulative shear angle and associated energy was derived from the global response of each specimen using Eq (27).

$$\gamma_{(i)} = maximum(\gamma_{G(i)}, \gamma_{(i-1)}) \tag{27}$$

$$W_{(i)} = \left(\left(\frac{F_{(i)} + F_{(i-1)}}{2}\right)\left(\gamma_{G(i)} - \gamma_{G(i-1)}\right) \cdot a\right) + W_{(i-1)}$$

where: γ is the shear angle (radians); γ_G is the global shear angle (radians); W is the dissipated energy (kip-in); F is the load corresponding to the global shear angle (kips); and a is the distance from the face of the shear wall to the centerline of loading (90 in.).

The resulting energy dissipation curve for each specimen is provided in Figure 5.12. The vertical jumps in each curve represent the second duplicate cycle of each load step where the dissipated energy increased while the shear angle remained the same. Specimen CD2's curve is excluded due to the uncertainty surrounding the global shear angle correction. When comparing each retrofitted specimen to the unretroffited control, no retrofit seemed to increase the energy dissipated. This implied that externally bonded FRP retrofits do not contribute any additional damping to the original system.

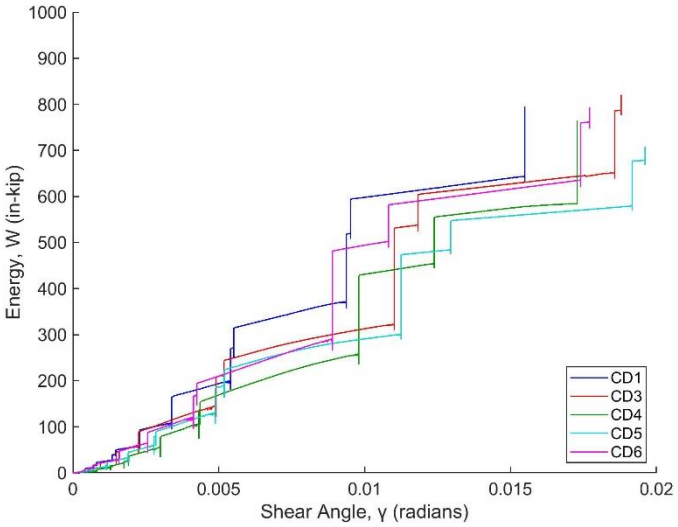

Figure 5.12. Comparison of Energy Dissipation.

Chapter 6. Discussion of Results

6.1. Overview

The purpose of this chapter is to examine the impact of test variables by comparing the performance of specimens with one another. For ductility-related comparisons, Specimen CD2 was excluded due to uncertainties in the global shear angle correction. To evaluate the effectiveness of the design guidance outlined in ACI PRC-440.2R (2017), the experimental data was compared to design strengths and limits. Finally, these comparisons will be used to propose design considerations for the use of externally bonded FRP for shear strengthening reinforced concrete diaphragms.

6.2. Effect of FRP Surface Coverage

The surface coverage of each specimen was defined as the percentage of surface area covered by FRP from the face of the shear wall to the interior edge beam boundary. To investigate the impact of surface coverage, the shear strength provided by FRP, $V_{f,exp}$, and the ductility ratio, μ, of Specimens CD2, CD4, and CD5 were compared. Each of these specimens utilized end anchorage only, were retrofitted parallel to the applied shear, and incorporated the same level of FRP axial stiffness. Figure 6.1(a) compares the effect of surface coverage on the in-plane strength provided by the retrofit, and Figure 6.1(b) compares the effect of surface coverage on the ductility ratio. The results in Figure 6.1(a) demonstrate that increasing the FRP surface coverage from 33% to 100% increases the shear strength provided by the retrofit by a factor of 1.625. Furthermore, increasing the surface coverage from 57% to 100% showed a negligible increase in the shear strength provided by FRP. Figure 6.1(b) shows that ductility was negligibly increased as the surface coverage was increased from 33% to 100%; however, the unretrofitted control specimen maintained a slightly larger ductility ratio in comparison.

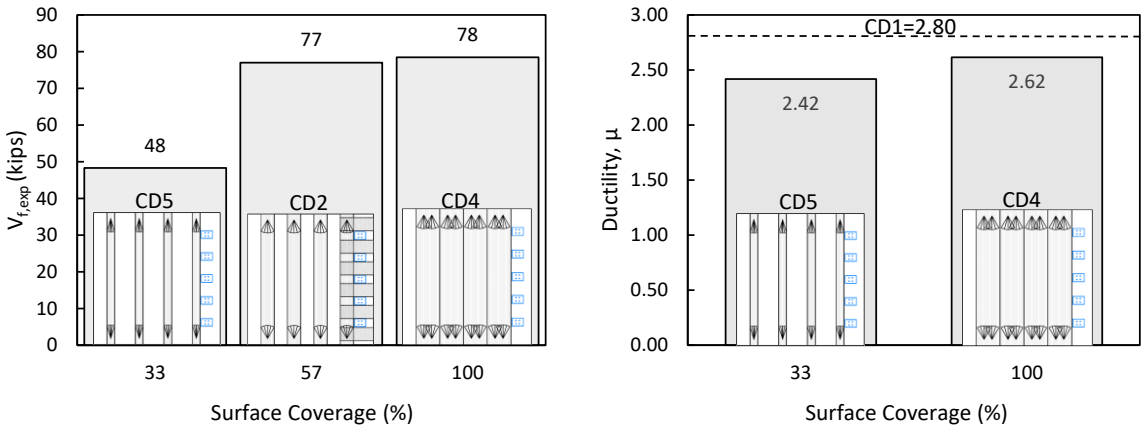

Figure 6.1. Surface Coverage Effects On: (a) In-plane Strength Provided by FRP; (b) Ductility.

FRP surface coverage also plays an important role in restraining crack widths in concrete. Large crack widths in concrete diaphragms are associated with inelastic behavior of diaphragm reinforcement, loss of aggregate interlock, and increase the likelihood of FRP debonding. The clear spacing of FRP sheets s_{fc}, which surface coverage is computed from, seemed to affect how well cracking was restrained. Specimen CD5's retrofit was characterized by 18.7 in. of clear spacing between sheets which narrowly exceeded the 18 in. maximum spacing requirement for reinforcing steel. This large clear spacing could be attributed to the approximate 62% difference in strength provided by FRP when compared to Specimens CD2 and CD4. Figure 6.2 compares the normalized clear spacing and shear capacity contribution of the retrofits corresponding to CD2 through CD5. Each of these retrofits were installed parallel to the applied shear and incorporated the same amount of FRP axial stiffness. The normalized clear spacing was calculated for each specimen by dividing the FRP clear spacing, s_{fc}, by the thickness of the diaphragm, t_c. The dotted trendline within Figure 6.2 shows the FRP shear strength contribution increased as the clear spacing between FRP sheets decreased until an optimal clear spacing was met. Based on this observation, the recommended maximum clear spacing was assumed to be 3 times the thickness of the diaphragm, $3t_c$. However, more tests that reflect a larger sample of strengthened diaphragms are recommended to confirm this limit.

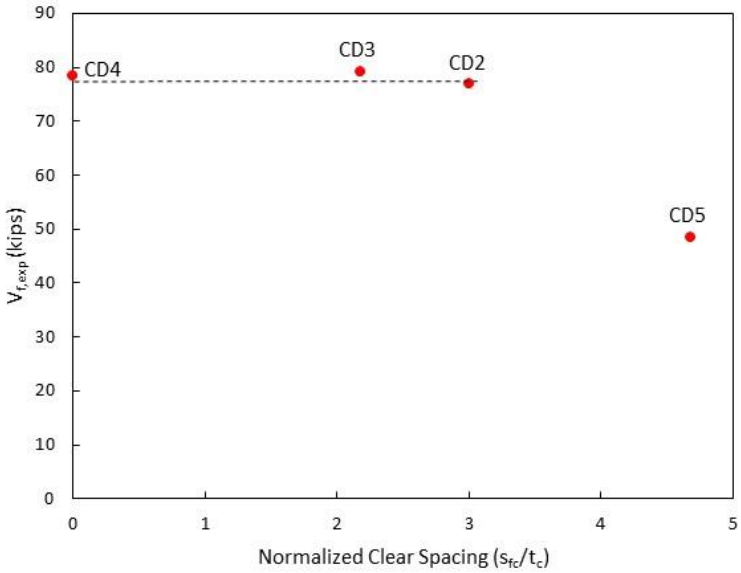

Figure 6.2. Effect of FRP Clear Spacing on the FRP Contribution to Shear Strength.

6.3. Effect of Anchorage Scheme

While all FRP sheets applied to reinforced concrete diaphragms should be anchored at the ends to prevent or delay debonding failures, engineers often try to further improve bond by arresting intermediate cracked induced debonding using intermediate anchors. To investigate the impact of using intermediate anchors designed to satisfy an overstrength factor of 1.5 times the area required to develop the tensile strength of the FRP sheet being anchored, the shear strength provided by FRP of Specimens CD2 and CD3 were compared. Each of these specimens were retrofitted parallel to the applied shear with CFRP and incorporated the same amount of FRP axial stiffness. Figure 6.3(a) compares the effect of anchorage on the in-plane strength provided by the retrofit. The results in Figure 6.3(a) demonstrate that installing intermediate anchors has negligible effect on the shear strength provided by the retrofit. This is because the concrete and reinforcing steel experience high levels of stress at peak diaphragm capacity. Due to this highly stressed condition, the base structure itself becomes the limiting factor, and the additional benefits provided by the intermediate anchors do not lead to any significant enhancement in diaphragm strength.

Furthermore, to investigate the ability of strengthened diaphragms to deform after peak load, the critical shear angle (*e.g.*, the shear angle prior to incipient failure) of Specimens CD3, CD4, and CD5 were compared. Values of critical shear angle were discussed in Section 5.6.

Specimens CD3 and CD4 were utilized in this comparison because they were both retrofitted parallel to the applied shear, Section 6.2 showed that surface coverage had relatively negligible impacts on ductility, and no data was provided for Specimen CD2. Figure 6.3(b) compares the effect of anchorage on the critical shear angle and shows that while no anchorage scheme increased the critical shear angle in comparison to the unretrofitted control, the critical shear angle of Specimen CD3 was substantially low in comparison to the others. This is due to the intermediate anchors causing stress concentrations resulting in localized areas of concentrated damage in the field of the diaphragm.

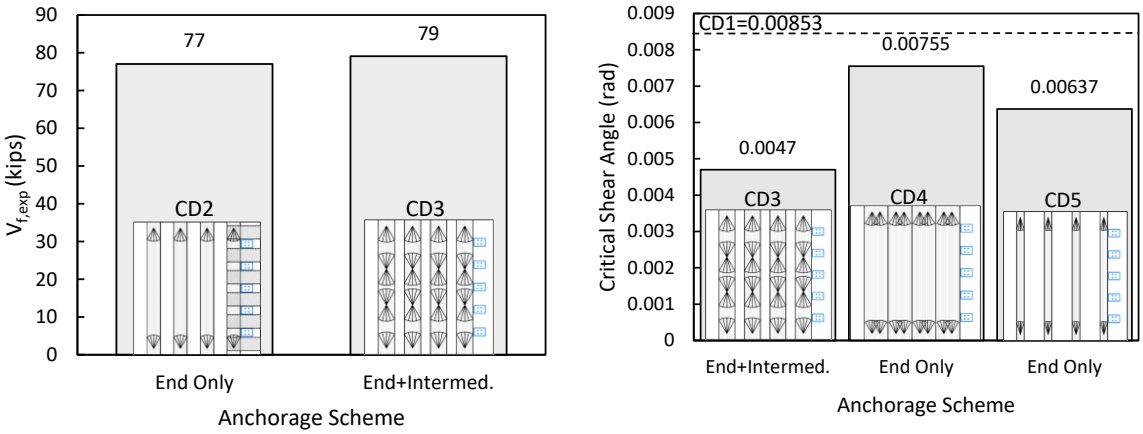

Figure 6.3. Effect of FRP Anchorage Scheme On: (a) In-plane Strength Provided by FRP; (b) Critical Shear Angle.

End anchors were found to prevent end peeling prior to intermediate crack induced debonding. However, installing intermediate anchors showed negligible benefit to the in-plane capacity provided by FRP and resulted in a decrease in the diaphragms ability to deform after peak load. The intermediate anchors, which were equivalently sized as the end anchors, were believed to cause areas of high stress concentrations resulting in increased damage propagation. This theory is supported by the failure mode of Specimen CD3 which was the only specimen to experience FRP sheet rupture in a localized area. Therefore, while end anchorage is recommended, the use of intermediate anchors is cautioned. If intermediate anchors are specified, it is recommended they be designed to satisfy a factor of 0.5 times the area required to develop the tensile strength of the FRP sheet being anchored. This recommendation serves to prevent localized damage in the diaphragm by allowing the intermediate anchors to fail first.

However, this recommendation should be confirmed and further developed through additional testing focused on the size and spacing of intermediate anchors.

6.4. Effect of FRP Orientation on Shear

While it is common to strengthen a reinforced concrete diaphragm with an orthogonal grid of FRP, the FRP applied in the perpendicular direction of applied shear is typically ignored in design scenarios (Dhakal et al. 2022). To investigate the impact of the FRP's orientation relative to the direction of applied loading, the shear strength provided by FRP and the ductility ratio of Specimens CD3 and CD6 were compared. Each of these specimens utilized end anchors with intermediate anchors and incorporated the same level of CFRP axial stiffness. Figure 6.4(a) compares the effect of orientation on the in-plane strength provided by the retrofit, and Figure 6.4(b) compares the effect of orientation on the ductility ratio. The results in Figure 6.4(a) demonstrate that installing the FRP parallel to the direction of loading provides more shear strength in comparison to a perpendicular installation. In terms of strength provided by FRP, the perpendicular retrofit was significant but approximately 75% as effective in comparison to the equivalent parallel retrofit. This indicates that ignoring FRP installed perpendicular to the applied shear is conservative in design scenarios. Figure 6.4(b) suggests that orienting the retrofit perpendicular to the applied shear can improve the ductility of a reinforced concrete diaphragm using externally bonded FRP. This is because FRP installed perpendicular to the direction of applied shear is thought to improve the flexural behavior of the diaphragm which consequently improves ductility.

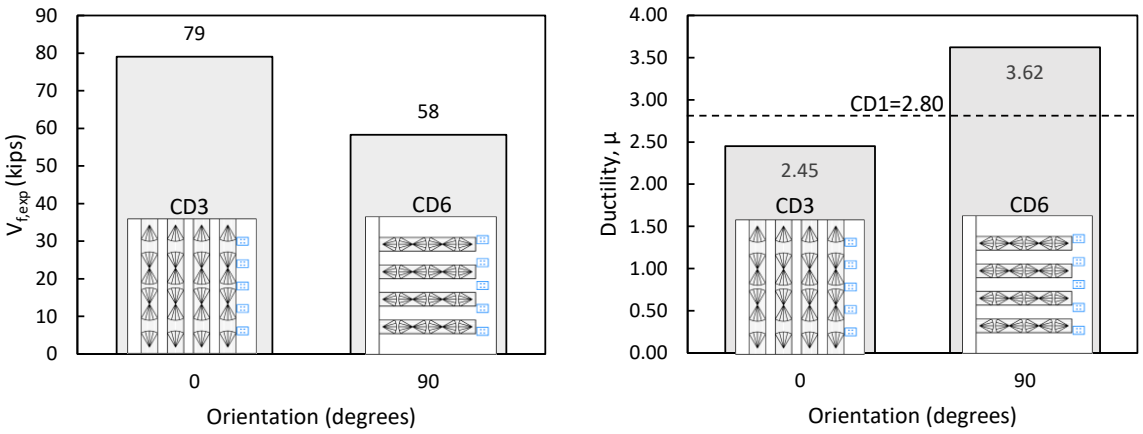

(a) (b)

Figure 6.4. Orientation to Shear Effects On: (a) In-plane Strength Provided by FRP; (b) Ductility.

6.5. Design Considerations

The following design considerations are provided for the use of externally bonded FRP for shear strengthening reinforced concrete diaphragms. These retrofit recommendations are focused on wet layup composites of unidirectional fiber reinforced fabric combined with a polymer resin. They are based on the limited results of this study and are intended to address gaps in existing FRP-related design documents, such as ACI PRC-440.2R (2017) and IAPMO EC038 (2019). Certain equations have been repeated from earlier sections of the thesis to improve readability of the design considerations.

6.5.1 Nominal Shear Strength of FRP Strengthened Diaphragms

The nominal shear strength V_n of reinforced concrete diaphragms may be proportioned according to:

$$V_n \geq \frac{V_u}{\phi} \tag{28}$$

where: ϕ is the strength reduction factor for shear-controlled elements and V_u is the factored shear demand defined according to Clause 12.5.3.2 of ACI 318-19 (2019). The strength reduction factor for shear is typically taken as 0.75, although it is equal to 0.60 when the provisions of ACI 318-19 Clause 21.2.4.1 are applicable. Further research is recommended to determine a specific strength reduction factor for shear-controlled elements strengthened with FRP.

The approach used to determine the nominal strength for diaphragm design relies on the type of model used to analyze the internal force distribution (CRSI 2019). The most commonly used approach is to represent the diaphragm using a beam analogy (Dhakal et al. 2022). In this approach, the load path is idealized such that a uniform shear flow is assumed over the diaphragm depth, d_{fv}. The diaphragm design requirements given in ACI 318-19 Clause 12.5.2 through 12.5.4 are based on the beam analogy. However, ACI 318-19 Clause 12.5.1.3(b-d) allows for the use of alternative approaches, such as strut-and-tie and finite element analysis.

The discussion that follows applies when determining the nominal shear strength of diaphragms strengthened with FRP when the internal force distribution is analyzed using the beam model.

The nominal shear strength V_n of a reinforced concrete diaphragm strengthened with externally bonded FRP is determined by Section 11.2 of ACI PRC-440.2R-17:

$$V_n = V_c + V_s + \psi_f V_f \tag{29}$$

where: V_c, V_s, and V_f are the concrete, reinforcing steel, and externally bonded FRP contributions to shear strength, respectively, and ψ_f is an additional reduction factor for FRP shear reinforcement intended to account for uncertainty inherent to FRP systems (ACI 2017).

The reduction factor ψ_f in Eq. (29) was developed based on a quasi-reliability calibration intended to provide an additional margin of safety depending on how the FRP is being applied to the element being strengthened (ACI 2017). Insufficient experimental data exists to perform a reliability analysis for one-sided diaphragm shear strengthening. However, more variability in performance can reasonably be expected for one-sided strengthening than fully wrapped, three sides U-wrapped, or two-opposite sides strengthening schemes. In the absence of further research, a reduction factor of $\psi_f = 0.75$ is recommended for diaphragms strengthened with FRP on one-side. This value was obtained by extrapolating values for completely wrapped members and members wrapped on two sides from Table 11.3 of ACI PRC-440.2R-17.

For a reinforced concrete diaphragm, the nominal shear strength provided by concrete and steel reinforcement, $V_c + V_s$, should be computed according to Clause 12.5.3.3 of ACI 318-19:

$$V_c + V_s = A_{cv}\left(2\lambda\sqrt{f_c'} + \rho_t f_y\right) \tag{30}$$

where: A_{cv} is the cross-sectional area at the section of interest (equal to the diaphragm depth d_{cv} minus the depth of any slab penetrations times the slab thickness h), λ is the modification factor that accounts for the reduced mechanical properties of lightweight concrete, f_c' is the compressive strength of concrete, and ρ_t is the ratio of distributed slab transverse reinforcement to gross concrete area of reinforcement oriented parallel to the in-plane shear.

6.5.2 Effective Strain in One-side Bonded Face Plies Applied to Concrete Diaphragms

The effective tensile stress f_{fe} in the FRP shear reinforcement at the nominal FRP shear strength V_f is directly proportional to the strain that can be developed in the composite:

$$f_{fe} = \varepsilon_{fe} E_f \tag{31}$$

where: ε_{fe} is the effective design strain and E_f is the tensile modulus of elasticity of FRP.

Diaphragm shear strengthening is considered a bond-critical application. This study revealed that the widespread cracks that propagate throughout the field of the diaphragm tend to precipitate intermediate crack debonding failures of the externally bonded composites. Therefore, the effective design strain ε_{fe} anticipated in diaphragm strengthening applications will be lower than the rupture strain ε_{fu} of the composite. According to ACI PRC-440.2R (2017) guidelines, the effective strain ε_{fe} for FRP shear strengthening should be calculated using a bond-reduction coefficient κ_v given below:

$$\varepsilon_{fe} = \kappa_v \varepsilon_{fu} \leq 0.004 \tag{32}$$

where:

$$\kappa_v = \frac{k_1 k_2 L_e}{468 \varepsilon_{fu}} \leq 0.75 \tag{33}$$

$$L_e = \frac{2500}{\left(n t_f E_f\right)^{0.58}} \tag{34}$$

$$k_1 = \left(\frac{f_c'}{4000}\right)^{2/3} \tag{35}$$

$$k_2 = \begin{cases} \dfrac{d_{fv} - L_e}{d_{fv}} \text{ for U} - \text{wraps} \\ \dfrac{d_{fv} - 2L_e}{d_{fv}} \text{ for two sides bonded} \end{cases} \tag{36}$$

The bond-reduction coefficient approach, presented in Equations (32)-(36), was developed by Khalifa et al. (1998) based on a database of mainly U-wrapped and two-sides bonded shear strengthened members, many of which were unusually shallow. Specifically, the

coefficient k_2 was developed to account for the effect of bonded surface configuration. The significance of k_2 is to account for the reduction in shear capacity of the FRP sheet due to the need to develop shear stresses at the strip termination points. Figure 6.5 illustrates how the effective width of FRP, $w_{fe} = d_f - 2L_e$, is reduced to account for the active bond length L_e extending past the crack over which most of the bond stresses are developed.

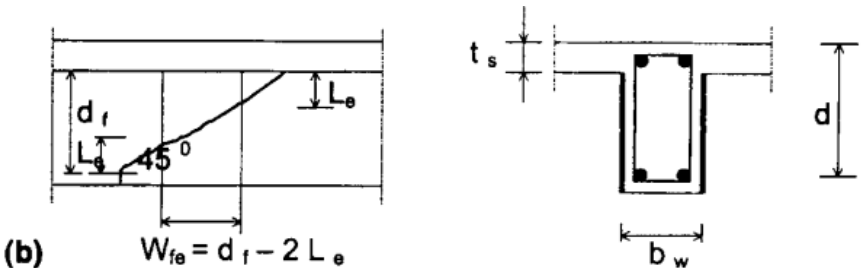

Figure 6.5. Definition of the Effective Width of an FRP Sheet Bonded on Two Sides of a Beam (from Khalifa et al. 1998).

Most beams and columns have geometric depths d that are only a few orders larger than the active bond length L_e of the FRP, which is approximately 6 in. or less. Consequently, the expected range of k_2 from Eq. (36) for beams and columns is typically less than 1.0. However, in the majority of buildings, the typical values of diaphragm depth d_{cv} are on the order of tens of feet, which is many times larger than L_e. As a result, when Eq. (I) is applied to diaphragms, it will lead to k_2 approaching 1.0.

Therefore, for the case of one-sided bonded face plies used for shear strengthening of diaphragms, it is recommended that $k_2 = 1.0$ be used with the bond-reduction coefficient approach of Section 11.4.1.2 of ACI PRC-440.2R-17.

A statistical analysis was conducted to assess the adequacy of using the bond-reduction approach $\kappa_v \varepsilon_{fu}$ given in Eq. (32) with $k_2 = 1.0$ for determining the design strain ε_{fe} of FRP strengthened diaphragms. The analysis was performed by comparing the design strain ε_{fe} for specimens CD2 through CD6 with $k_2 = 1.0$ against the estimated strains $\varepsilon_{f,exp}$ established in Section 5.4.1. Table 6.1 shows the results of the analysis. The average design-to-estimated strain ratio, $\varepsilon_{fe}/\varepsilon_{f,exp}$, was 0.82 with a coefficient of variance of 13% based on the 5 strengthened diaphragm tests of this study. The results indicate that using the bond-reduction procedure proposed by Khalifa et al. (1998) with the recommended value of $k_2 = 1.0$ to determine

the debonding strain of FRP retrofitting diaphragms is sufficiently conservative for the average of all cases considered. However, more research is recommended on the effective strain of FRP diaphragm shear strengthening, encompassing a broader range of retrofit configurations, including higher density fabrics of 40 oz/yd^2 commonly used in full-scale applications.

Table 6.1. Summary of Effective FRP Design Strain Calculations.

Test	**Active Bond Length L_e (in.)**	**Concrete Modification Factor, k_1**	**Retrofit Modification Factor, k_2 for diaphragm strengthening**	**FRP Rupture Strain, ε_{fu} (%)**	**Bond Coefficient for Shear, κ_v**	**Design Strain, $\varepsilon_{fe} = \kappa_v \varepsilon_{fu}$ (%)**	**Estimated FRP bonding strain $\varepsilon_{f,exp}$ (%)**	$\frac{\varepsilon_{fe}}{\varepsilon_{f,exp}}$
CD2	1.56	1.09	1.0	1.3	0.27	0.37	0.48	0.77
CD3	1.74	0.94	1.0	1	0.34	0.35	0.47	0.75
CD4	2.19	0.94	1.0	1.8	0.23	0.44	0.44	1.00
CD5	1.15	0.99	1.0	1.27	0.19	0.24	0.32	0.75
CD6	1.56	1.08	1.0	1.3	0.27	0.36	0.42	0.86
							Average COV	**0.82 13%**

In certain diaphragm strengthening applications, it may be necessary to further limit the effective FRP design strain ε_{fe}, to ensure force-controlled diaphragm behavior. While diaphragms are allowed to be analyzed as deformation-controlled according to ASCE 7-22, it may be necessary to ensure force-controlled behavior for diaphragms that are especially susceptible to brittle failure. This is particularly relevant for existing buildings constructed using Grade 40 reinforcing steel, along with other deficiencies (Dhakal et al. 2022). One of the concerns is that, when subjected to a lateral load event at the design level, the yielding of low-grade reinforcing steel at relatively low load levels may result in an extensive network of wide diaphragm cracks. This, in turn, is likely to increase the potential for FRP debonding due to the formation of stress concentrations in the composite at locations of intermediate cracks. Limiting the effective FRP design strain may also help prevent the loss of aggregate interlock necessary for concrete to contribute to shear strength V_c (Dhakal et al. 2022).

Therefore, when concerns regarding the capacity of the underlying reinforced concrete substrate are present, it is recommended that the effective design strain in FRP reinforcement be further limited to prevent yielding of reinforcing steel:

$$\varepsilon_{fe} = \kappa_v \varepsilon_{fu} \leq \frac{f_y}{E_s} \tag{37}$$

where: f_y and E_s are yield strength and modulus of elasticity of diaphragm reinforcing steel. The purpose of introducing the additional FRP design strain limitation in Eq. (37) is to maintain force-controlled diaphragm behavior in cases where the underlying substrate is particularly brittle, by ensuring that the FRP achieves its design stress concurrently with the yielding of reinforcing steel.

6.5.3 FRP Contribution to Shear Strength V_f

For design purposes, it is recommended to only consider the shear contribution of externally bonded FRP that is oriented parallel to the direction of applied shear. That is, FRP strips are inclined at an angle $\alpha = 90°$ relative to the longitudinal member axis. FRP placed perpendicular to the direction of applied shear ($\alpha = 0°$) can be conservatively ignored. This recommendation is consistent with the diaphragm design provisions in ACI 318 (2019) which neglect the contribution of reinforcing steel not parallel to the applied shear. Therefore, for design purposes, it is conservatively recommended to consider the shear strength contribution of externally bonded FRP V_f only when it is applied parallel to the direction of the applied shear force. For these cases,V_f can be established according to:

$$V_f = \frac{A_{fv} f_{fe} d_{fv}}{s_f} \tag{38}$$

where: A_{fv} is the cross-sectional area of composite fabric applied at center-to-center spacing s_f. The cross-sectional area of fabric A_{fv} can be taken as the width of the fabric strip w_f times the thickness of the composite t_f. If continuous strips are used, the width of the sheet w_f should be set equal to the spacing s_f.

In certain applications, it may be necessary to consider the contribution of FRP placed perpendicular to the direction of applied shear ($\alpha = 0°$). However, as was discussed in Section 6.4, perpendicular strengthening of specimen CD5 was only about 75% as effective as the nominally identical parallel strengthening applied to specimen CD3. This disparity could be attributed to the perpendicular FRP being less effective at restraining shear cracks, as well as

presence of shear-bending interaction which may have decreased the debonding failure load of the FRP.

The contribution of FRP shear reinforcement inclined at an angle α to the longitudinal member axis can be establishing using ACI PRC-440.2R (2017) Eq. 11.4a, given in Eq. (39) below:

$$V_f = \frac{A_{fv} f_{fe} d_{fv}}{s_f} (sin\alpha + cos\alpha) \tag{39}$$

In order to examine the validity of Eq. (39), the experimental shear strength provided by FRP $V_{f,exp}$ (see Section 5.3.3) was compared to the nominal design shear strength of FRP V_f. This comparison is summarized in Figure 6.6 which includes a ratio of $V_f/V_{f,exp}$. The average value of this ratio was 0.80 with a coefficient of variation (COV) of 14%. The design FRP shear strength contribution from Eq. (39) follows a similar trend as the corresponding experimental data and tends to give conservative results.

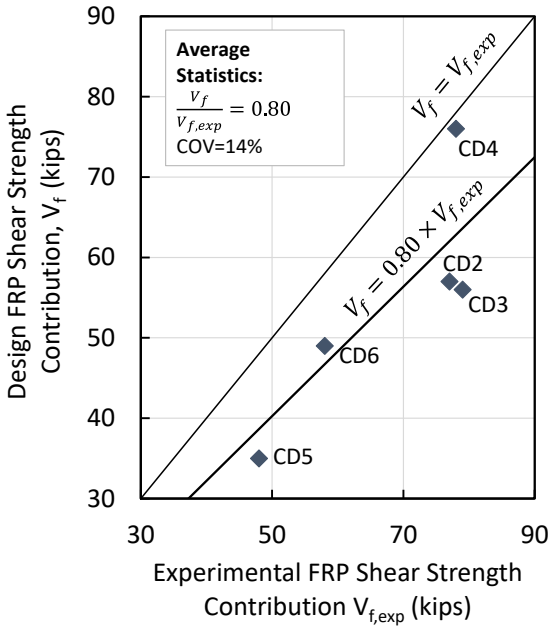

Figure 6.6. Comparison of Design and Experimental FRP Shear Strength Contribution.

It is important to acknowledge a potential issue associated with Eq. (39) for calculating the FRP shear strength contribution for strips oriented perpendicular to the direction of applied shear ($\alpha = 0°$). The expression in Eq. (39) can be traced back to Eq. (40), which was originally

developed for reinforcing steel inclined to the longitudinal member axis using the truss analogy shown in Figure 6.5. Eq. (39) was derived from Eq. (40) by first assuming concrete cracks occur at an angle $\theta = 45°$ and then simplifying the trigonometric terms.

$$V_f = \frac{A_{fv} f_{fe} d_{fv}}{s_f} sin\alpha(\cot\theta + \cot\alpha) \tag{40}$$

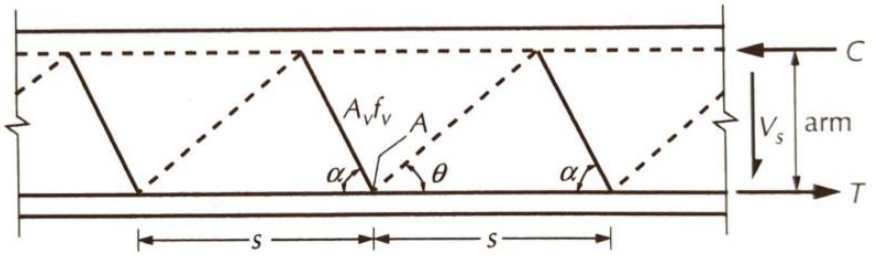

Figure 6.7. Truss Model for a Beam with Inclined Stirrups (from Pincheira et al. 2018).

A substantial body of work obtained from beam and column tests has substantiated the use of Eq. (39) and Eq. (40) for FRP strips oriented at approximately $\alpha \approx 45°$ to the longitudinal member axis (*e.g.*, Monti et al. 2005). However, very little data is available that examines the validity of these expressions for FRP placed perpendicular to the direction of applied shear. From Figure 6.7, it can be seen that these expressions necessitate equilibrium of the truss in the transverse direction. However, this can only be satisfied for non-zero angles of the inclined reinforcement. When the reinforcement inclination α is equal to 0°, the truss analogy shown in Figure 2 becomes invalid, and the trigonometric term $sin\alpha(\cot\theta + \cot\alpha)$ in Eq. (40) yields a divide by zero mathematical error. Although this error does not occur in Eq. (39) due to the trigonometric simplification, the truss analogy is still violated by the simplified expression commonly used in design.

Therefore, for designs considering unidirectional FRP strips placed perpendicular to the direction of applied shear, Eq. (39) and Eq. (40) may not be suitable, as they were intended for strengthening where the reinforcement inclination $\alpha \geq 45°$. Until more research becomes available, designers should use more refined methods of analysis for considering the shear strength contribution of unidirectional FRP placed perpendicular to the direction of applied shear.

6.5.4 Validity of the Expression for Design Nominal Strength V_n

The results of the six diaphragm tests were used to assess the validity of the design nominal shear strength V_n of FRP strengthened diaphragms calculated using Eq. (29). The values of V_n for the specimens were computed using: (i) the nominal material properties, geometry and reinforcing details from Chapter 3; (ii) $(V_c + V_s)$ computed using Eq. (30); (iii) the nominal shear strength of FRP V_f using ε_{fe} in Eq. (31) with $k_2 = 1.0$; and, (iv) taking the reduction factor $\psi_f = 0.75$.

Figure 6.8 presents a comparison between the design and experimental nominal shear strengths. The results indicate that the proposed design approach tends to be conservative, underestimating the actual shear strength observed during the experiments. The average ratio of $V_n/V_{n,exp} = 0.78$ with a $COV = 4\%$. Although these results are promising, more experimental tests are required to make definitive conclusions regarding the validity of this approach. The expanded dataset should encompass a wider range of retrofit schemes, concrete strengths, and diaphragm configurations. It is also important to consider that the experimental strengths are based on cyclic testing which has been found to reduce the in-plane capacity of diaphragms by up to 25% (Nakashima et al. 1981). While cyclic testing is most appropriate for seismic applications, monotonic testing may result in larger in-plane diaphragm capacity.

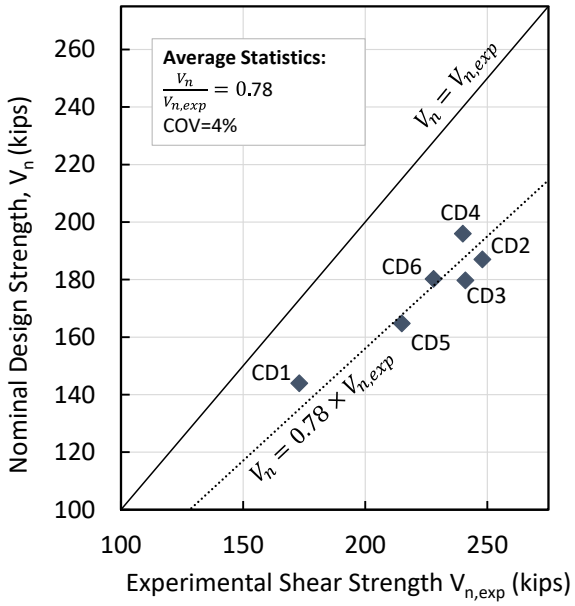

Figure 6.8. Comparison of Design and Experimental Nominal Diaphragm Shear Strengths.

6.5.5 Anchorage of Bonded FRP

Designers often feel more comfortable with FRP diaphragm strengthening when supplemental mechanical anchorages are provided (Dhakal et al. 2022). The purpose of these anchorage is not to increase the effective design strain of FRP retrofit system. Instead, they are provided to promote more favorable bond conditions and offer an additional margin of safety against debonding failures.

To promote favorable development of composite forces into concrete, mechanical anchorage should be provided at all FRP termination points or at the diaphragm shear span d_{fc}, whichever is less. These end anchorages should be designed to develop the full tensile capacity of the anchored sheets. If FRP anchors are used, the diameter of the anchors should be sized to develop at least 1.5 times the tensile capacity of the anchored fabric. Manufacturer specific requirements for anchor proportioning and installation should be followed.

In certain applications, intermediate FRP anchorages may be provided to promote favorable bond conditions in the field of the diaphragm between diagonal shear cracks. However, to prevent brittle diaphragm behavior, these intermediate anchorages should not be designed to develop the tensile capacity of anchored fabric. This recommendation is based on the results of specimen CD3, which demonstrated that using overstrength intermediate anchors resulted in a localized diaphragm failure between anchor locations that reduced global diaphragm ductility. Therefore, it is recommended that the intermediate FRP anchors should be designed to fail prior to the end FRP anchors. In the absence of further research, the intermediate FRP anchor diameter should be proportioned based on a factor of 0.5 times the area required to develop the tensile capacity of the FRP sheet being anchored. Although further research is required to determine acceptable intermediate anchor spacings, it is recommended that anchors be spaced no more than 9 ft apart. This recommendation is based on the approximate distance between the end anchors of each retrofitted specimen.

6.5.6 Clear Spacing of FRP Strips

The installation of FRP, either continuously along the diaphragm or in the form of discrete strips, was found to be effective strategies for shear strengthening. However, as described in Section 6.2, it was observed that the behavior of strengthened diaphragms was

negatively impacted when the clear spacing of discrete strips exceeded approximately three times the thickness of the diaphragm.

For the case of FRP strengthened diaphragms, it is recommended that the maximum clear spacing between FRP shear strips should be limited to the minimum of three times the thickness of the slab, or 18 in. The maximum clear spacing of 18 in. is recommended in absence of further research. Similar recommendations can also be found in IAPMO EC038 (2019) and Clause 13.7.3.1 in ACI PRC-440.2R (2017) which is intended for FRP strengthened shear walls.

6.5.7 Composite Material Selection

In practice, the majority of diaphragm shear strengthening applications use CFRP due to the high strength and stiffness of carbon fibers (Dhakal et al. 2022). However, the results of this study indicated that there was no significant difference in performance between diaphragm strengthened with GFRP and CFRP composites up to the ultimate limit state, as long the as the retrofits are proportioned to have levels of composite rigidity, $\rho_f E_f$. However, other factors, such as constructability, serviceability, and cost, may play a crucial role in making the appropriate choice between the two types of composites for a given retrofit application.

6.5.8 Reinforcement Limits

To prevent crushing of concrete struts in shear, the nominal diaphragm shear strength V_n cannot exceed the maximum nominal shear strength $V_{n,max}$ determined by ACI 318-19 Clause 12.5.3.4:

$$V_{n,max} = 8\sqrt{f_c'}A_{cv} \tag{41}$$

The applicability of this limit was assessed against the diaphragm tests results. The results of this analysis are shown in Figure 6.9. The contribution of the perimeter beams to shear strength V_{frame} was subtracted from the ultimate strength of the tests, $V_{u,exp}$, then normalized with respect to $A_{cv}\sqrt{f_c'}$. The results show that while the nominal shear strength of specimens CD3 and CD4 exceeded $V_{n,max}$, neither experienced a diagonal crushing failure.

Therefore, limiting $V_{n,max}$ to $\sqrt{f_c'}A_{cv}$ is believed to be appropriate for the design of FRP strengthened diaphragms.

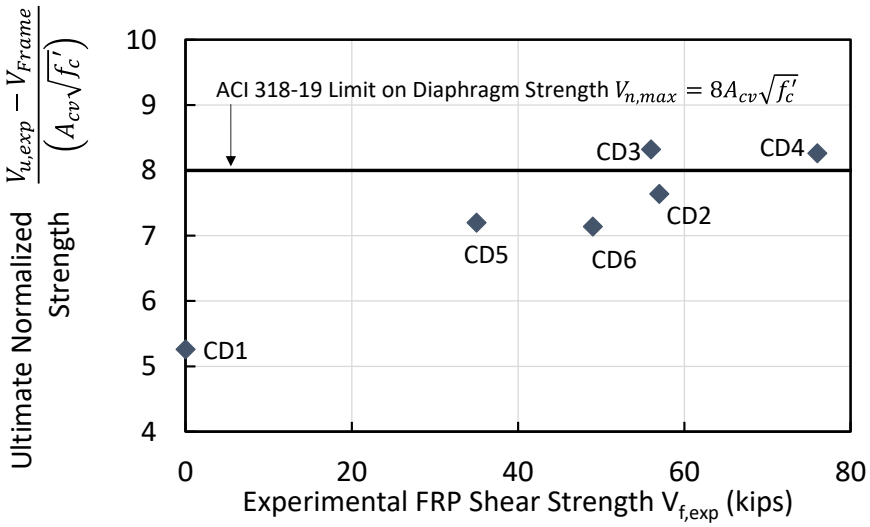

Figure 6.9. Comparison of the Ultimate normalized Diaphragm Strength Against the ACI 318-19 Diagonal Crushing Shear Limit.

Chapter 7. Conclusions

7.1. Summary of Research

This thesis summarizes results from an experimental study focused on the in-plane shear behavior of reinforced concrete diaphragms strengthened with FRP. A clear lack of data and industry need for design guidance motivated this study. Six half-scale diaphragms were tested to understand how externally bonded FRP improved the strength, ductility, and energy dissipation of the specimens. The results demonstrated that externally bonded FRP retrofitting improved both the shear strength and stiffness of the strengthened test specimens. The results also highlighted that the overall behavior of the specimens was influenced by the way the FRP retrofit schemes were proportioned and detailed. The impact of various test variables including spacing, anchorage, and orientation were analyzed to develop design recommendations and evaluate existing design provisions in ACI PRC-440.2R (2017). The key findings and recommendations based on this experimental study, along with recommendations for future research, are provided in this chapter.

7.2. Key Findings

From the experimental study on the behavior of reinforced concrete diaphragms strengthened with FRP, it was concluded that:

1. The strength of the reinforced concrete cantilever diaphragm test specimens was the sum of the shear strength contribution of concrete, reinforcing steel, and externally bonded FRP, as well as the additional strength provided by frame action of the perimeter beams.

2. Externally bonded FRP retrofits provided additional capacity that enhanced both the strength and stiffness of strengthened diaphragms.

3. In retrofit schemes proportioned to maintain a constant total ply stiffness, the peak strength of retrofitted diaphragms was approximately 1.38 times greater than that of the unstrengthened control specimen.

4. The unstrengthened control specimen experienced a diagonal tension shear failure. The FRP strengthened specimens all exhibited an FRP debonding failure, which was initiated by intermediate shear cracks occurring within the field of the diaphragm.

5. Complete debonding of externally bonded FRP consistently occurred after the yielding of the internal diaphragm steel reinforcement.

6. The retrofit surface coverage affected the shear strength contribution of externally bonded FRP, $V_{f,exp}$. Higher surface coverages of externally bonded FRP were found to result in superior diaphragm performance than lower surface coverages of narrow strips of high-density fabric. This was attributed to improved control of shear cracks from more uniform surface coverage within the diaphragm field. For example, FRP retrofits designed with a surface coverage ranging from 57% to 100% demonstrated similar values of $V_{f,exp}$, approximately 80 kips, along with similar estimated debonding strains, $\varepsilon_{f,exp}$, of 0.46%. However, retrofits with a surface coverage of 33% performed less effectively, yielding a lower value of $V_{f,exp}$, approximately 48 kips, and an estimated debonding strain, $\varepsilon_{f,exp}$, of 0.32%.

7. No significant difference in performance was observed between diaphragms strengthened with GFRP and CFRP composites, indicating either type of fabric may be suitable, as long as the retrofits were proportioned to achieve comparable levels of composite stiffness and had a surface coverage exceeding 57%.

8. Although unanchored FRP retrofits were not specifically tested in this study, it was believed that the presence of end anchors, designed to satisfy a factor of 1.5 times the area required to develop the tensile capacity of the FRP sheet being anchored, would promote favorable bond conditions during the diaphragm tests.

9. The use of intermediate FRP anchors, designed to satisfy a factor of 1.5 times the area required to develop the tensile capacity of the FRP sheet being

anchored, did not significantly impact the shear strength contribution of externally bonded FRP, $V_{f,exp}$, or the estimated debonding strain of the composite, $\varepsilon_{f,exp}$.

10. However, the one test with intermediate overstrength anchorages led to localized failures that concentrated inelastic diaphragm response between anchor locations, resulting in a significant reduction in diaphragm deformation capacity.

11. The secant stiffness of FRP strengthened diaphragms up to their peak strength, K_{SPeak}, was observed to increase proportionally with the shear strength contribution of externally bonded FRP, $V_{f,exp}$.

12. The application of FRP parallel to the direction of applied shear was identified as the most effective approach in terms of achieving the highest increases in the shear strength contribution of FRP, $V_{f,exp}$.

13. The application of FRP perpendicular to the applied shear was less effective than parallel retrofitting, but still contributed to enhancing the diaphragm shear strength. The FRP contribution to shear strength, $V_{f,exp}$, of perpendicular retrofits was approximately 75% as effective as similar diaphragms strengthened with parallel retrofitting.

14. Parallel retrofitting did not substantially enhance the deformation at peak load of the diaphragms compared to the unretrofitted control. However, with exception of Specimen CD3, parallel retrofitting did not significantly reduce diaphragm deformability compared with the control specimen.

15. Perpendicular retrofitting increased the ductility of reinforced concrete diaphragms by a factor of 1.29. This was attributed to enhancements in flexural behavior.

16. The energy dissipation of reinforced concrete diaphragms was not increased by FRP strengthening.

17. Analytical methods based on the Modified Compression Field Theory (MCFT) and considering frame action of the perimeter beams were found to provide reasonable predictions of the peak strength of the unretrofitted concrete diaphragm.

18. When the debonding strain of retrofitted diaphragms is known, the shear strength contribution of externally bonded FRP applied parallel to the direction of applied shear can be reasonably predicted using design equations provided in ACI PRC-440.2R-17 (2017).

19. Taking a value of $k_2 = 1.0$ for one-sided diaphragm strengthening, the expression for effective design strain, $\varepsilon_{fe} = \kappa_v \varepsilon_{fu}$, in Chapter 11 of ACI PRC-440.2R-17 (2017) was found to conservatively underpredict the experimental debonding strains observed during the diaphragm tests by an average of 18%.

20. Chapter 6.5 of this thesis proposed an approach for establishing the nominal design shear strength of reinforced concrete diaphragms strengthened with FRP, V_n. This approach was found to conservatively underpredict the nominal experimental shear strength observed by an average of 22%.

7.3. Design Recommendations

Design recommendations were prepared based on the analysis and discussion of results presented in Chapter 5 and Chapter 6. The recommendations incorporated key findings from this research and validate certain existing provisions within ACI PRC-440.2R-17 (2017). The following design recommendations are suggested for shear strengthening reinforced concrete diaphragms with externally bonded FRP:

1. The current practice for diaphragm retrofit design lacks specific guidance and often relies on two separate reduction factors applied to V_f. Designers typically use a value of $\psi_f = 0.85$ for both three-sided and two-sided wrapped members and apply an additional reduction factor of 0.75 is applied to V_f, originally intended for shear wall strength applications. To simplify the design process and

minimize potential confusion, it is recommend introducing that a single reduction factor ψ_f for one-sided diaphragm strengthening applications, eliminating the need for any further reduction factors.

2. The required shear contribution of externally bonded FRP can be calculated with Equation (42):

$$V_f \geq \frac{1}{\Psi_f}\left(\frac{V_u}{\phi} - V_c - V_s\right) \tag{42}$$

where: V_f is the nominal shear strength provided by FRP; Ψ_f is the FRP strength reduction factor that accounts for bond reliability; V_u is the factored shear demand of the diaphragm; V_c is the nominal shear strength provided by concrete; V_s is the nominal shear strength provided by reinforcing steel; and, ϕ is the shear strength reduction factor of 0.75 for shear-controlled elements in ACI 318 (2019).

3. In absence of further research, the FRP strength reduction factor, Ψ_f, is recommended to be taken as 0.75 for diaphragms strengthened on one side only. This value was obtained by extrapolating values for completely wrapped and members wrapped on two sides from Table 11.3 of ACI 440.2R-17 (2017).

4. The nominal shear strength contribution of externally bonded FRP, V_f, applied parallel to the direction of applied shear can be determined with Equation (43):

$$V_f = \frac{A_{fv} f_{fe} d_{fv}}{s_f} \tag{43}$$

where: V_f is the nominal shear strength provided by FRP (lbs); A_{fv} is the area of FRP shear reinforcement (in.^{2}); f_{fe} is the effective stress in FRP (psi); d_{fv} is the effective depth of FRP shear reinforcement (in.); s_f is the center-to-center spacing of FRP strips (in.); and Ψ_α is the FRP orientation factor.

5. The shear strength contribution of externally bonded FRP applied perpendicular to the direction of applied shear can be conservatively ignored. This recommendation is consistent with diaphragm design provisions in ACI 318-19

(2019) which neglect the contribution of reinforcing steel not parallel to the applied shear.

6. The effective FRP design strain may be established with Equation 11.4.1.2 of ACI PRC-440.2R-17 (2017), with the exception that the retrofit scheme modification factor, k_2, be taken as 1.0 for one-sided diaphragm strengthening.

7. At a minimum, mechanical anchorage should be provided to promote favorable development of composite forces into concrete at the ends of the FRP laminates or at the effective depth of the FRP reinforcement, d_{fv}, whichever is less. These end anchorages should be designed to develop the full tensile capacity of the anchored sheets. If FRP anchors are used, the diameter of the anchors should be sized to satisfy a factor of 1.5 times the area required to develop the tensile capacity of the FRP sheet being anchored. Manufacturer specific design requirements for anchors should be followed.

8. The following recommendations relate to the use of intermediate anchors:

a. Intermediate anchorage is recommended to mitigate intermediate crack induced debonding in the field of typical large span diaphragms.

b. However, to prevent brittle diaphragm response, intermediate anchors should not be designed to develop the full tensile capacity of anchored fabric. FRP anchors should be designed to fail after debonding of the FRP sheet but before failure of the end anchors.

c. In the absence of further research, intermediate FRP anchors should designed to satisfy a factor of 0.5 times the area required to develop the tensile strength of the FRP sheet being anchored.

d. In the absence of further research, intermediate FRP anchors should be spaced no more than 9 ft apart.

9. In certain diaphragm strengthening applications, it may be necessary to limit the effective design strain to limit steel yielding and control the width and

extent of cracking. This could be done enforcing the limit presented as Equation (44); however, further research is required to verify the applicability of this limit.

$$\varepsilon_{fe} \leq \frac{f_y}{E_s} \tag{44}$$

where: ε_{fe} is the effective FRP design strain (in./in.); f_y is the yield strength of reinforcing steel (psi); and E_s is the modulus of elasticity of reinforcing steel (psi).

10. The total quantity of steel and FRP reinforcement should be limited to prevent crushing of concrete struts in shear. The limit proposed by ACI PRC-440.2R-17 is presented as Equation (45) and seems to be appropriate for design.

$$V_s + V_f \leq 8\sqrt{f_c'}\, b_w d \tag{45}$$

where: V_s is the nominal shear strength provided by steel (lbs); V_f is the nominal shear strength provided by FRP (lbs); f_c' is the compressive strength of concrete (psi); b_w is the web width (in.); and d is the distance from the extreme compression fiber to the centroid of the tension reinforcement (in.).

11. For externally bonded FRP reinforcement in the form of discrete strips with defined widths, the clear spacing between strips should not exceed three times the diaphragm thickness, $3t_c$. This is intended to limit crack widths between strips which may degrade bond performance.

7.4. Suggestions for Future Research

This research initiative was limited to strengthening reinforced concrete diaphragms with single ply externally bonded FRP retrofits oriented in one direction and anchored with FRP splay anchors. While this focus helped form design recommendations intended to further develop the existing design provisions within ACI PRC-440.2R (2017), additional research is needed to address topics not included in this study. It is also important to note that the tested specimens were relatively small and included large proportions of reinforcing steel in

comparison to existing diaphragms encountered in practice. The following topics are suggested for future research:

1. Testing of reinforced concrete diaphragms strengthened with FRP and constructed using A615 deformed reinforcement to produce a ratio of $V_f/V_s > 2.0$.

2. Testing of reinforced concrete diaphragms strengthened with multiple layered plies of FRP.

3. Testing of reinforced concrete diaphragms strengthened with an orthogonal grid of FRP, as well as FRP oriented at an angle to the direction of applied shear.

4. Testing of alternative anchoring techniques, such as techniques based on bonded steel plates bolted to concrete, as well as alternative FRP anchor design methodologies.

5. A computational study on the effect of limiting the effective FRP debonding strain to the internal steel reinforcement strain on diaphragm response.

6. A computational study on the effect of under-designing intermediate anchorages on the bond behavior and global performance of FRP strengthened diaphragms.

7. Research on the potential shear lag mechanics related to the bond of the FRP composite and concrete.

References

ACI Committee 318 (1992) *Building code requirements for structural concrete (ACI 318-92) and commentary (ACI 318R-92)*, Published by the American Concrete Institute.

ACI Committee 318 (2019) *Building code requirements for structural concrete (ACI 318-19) and commentary (ACI 318R-19)*, Published by the American Concrete Institute.

ACI Committee 435 (2020) *Report on Deflection of Nonprestressed Concrete Structures (ACI 435R-20)*, Published by the American Concrete Institute.

ACI Committee 440 (2017) *Guide for the design and construction of externally bonded FRP systems for strengthening concrete structures (ACI PRC-440.2R-17)*, Published by the American Concrete Institute.

ASCE (2022) *Minimum Design Loads and Associated Criteria for Buildings and Other Structures (ASCE 7-22)*, Published by the American Society of Civil Engineers.

Aegion (2016) *Tyfo FRP Seismic to Floor Diaphragm Strengthening*, Webpage http://concretesolutions.co.nz/tyfo-frp-seismic-floor-diaphragm-strengthening/ last accessed August 27, 2019.

Aryan, H., Gencturk, B., and Alkhrdaji, T.. (2022) "In-plane shear strengthening of reinforced concrete diaphragms using fiber reinforced polymer composites." *Advances in Structural Engineering*, 0(0), 1-17.

Arnold, S.F., Chiewanichakorn, M., and Toranzo, L. (2011) "Seismic retrofit of St. Joseph Hospital Using Advanced Composite Materials for the Enhancement of Column, Slab, Wall and Beam Elements," *Proceedings, Ninth Pacific Conference on Earthquake Engineering, Building an Earthquake-resilient Society*, Auckland, New Zealand, 14-16 April 2011.

ASTM (2008) *Standard Test Method for Tensile Properties of Polymer Matrix Composite Materials (D3039-08)*, Published by ASTM International.

ASTM (2017) *Standard Test Method for Splitting Tensile Strength of Cylindrical Concrete Specimens (C496-17),* Published by ASTM International.

ASTM (2021) *Standard Test Method for Compressive Strength of Cylindrical Concrete Specimens (C39-22),* Published by ASTM International.

ASTM (2022) *Standard Practice for Making and Curing Concrete Test Specimens in the Field (C31-22),* Published by ASTM International.

ASTM (2022) *Standard Test Method for Static Modulus of Elasticity and Poisson's Ratio of Concrete in Compression (C439-22),* Published by ASTM International.

ASTM (2022) *Standard Test Methods and Definitions for Mechanical Testing of Steel Products (A370-22),* Published by ASTM International.

Avellaneda-Ramirez, R., (2021) "Experimental Behavior of Concrete Filled Steel Deck Diaphragms" Personal Communication, Virginia Tech, Blacksburg, VA.

Avellaneda-Ramirez, R., Eatherton, M.R., Easterling, W.S., Schafer, B., Hajjar, J.F., (2022) "Stiffness of Concrete Filled Steel Deck Diaphragms" *Cold-Formed Steel Research Consortium (CFSRC R-2022-01), 1-62*.

Bentz, E. (2001) *Response-2000, Shell-2000, Triax-2000, Membrane-2000 User Manual.*

Bentz, E., Vecchio, F., and Collins, M. (2006) "Simplified Modified Compression Field Theory for Calculating Shear Strength of Reinforced Concrete Elements" *ACI Structural Journal,* 0(0), 1-11.

del Rey Castillo, E., Ravi, K., and Smith, S. (2019) "Floor Diaphragm Strengthening of Concrete Structures with FRP," *Proceedings, 2019 Concrete for Life, Concrete NZ Conference,* Auckland, NZ, 13-14 September 2019.

Dhakal, P., Hutton, H., Eatherton, M.R., and Jacques, E. (2022) "Workshop Report: Development of FRP Retrofit Guidelines for Deficient Reinforced Concrete Horizontal Lateral Force Resisting Systems." *VTechWorks,* 0(0), 1-33.

Ellsworth, D. (2013) *Memo regard FRP Bond Pull-out Test – Wilson High School*, Personal Communication, Contech Services Inc., Vancouver, WA, 10 pages.

Erickson, B. (2019) "*IAPMO UES EC038 Revision Recommendation*", Simpson Strong-Tie. Accessed from: https://www.iapmo.org/media/21962/ec_038-revision-recommendations-from-simpson-strong-tie.pdf on July 11, 2020.

FEMA (2006) *Techniques for the seismic rehabilitation of existing buildings (FEMA 547)*, Published by the Federal Emergency Management Agency.

FEMA (2007) *Interim testing protocols for determining the seismic performance characteristics of structural and nonstructural components (FEMA 461)*, Published by the Federal Emergency Management Agency.

FEMA (2009) *Quantification of Building Seismic Performance Factors (FEMA P695)*, Published by the Federal Emergency Management Agency.

Fyfe (2022) *Tyfo SCH Composite Anchors*, Published by FyfeFRP.

Fyfe (2022a) *Tyfo SCH-11UP*, Published by FyfeFRP.

Fyfe (2022b) *Tyfo SEH-51A*, Published by FyfeFRP.

Harries, K.A., and Witt, S. (2019) "*Comments on EC-038 Evaluation criteria for diaphragm strengthening using fiber reinforced polymers from ACI 440F*". Accessed from: http://www.iapmoes.org/media/21966/ec_038-2019-aci-440f.pdf on August 26, 2019

IAPMO (2019) *Evaluation Criteria for Diaphragm Strengthening Using Fiber Reinforced Polymers* (IAPMO EC038), Published by the International Association of Plumbing and Mechanical Officials

Khalifa, A., Gold, W.J., Nanni, A., Abdel-Aziz, M.I. (1998) "Contribution of Externally Bonded FRP to Shear Capacity of RC Flexural Members". *Journal of Composites for Construction*, 2(4), 195-202.

MacFarlane, E.R, and Gold, W.J. (2016) *A Guide to the Use of Fiber Reinforced Polymers for Strengthening Department of Energy Facilities*, Report LA-UR-16-26728, Published by the U.S. Department of Energy, 66 pg.

Monti, G., and Liotta, M.A. (2005) "FRP-strengthening in shear: Tests and design equations", ACI Special Publication SP-230, *International Symposium on Fiber-Reinforced Polymer Reinforcement for Reinforced Concrete Structures, FRPRCS 2005,* American Concrete Institute, pp. 543-562.

Nakashima, M., Huang, T., and Lu, L.-W. (1981) "Seismic Resistance Characteristics of Reinforced Concrete Beam-Supported Floor Slabs in Building Structures." *Fritz Laboratory Reports,* Bethlehem, Pennsylvania.

Ormeno, M., Jing, J., Rogers, R., and del Rey Castillo, E. (2019) "Capacity of diaphragm strengthened with FRP: comparison between ACI 440.2R and in-situ tests," *Proceedings, 2019 Pacific Conference on Earthquake Engineering, New Zealand Society for Earthquake Engineering,* Auckland, NZ, 4–6 April 2019.

Pincheira, J.A., Parra-Montesinos, G.J., Wang, C.K., and Salmon, C. (2018) *Reinforced Concrete Design,* Oxford University Press, 9th Edition.

Priestly, M.J.N, and Park, R. (1987) "Strength and Ductility of Concrete Bridge Columns Under Seismic Loading", *ACI Structural Journal.* 61-76.

Rosenboom, O.A., and Kehoe, B.E. (2009) "CFRP seismic collector for concrete diaphragms", *Proceedings, 9th International Conference on Fiber Reinforced Polymer Reinforcement for Reinforced Concrete Structures (FRPRCS9),* Sydney, Australia, 13-15 July, 2009.

Rosenboom, O.A., Paret, T.F., Corbeen, K. (2017) "Seismic strengthening of a 19th century banking template, 16th World Conference on Earthquake" *Proceedings, The 16th World Conference on Earthquake Engineering (16WCEE 2017),* Santiago Chile, 9-13 January 2017.

Simpson Strong-Tie (2022a) *CSS V-Wrap C100HM,* Published by Simpson Strong-Tie Company.

Simpson Strong-Tie (2022b) *CSS V-Wrap C200HM,* Published by Simpson Strong-Tie Company.

Simpson Strong-Tie (2022) *CSS V-Wrap HMCA,* Published by Simpson Strong-Tie Company.

Appendix A. Specimen Details

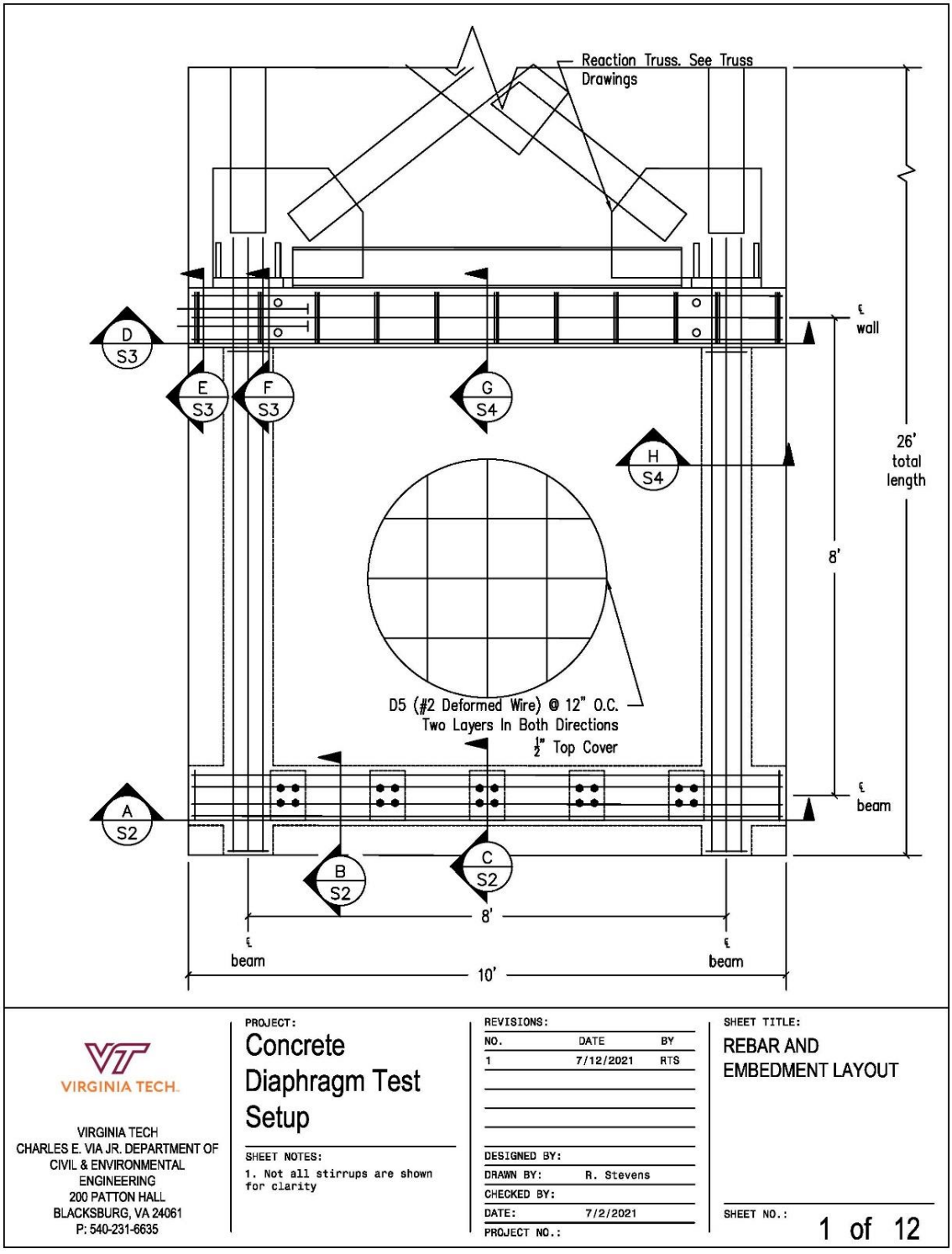

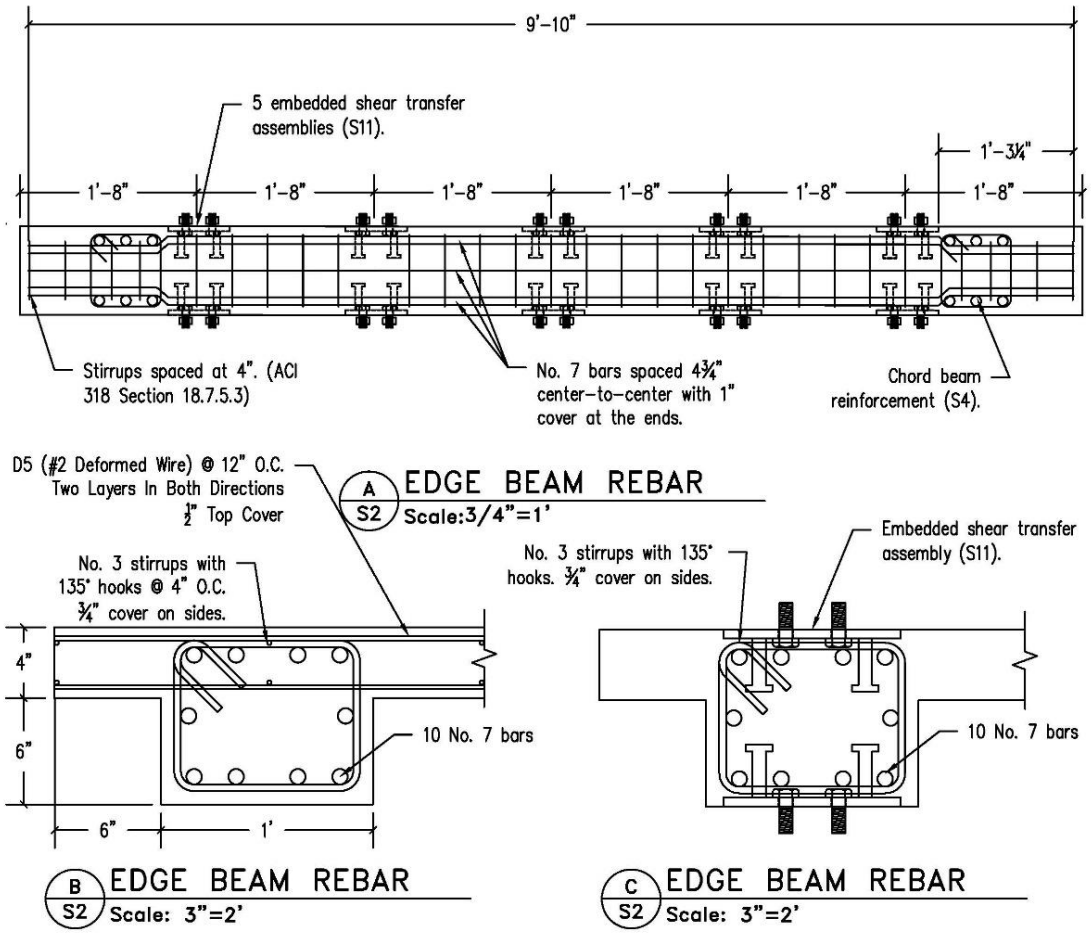

VIRGINIA TECH

VIRGINIA TECH
CHARLES E. VIA JR. DEPARTMENT OF CIVIL & ENVIRONMENTAL ENGINEERING
200 PATTON HALL
BLACKSBURG, VA 24061
P: 540-231-6635

PROJECT:
Concrete Diaphragm Test Setup

SHEET NOTES:

REVISIONS:

NO.	DATE	BY
1	7/12/2021	RTS
2	7/14/2021	RTS

DESIGNED BY:
DRAWN BY: R. Stevens
CHECKED BY:
DATE: 7/1/2021
PROJECT NO.:

SHEET TITLE:
SECTION VIEWS

SHEET NO.: 2 of 12

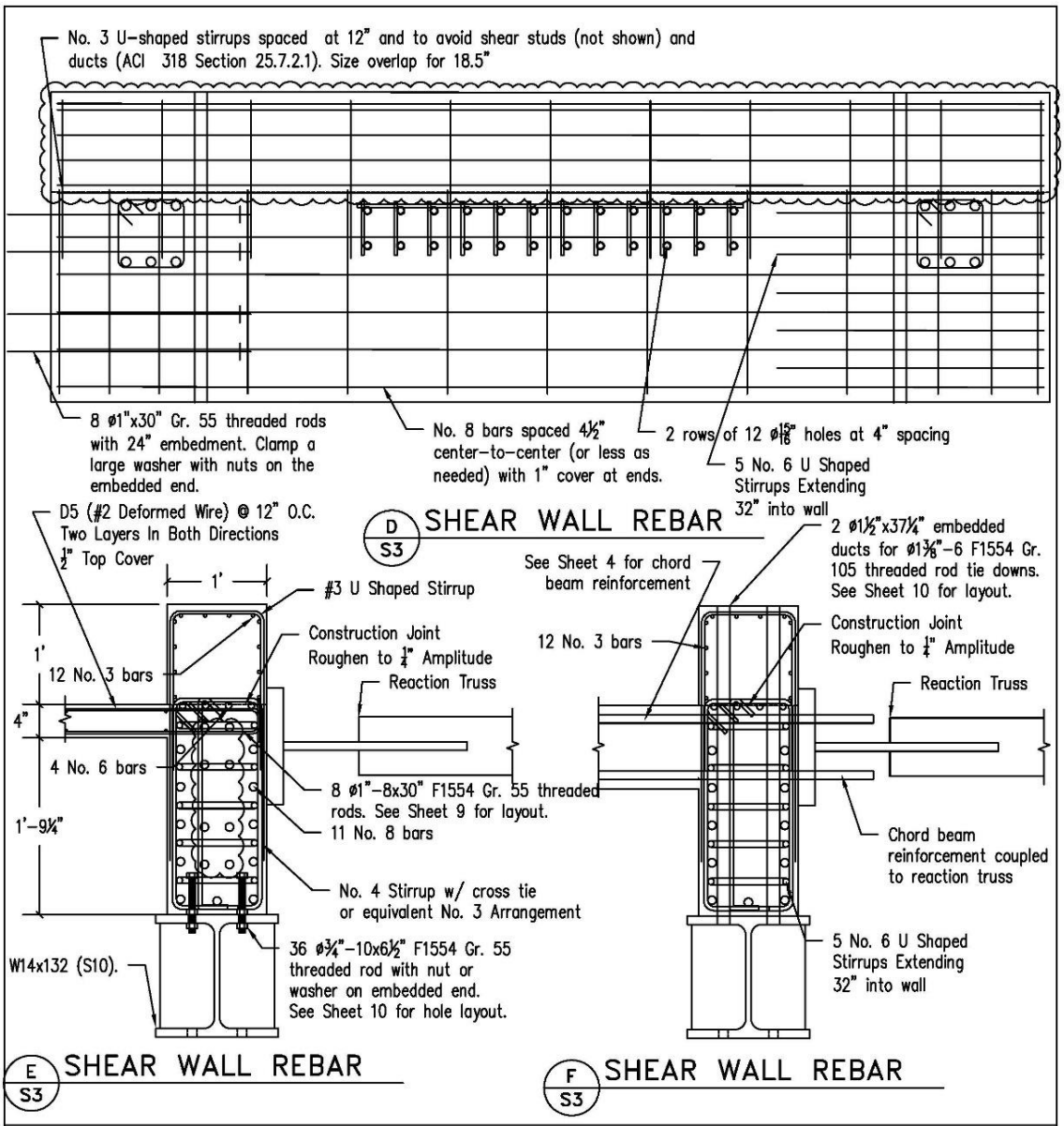

VIRGINIA TECH

VIRGINIA TECH
CHARLES E. VIA JR. DEPARTMENT OF CIVIL & ENVIRONMENTAL ENGINEERING
200 PATTON HALL
BLACKSBURG, VA 24061
P: 540-231-6635

PROJECT:
Concrete Diaphragm Test Setup

SHEET NOTES:
1. Scale is 3/4"=1'

REVISIONS:

NO.	DATE	BY
1	7/8/2021	RTS
2	7/14/2021	RTS

DESIGNED BY:
DRAWN BY: R. Stevens
CHECKED BY:
DATE: 7/1/2021
PROJECT NO.:

SHEET TITLE:
SECTION VIEWS

SHEET NO.: 3 of 12

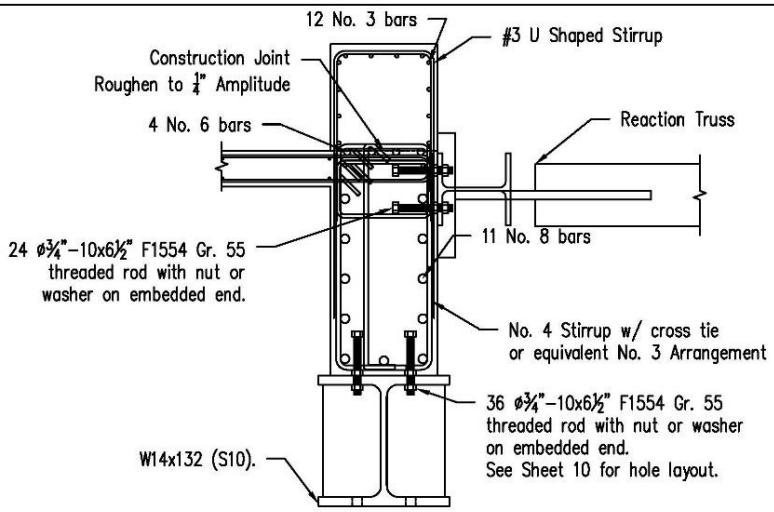

G/S4 SHEAR WALL REBAR
Scale:3/4"=1'

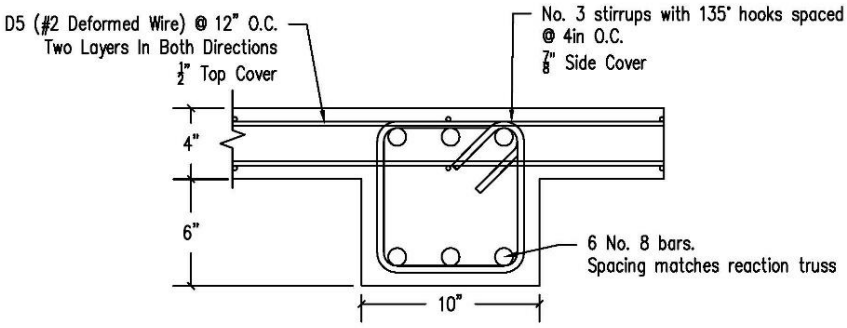

H/S4 CHORD BEAM REBAR
Scale: 3"=2'

VIRGINIA TECH
VIRGINIA TECH
CHARLES E. VIA JR. DEPARTMENT OF
CIVIL & ENVIRONMENTAL
ENGINEERING
200 PATTON HALL
BLACKSBURG, VA 24061
P: 540-231-6635

PROJECT:
Concrete Diaphragm Test Setup

SHEET NOTES:

REVISIONS:

NO.	DATE	BY
1	7/8/2021	RTS
2	7/14/2021	RTS

DESIGNED BY:
DRAWN BY: R. Stevens
CHECKED BY:
DATE: 7/2/2021
PROJECT NO.:

SHEET TITLE:
SECTION VIEWS

SHEET NO.: 4 of 12

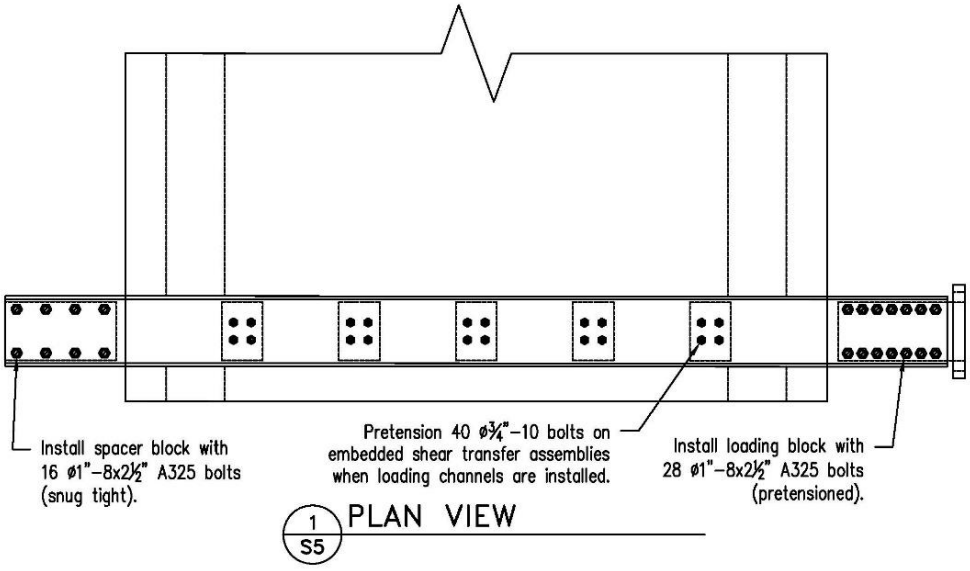

1/S5 PLAN VIEW

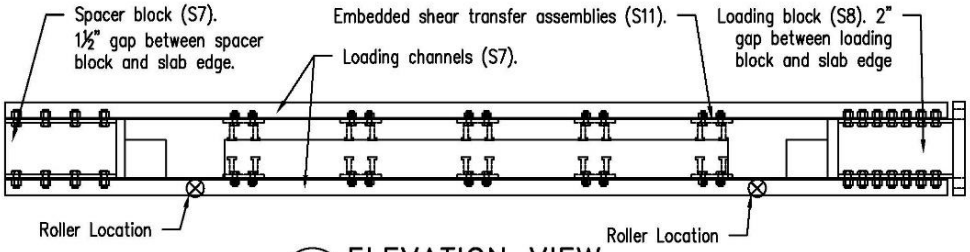

2/S5 ELEVATION VIEW

VIRGINIA TECH

VIRGINIA TECH
CHARLES E. VIA JR. DEPARTMENT OF
CIVIL & ENVIRONMENTAL
ENGINEERING
200 PATTON HALL
BLACKSBURG, VA 24061
P: 540-231-6635

PROJECT:
Concrete Diaphragm Test Setup

SHEET NOTES:
1. Scale is 1/2"=1'

REVISIONS:

NO.	DATE	BY
1	7/12/2021	RTS
2	7/14/2021	RTS

DESIGNED BY:
DRAWN BY: R. Stevens
CHECKED BY:
DATE: 7/2/2021
PROJECT NO.:

SHEET TITLE:
LOADING CHANNEL INSTALLATION

SHEET NO.: 5 of 12

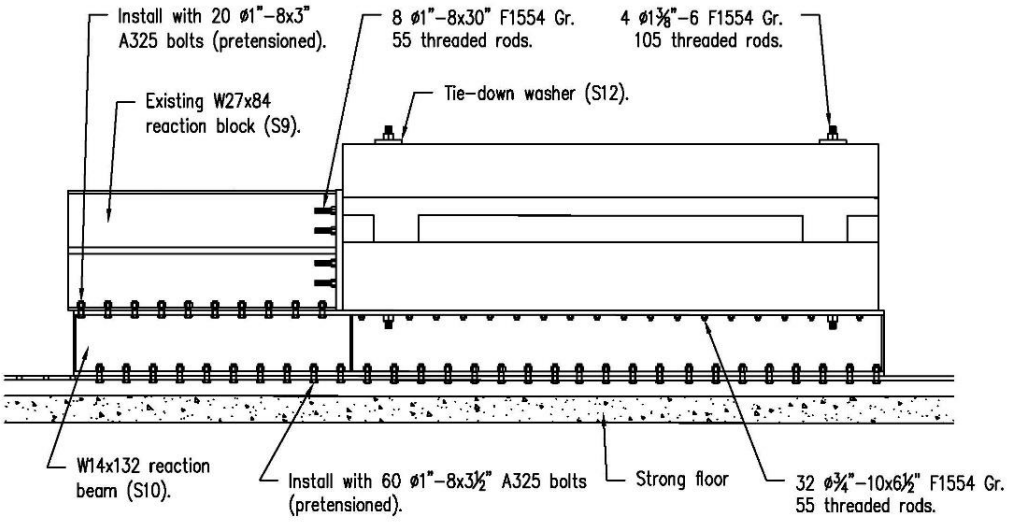

VIRGINIA TECH

VIRGINIA TECH
CHARLES E. VIA JR. DEPARTMENT OF CIVIL & ENVIRONMENTAL ENGINEERING
200 PATTON HALL
BLACKSBURG, VA 24061
P: 540-231-6635

PROJECT:
Concrete Diaphragm Test Setup

SHEET NOTES:
1. Scale is 3/8"=1'

REVISIONS:

NO.	DATE	BY
1	7/8/2021	RTS
2	7/14/2021	RTS

DESIGNED BY:
DRAWN BY: R. Stevens
CHECKED BY:
DATE: 7/2/2021
PROJECT NO.:

SHEET TITLE:
REACTION ASSEMBLY

SHEET NO.: 6 of 12

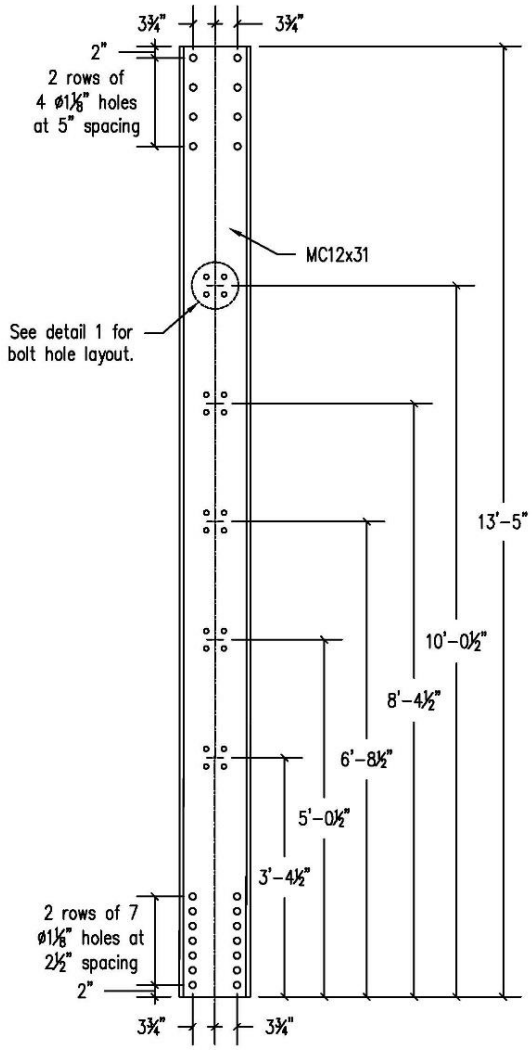

3 S7 LOADING CHANNEL (QTY: 2)
Scale:1/2"=1'

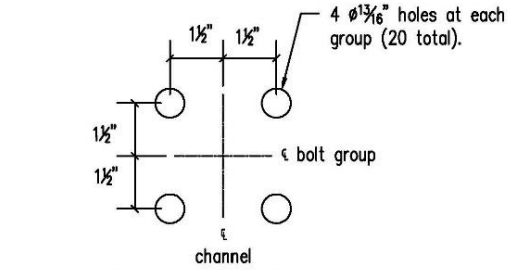

1 S7 HOLE LAYOUT
Scale: 3"=1'

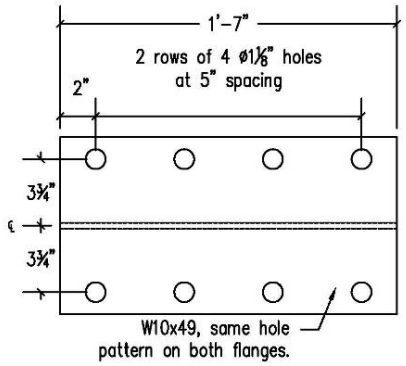

2 S7 SPACER BLOCK (QTY: 1)
Scale: 3"=2'

VIRGINIA TECH

VIRGINIA TECH
CHARLES E. VIA JR. DEPARTMENT OF
CIVIL & ENVIRONMENTAL
ENGINEERING
200 PATTON HALL
BLACKSBURG, VA 24061
P: 540-231-6635

PROJECT:
Concrete Diaphragm Test Setup

SHEET NOTES:

REVISIONS:

NO.	DATE	BY
1	7/14/2021	RTS

DESIGNED BY:
DRAWN BY: R. Stevens
CHECKED BY:
DATE: 7/1/2021
PROJECT NO.:

SHEET TITLE:
LOADING CHANNEL AND SPACER BLOCK

SHEET NO.: 7 of 12

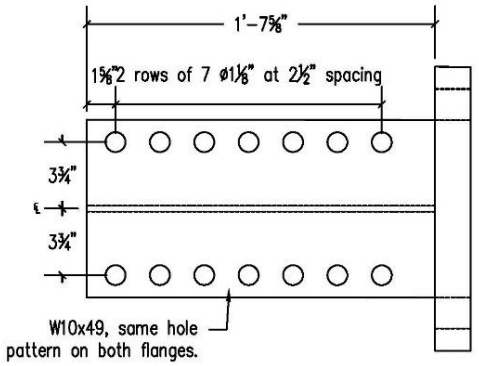

1 S8 LOADING BLOCK

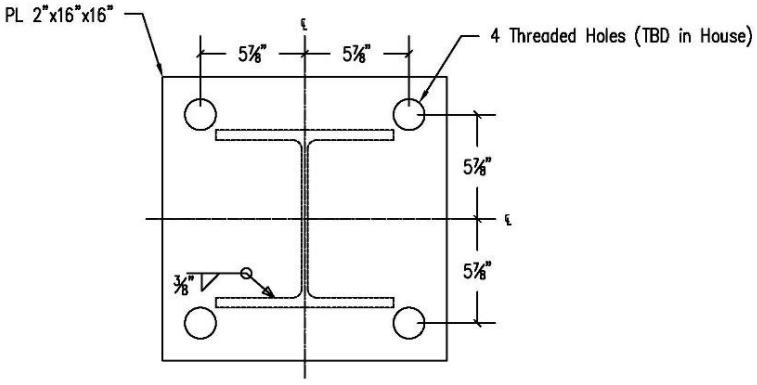

2 S8 END-PLATE

VIRGINIA TECH

VIRGINIA TECH
CHARLES E. VIA JR. DEPARTMENT OF CIVIL & ENVIRONMENTAL ENGINEERING
200 PATTON HALL
BLACKSBURG, VA 24061
P: 540-231-6635

PROJECT:
Concrete Diaphragm Test Setup

SHEET NOTES:
1. Scale is 1 1/2"=1'
2. W10x49 is centered on the end-plate

REVISIONS:

NO.	DATE	BY
1	7/8/2021	RTS

DESIGNED BY:
DRAWN BY: R. Stevens
CHECKED BY:
DATE: 7/1/2021
PROJECT NO.:

SHEET TITLE:
LOADING BLOCK (QTY: 1)

SHEET NO.: 8 of 12

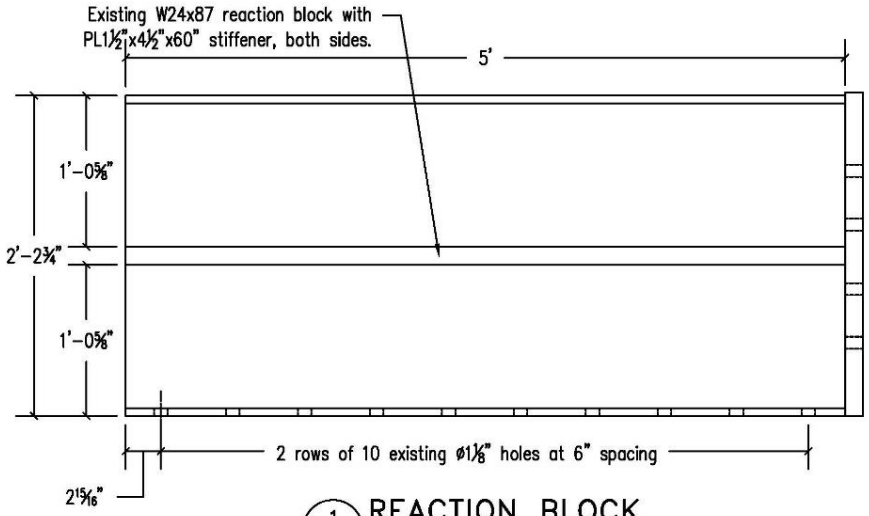

1 S9 REACTION BLOCK

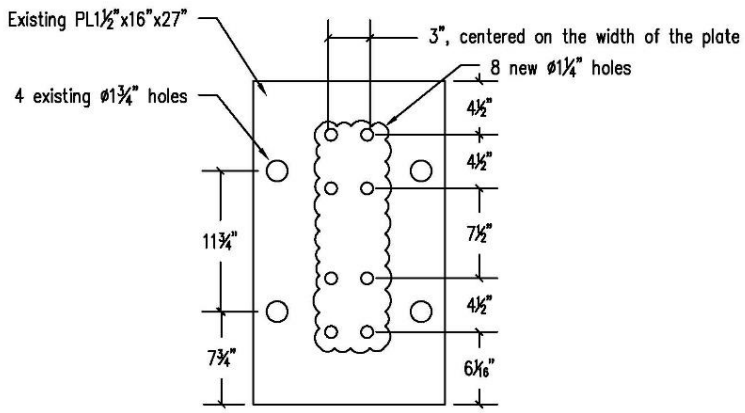

2 S9 NEW HOLE LAYOUT

VIRGINIA TECH

VIRGINIA TECH
CHARLES E. VIA JR. DEPARTMENT OF CIVIL & ENVIRONMENTAL ENGINEERING
200 PATTON HALL
BLACKSBURG, VA 24061
P: 540-231-6635

PROJECT:
Concrete Diaphragm Test Setup

SHEET NOTES:
1. Scale is 1"=1'
2. Work to be done by VT

REVISIONS:

NO.	DATE	BY
1	7/8/2021	RTS

DESIGNED BY:
DRAWN BY: R. Stevens
CHECKED BY:
DATE: 6/28/2021
PROJECT NO.:

SHEET TITLE:
END REACTION BLOCK (QTY: 2)

SHEET NO.: 9 of 12

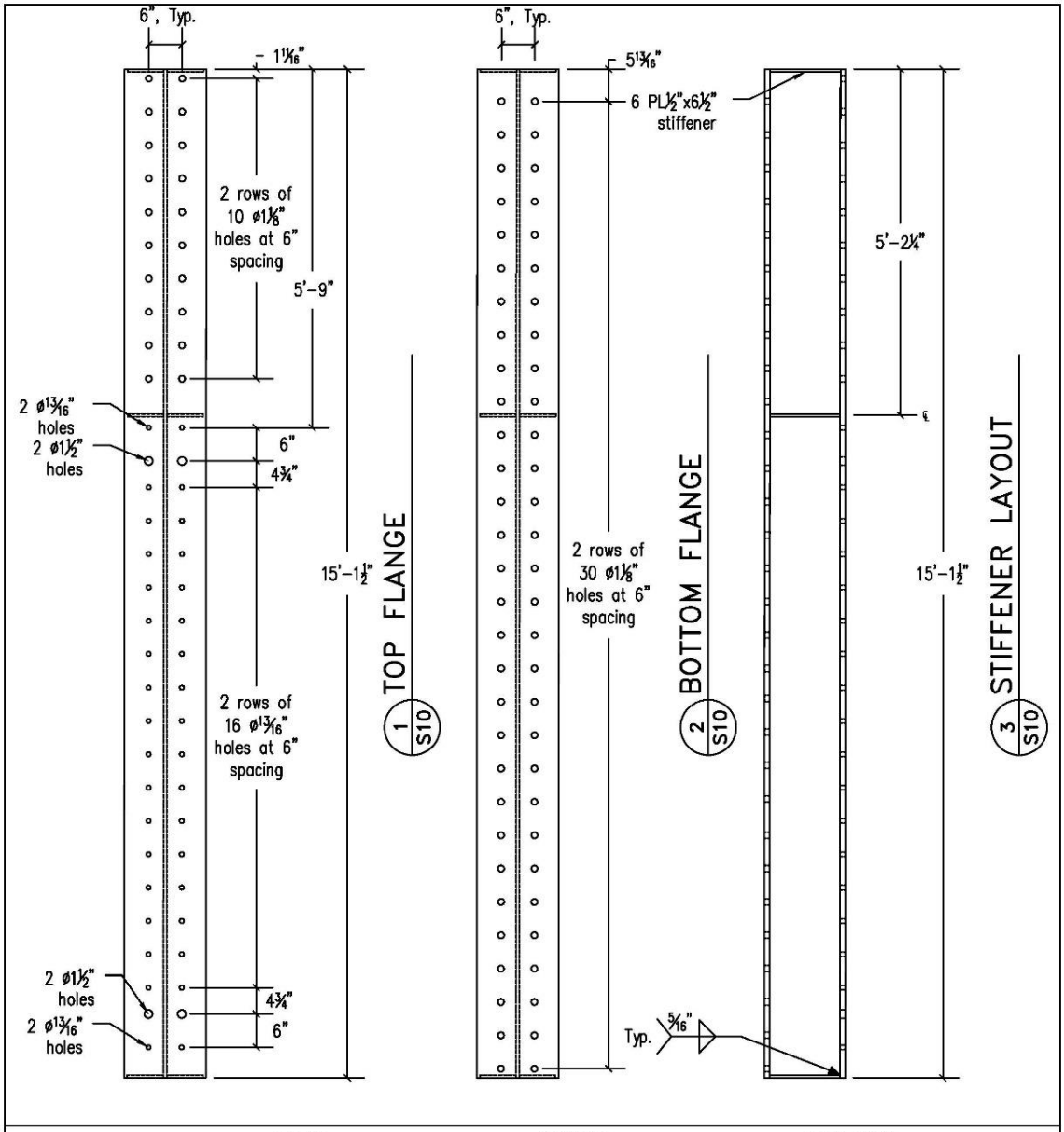

VIRGINIA TECH

VIRGINIA TECH
CHARLES E. VIA JR. DEPARTMENT OF CIVIL & ENVIRONMENTAL ENGINEERING
200 PATTON HALL
BLACKSBURG, VA 24061
P: 540-231-6635

PROJECT:
Concrete Diaphragm Test Setup

SHEET NOTES:
1. Scale is 1/2"=1'
2. The two lines of bolts are centered across the flange width.

REVISIONS:

NO.	DATE	BY
1	7/8/2021	RTS

DESIGNED BY:
DRAWN BY: R. Stevens
CHECKED BY:
DATE: 7/1/2021
PROJECT NO.:

SHEET TITLE:
BEARING BEAM (QTY: 2)

SHEET NO.: 10 of 12

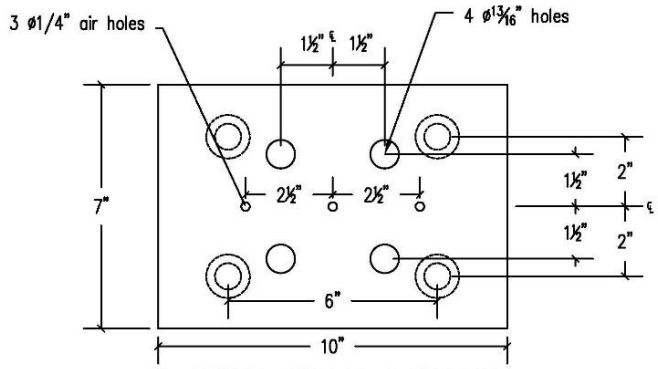

1 S11 BOLT HOLE LAYOUT

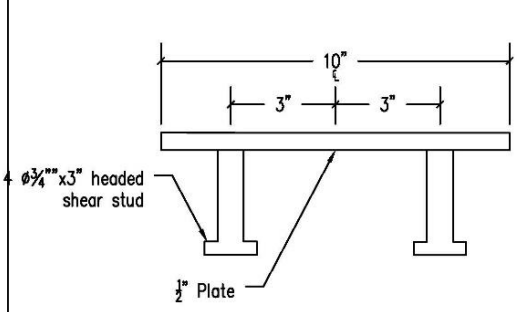

2 S11 SHEAR STUD LAYOUT

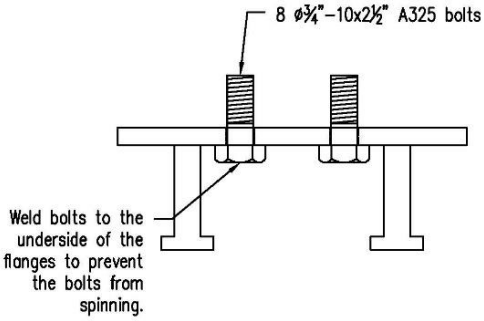

3 S11 BOLT INSTALLATION

VIRGINIA TECH

VIRGINIA TECH
CHARLES E. VIA JR. DEPARTMENT OF CIVIL & ENVIRONMENTAL ENGINEERING
200 PATTON HALL
BLACKSBURG, VA 24061
P: 540-231-6635

PROJECT:
Concrete Diaphragm Test Setup

SHEET NOTES:
1. Scale is 3"=1'

REVISIONS:

NO.	DATE	BY
1	7/12/2021	RTS
2	7/14/2021	RTS

DESIGNED BY:
DRAWN BY: R. Stevens
CHECKED BY:
DATE: 7/2/2021
PROJECT NO.:

SHEET TITLE:
SHEAR TRANSFER ASSEMBLY
(QTY: 10 PER SPECIMEN)

SHEET NO.: 11 of 12

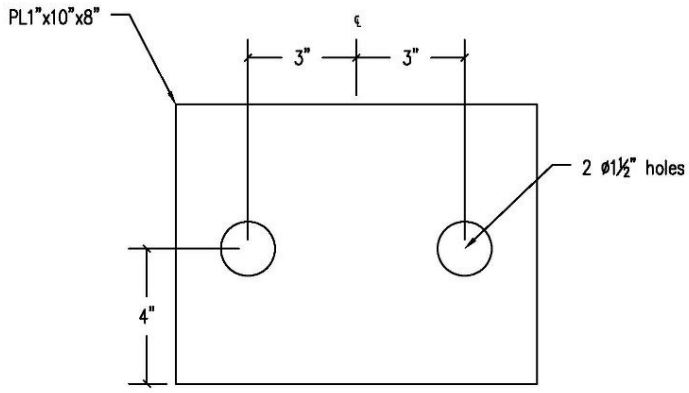

1/S12 HOLE LAYOUT

VIRGINIA TECH

VIRGINIA TECH
CHARLES E. VIA JR. DEPARTMENT OF CIVIL & ENVIRONMENTAL ENGINEERING
200 PATTON HALL
BLACKSBURG, VA 24061
P: 540-231-6635

PROJECT:
Concrete Diaphragm Test Setup

SHEET NOTES:
1. Scale is 3"=1'

REVISIONS:

NO.	DATE	BY

DESIGNED BY:
DRAWN BY: R. Stevens
CHECKED BY:
DATE: 7/12/2021
PROJECT NO.:

SHEET TITLE:
TIE-DOWN WASHER (QTY: 2)

SHEET NO.: 12 of 12

Appendix B. Design of Testing Setup

Design Calcs for Concrete Diaphragm Setup

Design Forces

$P_{act} := 330\ kip$

$V_u := 2 \cdot P_{act} = 660\ kip$

Calculate how many 1-3/8 in. diameter F1554 Gr. 105 hold downs are needed. The floor beam is a W14x120, which has a depth of $d_{beam} := 14.5\ in$, and the centerline of the actuator is $34.5\ in$ above the strong floor.

$T_u := \frac{V_u \cdot (34.5\ in - d_{beam})}{96\ in} = 138\ kip$

$A_{thbar} := 1.48\ in^2$

$F_{y.thbar} := 105\ ksi$

$n_r := \frac{T_u}{A_{thbar} \cdot F_{y.thbar}} = 0.885$

Round up the number of bars to 2 at each end for symmetry.

Determine if bearing stiffeners are needed in the floor beam to resist the tension force from the hold down bars. Check flange local bending.

$\phi := 0.90$

$F_{y.flange} := 50\ ksi$

$t_f := 0.94\ in$

$\phi R_n := \phi \cdot 6.25 \cdot F_{y.flange} \cdot t_f^{\ 2} = 249\ kip$ Eq. J10-1 Greater than $T_u = 138\ kip$, OKAY

Check web local yielding in tension. On one end of the beam, the tension force is applied at distance from the end of the beam that is less than the depth of the floor beam.

$\phi := 1.0$

$F_{y.web} := 50\ ksi$

$t_w := 0.59\ in$

$k := 1.31\ in$

$l_b := 2.188\ in$ Width across the flats of a nut for a 1 3/8 in. threaded rod

$\phi R_n := \phi \cdot F_{y.web} \cdot t_w \cdot (2.5 \cdot k + l_b) = 161\ \textit{kip}$ Eq. J10-3 Greater than $T_u = 138\ \textit{kip}$, OKAY

Check web local yielding for compression. The bearing length is assumed to be the width of the chord beam. In reality, the compressive force would be distributed over a longer length of the shear wall. The centroid of this bearing length is at a distance from the end of the bearing beam ($14.75\ in$) that is greater than the full nominal depth of the member.

$l_b := 10\ \textit{in}$

$\phi R_n := \phi \cdot F_{y.web} \cdot t_w \cdot (5 \cdot k + l_b) = 488\ \textit{kip}$ Eq. J10-2 Greater than $T_u = 138\ \textit{kip}$, OKAY

If the bearing length is assumed to be the distance from the inside face of the chord beam to the end of the shear wall, then the centroid of the bearing length is at a distance from the member end ($11.25\ in$) that is less than the full nominal depth of the member.

$l_b := 17\ \textit{in}$

$\phi R_n := \phi \cdot F_{y.web} \cdot t_w \cdot (2.5 \cdot k + l_b) = 598\ \textit{kip}$ Eq. J10-3 Greater than $T_u = 138\ \textit{kip}$, OKAY

Check web local crippling. The same assumption about bearing length applies. The centroid of this bearing length is at a distance from the end of the bearing beam that is greater than half of the full nominal depth of the member.

$\phi := 0.75$

$l_b := 10\ \textit{in}$

$E := 29000\ \textit{ksi}$

$Q_f := 1.0$

$$\phi R_n := \phi \cdot 0.80 \cdot t_w^{\,2} \cdot \left(1 + 3 \cdot \left(\frac{l_b}{d_{beam}}\right) \cdot \left(\frac{t_w}{t_f}\right)^{1.5}\right) \cdot \sqrt{\frac{E \cdot F_{y.web} \cdot t_f}{t_w}} \cdot Q_f = 644\ \textit{kip}$$ Eq. J10-4

Greater than $T_u = 138\ \textit{kip}$, OKAY

Check web sidesway buckling.

$\phi := 0.85$

$L_b := 10\ \textit{ft}$

$h := 10\ \textit{in}$

$b_f := 14.7\ \textit{in}$

$$\frac{\frac{h}{t_w}}{\frac{L_b}{b_f}} = 2.076$$

$C_r := 960000\ \textbf{ksi}$

$$\phi R_n := \phi \cdot \frac{C_r \cdot {t_w}^3 \cdot t_f}{h^2} \cdot \left(1 + 0.4 \cdot \left(\frac{\frac{h}{t_w}}{\frac{L_b}{b_f}}\right)^3\right) = \left(7.22 \cdot 10^3\right)\ \textbf{kip} \quad \text{Eq. J10-6}$$

Greater than $T_u = 138\ \textbf{kip}$, OKAY

Check web compression buckling.

$\phi := 0.90$

$$\phi R_n := \phi \cdot \left(\frac{24 \cdot {t_w}^3 \cdot \sqrt{E \cdot F_{y.web}}}{h}\right) \cdot Q_f = 534\ \textbf{kip} \quad \text{Eq. J10-8}$$

Greater than $T_u = 138\ \textbf{kip}$, OKAY

No bearing stiffeners are required, but stiffeners will be provided at the tie down points and at the end of the reaction block for peace of mind.

Calculate the slip-critical capacity of the floor beam-to-strong floor connection, assuming the six bolts nearest to the hold down bars transfer the tension force. The tension force at the strong floor is

$$T_{u.sf} := \frac{V_u \cdot 34.5\ \textbf{in}}{96\ \textbf{in}} = 237\ \textbf{kip}$$

$\phi := 1.0$

$T_b := 51\ \textbf{kip}$ Table J3.1, 1 in. A325 bolts

$n_b := 6$

$D_u := 1.13$

$$k_{sc} := 1 - \frac{T_{u.sf}}{D_u \cdot T_b \cdot n_b} = 0.314 \quad \text{Eq. J3-5a}$$

$\phi R_{n.bolt} := 17.3\ \textbf{kip}$ AISCM Table 7.3, 1 in. A325 bolts

$\phi R_{n.beam} := 56 \cdot \phi R_{n.bolt} + \phi R_{n.bolt} \cdot n_b \cdot k_{sc} = 1001\ \textbf{kip}$ Greater than $V_u = 660\ \textbf{kip}$, OKAY

Check the tension capacity of the six bolts nearest the hold downs.

$A_{bolt} := 0.785\ \textbf{in}^2$

$f_{bolt} := \frac{T_{u.sf}}{n_b \cdot A_{bolt}} = 50.4\ \textbf{ksi}$

$\frac{f_{bolt}}{90\ \textbf{ksi}} = 0.56$

This is greater than 0.3, so combined shear and tension must be checked using Section J3.7.

$\phi := 0.75$

$F_{nt} := 90\ \textbf{ksi}$ AISC Table J3.2

$F_{nv} := 54\ \textbf{ksi}$ AISC Table J3.2

$f_{rv} := \frac{V_u}{61 \cdot A_{bolt}} = 13.8\ \textbf{ksi}$ $< F_{nv}$

$F'_{nt} := 1.3 \cdot F_{nt} - \frac{F_{nt}}{\phi \cdot F_{nv}} \cdot f_{rv} = 86.4\ \textbf{ksi}$ $< F_{nt}$ Eq. J3-3a

$\phi R_{n.boltT} := \phi \cdot F'_{nt} \cdot A_{bolt} = 50.9\ \textbf{kip}$

The combined tensile strength of the 6 bolts in combined shear and tension is

$\phi T_n := n_b \cdot \phi R_{n.boltT} = 305\ \textbf{kip}$ Greater than $T_{u.sf} = 237\ \textbf{kip}$, OKAY

Calculate how many shear studs are needed on the top flange to transfer shear into the floor beam. For a 3/4 in. diameter studs, $Q_n := 21.5\ \textbf{kip}$ from AISCM Table 3-21. Assume a 3/4 in. bolt has the same capacity.

$N := \frac{V_u}{Q_n} = 31$ Round up to 32 in 2 rows

Calculate the slip-critical capacity of the connection between the floorbeam and the end reaction.

$\phi R_n := 17.3\ \textbf{kip}$ AISCM Table 7.3, 1 in. A325 bolts

$V_n := \phi R_n \cdot 20 = 346\ \textbf{kip}$

Calculate the number of 1 in. diameter threaded rods required to transfer this force.

$d_{bar} := 1\ in$

$F_{y.bar} := 55\ ksi$

$$n_{bar} := \frac{V_n}{F_{y.bar} \cdot \frac{\pi \cdot d_{bar}^{\ 2}}{4}} = 8$$

8 threaded rods are needed to transfer the force.

Calculate the required development length of the threaded rods, assuming a large washer and nut is used on the embedded end.

$\psi_e := 1.0$

$f'_c := 4000\ psi$

$$l_{dt} := \left(\frac{0.016 \cdot \psi_e \cdot F_{y.bar}}{\sqrt{4000\ psi}} \right) \cdot d_{bar} = 13.9\ in$$

Round the development length up to $24\ in$. to make it a round number and put the ends of the bars past the slab beams.

Design the loading assembly. Calculate how many 1" A325 bolts are needed to transfer the actuator force into the loading channels.

$\phi r_n := 17.3\ kip$ AISCM Table 7.3

$n_b := \frac{P_{act}}{\phi r_n} = 19$ Round up to at least 20 bolts.

Assume a W10x49 loading block with 2 rows of 7 bolts on each flange and 2 C12x20.7 channels. $n_b := 4 \cdot 7 = 28$ bolts total. This is enough bolts for sufficient slip-critical capacity.

$b_f := 10\ in$ $d := 10\ in$ $t_{wch} := 0.282\ in$

$t_f := 0.56\ in$ $t_w := 0.34\ in$ $d_{ch} := 12\ in$

$A := 14.4\ in^2$ $A_{ch} := 6.08\ in^2$

$F_y := 55\ ksi$

$F_u := 65\ ksi$

Calculate the strength of the bolted connection if there is slip between the loading channels and loading block.

Since the channel has the thinner web thickness, it will control the capacity of the connection when considering bolt limit states.

Calculate the bearing strength of a bolt on the loading channel.

$d_b := 1.0\ \textbf{in}$

$\phi := 0.75$

$\phi r_{n.2} := \phi \cdot 2.4 \cdot d_b \cdot t_{wch} \cdot F_u = 33\ \textbf{kip}$

Calculate the bolt tearout strength of interior and exterior bolts.

$l_{c1} := 2\ \textbf{in} - \left(d_b + 0.125\ \textbf{in}\right) \cdot 0.5 = 1.438\ \textbf{in}$

$l_{c2} := 2.5\ \textbf{in} - \left(d_b + 0.125\ \textbf{in}\right) = 1.375\ \textbf{in}$

$\phi r_{n.2} := \phi \cdot 1.2 \cdot l_{c1} \cdot t_{wch} \cdot F_u = 23.7\ \textbf{kip}$

$\phi r_{n.3} := \phi \cdot 1.2 \cdot l_{c2} \cdot t_{wch} \cdot F_u = 22.7\ \textbf{kip}$

The capacity of the connection considering bolt limit states is

$\phi R_n := 4 \cdot \phi r_{n.3} + 24 \cdot \phi r_{n.2} = 660\ \textbf{kip}$ Greater than $P_{act} = 330\ \textbf{kip}$, OKAY

Calculate the required edge distance to prevent bolt tearout and reach the full shear capacity of the bolt on the loading block.

$$l_{c.req} := \frac{31.8\ \textbf{kip}}{\phi \cdot 1.2 \cdot t_f \cdot F_u} = 0.971\ \textbf{in}$$

Provide a minimum edge distance of 1 in. to reach the full bolt capacity.

Calculate the capacity of the W10x49 loading block considering tensile yield on the gross section.

$\phi := 0.90$

$F_y := 50\ \textbf{ksi}$

$\phi R_n := \phi \cdot A \cdot F_y = 648\ \textbf{kip}$ Greater than $P_{act} = 330\ \textbf{kip}$, OKAY

Calculate the capacity of the loading block considering tensile rupture on the net section.

$\phi := 0.75$

$U := 1.0$

$A_n := A - 4 \cdot \left(d_b + 0.125\ \textbf{in} + 0.0625\ \textbf{in}\right) \cdot t_f = 11.7\ \textbf{in}^2$

$A_e := A_n \cdot U$

$\phi R_n := \phi \cdot A_e \cdot F_u = 572\ \textbf{kip}$ Greater than $P_{act} = 330\ \textbf{kip}$, OKAY

Calculate the tensile capacity of the loading channels considering tensile yield on the gross section.

$\phi := 0.90$

$\phi R_n := 2 \cdot \phi \cdot A_{ch} \cdot F_y = 547\ \textbf{kip}$ Greater than $P_{act} = 330\ \textbf{kip}$, OKAY

Calculate the tensile capacity of the loading channels considering tensile rupture on the net section considering shear lag.

$\phi := 0.75$

$x := 0.698\ \textbf{in}$

$L := 15.125\ \textbf{in}$

$U := 1 - \frac{x}{L} = 0.954$

$A_e := \left(A_{ch} - 2 \cdot t_{wch} \cdot \left(d_b + 0.125\ \textbf{in} + 0.0625\ \textbf{in}\right)\right) \cdot U = 5.16\ \textbf{in}^2$

$\phi P_n := 2 \cdot \phi \cdot F_u \cdot A_e = 503\ \textbf{kip}$ Greater than $P_{act} = 330\ \textbf{kip}$, OKAY

Calculate the length of fillet weld needed to transfer the force from the end-plate to the W-shape.

$t_{eff} := 0.707 \cdot \frac{3}{8}\ \textbf{in} = 0.265\ \textbf{in}$

$\phi := 0.75$

$F_{EXX} := 70\ \textbf{ksi}$

$\theta := 0\ \textbf{rad}$

$F_{nw} := 0.6 \cdot F_{EXX} \cdot \left(1 + 0.5 \cdot \left(\sin\left(\theta\right)\right)^{1.5}\right) = 42\ \textbf{ksi}$

$l_{req} := \frac{P_{act}}{\phi \cdot F_{nw} \cdot t_{eff}} = 39.5\ \textbf{in}$

The perimeter of the W-shape, minus the flange tips and the fillets is $52\ in$.

If the total length is used, the capacity of the fillet weld is

$\phi R_n := \phi \cdot F_{nw} \cdot t_{eff} \cdot 52\ in = 434\ kip$ Greater than $P_{act} = 330\ kip$, OKAY

Calculate the shear rupture strength of the base metal at the end-plate weld.

$A_{nv} := 0.3125\ in \cdot 52\ in = 16.3\ in^2$

$\phi := 0.75$

$\phi R_n := \phi \cdot 0.60 \cdot F_u \cdot A_{nv} = 475\ kip$ Greater than $P_{act} = 330\ kip$, OKAY

Calculate the shear yield strength of the W-shape base metal at the end-plate weld.

$\phi := 1.0$

$\phi R_n := \phi \cdot 0.60 \cdot F_y \cdot A_{nv} = 488\ kip$ Greater than $P_{act} = 330\ kip$, OKAY

Calculate the number of 3/4 in bolts needed for sufficient slip critical capacity.

$\phi r_n := 9.49\ kip$ AISCM Table 7-2

$$n_{b.req} := \frac{P_{act}}{\phi r_n} = 34.8$$

Round up to 35. 40 are provided so this is sufficient.

Calculate the strength of a steel headed stud welded to the web of the embedded shape.

$\phi := 0.65$

$d_{stud} := 0.75\ in$

$$A_{sa} := \frac{\pi \cdot d_{stud}^{\ 2}}{4} = 0.442\ in^2$$

$F_u := 65\ ksi$

$\phi Q_{nv} := \phi \cdot F_u \cdot A_{sa} = 18.7\ kip$

Calculate how many shear studs are needed to transfer the shear force to the concrete.

$$n_s := \frac{P_{act}}{\phi Q_{nv}} = 17.7$$

Round up to 18. 40 are provided so this is sufficient. Minimum length is $4 \cdot d_{stud} = 3\ in$. Minimum spacing is $4 \cdot d_{stud} = 3\ in$ in any direction. Minimum cover is in accordance with ACI

318.

The strength of the loading fixture is controlled by the fillet weld strength, $434\ kip$.

Calculate the required strength of the loading channel accounting for out of plane bending.

$$P := 0.05 \cdot P_{act} = 16.5\ \textbf{kip}$$

The distance from the top roller to the centerline of the nearest chord beam is $23\ in$. The distance from the centerline of the chord beam to the farthest top roller is $119\ in$.

$$M_{max} := \frac{P \cdot (119\ \textbf{in} \cdot 23\ \textbf{in})}{119\ \textbf{in} + 23\ \textbf{in}} = 26.5\ \textbf{kip} \cdot \textbf{ft}$$

The moment of inertia of the combined channels is

$$I_{ch} := 3.86\ \textbf{in}^4$$

$$I_{total} := 2 \cdot \left(I_{ch} + A_{ch} \cdot \left(5\ \textbf{in} + 0.698\ \textbf{in}\right)^2\right) = 403\ \textbf{in}^4$$

$$\sigma := \frac{M_{max} \cdot \left(5\ \textbf{in} + 0.698\ \textbf{in}\right)}{I_{total}} = 4.5\ \textbf{ksi}$$

Design calculations for a cellular loading beam option.

Calculate what area of steel is needed to transfer the actuator force in the cellular beam.

$$A_{s.req} := \frac{P_{act}}{F_y} = 6.6\ \textbf{in}^2$$

Assuming a W10x45 is used, calculate the maximum hole diameter that can be used in the web.

$$A_{W10x45} := 13.3\ \textbf{in}^2$$

$$t_{w.W10x45} := 0.35\ \textbf{in}$$

$$d_{max} := \frac{A_{W10x45} - A_{s.req}}{t_{w.W10x45}} = 19.143\ \textbf{in}$$

This is larger than the depth of the section, so any size hole will work. For simplicity, use a $6\ in$ diameter holes in the web with an $18\ in$ spacing.

Appendix C. Reaction Truss Details

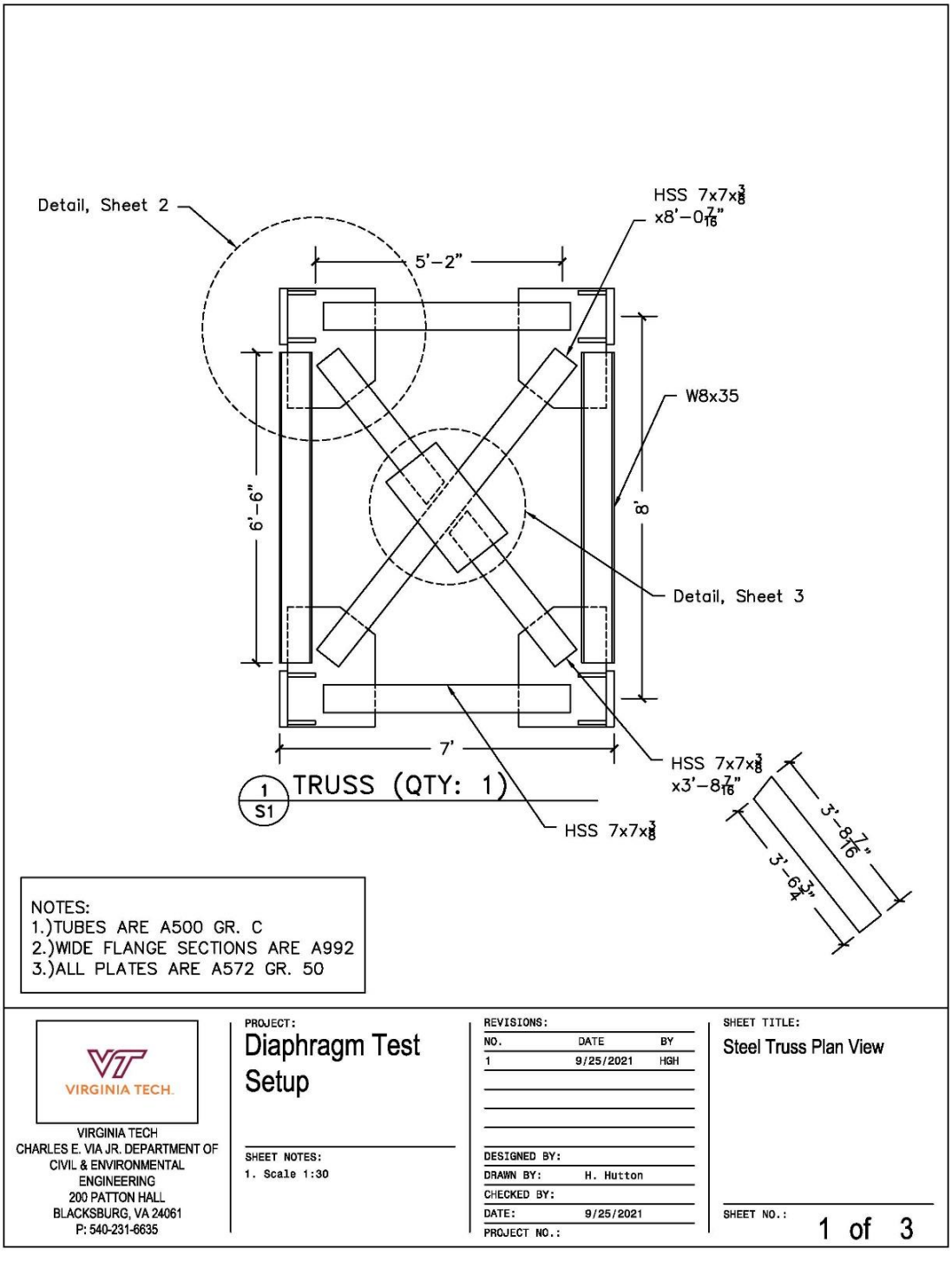

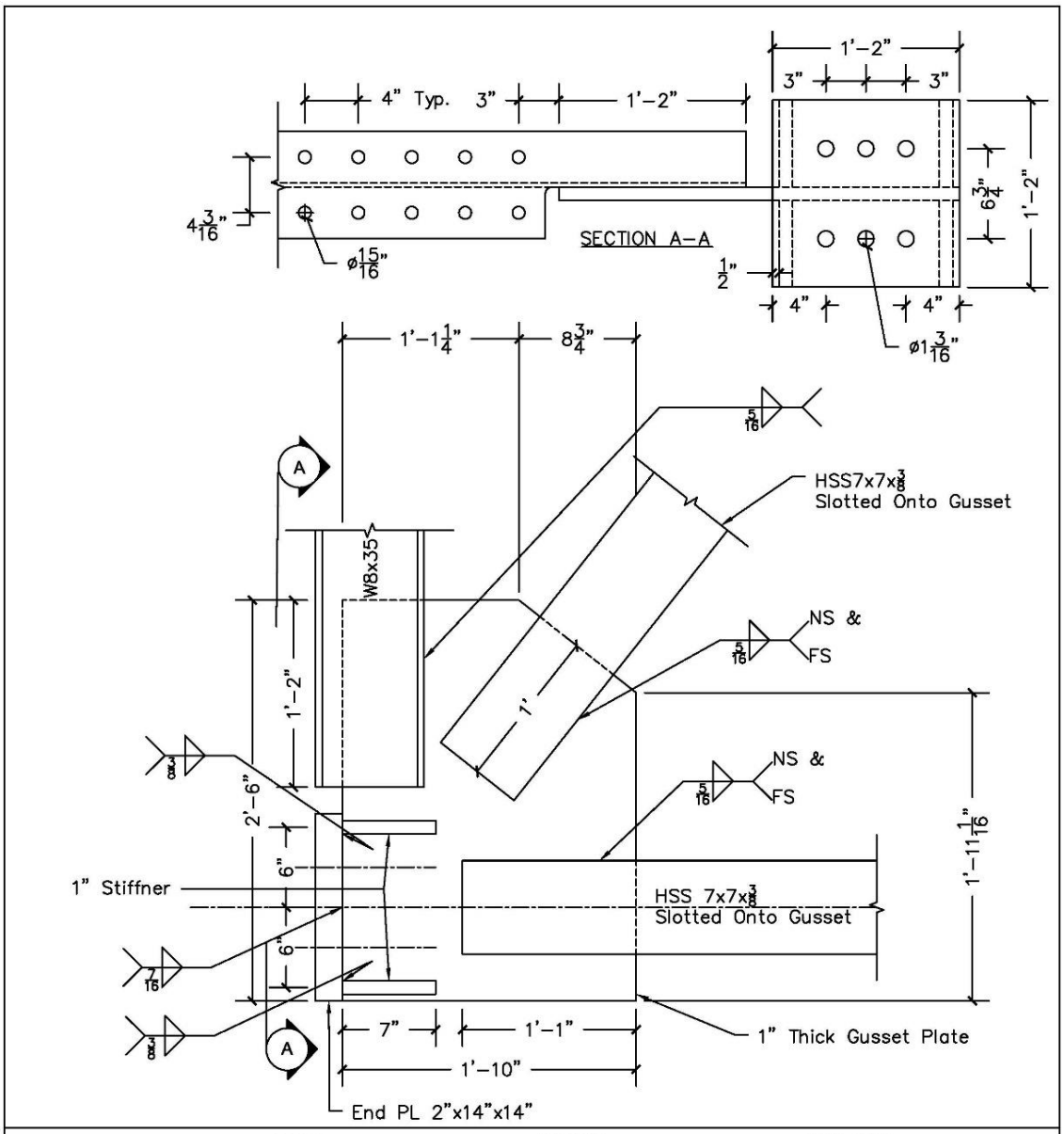

VIRGINIA TECH

VIRGINIA TECH
CHARLES E. VIA JR. DEPARTMENT OF CIVIL & ENVIRONMENTAL ENGINEERING
200 PATTON HALL
BLACKSBURG, VA 24061
P: 540-231-6635

PROJECT:
Diaphragm Test Setup

SHEET NOTES:
1. Scale 1:10

REVISIONS:

NO.	DATE	BY
1	9/25/2021	HGH

DESIGNED BY:
DRAWN BY: H. Hutton
CHECKED BY:
DATE: 9/25/2021
PROJECT NO.:

SHEET TITLE:
Steel Truss Connection Detail 1

SHEET NO.: 2 of 3

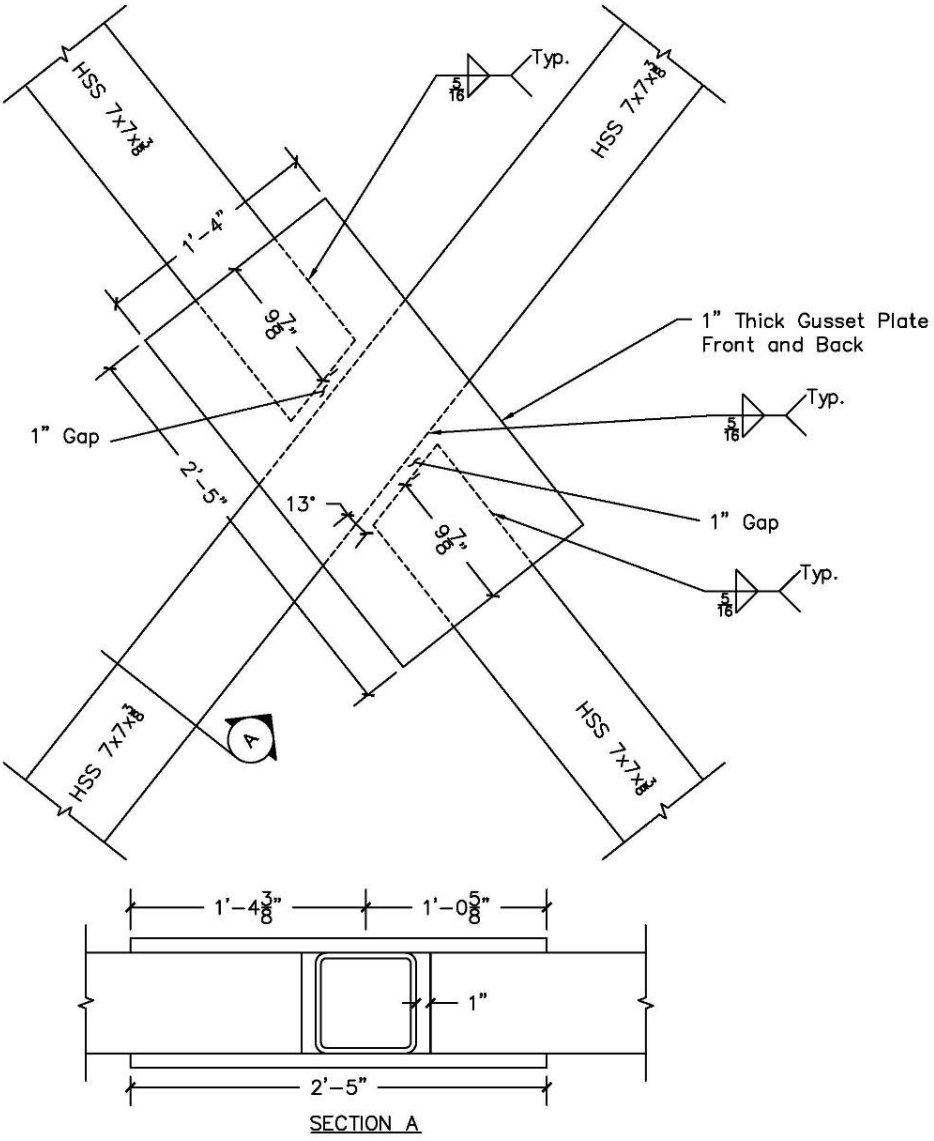

SECTION A

VIRGINIA TECH

VIRGINIA TECH
CHARLES E. VIA JR. DEPARTMENT OF CIVIL & ENVIRONMENTAL ENGINEERING
200 PATTON HALL
BLACKSBURG, VA 24061
P: 540-231-6635

PROJECT:
Diaphragm Test Setup

SHEET NOTES:
1. Scale 1:10

REVISIONS:		
NO.	DATE	BY
1	9/25/2021	HGH

DESIGNED BY:
DRAWN BY: H. Hutton
CHECKED BY:
DATE: 9/25/2021
PROJECT NO.:

SHEET TITLE:
Steel Truss Connection Detail 2

SHEET NO.: 3 of 3

Appendix D. Design of Reaction Truss

Truss Design

Virginia Tech Diaphragm Initiatives
Designed By: Hunter Hutton
January 31, 2022

The following model was created to determine design forces:

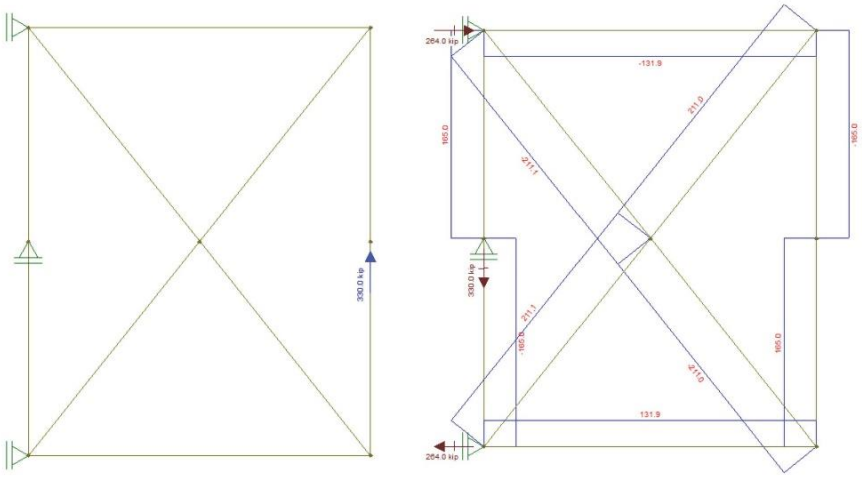

Expected Forces From Model

$P_{cross} := 211\ kip$ Axial force in members crossing

$P_{chord} := 132\ kip$ Axial force in members in line with chord beams

$P_{wall} := 165\ kip$ Axial force in member parallel to shear wall

Factored Design Forces $FS := 1.5$

$PU_{cross} := P_{cross} \cdot FS = 316.5\ kip$ Design force in members crossing

$PU_{chord} := P_{chord} \cdot FS = 198\ kip$ Design force in members in line with chord beams

$PU_{wall} := P_{wall} \cdot FS = 247.5\ kip$ Design force in member parallel to shear wall

Cross Member Design

$l := 12.8\ ft$ Axial Length
$k := 1$ Effective Length Factor
$l_c := l \cdot k = 12.8\ ft$
$E := 29000\ ksi$
$F_y := 46\ ksi$ Grade B HSS (AISC Table 2-4)
$F_u := 58\ ksi$ Grade B HSS (AISC Table 2-4)
$\phi_c := 0.9$

Try HSS 7x7x3/8

$A_g := 8.97\ in^2$
$r_x := 2.69\ in$
$r_y := 2.69\ in$
$b\_over\_t := 17.1$
$B := 7\ in$
$H := 7\ in$
$t := 0.349\ in$

$W := 32.58\ \frac{lbf}{ft}$

+Check Limiting Width to Thickness Ratio for Axial Compression

$\lambda_r := 1.40 \cdot \sqrt{\frac{E}{F_y}} = 35.152$ > $b\_over\_t = 17.1$ (AISC Table B4.1a)

+Compression Design

$\frac{l_c}{r_x} = 57.1$ $\frac{l_c}{r_y} = 57.1$ (Round Down to 57)

$\phi_c F_{cr} := 33.3\ ksi$ (AISC Table 4-14 For 46 ksi Steel)

$F_{cr} := \frac{\phi_c F_{cr}}{\phi_c} = 37\ ksi$ Compression Critical Stress

$P_n := F_{cr} \cdot A_g = 331.89\ kip$ > $PU_{cross} = 316.5\ kip$

+Tension Yield Design

$A_{req} := \frac{PU_{cross}}{F_y} = 6.88\ in^2$ < $A_g = 8.97\ in^2$

$P_n := F_y \cdot A_g = 412.62\ kip$ > $PU_{cross} = 316.5\ kip$ (AISC Eqn D2-1)

+Weld Design

$R_n := PU_{cross}$ Design Force

$n := 4$ Number of Welds

$F_{EXX} := 70\ ksi$ Weld Strength

$D := 5\ in$ 5/16" Weld

$l := \frac{R_n}{0.6 \cdot F_{EXX} \cdot \frac{\sqrt{2}}{2} \cdot \frac{D}{16}} = 34.103\ in$ Total Required Weld Length (AISC Eqn 8-1)

$\frac{l}{n} = 8.526\ in$ Required Length Per Weld (Round to 9")

Minimum of (4), 9" welds.... $lengthperweld := 9\ in$

Note that the cross members will be connected using two different methods. Method (1) will be a slotted gusset & Method (2) will be a sandwiched gusset.

+Tension Rupture Design at (1) Slotted Gusset

$l := lengthperweld$

$t_g := 1\ in$ Gusset Thickness

$xbar_{slot} := \frac{B^2 + 2 \cdot B \cdot H}{4\,(B + H)} = 2.625\ in$ (AISC Table D3.1)

$U := 1 - \frac{xbar_{slot}}{l} = 0.708$ Shear Lag Factor (AISC Table D3.1)

$A_n := A_g - (2 \cdot t_g \cdot t) = 8.272\ in^2$ Net Area

$A_e := U \cdot A_n = 5.859\ in^2$ Effective Net Area (AISC Eqn D3-1)

$P_n := F_u \cdot A_e = 339.841\ kip$ > $PU_{cross} = 316.5\ kip$ (AISC Eqn D2-2)

+Tension Rupture Design at (2) Sandwich Gusset

$l := lengthperweld$

$t_g := 1\ in$ Gusset Thickness

$xbar_{slot} := \frac{B^2}{4\,(B+H)} = 0.875\ in$ (AISC Table D3.1)

$U := 1 - \frac{xbar_{slot}}{l} = 0.903$ Shear Lag Factor (AISC Table D3.1)

$A_n := A_g$ Net Area

$A_e := U \cdot A_n = 8.098\ in^2$ Effective Net Area (AISC Eqn D3-1)

$P_n := F_u \cdot A_e = 469.679\ kip$ > $PU_{cross} = 316.5\ kip$ (AISC Eqn D2-2)

Chord Member Design

$l := 8\ ft$ Axial Length
$k := 1$ Effective Length Factor
$l_c := l \cdot k = 8\ ft$
$E := 29000\ ksi$
$F_y := 46\ ksi$ Grade B HSS (AISC Table 2-4)
$F_u := 58\ ksi$ Grade B HSS (AISC Table 2-4)
$\phi_c := 0.9$

Try HSS 7x7x3/8

$A_g := 8.97\ in^2$
$r_x := 2.69\ in$
$r_y := 2.69\ in$
$b\_over\_t := 17.1$
$B := 7\ in$
$H := 7\ in$
$t := 0.349\ in$

$W := 32.58\ \frac{lbf}{ft}$

+Check Limiting Width to Thickness Ratio for Axial Compression

$\lambda_r := 1.40 \cdot \sqrt{\frac{E}{F_y}} = 35.152$ > $b\_over\_t = 17.1$ (AISC Table B4.1a)

+Compression Design

$\frac{l_c}{r_x} = 35.688$ $\frac{l_c}{r_y} = 35.688$ (Round Up to 36)

$\phi_c F_{cr} := 37.9\ ksi$ (AISC Table 4-14 For 46 ksi Steel)

$F_{cr} := \frac{\phi_c F_{cr}}{\phi_c} = 42.111\ ksi$ Compression Critical Stress

$P_n := F_{cr} \cdot A_g = 377.737\ kip$ > $PU_{chord} = 198\ kip$

+Tension Yield Design

$A_{req} := \frac{PU_{chord}}{F_y} = 4.304\ in^2$ < $A_g = 8.97\ in^2$

$P_n := F_y \cdot A_g = 412.62\ kip$ > $PU_{chord} = 198\ kip$ (AISC Eqn D2-1)

+Weld Design

$R_n := PU_{chord}$ Design Force

$n := 4$ Number of Welds

$F_{EXX} := 70\ ksi$ Weld Strength

$D := 5\ in$ 5/16" Weld

$l := \frac{R_n}{0.6 \cdot F_{EXX} \cdot \frac{\sqrt{2}}{2} \cdot \frac{D}{16}} = 21.334\ in$ Total Required Weld Length (AISC Eqn 8-1)

$\frac{l}{n} = 5.334\ in$ Required Length Per Weld (Round to 7" so l=H)

Minimum of (4), 7" welds.... $lengthperweld := 7\ in$

Note that the chord members will only have one connection type which will be a slotted gusset.

+Tension Rupture Design at Slotted Gusset

$l := lengthperweld$

$t_g := 1\ in$ Gusset Thickness

$xbar_{slot} := \frac{B^2 + 2 \cdot B \cdot H}{4\,(B+H)} = 2.625\ in$ (AISC Table D3.1)

$U := 1 - \frac{xbar_{slot}}{l} = 0.625$ Shear Lag Factor (AISC Table D3.1)

$A_n := A_g - (2 \cdot t_g \cdot t) = 8.272\ in^2$ Net Area

$A_e := U \cdot A_n = 5.17\ in^2$ Effective Net Area (AISC Eqn D3-1)

$P_n := F_u \cdot A_e = 299.86\ kip$ > $PU_{chord} = 198\ kip$ (AISC Eqn D2-2)

Shear-Wall Member Design

$l := 3\ ft$ Axial Length
$k := 1$ Effective Length Factor
$l_c := l \cdot k = 3\ ft$
$E := 29000\ ksi$
$F_y := 50\ ksi$ A992 (AISC Table 2-4)
$F_u := 65\ ksi$ A992 (AISC Table 2-4)
$\phi_c := 0.9$

Try W8x40

$A_g := 11.7\ in^2$
$r_x := 3.53\ in$
$r_y := 2.04\ in$
$bf\_over\_2tf := 7.21$
$h\_over\_tw := 17.6$
$d := 8.25\ in$
$T := 5.75\ in$
$t_w := 0.36\ in$
$b_f := 8.07\ in$
$t_f := 0.56\ in$

$W := 40\ \frac{lbf}{ft}$

+Check Limiting Width to Thickness Ratio for Axial Compression

$\lambda_f := 0.56 \cdot \sqrt{\frac{E}{F_y}} = 13.487$ > $bf\_over\_2tf = 7.21$ (AISC Table B4.1a)

$\lambda_w := 1.49 \cdot \sqrt{\frac{E}{F_y}} = 35.884$ > $h\_over\_tw = 17.6$ (AISC Table B4.1a)

+Compression Design

$\frac{l_c}{r_x} = 10.198$ $\frac{l_c}{r_y} = 17.647$ (Round Up to 18)

$\phi_c F_{cr} := 43.9\ ksi$ (AISC Table 4-14 For 50 ksi Steel)

$F_{cr} := \frac{\phi_c F_{cr}}{\phi_c} = 48.778\ ksi$ Compression Critical Stress

$P_n := F_{cr} \cdot A_g = 570.7\ kip$ > $PU_{wall} = 247.5\ kip$

+Tension Yield Design

$A_{req} := \frac{PU_{wall}}{F_y} = 4.95\ in^2$ < $A_g = 11.7\ in^2$

$P_n := F_y \cdot A_g = 585\ kip$ > $PU_{wall} = 247.5\ kip$ (AISC Eqn D2-1)

+Weld Design

$R_n := PU_{wall}$ Design Force

$n := 2$ Number of Welds

$F_{EXX} := 70\ ksi$ Weld Strength

$D := 5\ in$ 5/16" Weld

$l := \frac{R_n}{0.6 \cdot F_{EXX} \cdot \frac{\sqrt{2}}{2} \cdot \frac{D}{16}} = 26.668\ in$ Total Required Weld Length (AISC Eqn 8-1)

$\frac{(l-d)}{n} = 9.209\ in$ Required Length Per Weld (Round to 9.5")

Minimum of (2), 9.5" welds.... $lengthperweld := 9.5\ in$

Note that the wall members will only have one connection type which will involve 2 half flanges to be coped from one side.

+Tension Rupture Design at Coped Joint

$l := lengthperweld$

$t_g := 1\ in$ Gusset Thickness

$xbar := \frac{T \cdot t_w \cdot \left(\frac{t_w}{2}\right) + 2 \cdot \left(t_f \cdot \frac{b_f}{2} \cdot \frac{b_f}{4}\right)}{T \cdot t_w + 2 \cdot \left(t_f \cdot \frac{b_f}{2}\right)} = 1.44\ in$

$U := 1 - \frac{xbar}{l} = 0.848$ Shear Lag Factor (AISC Table D3.1)

$A_n := A_g - (b_f \cdot t_f) = 7.181\ in^2$ Net Area

$A_e := U \cdot A_n = 6.092\ in^2$ Effective Net Area (AISC Eqn D3-1)

$P_n := F_u \cdot A_e = 395.99\ kip$ > $PU_{wall} = 247.5\ kip$ (AISC Eqn D2-2)

+Shear Stud Design (Connecting W Shape to Shear Wall)

$V := 330\ \textbf{kip}$ Shear Force

$V_u := FS \cdot V = 495\ \textbf{kip}$ Factored Shear Force

$V_{uflange} := \frac{V_u}{2} = 247.5\ \textbf{kip}$ Design shear per flange

$Q_n := 21.5\ \textbf{kip}$ 3/4" Stud Capacity for 4000 psi Concrete and No Deck (AISC Table 3-21)

$Required\_Studs\_Per\_Flange := \frac{V_{uflange}}{Q_n} = 11.512$ Round to 12

(12), 3/4" Shear Studs are Required Per Flange.

$Total\_Studs\_Required := 12 \cdot 2 \cdot 2 = 48$ Required Amount of 3/4" Shear Studs for 2 Members with 2 Flanges Each

End Plate Design

The chord beam includes (6) #8 reinforcing bars that will be coupled with the end plate. This will create a bending condition.

$A_s := 0.79\ \textbf{in}^2$ Area of 1 #8 Bar

$f_y := 60\ \textbf{ksi}$ Yield Strength of Reinforcing Bars

$n := 6$ Number of Bars

$b := 14\ \textbf{in}$ 14" Square Plate

$F_y := 50\ \textbf{ksi}$ Yield Strength of End Plate

$P := f_y \cdot \left(\frac{n}{2}\right) \cdot A_s = 142.2\ \textbf{kip}$ Expected Force on End Plate

$P_u := P \cdot FS = 213.3\ \textbf{kip}$ Factored Force on End Plate

$e := 3.375\ \textbf{in}$ Eccentricity of Force

$M_u := P_u \cdot e = 719.888\ \textbf{kip} \cdot \textbf{in}$ $M_p := M_u$ Factored Moment on End Plate

$z := \frac{M_p}{F_y} = 14.398\ \textbf{in}^3$ Required Plastic Section Modulus

$t_{req} := \sqrt{\frac{4 \cdot z}{b}} = 2.028\ \textbf{in}$ Required Thickness of End Plates

Specify 2"x14"x14" Plate w/ Stiffeners for Peace of Mind

Gusset Plate Design

$P := 330\ kip$ Chord Force

$P_u := FS \cdot P = 495\ kip$ Factored Chord Force

$F_y := 50\ ksi$ Yield Strength of Gusset Plate

$A_{req} := \frac{P_u}{F_y} = 9.9\ in^2$ Required Gusset Plate Area

+Weld Design for Gusset & Edge Plate

$R_n := P$ Design Force

$n := 2$ Number of Welds

$F_{EXX} := 70\ ksi$ Weld Strength

$D := 7\ in$ 7/16" Weld

$l := \frac{R_n}{0.6 \cdot F_{EXX} \cdot \frac{\sqrt{2}}{2} \cdot \frac{D}{16}} = 25.398\ in$ Total Required Weld Length (AISC Eqn 8-1)

$\frac{l}{n} = 12.699\ in$ Required Length Per Weld

Minimum of (2), 14" welds.... $lengthperweld := 14\ in$

Note that the design force for this weld was not factored as we expect some load to go through the specified stiffeners.

Appendix E. String Potentiometer Locations

The distances between the mounting points of each string potentiometer were measured and recorded prior to each test to calculate the local and global shear angles. Figure E1 shows the labeling system used to record each measurement. The recorded distances for each test are provided in Table E1.

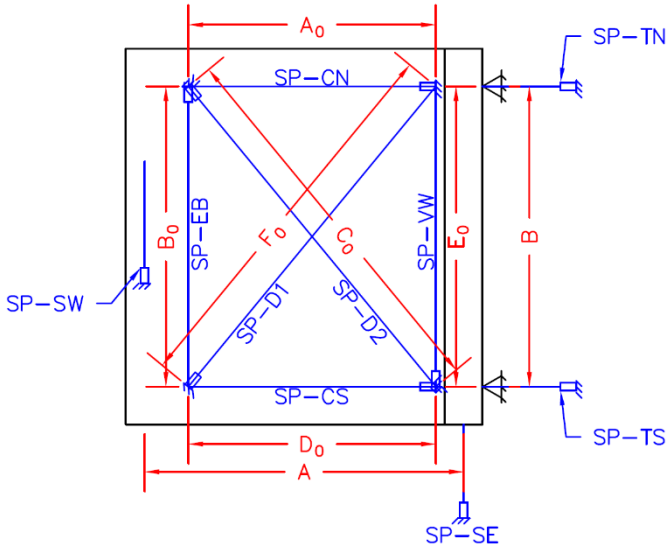

Figure E1. String Potentiometer Location Legend.

Table E1. Distance Between String Potentiometers.

Specimen	A_0 (in.)	B_0 (in.)	C_0 (in.)	D_0 (in.)	E_0 (in.)	F_0 (in.)	A (in.)	B (in.)
CD1	77.25	98	125.25	77	97.25	123.5	101.5	114.5
CD2	76.5	96.625	125	76.3125	97.8125	122.25	90	114.625
CD3	76.25	97.125	122.875	76.75	95.5	123.5	101.875	115.5
CD4	76.5	95.5	122.75	76.75	96.125	122.875	101.5	115
CD5	73.75	97.625	122.625	73.0625	98.75	122.625	102.75	114.125
CD6	76.25	97.375	121.375	73.25	97.375	123.625	100.125	115.25

Appendix F. Reaction Truss Forces

The averaged strain values for each instrumented truss member were multiplied by an elastic modulus of 29000 ksi to obtain an average stress. The average stress values were then multiplied by the nominal area of each respective truss member to obtain an average force. To check the design and force transfer of the reaction truss, the average experimental force values are compared to the expected design forces for Specimen CD1. The forces for sections a-a and b-b are compared in Figure F1(a), and the forces for sections c-c and d-d are compared in Figure F1(b). Additionally, Figure F1(c) provides the labeling system used for the truss members. It was concluded that the average experimental force values generally agree with the design values with no more than 25% variance.

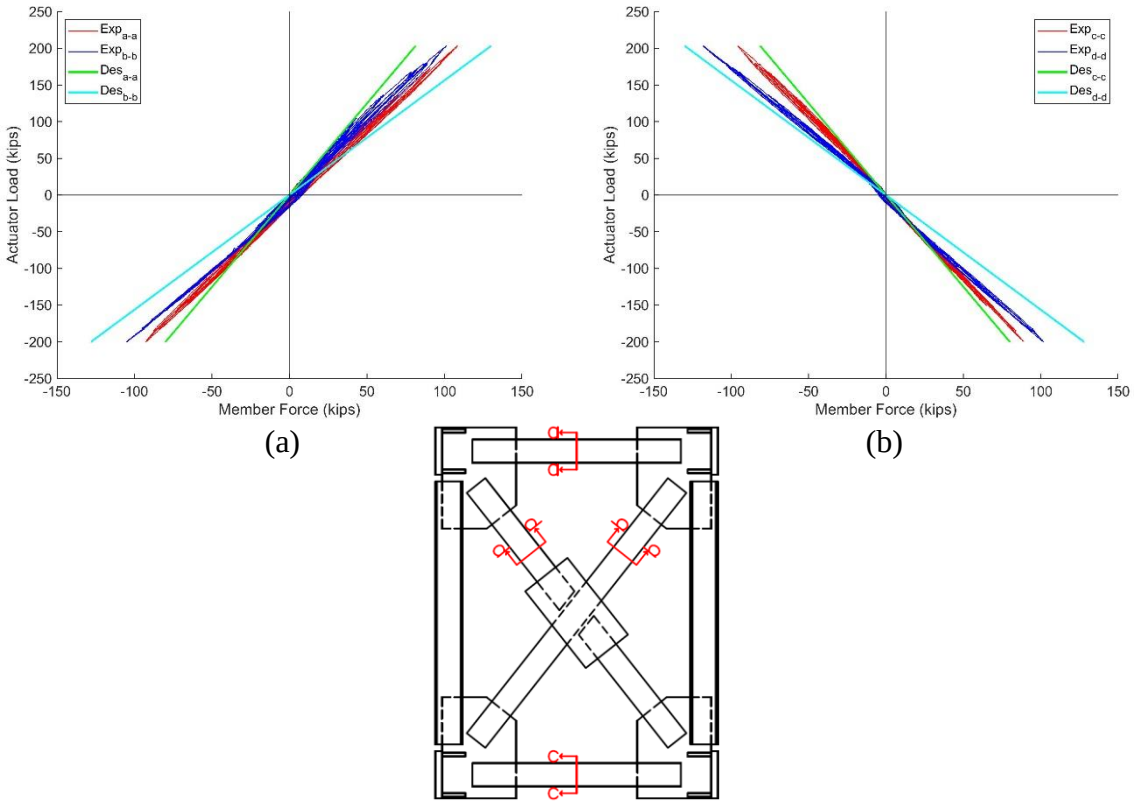

Figure F1. Reaction Truss Force Analysis: (a) Average Experimental Forces Versus Design Forces for Sections a-a and b-b; (b) Average Experimental Forces Versus Design Forces for Sections c-c and d-d; and (c) Reaction Truss Legend.

Appendix G. Formwork Details

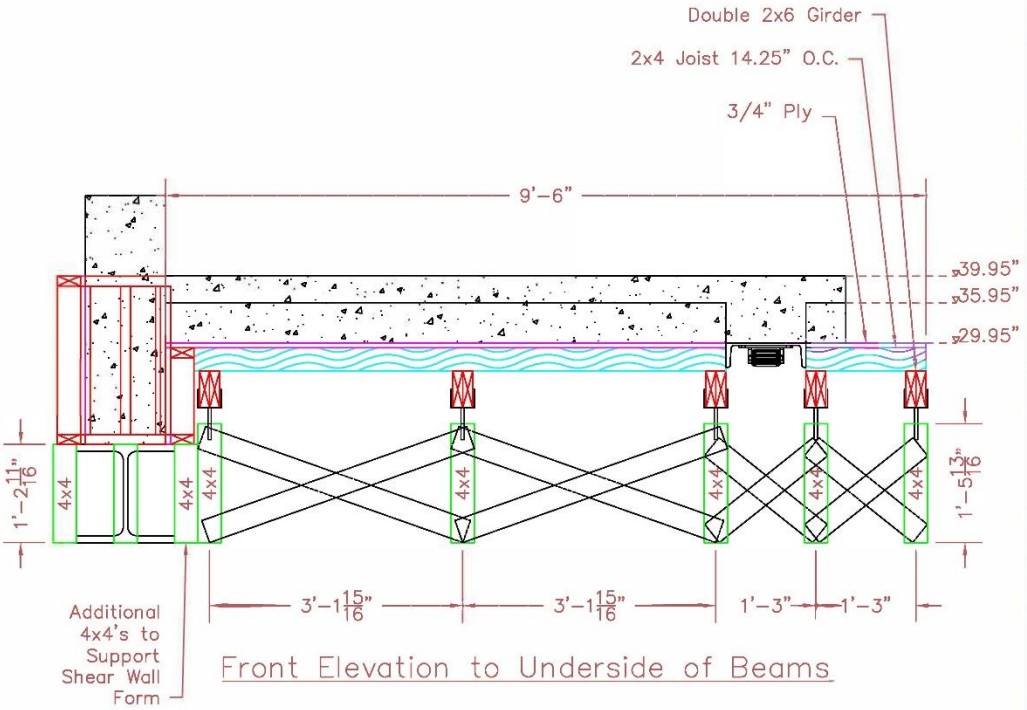

Notes:
(1.) Provide 2x4 Blocking Along Length of Channel on Both Sides (Between Joists). Fasten Blocking to Joists and Channel.
(2.) See Shear Wall Form Details on Sheet 6

VIRGINIA TECH
VIRGINIA TECH
CHARLES E. VIA JR. DEPARTMENT OF CIVIL & ENVIRONMENTAL ENGINEERING
200 PATTON HALL
BLACKSBURG, VA 24061
P: 540-231-6635

PROJECT: Concrete Diaphragm Test Setup

SHEET NOTES:
1. Scale 1:50

REVISIONS:

NO.	DATE	BY
1	10/1/2021	HGH

DESIGNED BY:
DRAWN BY: H. Hutton
CHECKED BY:
DATE: 10/1/2021
PROJECT NO.:

SHEET TITLE: Front Elevation to Underside of Beams

SHEET NO.: 1 of 6

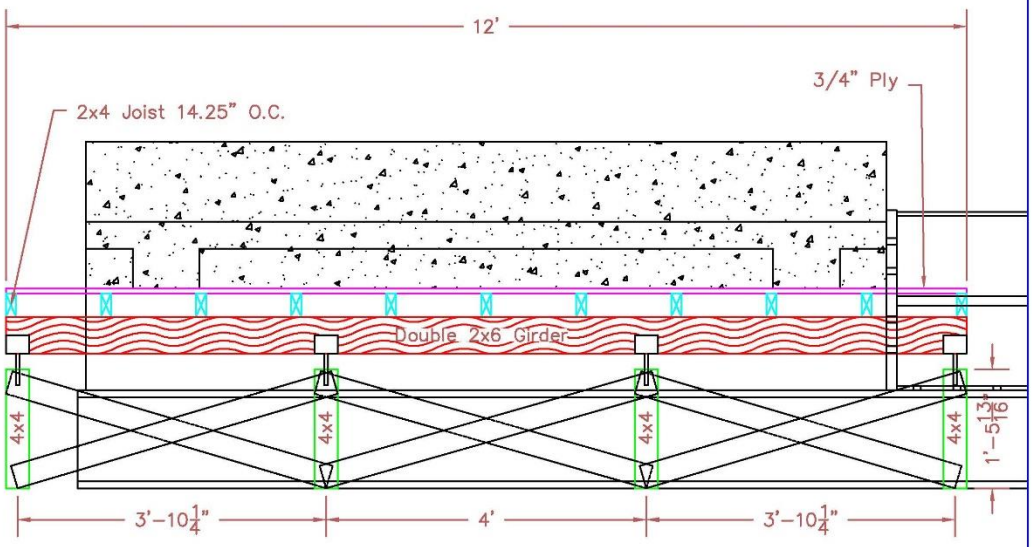

Side Elevation to Underside of Beams

VIRGINIA TECH
CHARLES E. VIA JR. DEPARTMENT OF CIVIL & ENVIRONMENTAL ENGINEERING
200 PATTON HALL
BLACKSBURG, VA 24061
P: 540-231-6635

PROJECT:
Concrete Diaphragm Test Setup

SHEET NOTES:
1. Scale 1:50

REVISIONS:

NO.	DATE	BY
1	10/1/2021	HGH

DESIGNED BY:
DRAWN BY: H. Hutton
CHECKED BY:
DATE: 10/1/2021
PROJECT NO.:

SHEET TITLE:
Side Elevation to Underside of Beams

SHEET NO.: 2 of 6

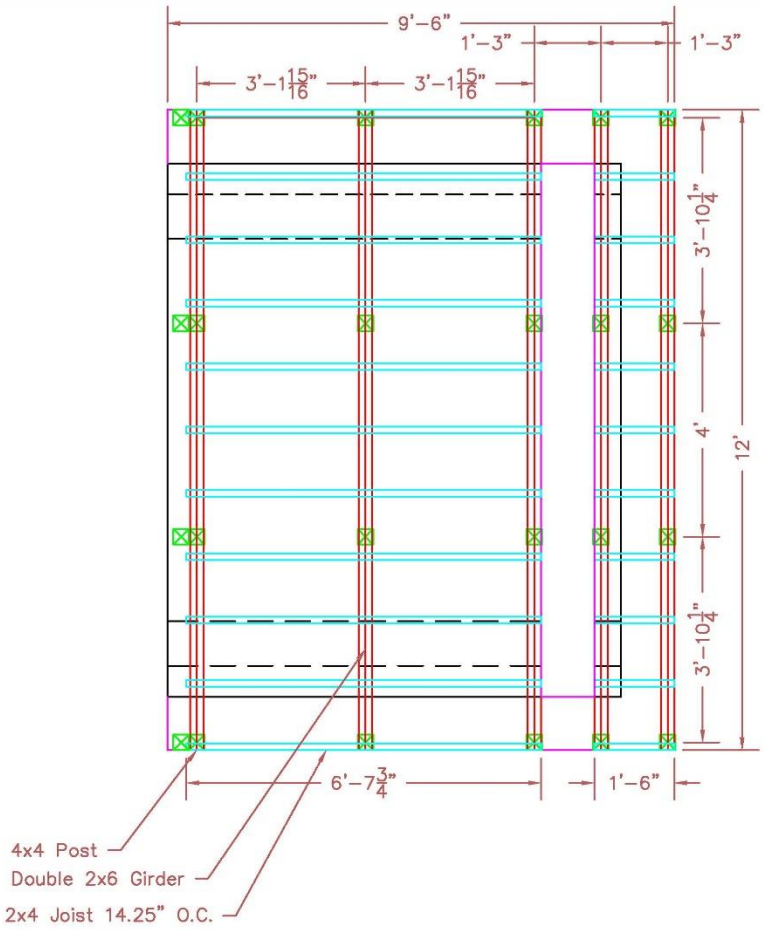

Plan View to Underside of Beams

VIRGINIA TECH
CHARLES E. VIA JR. DEPARTMENT OF CIVIL & ENVIRONMENTAL ENGINEERING
200 PATTON HALL
BLACKSBURG, VA 24061
P: 540-231-6635

PROJECT:
Concrete Diaphragm Test Setup

SHEET NOTES:
1. Scale 1:50

REVISIONS:

NO.	DATE	BY
1	10/1/2021	HGH

DESIGNED BY:
DRAWN BY: H. Hutton
CHECKED BY:
DATE: 10/1/2021
PROJECT NO.:

SHEET TITLE:
Plan View to Underside of Beams

SHEET NO.: 3 of 6

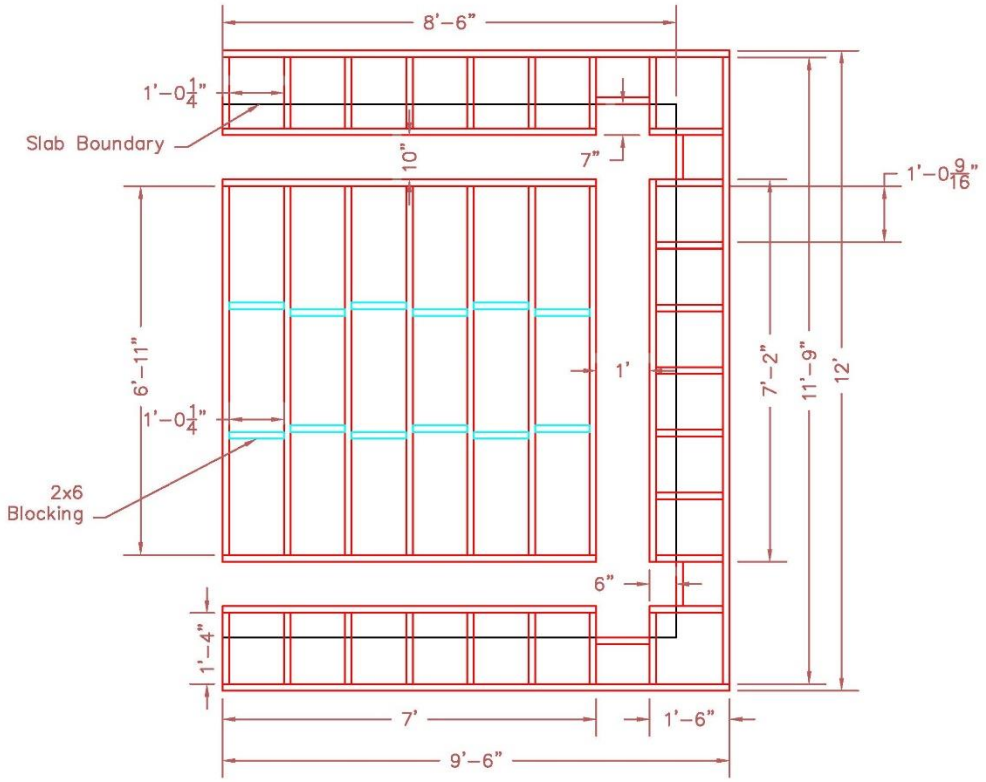

Notes:
(1.) All material in this Block–Out is 2x6
(2.) Top This 2x6 Block Out with ½" Ply to Obtain the Desired Beam Depth of 6"

Block Out For Beams

VIRGINIA TECH
CHARLES E. VIA JR. DEPARTMENT OF CIVIL & ENVIRONMENTAL ENGINEERING
200 PATTON HALL
BLACKSBURG, VA 24061
P: 540-231-6635

PROJECT:
Concrete Diaphragm Test Setup

SHEET NOTES:
1. Scale 1:50

REVISIONS:

NO.	DATE	BY
1	10/1/2021	HGH

DESIGNED BY:
DRAWN BY: H. Hutton
CHECKED BY:
DATE: 10/1/2021
PROJECT NO.:

SHEET TITLE:
Block-Out Arrangement

SHEET NO.: 4 of 6

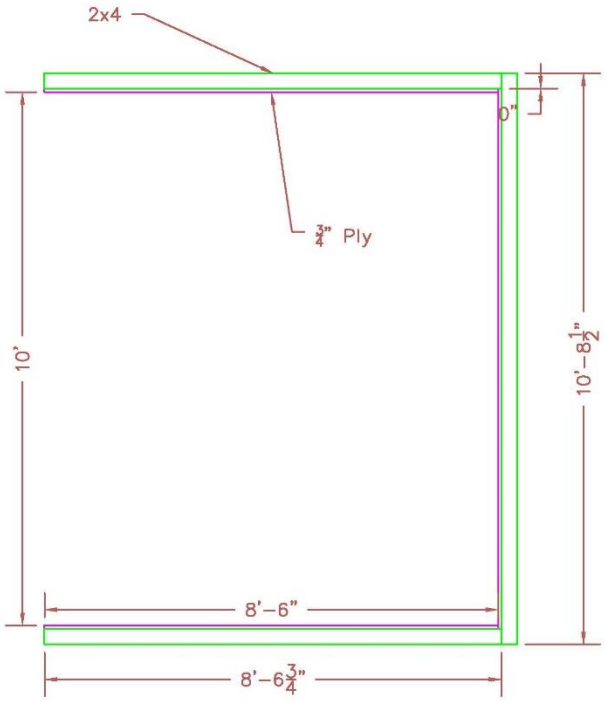

Slab Formwork

Notes:
(1.) Provide Stacked 2x4, 12" O.C. See Detail

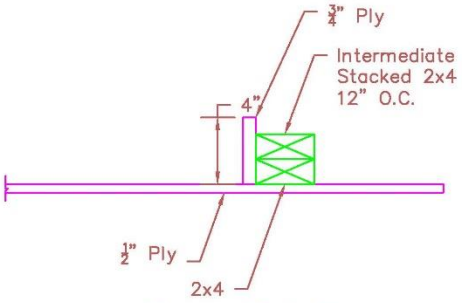

Brace Detail

VIRGINIA TECH
CHARLES E. VIA JR. DEPARTMENT OF CIVIL & ENVIRONMENTAL ENGINEERING
200 PATTON HALL
BLACKSBURG, VA 24061
P: 540-231-6635

PROJECT:
Concrete Diaphragm Test Setup

SHEET NOTES:
1. Scale 1:50

REVISIONS:

NO.	DATE	BY
1	10/1/2021	HGH

DESIGNED BY:
DRAWN BY: H. Hutton
CHECKED BY:
DATE: 10/1/2021
PROJECT NO.:

SHEET TITLE:
Slab Arrangement

SHEET NO.: 5 of 6

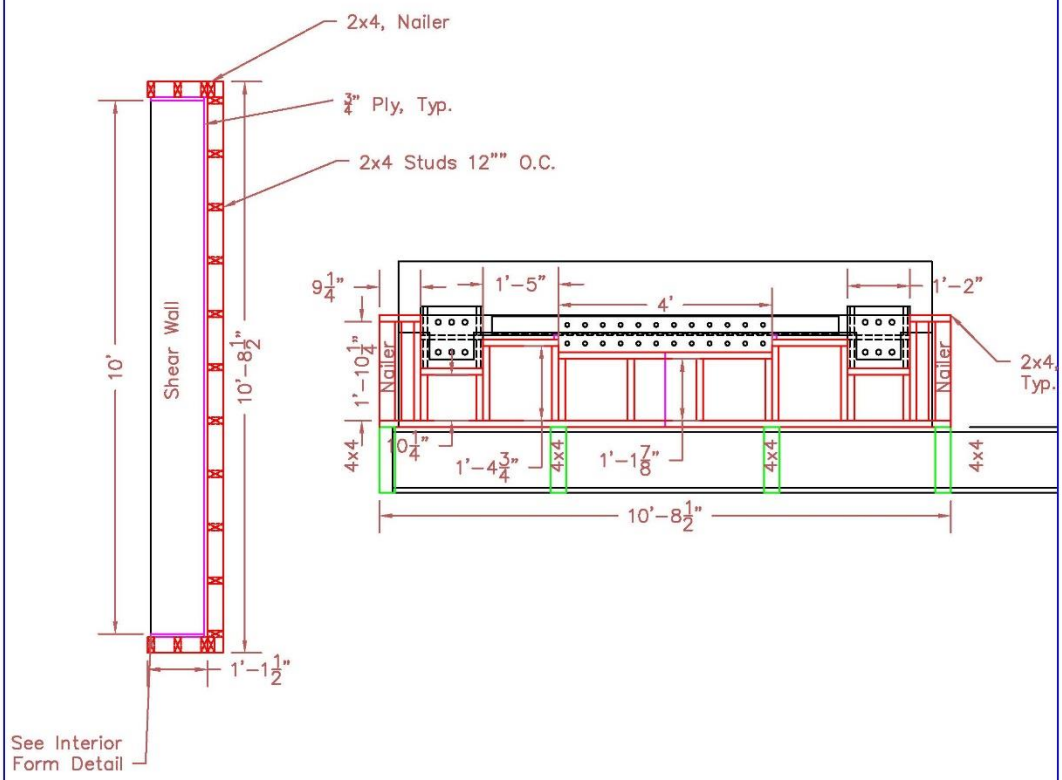

Shear Wall Formwork

VIRGINIA TECH
CHARLES E. VIA JR. DEPARTMENT OF CIVIL & ENVIRONMENTAL ENGINEERING
200 PATTON HALL
BLACKSBURG, VA 24061
P: 540-231-6635

PROJECT:
Concrete Diaphragm Test Setup

SHEET NOTES:
1. Scale 1:50

REVISIONS:

NO.	DATE	BY
1	10/1/2021	HGH

DESIGNED BY:
DRAWN BY: H. Hutton
CHECKED BY:
DATE: 10/1/2021
PROJECT NO.:

SHEET TITLE:
Shear Wall Arrangement

SHEET NO.: 6 of 6

Appendix H. FRP Technical Data Sheets

Smarter Strengthening Solutions™

CSS V-Wrap™ C100HM

High-Modulus Code-Listed Unidirectional Carbon Fabric

SIMPSON Strong-Tie | structural TECHNOLOGIES

DESCRIPTION

CSS V-Wrap C100HM is a high-modulus unidirectional carbon fiber fabric with fibers oriented in the 0° direction. The CSS V-Wrap C100HM system is field laminated using a two-part 100% solids and high-strength CSS V-Wrap-approved structural adhesives to form a carbon fiber reinforced polymer (CFRP) system used to reinforce and strengthen structural elements.

CODE REPORTS AND COMPLIANCE

ICC-ES ESR-4930

MATERIAL PROPERTIES

Typical Data

Storage Conditions	Store dry at 40°F – 90°F (4°C – 32°C)
Color	Black
Primary Fiber Direction	0° (unidirectional)
Weight	9.7 oz./yd.² (330 g/m²)
Shelf Life	10 years

Dry Fiber Properties	
Tensile Strength	790,000 psi (5,440 MPa)
Tensile Modulus	42 x 10^6 psi (289,550 MPa)
Elongation at Break	1.9%

Cured Laminate Properties	Average Values	Design Values*
Tensile Strength	216,000 psi (1,490 MPa)	165,000 psi (1,138 MPa)
Modulus of Elasticity	16.7 x 10^6 psi (115,100 MPa)	15 x 10^6 psi (103,400 MPa)
Elongation at Break	1.3%	1.1%
Thickness	0.02 in. (0.51 mm)	0.02 in. (0.51 mm)
Strength per Unit Width	4,320 lb./in. (0.76 kN/mm)	3,300 lb./in. (0.58 kN/mm)

*Design properties are based on ACI 440.2R using average minus three standard deviations.

MADE IN USA with GLOBAL MATERIALS

PERFORMANCE FEATURES

- ICC-ES ESR-4930 listed product
- UL Listed (ul.com/database)
- NSF/ANSI Standard 61 listed product for drinking water systems
- 0% VOC
- 100% solvent-free
- Non-corrosive reinforcement system
- Lightweight flexible fabric can be wrapped around complex shapes
- Used for shear, confinement or flexural strengthening
- High strength and high modulus
- Lightweight
- Reduces crack width
- Low aesthetic impact

APPLICATIONS

CSS V-Wrap fabrics can be used to resolve strength deficiencies and increase the load-carrying capacity of buildings, bridges, silos, chimneys and other structures.

- Load increases
- Seismic strengthening
- Repair structural elements
- Change in structural system
- Design or construction defects

PACKAGING

Roll Size (Width x Length)	Model No.
24 in. x 150 ft. / 50 yd. (610 mm x 45.7 m)	CV-C100HM24-50

HOW TO USE

Design
Design should comply with ACI 440.2R or another recognized design/specification entity and is typically based on CFRP contribution determined by detailed analysis. Design values will vary based on project requirements and applicable environmental and strength reduction factors. Contact STRUCTURAL TECHNOLOGIES at (410) 859-6502 to determine applicable design factors.

Surface Preparation
Surfaces to receive CSS V-Wrap C100HM must be clean and sound. They must be dry and free of frost. All dust, laitance, grease, curing compounds, waxes, deteriorated materials and other bond-inhibiting materials must be removed from the surface prior to application. Existing uneven surfaces must be filled with appropriate epoxy putty or repair mortar. Use abrasive blasting, pressure washing, shotblasting, grinding or other approved mechanical means to achieve an open-pore texture with a concrete surface profile of not less than CSP-3 (ICRI). In certain applications and at the engineer's discretion, the bond between the substrate and the fabric may be determined to be non-critical (such as in column confinement applications). All corners must be rounded to ½" radius minimum. The adhesive bond strength of the concrete may be verified after surface preparation by random pull-off testing (ASTM C1583) at the discretion of the engineer. Minimum tensile strength of 200 psi must be achieved for concrete.

Handling
Approved personal protection equipment should be worn at all times. Particle mask is recommended for possible airborne particles. Gloves are recommended when handling fabrics and resins to avoid skin irritation. Safety glasses are recommended to prevent eye irritation. Wear chemical-resistant clothing/gloves/goggles. Ventilate area. In absence of adequate ventilation, use a properly fitted NIOSH respirator.

Cutting
Fabric can be cut to appropriate length by using commercial quality heavy-duty scissors.

Application
Installation of the CSS V-Wrap strengthening system should be performed only by a specially trained, approved contractor. The CSS V-Wrap strengthening system shall consist of CSS V-Wrap carbon fabric and CSS V-Wrap 770 epoxy.

Note the specified number of plies, ply widths and fiber orientation. Mix resin components using recommended procedures on product datasheet. Apply one coat of CSS V-Wrap 770 epoxyy as a primer to the surface using a nap roller. Fill minor concrete defects such as bug holes and other imperfections using CSS V-Wrap 770 epoxy mixed with fumed silica (thickened epoxy) or CSS V-Wrap PF putty filler. Apply thickened epoxy or putty using a trowel. Adjust the gap between saturator rollers to approximately 42 mils. Using a saturator machine, pre-saturate the appropriate length of CSS V-Wrap fabric with CSS V-Wrap 770 epoxy as a saturant. Install the saturated CSS V-Wrap fabric. Use a rib roller to remove all air pockets and ensure intimate contact with the surface. If a splice is needed, a minimum 6" overlap is required to achieve continuity. On multiple plies with splices, stagger the splice locations. If required, apply topcoat material.

Limitations
- Design calculations must be approved by a licensed professional engineer.
- System is a vapor barrier.
- Concrete deterioration and steel corrosion must be resolved prior to application.
- Minimum application temperature is 40°F.

Storage
Store material in a cool, dark space. Low humidity is recommended.

CAUTION

Protective Measures: The use of safety glasses and chemically-resistant gloves is recommended. Use appropriate clothing to minimize skin contact. The use of a NIOSH-approved respirator is required to protect respiratory tract when ventilation is not adequate to limit exposure below the PEL. Refer to Safety Data Sheets (SDS) available at **strongtie.com/sds** for detailed information.

FIRST AID

Skin: Wash fibers off skin with water and soap. If fibers are embedded in the skin, remove with tweezers. Discard clothing that may contain embedded fibers. Seek medical advice if exposure results in adverse effects.

Eyes: Immediately flush with a continuous water stream for at least 20 minutes. Washing immediately after exposure is expected to be effective in preventing damage to the eyes. Seek medical advice.

Inhalation: If there is inhalation exposure to the fibers of this product, remove source of exposure and move affected person to fresh air. If not breathing, give artificial respiration. If there is breathing difficulty, give oxygen. Seek medical advice for any respiratory problems.

Ingestion: Not expected to occur since ingestion is not a likely route of exposure for this product. If ingestion does occur, DO NOT INDUCE VOMITING. Nothing by mouth if unconscious. Seek medical advice.

CLEAN-UP

Environmental Precautions

Spill/Release and Cleanup Procedures: In case of spill, collect (e.g., sweep up, vacuum, etc.) spilled material and either reuse or dispose of properly. Chopped or milled carbon fibers may be slippery if spilled, posing an accident risk. Wear personal protective equipment as described in the SDS during cleanup activities.

LIMITED WARRANTY

This product is covered by the Simpson Strong-Tie RPS Product Limited Warranty, which is available at **strongtie.com/limited-warranties** or by calling Simpson Strong-Tie at (800) 999-5099.

Smarter Strengthening Solutions™

CSS V-Wrap™ C200HM

High-Modulus Code-Listed Unidirectional Carbon Fabric

SIMPSON Strong-Tie | structural TECHNOLOGIES

DESCRIPTION

CSS V-Wrap C200HM is a code-listed unidirectional carbon fiber fabric with fibers oriented in the 0° direction. The CSS V-Wrap C200HM system is field laminated using CSS V-Wrap-approved structural adhesives to form a carbon fiber reinforced polymer (CFRP) system used to reinforce and strengthen structural elements.

CODE REPORTS AND COMPLIANCE

ICC ES **ICC-ES ESR-4930**

MATERIAL PROPERTIES

Typical Data

Storage Conditions	Store dry at 40°F – 90°F (4°C – 32°C)
Color	Black
Primary Fiber Direction	0° (unidirectional)
Weight	17.7 oz./yd.² (600 g/m²)
Shelf Life	10 years

Dry Fiber Properties	
Tensile Strength	790,000 psi (5,440 MPa)
Tensile Modulus	42 x 10^6 psi (290,000 MPa)
Elongation at Break	1.9%

Cured Laminate Properties	Average Values	Design Values*
Tensile Strength	180,000 psi (1,240 MPa)	155,000 psi (1,070 MPa)
Modulus of Elasticity	14.24 x 10^6 psi (98,100 MPa)	14.0 x 10^6 psi (96,500 MPa)
Elongation at Break	1.27%	1.1%
Thickness	0.04 in. (1.02 mm)	0.04 in. (1.02 mm)
Strength per Unit Width	7,200 lb./in. (1.26 kN/mm)	6,200 lb./in. (1.09 kN/mm)

*Design properties are based on ACI 440.2R using average minus three standard deviations.

MADE IN USA with GLOBAL MATERIALS

PERFORMANCE FEATURES

- ICC-ES ESR-4930 listed product
- UL Listed (ul.com/database)
- NSF/ANSI Standard 61 listed product for drinking water systems
- 0% VOC
- 100% solvent-free
- Non-corrosive reinforcement system
- Lightweight flexible fabric can be wrapped around complex shapes
- Used for shear, confinement or flexural strengthening
- High strength and high modulus
- Lightweight
- Reduces crack width
- Low aesthetic impact

APPLICATIONS

CSS V-Wrap fabrics can be used to resolve strength deficiencies and increase the load-carrying capacity of buildings, bridges, silos, chimneys and other structures.

- Load increases
- Seismic strengthening
- Repair structural elements
- Change in structural system
- Design or construction defects

PACKAGING

Roll Size (Width x Length)	Model No.
8 in. x 150 ft. / 50 yd. (203 mm x 45.7 m)	CV-C200HM8-50
12 in. x 150 ft. / 50 yd. (305 mm x 45.7 m)	CV-C200HM12-50
24 in. x 150 ft. / 50 yd. (610 mm x 45.7 m)	CV-C200HM24-50
24 in. x 300 ft. / 100 yd. (610 mm x 91.4 m)	CV-C200HM24-100

HOW TO USE

Design
Design should comply with ACI 440.2R or another recognized design/specification entity and is typically based on CFRP contribution determined by detailed analysis. Design values will vary based on project requirements and applicable environmental and strength reduction factors. Contact STRUCTURAL TECHNOLOGIES at (410) 859-6502 to determine applicable design factors.

Surface Preparation
Surfaces to receive CSS V-Wrap C200HM must be clean and sound. They must be dry and free of frost. All dust, laitance, grease, curing compounds, waxes, deteriorated materials and other bond-inhibiting materials must be removed from the surface prior to application. Existing uneven surfaces must be filled with appropriate epoxy putty or repair mortar. Use abrasive blasting, pressure washing, shotblasting, grinding or other approved mechanical means to achieve an open-pore texture with a concrete surface profile of not less than CSP-3 (ICRI). In certain applications and at the engineer's discretion, the bond between the substrate and the fabric may be determined to be non-critical (such as in column confinement applications). All corners must be rounded to ½" radius minimum. The adhesive bond strength of the concrete may be verified after surface preparation by random pull-off testing (ASTM C1583) at the discretion of the engineer. Minimum tensile strength of 200 psi must be achieved for concrete.

Handling
Approved personal protection equipment should be worn at all times. Particle mask is recommended for possible airborne particles. Gloves are recommended when handling fabrics and resins to avoid skin irritation. Safety glasses are recommended to prevent eye irritation. Wear chemical-resistant clothing/gloves/goggles. Ventilate area. In absence of adequate ventilation, use a properly fitted NIOSH respirator.

Cutting
Fabric can be cut to appropriate length by using commercial quality heavy-duty scissors.

Application
Installation of the CSS V-Wrap strengthening system should be performed only by a specially trained, approved contractor. The CSS V-Wrap strengthening system shall consist of CSS V-Wrap carbon fabric and CSS V-Wrap 770 epoxy.

Note the specified number of plies, ply widths and fiber orientation. Mix resin components using recommended procedures on product datasheet. Apply one coat of CSS V-Wrap 770 epoxy as a primer to the surface using a nap roller. Fill minor concrete defects such as bug holes and other imperfections using CSS V-Wrap 770 epoxy mixed with fumed silica (thickened epoxy) or CSS V-Wrap PF putty filler. Apply thickened epoxy or putty using a trowel. Adjust the gap between saturator rollers to approximately 42 mils. Using a saturator machine, pre-saturate the appropriate length of CSS V-Wrap fabric with CSS V-Wrap 770 epoxy as a saturant. Install the saturated CSS V-Wrap fabric. Use a rib roller to remove all air pockets and ensure intimate contact with the surface. If a splice is needed, a minimum 6" overlap is required to achieve continuity. On multiple plies with splices, stagger the splice locations. If required, apply topcoat material.

Limitations
- Design calculations must be approved by a licensed professional engineer.
- System is a vapor barrier.
- Concrete deterioration and steel corrosion must be resolved prior to application.
- Minimum application temperature is 40°F.

Storage
Store material in a cool, dark space. Low humidity is recommended.

CAUTION

Protective Measures: The use of safety glasses and chemically-resistant gloves is recommended. Use appropriate clothing to minimize skin contact. The use of a NIOSH-approved respirator is required to protect respiratory tract when ventilation is not adequate to limit exposure below the PEL. Refer to Safety Data Sheets (SDS) available at **strongtie.com/sds** for detailed information.

FIRST AID

Skin: Wash fibers off skin with water and soap. If fibers are embedded in the skin, remove with tweezers. Discard clothing that may contain embedded fibers. Seek medical advice if exposure results in adverse effects.

Eyes: Immediately flush with a continuous water stream for at least 20 minutes. Washing immediately after exposure is expected to be effective in preventing damage to the eyes. Seek medical advice.

Inhalation: If there is inhalation exposure to the fibers of this product, remove source of exposure and move affected person to fresh air. If not breathing, give artificial respiration. If there is breathing difficulty, give oxygen. Seek medical advice for any respiratory problems.

Ingestion: Not expected to occur since ingestion is not a likely route of exposure for this product. If ingestion does occur, DO NOT INDUCE VOMITING. Nothing by mouth if unconscious. Seek medical advice.

CLEAN-UP

Environmental Precautions

Spill/Release and Cleanup Procedures: In case of spill, collect (e.g., sweep up, vacuum, etc.) spilled material and either reuse or dispose of properly. Chopped or milled carbon fibers may be slippery if spilled, posing an accident risk. Wear personal protective equipment as described in the SDS during cleanup activities.

LIMITED WARRANTY

This product is covered by the Simpson Strong-Tie RPS Product Limited Warranty, which is available at **strongtie.com/limited-warranties** or by calling Simpson Strong-Tie at (800) 999-5099.

FYFE®

TYFO® SCH-11UP COMPOSITE

using Tyfo® S Epoxy

DESCRIPTION

The Tyfo® SCH-11 UP Composite is comprised of Tyfo® S Epoxy and Tyfo® SCH-11UP reinforcing fabric. Tyfo® SCH-11UP is a custom, unidirectional carbon fabric. The Tyfo® S Epoxy is a two-component epoxy matrix.

USE

Tyfo® SCH-11UP Fabric is combined with Tyfo® epoxy to add strength to bridges, buildings, and other structures.

ADVANTAGES

- Good high & low temperature properties
- Long working time
- High tensile modulus and strength
- Ambient cure
- 100% solvent-free
- Rolls can be cut to desired widths prior to shipping

COVERAGE

Approximately 1,200 sq. ft. surface area with 3 to 4 units of Tyfo® S Epoxy and 1 roll of Tyfo® SCH-11UP Fabric when used with the Tyfo® Saturator.

PACKAGING

Order Tyfo® S Epoxy in 55-gallon (208L) drums or pre-measured units in 5-gallon (19L) containers. Tyfo® SCH-11UP Fabric typically shipped in 24" x 600 lineal foot (0.6m x 182.9m) rolls. Typically ships in 14" x 14" x 27" (356mm x 356mm x 686mm) boxes.

EPOXY MIX RATIO

100.0 component A to 42.0 component B by volume. (100 oomponent A to 34.5 component B by weight.)

SHELF LIFE

Epoxy – two years in original, unopened and properly stored containers.

Fabric – ten years in proper storage conditions.

STORAGE CONDITIONS

Store epoxy at 40° to 90° F (4° to 32° C). Avoid freezing. Store rolls flat, not on ends, at temperatures below 100° F (38° C). Avoid moisture and water contamination.

CERTIFICATE OF COMPLIANCE

- Will be supplied upon request, complete with state and federal packaging laws with copy of labels used.
- Material safety data sheets will be supplied upon request.
- Possesses 0% V.O.C. level.

Typical Dry Fiber Properties

Property	Typical Test Value
Tensile Strength	550,000 psi (3.79 GPa)
Tensile Modulus	33.4 x 10^6 psi (230 GPa)
Ultimate Elongation	1.7%
Density	0.063 lbs./in.^{3} (1.8 g/cm^3)
Minimum weight per sq. yd.	11.6 oz. (393 g/m^2)

Composite Gross Laminate Properties

Property[1]	ASTM Method	Typical Test Value	Design Value*
Ultimate Tensile Strength in Primary Fiber Direction	D3039	143,000 psi (986 MPa) (2.8 kip/in. width)	121,000 psi (834.3 MPa) (2.4 kip/in. width)
Elongation at Break		1.0%	0.85%
Tensile Modulus		13.9 x 10^6 psi (95.8 GPa)	11.9 x 10^6 psi (82 GPa)
Nominal Laminate Thickness		0.02 in. (0.51mm)	0.02 in. (0.51mm)

* Design and specification values will vary based on individual project requirements and applicable safety factors. Contact FyfeFRP LLC engineers to determine appropriate specification values.

Epoxy Material Properties

Curing Schedule 72 hours post cure at 140° F (60° C).

Property	ASTM Method	Typical Test Value
Glass Transition Temperature, T_g	D4065	180°F (82°C)
Tensile Strength[1], psi	D638 Type 1	10,500 psi (72.4 MPa)
Tensile Modulus, psi		461,000 psi (3.18 GPa)
Elongation Percent		5.0%
Flexural Strength, psi	D790	17,900 psi (123.4 MPa)
Flexural Modulus, psi		452,000 psi (3.12 GPa)

[1] Testing temperature: 70° F (21° C)
Crosshead speed: 0.5 in. (13mm)/min. Grips Instron 2716-0055 - 30 kips
[2] Specification values can be provided upon request.

INSTALLATION OF THE TYFO® COMPOSITE SYSTEM

DESIGN
The Tyfo® Fibrwrap® System shall be designed to meet specific design criteria. The criteria for each project is dictated by the engineer of record and any relevant building codes and/or guidelines. The design should be based on the allowable strain for each type of application and the design modulus of the material. The FyfeFRP LLC engineering staff will provide preliminary design at no obligation.

INSTALLATION
Tyfo® System to be installed by FyfeFRP LLC trained and certified applicators. Installation shall be in strict compliance with the FyfeFRP LLC Quality Control Manual.

SURFACE PREPARATION
The required surface preparation is largely dependent on the type of element being strengthened. In general, the surface must be clean, dry and free of protrusions or cavities, which may cause voids behind the Tyfo® composite. Column surfaces that will receive continuous wraps typically require only a broom cleaning. Discontinuous wrapping surfaces (walls, beams, slabs, etc.) typically require a light sandblast, grinding or other approved methods to prepare for bonding. Tyfo® Composite Anchors are incorporated in some designs. The FyfeFRP LLC engineering staff will provide the proper specifications and details based on the project requirements.

MIXING
For pre-measured units in 5-gallon containers, pour the contents of component B into the pail of component A. For drums, premix each component: 100.0 parts of component A to 42.0 parts of component B by volume (100 parts of component A to 34.5 parts of component B by weight). Mix thoroughly for five minutes with a Tyfo® low speed mixer at 400-600 RPM until uniformly blended.

APPLICATION
Apply one prime coat of Tyfo® S epoxy on the substrate by using a roller. Saturate the fabric by feeding ii through the Tyfo®Saturator or by approved hand methods (See the Tyfo® Saturator Manual). Prior to the application of the saturated fabric, fill any uneven surface. Saturate and apply subsequent layers of the fabric according to the Specifications and the Design Requirements. With the use of a roller or hand pressure, ensure proper orientation f fibers. Release or roll out entrapped air and ensure that each individual layer is firmly bedded and adhered to the preceding layer or substrate. Apply a final coat of thickened Tyfo® S Epoxy and detail all fabric edges, including butt splice, termination points and jacket edges.

PROTECTIVE COATINGS
In case of plaster final coaling, apply sand by hand for better bonding surface while the final coat of epoxy is still tacky. In case of paint final coating, paint between 24 and 72 hours after final application of epoxy. If more than 72 hours after application, prepare the surface of the final coat of epoxy by light sandblast or hand sanding to slightly etch the surface.

LIMITATIONS
Recommended substrate temperature range is 50°F to 100°F (10°C to 38°C). All coating applications to be performed at a minimum of 5.4°F above the dew point. Maintain conditions for the first 48 hours of cure. Temperatures below 50°F will significantly increase the viscosity of the mixed product. Higher viscosity will reduce fabric penetration, introduce additional air into the system, and extend the cure times beyond 48 hours. DO NOT THIN. Solvents will prevent proper cure.

FIELD QUALITY CONTROL
Record batch numbers for fabric and epoxy used each day and note locations of installations. Measure square feet of fabric and volume of epoxy used each day.

CAUTION!

CLEANUP
Collect with absorbent material. Dispose in accordance with local disposal regulations. Uncured material can be removed with approved solvent. Cured materials must be mechanically removed.

HAZARDS
Consult the Safety Data Sheets (SDS) for associated hazards. SDS will be supplied upon request.

Consult safety data sheet (SDS) for more information. For industrial use only.

FyfeCo.com | FyfeInfo@cs-nri.com | +1.855.708.3617

V: 07.13.2022

FYFE®

TYFO® SEH-51A Composite

using Tyfo® S Epoxy

DESCRIPTION
The Tyfo® SEH-51A Composite is comprised of the Tyfo® S Epoxy and Tyfo® SEH-51A reinforcing fabric. Tyfo® SEH-51A is a custom weave, uni-directional glass fabric orientated in the 0° direction. The Tyfo® S Epoxy is a two-component epoxy matrix.

USE
The Tyfo® SEH-51A fabric is combined with Tyfo® S Epoxy to provide an ambient-cure, wet-layup, composite system for strengthening and increasing the ductility of bridges, buildings, and other structures.

ADVANTAGES
- ICC-ES ESR-2103 listed product
- IAPMO UES ER-595 listed product
- UL listed, fire-rated assembly component
- Tyfo® Systems are NSF/ANSI Standard 61-G certified
- Proven long-term performance and durability
- Excellent wet-out and handling properties
- 100% solids, solvent-free epoxy matrix
- Low viscosity, long working time
- Ambient cure application

PACKAGING
Tyfo® SEH-51A: 24" width x 150 lineal ft. (300 sq. ft.) Typically ships in 12" x 13" x 26" boxes.

Tyfo® S Epoxy: Pre-measured 5-gallon units with a combined material volume of 4 gallons or in 55-gallon drums.

COVERAGE
Approximately 2 to 3 units per roll of the Tyfo® SEH-51A fabric.

CONSUMPTION RATE
Fabric-to-epoxy ratio by weight:
For Tyfo® SCH Fabrics: 1 : 1
For Tyfo® SEH Fabrics: 1 : 0.8

SHELF LIFE
Epoxy - two years in original, unopened and properly stored containers.
Fabric - 10 years in proper storage conditions.

STORAGE CONDITIONS
Store epoxy at 60°F to 100°F (15°C to 38°C). Resin is susceptible to crystallization at temperatures below 50°F. If crystallized, epoxy must be reheated until clear. Store fabric rolls flat, not on ends, and at temperatures below 100°F (38°C). Avoid moisture and water contamination.

Typical Dry Fiber Properties

Property	Typical Test Value
Tensile Strength	470,000 psi (3.24 GPa)
Tensile Modulus	10.5 x 10^6 psi (72.4 GPa)
Ultimate Elongation	4.5%
Density	0.092 lbs./in.^{3} (2.55 g/cm^3)
Minimum weight per sq. yd.	27 oz. (915 g/m^2)

Composite Gross Laminate Properties

Property[3]	ASTM Method	ACI 440.2R Properties[1]	Design Properties[2]
Ultimate Tensile Strength in Primary Fiber Direction	D3039	66,000 psi (455 MPa)	66,000 psi (455 MPa)
Elongation at Break		1.80%	1.80%
Tensile Modulus		3.73 x 10^6 psi (25.7 GPa)	3.40 x 10^6 psi (23.4 GPa)
Tensile Strength per inch width	D7565	3,300 lbf/in width (578 N/mm)	3,300 lbf/in width (578 N/mm)
Tensile Stiffness per inch width		187 x 10^3 lbf/in width (32.7 kN/mm)	170 x 10^3 lbf/in width (29.8 kN/mm)
Nominal Laminate Thickness	D1777	0.05 in. (1.3 mm)	0.05 in. (1.3 mm)

[1] Strength is defined as the mean strength (83 ksi) minus 3 standard deviations. Modulus is defined as the reported mean modulus, and elongation is defined as the calculated strain from the design strength and modulus.
[2] Tensile modulus is defined as the 5th percentile value representing the 80% lower confidence bound of a 2 parameter Weibull distribution (ASTM D7290).
[3] Design values may require additional reduction factors based on expected exposure conditions, type of application, and design life assumptions.

Additional Composite Properties

Property[4]	ASTM Method	Typical Test Values	Design Values
Flexural Strength	D790	80,000 psi (551.6 MPa)	68,000 psi (468.9 MPa)
Flexural Modulus		3.5 x 10^6 psi (24.1 GPa)	2.98 x 10^6 psi (20.5 GPa)
Cathodic Disbondment	G8	PASSED, <1mm	
Dielectric Breakdown Voltage	D149	26.1 kV	
Dielectric Strength		5.7 kV/mm	
Water Absorption (24 hours)	D570	.08%	
Barcol Hardness	D2583	52	
Notched IZOD Impact Resistance	D256 Method D	30 ft-lbs/in width	

[4] Contact FyfeFRP LLC engineers to confirm project specification values and design methodology.

INSTALLATION OF THE TYFO® SEH-51A SYSTEM

DESIGN
The Tyfo® SEH-51A system is designed to meet specific project criteria dictated by the engineer of record and any relevant building codes and/or guidelines. The design shall be based on the allowable strain for each type of application and the design modulus of the material. FyfeFRP LLC engineering staff may provide preliminary design, specification wording and application details based on the project requirements.

INSTALLATION
The Tyfo® system is to be installed by FyfeFRP LLC trained and certified applicators in accordance with the FyfeFRP LLC quality control manual, project specifications, and design requirements.

SURFACE PREPARATION
The required surface preparation is dependent on the type of element being strengthened. In general, the surface must be clean, dry and free of protrusions or cavities to prevent voids behind the Tyfo® system. Column surfaces that will receive continuous wraps typically only require a clean, sound substrate. Discontinuous wrapping surfaces (walls, beams, slabs, etc.) require a minimum CSP-2 profile to prepare for bonding, achieved by light sandblast, grinding or other approved methods per ICRI 310.2R. Tyfo® Composite Anchors may be incorporated in the designs. FyfeFRP LLC engineering staff will provide the proper specifications and details based on project requirements.

MIXING TYFO® S EPOXY
For pre-measured units in 5-gallon containers, pour the contents of component B into the component A container. Mix thoroughly with a low speed mixer at 400 to 600 RPM until uniformly blended. Ensure epoxy is transferred between the A and B buckets. For 55-gallon drums, mix component A and component B per the appropriate weight or volumetric mix ratio. Resin may be heated to achieve desired viscosity (i.e. radiant heating, drum heaters, water bath). Mixed Tyfo® S Epoxy may be thickened by adding up to 7 percent by weight of fumed silica (such as Cab-o-sil TS-720) or approved filler such as HDPE fibers. DO NOT THIN. Solvents will prevent proper cure.

PROTECTIVE COATINGS
Apply a final coat of thickened Tyfo® S Epoxy to all fabric edges, including butt splice, termination points and jacket edges. Paint between 24 and 72 hours after final application of epoxy. If more than 72 hours after application, prepare the surface by light sandblast or hand sanding to lightly etch the surface. Please refer to FyfeFRP LLC 's NSF Listing for the NSF-61G listed application method (www.NSF.org).

LIMITATIONS
Recommended substrate temperature range is 50°F to 100°F (10°C to 38°C). All coating applications to be performed at a minimum of 5.4°F above the dew point. Maintain conditions for the first 48 hours of cure. Temperatures below 50°F will significantly increase the viscosity of the mixed product. Higher viscosity will reduce fabric penetration, introduce additional air into the system, and extend the cure times beyond 48 hours. DO NOT THIN. Solvents will prevent proper cure.

Epoxy Material Properties		
Cure schedule: 72 hour post-cure at 140°F (60°C)[1]		
Property	**ASTM Method**	**Typical Test Value**
Glass Transition Temperature, T_g	D4065/E1356	180°F (82°C)
Tensile Strength	D638 Type 1	10,500 psi (72.4 MPa)
Tensile Modulus		461,000 psi (3.18 GPa)
Elongation		5.0%
Compressive Strength	D695	12,500 psi (86.2 MPa)
Compressive Modulus		465,000 psi (3.2 GPa)
Flexural Strength	D790	17,900 psi (123.4 MPa)
Flexural Modulus		452,000 psi (3.12 GPa)
Shore D Hardness	D2240	87±3
Water Absorption (24 hours) Water Absorption (13 weeks)	D570	0.33% 1.98%
Adhesion Strength[2] Concrete (ASTM D7522) Steel Epoxy	D4541	>400 psi (concrete failure typ.) >1200 psi >1200 psi

[1] Testing temperature: 73°F (23°C).
[2] Adhesion strength dependent on surface preparation and substrate thickness. Concrete adhesion strength is dependent on the concrete strength and is based on a minimum CSP-2 profile. Steel adhesion strength is based on SSPC-SP10 and SSPC-SP11 surface preparation methods. Cure schedule: 7 days at 73°F (23°C).

CAUTION!

CLEANUP
Collect with absorbent material. Dispose in accordance with local disposal regulations. Uncured material can be removed with approved solvent. Cured materials must be mechanically removed.

HAZARDS
Consult the Safety Data Sheets (SDS) for associated hazards. SDS will be supplied upon request.

Consult safety data sheet (SDS) for more information.
For industrial use only.

FyfeCo.com | FyfeInfo@cs-nri.com | +1.855.708.3617

V: 03.06.2022

Smarter Strengthening Solutions™

CSS V-Wrap™ HMCA

Carbon Fiber Anchor

DESCRIPTION

CSS V-Wrap HMCA is a high-strength, high-modulus unidirectional carbon fiber anchor designed to be field laminated with CSS V-Wrap 770 epoxy to create a carbon-fiber-reinforced polymer (CFRP) composite anchor for improving force transfer.

MATERIAL PROPERTIES

Typical Data

Storage Conditions	Store dry at 40°F – 90°F (4°C – 32°C)
Color	Black
Shelf Life	10 years

Dry Fiber Properties	
Tensile Strength	790,000 psi (5,440 MPa)
Tensile Modulus	42 x 10^6 psi (289,550 MPa)
Elongation at Break	1.9%

Cured Laminate Properties	Design Values
Tensile Strength	165,000 psi (1,138 MPa)
Modulus of Elasticity	15.0 x 10^6 psi (103,400 MPa)
Elongation at Break	1.1%

MADE IN USA with GLOBAL MATERIALS

PERFORMANCE FEATURES

- Manufactured using ICC-approved raw materials
- High tensile modulus and strength
- Lightweight
- Noncorrosive
- Flexible
- Various finish options

APPLICATIONS

The CSS V-Wrap HMCA carbon fiber anchor is combined with CSS V-Wrap epoxies and can be used as a standalone reinforcement or to improve end details and anchorage of various CSS V-Wrap designs.

- Load increases
- Seismic strengthening
- Repair of structural elements
- Change in structural system
- Design or construction defects

PACKAGING

Custom anchor lengths and diameters are available in diameters ranging from 0.375" to 1.5" (9 mm to 37 mm) in ⅛" increments.

HOW TO USE

Design
The CSS V-Wrap HMCA carbon fiber anchors shall be designed to meet specific design criteria. The criteria for each project is dictated by the Engineer of Record and any relevant building codes and/or guidelines. Contact Structural Technologies at (410) 859-6502 for engineering support with anchor design.

Surface Preparation
Surfaces to receive CSS V-Wrap HMCA must be clean and sound. They must be dry and free of frost. All dust, laitance, grease, curing compounds, waxes, deteriorated materials and other bond-inhibiting materials must be removed from the surface prior to application. Existing uneven surfaces must be filled with appropriate epoxy putty or repair mortar. Use abrasive blasting, pressure washing, shotblasting, grinding or other approved mechanical means to achieve an open-pore texture with a concrete surface profile of not less than CSP-3 (ICRI). In certain applications and at the engineer's discretion, the bond between the substrate and the fabric may be determined to be non-critical (such as in column confinement applications). The adhesive bond strength of the concrete may be verified after surface preparation by random pull-off testing (ASTM C1583) at the discretion of the engineer. Minimum tensile strength of 200 psi must be achieved for concrete.

Drilled Hole Preparation
Drill holes to specified diameter, depth and angle according to approved drawings using a rotary hammer drill, a carbide-tipped drill bit conforming to ANSI B212.15-1994, router bits, and a Simpson Strong-Tie® ETB brush.

Drilled hole diameter shall be anchor diameter plus ⅛" (3.18 mm). Round the top edge of the drilled hole using router bits to specified radius. Using clean, compressed air, blow out any remaining debris for four seconds, then clean with the appropriate sized Simpson Strong-Tie ETB brush for a minimum of four cycles, and again blowing out any remaining debris for another four seconds with compressed air.

Application
Manually saturate the anchor and ensure full fiber saturation is achieved. Install the saturated anchor in accordance with the approved project drawings and specifications. Refer to the CSS V-Wrap 770 Epoxy Saturant Technical Data Sheet for all information on the approved epoxy.

Limitations
Minimum application temperature is 40°F.

Storage
Store material in a cool, dark space. Low humidity is recommended. Store at 40°F to 90°F (4°C to 32°C). Avoid freezing. Avoid moisture and water contamination.

CAUTION

Protective Measures: The use of safety glasses, chemical-resistant gloves and appropriate clothing to minimize skin contact is recommended. The use of a NIOSH-approved respirator is required to protect respiratory tract when ventilation is not adequate to limit exposure below the PEL. Refer to Safety Data Sheets (SDS) available at **strongtie.com/sds** for detailed information.

FIRST AID

Skin: Wash fibers off skin with water and soap. If fibers are embedded in the skin, remove with tweezers. Discard clothing that may contain embedded fibers. Seek medical advice if exposure results in adverse effects.

Eyes: Immediately flush with a continuous water stream for at least 20 minutes. Washing immediately after exposure is expected to be effective in preventing damage to the eyes. Seek medical advice.

Inhalation: If there is inhalation exposure to the fibers of this product, remove source of exposure and move affected person to fresh air. If not breathing, give artificial respiration. If there is breathing difficulty, give oxygen. Seek medical advice for any respiratory problems.

Ingestion: Not expected to occur since ingestion is not a likely route of exposure for this product. If ingestion does occur, DO NOT INDUCE VOMITING. Nothing by mouth if unconscious. Seek medical advice.

CLEAN-UP

Spill/Release and Cleanup Procedures: In case of spill, collect (e.g., sweep up, vacuum, etc.) spilled material and either reuse or dispose of properly. Chopped or milled carbon fibers may be slippery if spilled, posing an accident risk. Wear personal protective equipment as described in the SDS during cleanup activities.

LIMITED WARRANTY

This product is covered by the Simpson Strong-Tie RPS Product Limited Warranty, which is available at **strongtie.com/limited-warranties** or by calling Simpson Strong-Tie at (800) 999-5099.

TYFO® SCH COMPOSITE ANCHORS

Carbon Tyfo® Fiber Anchor Systems

DESCRIPTION

The Tyfo® SCH Composite Anchors are custom, uni-directional reinforcing carbon fiber bundles that are combined with the Tyfo® S Epoxy for anchoring applications.

USE

Tyfo® SCH Composite Anchors are manually saturated with Tyfo® S Epoxy and installed to improve end details, anchoring or development of tension or shear forces in various Tyfo® designs.

ADVANTAGES

- IAPMO UES ER-595 listed product
- System-compatible anchoring designs
- Excellent wet-out and handling properties
- 100% solids, solvent-free epoxy matrix
- Low viscosity, long working time
- Ambient cure application

PACKAGING

Packaging and weight will vary based on anchor design requirements.

CONSUMPTION RATE

Fiber-to-epoxy ratio by weight:
For Tyfo® SCH Fiber Anchors: 1 : 1.35

SHELF LIFE

Epoxy – two years in original, unopened and properly stored containers.
Anchors – ten years in proper storage conditions.

STORAGE CONDITIONS

Store epoxy at 60°F to 100°F (15°C to 38°C). Resin is susceptible to crystallization at temperatures below 50°F. If crystallized, epoxy must be reheated until clear. Store fabric rolls flat, not on ends, and at temperatures below 100°F (38°C). Avoid moisture and water contamination.

Typical Dry Fiber Properties

Property	Typical Test Value
Tensile Strength	620,000 psi (4.3 GPa)
Tensile Modulus	36 x 10^6 psi (250 GPa)
Ultimate Elongation	1.7%
Density	0.064 lbs/in^3 (1.77 g/cm^3)

Composite Gross Laminate Properties

Property[1]	ASTM Method	Typical Test Value	ACI 355.4 Design Value[2]
Ultimate Tensile Strength	E488	140,000 psi	110,000 psi
Ultimate Shear Strength		59,000 psi	40,000 psi
Bond Shear Strength in uncracked concrete		4,100 psi	3,000 psi
Bond shear Strength in cracked concrete, crack width = 0.012"		2,700 psi	2,300 psi
Bond shear Strength in cracked concrete, crack width = 0.020"		2,600 psi	1,600 psi

[1] Properties based on testing ⅝" and ⅞" anchors in low strength concrete.
[2] Design properties calculated per ACI 355.4.

Anchor Construction Detailing

Use carbide-tipped masonry and concrete hammer bit meeting requirements of ANSI B212.15.

Composite Anchor Diameter, in.	Weight per unit length, oz./in.	Concrete Bit Size, in.
¼	0.02	⅜
⅜	0.04	½
½	0.08	¾
⅝	0.12	⅞
¾	0.17	1
⅞	0.23	1-⅛

INSTALLATION OF THE TYFO® SCH ANCHORS

DESIGN

The Tyfo® SCH Anchors are designed to meet specific project criteria dictated by the engineer of record and any relevant building codes and/ or guidelines. Tyfo® SCH Anchors are incorporated for additional development, anchorage, or end detailing of strengthening systems. The size and area of the Tyfo® SCH anchors are directly correlated to the equivalent fiber area of the Tyfo® SCH-41 and Tyfo® SCH-41-2X laminates. The design shall be based on the amount of tension force transferred as described in the Fyfe Company Design Manual v10. FyfeFRP LLC engineering staff may provide preliminary design, specification wording and application details based on the project requirements.

INSTALLATION

The Tyfo® system is to be installed by FyfeFRP LLC trained and certified applicators in accordance with the FyfeFRP LLC quality control manual, project specifications, and design requirements.

Drilling

1. Drill anchor holes with rotary hammer drill and carbide bit to the required depth.
2. Grind edges around anchor holes for smooth transitions as required by the drawings.
3. HEPA-Vacuum the concrete dust generated during drilling, whenever possible.

Cleaning

1. Vacuum the concrete dust from the anchor hole. Alternatively, blow out anchor hole with compressed air in combination with vacuum collection to clean the anchor hole.
2. Use a steel bristle brush to clean out the hole walls. Perform 5 insertions. (diameter of brush to be equal to or greater than concrete bit diameter)
3. Vacuum anchor hole.
4. Use the pipe brush to clean out the hole walls. Perform 5 insertions.
5. Vacuum anchor hole.

Anchor Embedment

1. Prime the anchor hole with Thickened Tyfo® S, using a syringe with flexible tip capable of filling from max depth of hole. Fill hole up to 75%.
2. Embed saturated anchor into hole to the specified depth with anchor insertion tool.
3. Keep tool inserted and anchor tensioned while free end is splayed as required.
4. Remove insertion tool and backfill cavity with thickened Tyfo® S.
5. Apply skim coat of thickened Tyfo® S over anchor hole and splay area.
6. Continue with installation as detailed in drawings

MIXING TYFO® S EPOXY

For pre-measured units in 5-gallon containers, pour the contents of component B into the component A container. Mix thoroughly with a low speed mixer at 400 to 600 RPM until uniformly blended. Ensure epoxy is transferred between the A and B buckets. For 55-gallon drums, mix component A and component B per the appropriate weight or volumetric mix ratio. Resin may be heated to achieve desired viscosity (i.e. radiant heating, drum heaters, water bath). Mixed Tyfo® S Epoxy may be thickened by adding up to 7 percent by weight of fumed silica (such as Cab-o-sil TS-720).

APPLICATION NOTES

Manually saturate the Tyfo® SCH Composite Anchors with Tyfo® S Epoxy. The fully saturated anchor is then applied as detailed on the project drawings. Maintain an appropriate slope when transitioning fibers over uneven surfaces. If anchor penetrations are elevated from the bonding surface, use an appropriate transition to slope the anchors from the anchor penetrations onto the bonding surface. A typical slope requirement is a 4:1 transition. Refer to project drawings for the slope detail or contact FyfeFRP LLC. Slope to be filled with a thickened epoxy or epoxy mortar. For slopes greater than 1" height, use an approved epoxy mortar.

PROTECTIVE COATINGS

Apply a final coat of thickened Tyfo® S Epoxy to all fabric edges, including butt splice, termination points and jacket edges. Paint between 24 and 72 hours after final application of epoxy. If more than 72 hours after application, prepare the surface by light sandblast or hand sanding to lightly etch the surface.

LIMITATIONS

Recommended substrate temperature range is 50°F to 100°F (10°C to 38°C). All coating applications to be performed at a minimum of 5°F (3°C) above the dew point. Maintain conditions for the first 48 hours of cure. Temperatures below 50°F will significantly increase the viscosity of the mixed product. Higher viscosity will reduce fabric penetration, introduce additional air into the system, and extend the cure times beyond 48 hours. DO NOT THIN. Solvents will prevent proper cure.

CAUTION!

CLEANUP

Collect with absorbent material. Dispose in accordance with local disposal regulations. Uncured material can be removed with approved solvent. Cured materials must be mechanically removed.

HAZARDS

Consult the Safety Data Sheets (SDS) for associated hazards. SDS will be supplied upon request. Carbon fiber is electro-conductive.

Consult safety data sheet (SDS) for more information. For industrial use only.

FyfeCo.com | FyfeInfo@cs-nri.com | +1.855.708.3617

V: 07.13.2022

Smarter Strengthening Solutions™

CSS V-Wrap™ 770

Epoxy Saturant

SIMPSON Strong-Tie | structural TECHNOLOGIES

DESCRIPTION

CSS V-Wrap 770 is a two-part, 100% solids epoxy for high-strength composite bonding applications. CSS V-Wrap 770 matrix material is combined with CSS V-Wrap carbon and glass fabrics to provide a wet-layup composite for strengthening of structural members. It is formulated to provide high elongation to optimize properties of the CSS V-Wrap composite systems. It provides a long working time for application, with no offensive odor. CSS V-Wrap 770 may be thickened with fumed silica to produce a tack coat/putty or a finishing coat, depending upon the project requirements. CSS V-Wrap 770 contains no Volatile Organic Compounds (VOC) or solvents.

CODE REPORTS AND COMPLIANCE

ICC-ES ESR-4930

MATERIAL PROPERTIES*

Part A & B Properties

Approximate Pot Life	3 to 6 hours at 68°F (20°C)
Color	**Part A:** Clear **Part B:** Clear **Mixed:** Clear
Density	**Part A:** 9.7 lb./gal (1.16 kg/L) **Part B:** 7.9 lb./gal (0.95 kg/L) **Mixed:** 9.17 lb./gal (1.11 kg/L)
Mixing Ratio	100A:41B by volume 100A:33B by weight
Shelf Life	24 months stored in unopened containers at 70°F (21°C)
Storage	Store material in a dry area between 40°F (4°C) and 100°F (38°C) with no exposure to moisture.

Cured Epoxy Properties	Average Values
Tensile Strength (ASTM D638)	8,800 psi (60.7 MPa)
Tensile Modulus (ASTM D638)	400,000 psi (2,760 MPa)
Elongation at Break (ASTM D638)	4.4%
Flexural Strength (ASTM D790)	16,000 psi (110.3 MPa)
Flexural Modulus (ASTM D790)	420,000 psi (2,896 MPa)
Compressive Strength (ASTM D695)	12,200 psi (84.1 MPa)
Compressive Modulus (ASTM D695)	440,000 psi (3,304 MPa)
T_g (ASTM E1640)	187°F (86°C)
VOC Content (ASTM D2369)	0% VOC

* Curing schedule: 72 hours post cure at 140°F (60°C)

MADE IN USA with GLOBAL MATERIALS

PERFORMANCE FEATURES

- ICC-ES ESR-4930 listed product
- UL listed (ul.com/database)
- 100% solvent-free
- Good high / low temperature properties
- High elongation
- NSF/ANSI Standard 61 listed product for drinking water systems

APPLICATIONS

CSS V-Wrap 770 is a multi-use epoxy that performs as a primer, tack coat/putty, and saturating resin for the CSS V-Wrap carbon and glass fiber systems. Fumed silica may be added to thicken the resin. The maximum ratio by volume is 1.5 of fumed silica to 1 part of resin.

PACKAGING

Kit Size	Model No.
4 US gallon (15.1 L)	CV-ES7704KT

HOW TO USE

Surface Preparation
CSS V-Wrap 770 should be applied to substrates that are free of protrusions, dust, oils, and other surface contaminates or bond-inhibiting materials. Substrates should be dry and exhibit an open pore structure.

Application
Apply primer to repair surfaces with a medium nap roller or non-shedding brush. Ensure full saturation of fabric sheets is achieved before installation. Heavier fabrics typically require mechanical saturation. Apply thickened CSS V-Wrap epoxy using trowels.

Basic Application Equipment
Application processes for CSS V-Wrap 770 will require mixing drill, mixing paddle, ¼" nap rollers, steel rollers, paint brushes, trowels and saturator.

Mixing
Combine the contents of CSS V-Wrap 770-A pail and CSS V-Wrap 770-B pail together making sure to scrape all material from the sides of the pail and mix for 3 minutes using a mixer at a speed of 400–600 RPM until uniformly blended. Transfer the mixed epoxy into the other pail and mix for an additional 2 minutes. Mix ratio: by volume 100A:41B, by weight 100A:33B.

Observe Working Time Limitations
Mix no more material than can be applied within the working time. Available work time, temperature and complexity of the application will determine how much material should be mixed at one time. Keep material cool and in shaded area, away from direct sunlight in warm weather. During hot weather, work time can be extended by keeping the material cool before and after mixing or by immersing the pot in ice water.

Maintenance
Periodically inspect the applied material and repair localized areas as needed.

Coverage Rates
As a Primer:

Concrete:	225 ft.²/gal (5.5 m²/L)
Masonry (Concrete):	125 ft.²/gal (3.0 m²/L)
Masonry (Clay):	200 ft.²/gal (4.9 m²/L)

As a Putty/Tack Coat:

Filler:	60 ft.²/gal (1.5 m²/L)

(Depending on surface roughness)

As Saturant:

CSS V-Wrap C100H / C100HM	80 ft.²/gal (1.9 m²/L)
CSS V-Wrap C200H / C200HM	60 ft.²/gal (1.5 m²/L)
CSS V-Wrap C400H / C400HM	40 ft.²/gal (1 m²/L)
CSS V-Wrap C220B	60 ft.²/gal (1.5 m²/L)
CSS V-Wrap EG50 / EG50B	60 ft.²/gal (1.5 m²/L)

Coverage rates may vary based on installation procedure and fabric type. Contact STRUCTURAL TECHNOLOGIES at (410) 859-6502 for coverage rates.

Limitations
Only apply CSS V-Wrap 770 when the ambient temperature is between 40°F and 100°F (4°C to 38°C). Topcoat selection should be based upon requirements for protection from environmental exposures, aesthetics and fire protection/burn characteristics.

Storage
Store in a cool, dry area (40°F and 100°F [4°C to 38°C]) away from direct sunlight, flame or other hazards.

CAUTION

Component "A": Causes skin and serious eye irritation. May cause an allergic skin reaction.

Component "B": CORROSIVE! Harmful if swallowed. Causes severe skin burns and eye damage. May cause an allergic skin reaction.

Protective Measures: The use of safety glasses and chemically-resistant gloves is recommended. Use appropriate clothing to minimize skin contact. The use of NIOSH-approved respirator is required to protect respiratory tract when ventilation is not adequate to limit exposure below the PEL. Refer to Safety Data Sheets (SDS) available at **strongtie.com/sds** for detailed information.

These products are for professional and industrial use only and are to be installed by trained and qualified applicators. Trained applicators must follow installation instructions.

FIRST AID

Eye Contact: Immediately flush eyes with plenty of cool water for at least 15 minutes while holding the eyes open. If redness, burning, blurred vision, or swelling persists, seek medical advice.

Skin Contact: In case of contact, remove product and immediately wash affected area with plenty of soap and water for at least 5 minutes. Do not apply greases or ointments. Remove contaminated clothing. Clean contaminated clothing with soap and water before re-use. If redness, burning or swelling persists, seek medical advice.

Ingestion: DO NOT INDUCE VOMITING. Never administer anything by mouth to an unconscious person. Rinse out mouth with water, then drink sips of water to remove taste from mouth. Seek medical advice. Do not leave victim unattended. If vomiting occurs spontaneously, lay victim on side and keep head lower than waist to prevent aspiration.

Inhalation: If respiratory irritation or distress occurs, remove victim to fresh air. If breathing is difficult, give oxygen. If breathing stops, apply artificial respiration. Seek medical advice.

CLEAN-UP

Environmental Precautions: Construct a dike to prevent spreading. Keep out of sewers, storm drains, surface waters and soils.

Equipment: Use methyl ethyl ketone or acetone. Observe fire and health precautions when using solvents. Dispose of in accordance with local regulations.

Small Spills: Soak up with an absorbent material, such as clay, sand or other suitable non-reactive material. Place in leak-proof containers. Seal tightly for proper disposal.

Large Spills: Approach suspected leaks with caution. Construct a dike or trench to contain material. Soak up with an absorbent material, such as clay, sand or other suitable non-reactive material. Place in leak-proof containers. Seal tightly for proper disposal.

Disposal: Dispose of container and unused portions in accordance with local, state and federal regulations. Emptied container may contain product residue and should not be reused.

LIMITED WARRANTY

This product is covered by the Simpson Strong-Tie RPS Product Limited Warranty, which is available at **strongtie.com/limited-warranties** or by calling Simpson Strong-Tie at (800) 999-5099.

FYFE®

TYFO® S
Saturant Epoxy

DESCRIPTION
The Tyfo® S Epoxy is a two-component epoxy matrix material for bonding applications. The Tyfo® S Epoxy combined with the Tyfo® fabrics make up the Tyfo® Systems which are NSF/ANSI Standard 61-G certified for drinking water systems. It is a high elongation material which gives optimum properties as a matrix for the Tyfo® system. It provides a long working time for application, with no offensive odor.

USE
The Tyfo® S Epoxy matrix material is combined with the Tyfo® fabrics to provide an ambient-cure wet-layup composite system for strengthening structural members. Tyfo® S Epoxy may be thickened with fumed silica (such as Cab-O-Sil TS-720) to be used as a primer, tack coat or finish depending on project requirements.

ADVANTAGES
- ICC-ES ESR-2103 listed product
- IAPMO UES ER-595 listed product
- Tyfo® Systems are NSF/ANSI Standard 61-G certified
- Good high and low temperature properties
- 100% solids, solvent-free
- Long working time
- High elongation
- Ambient cure

PACKAGING
Pre-measured 5-gallon units with a combined material volume of 4 gallons or in 55-gallon drums.

EPOXY MIX RATIO
100A : 34.5B by weight
100A : 42.0B by volume

CONSUMPTION RATE
Fabric-to-epoxy ratio by weight:
For Tyfo® SCH Fabrics: 1 : 1
For Tyfo® SEH Fabrics: 1 : 0.8

SHELF LIFE
Epoxy - two years in original, unopened and properly stored containers.
Fabric - 10 years in proper storage conditions.

STORAGE CONDITIONS
Store epoxy at 60°F to 100°F (15°C to 38°C). Resin is susceptible to crystallization at temperatures below 50°F. If crystallized, epoxy must be reheated until clear. Store fabric rolls flat, not on ends, and at temperatures below 100°F (38°C). Avoid moisture and water contamination.

Epoxy Material Properties

Material properties are based on standard laboratory conditions (23°C, 50 percent relative humidity.)

Property	Typical Test Value	
Net Weight	Component A Component B Mixed	27.4 lbs. (2.8 gal) 9.60 lbs. (1.2 gal) 37.0 lbs. (4.0 gal)
Color	Component A Component B Mixed	Clear to amber Clear to yellow Clear to amber
Viscosity	Component A Component B Mixed	11,000-13,000 cps 11 cps 600-700 cps
Density (D792) Pounds/Gallon	Component A Component B Mixed	9.7 (1.16 kg/L) 7.9 (0.95 kg/L) 9.2 (1.11 kg/L)
Pot Life (Working Time)	Mixed	3 to 4 hours
Gel Time (Time to Gelation)	Mixed	10 hours

Epoxy Material Properties

Cure schedule: 72 hour post-cure at 140°F (60°C)[1]

Property	ASTM Method	Typical Test Values
Glass Transition Temperature, T_g	D4065 E1356	180°F (82 C)
Tensile Strength	D638 Type 1	10,500 psi (72.4 MPa)
Tensile Modulus		461,000 psi (3.18 GPa)
Elongation		5.0%
Compressive Strength	D695	12,500 psi (86.2 MPa)
Compressive Modulus		465,000 psi (3.2 GPa)
Flexural Strength	D790	17,900 psi (123.4 MPa)
Flexural Modulus		452,000 psi (3.12 GPa)
Shore D Hardness	D2240	87±3
Water Absorption (24 hours) Water Absorption (13 weeks)	D570	0.33% 1.98%
Adhesion Strength[2] Concrete (ASTM D7522) Steel Epoxy	D4541	 >400 psi (concrete failure typ.) >1200 psi >1200 psi

[1] Testing temperature: 73°F (23°C).
[2] Adhesion strength dependent on surface preparation and substrate thickness. Concrete adhesion strength is dependent on the concrete strength and is based on a minimum CSP-2 profile. Steel adhesion strength is based on SSPC-SP10 and SSPC-SP11 surface preparation methods. Cure schedule: 7 days at 73°F (23°C).

HOW TO USE THE TYFO® S SATURANT EPOXY

INSTALLATION
The Tyfo® system is to be installed by FyfeFRP LLC trained and certified applicators in accordance with the FyfeFRP LLC quality control manual, project specifications, and design requirements.

SURFACE PREPARATION
The required surface preparation is dependent on the type of element being strengthened. In general, the surface must be clean, dry and free of protrusions or cavities to prevent voids behind the Tyfo® system. Column surfaces that will receive continuous wraps typically only require a clean, sound substrate. Discontinuous wrapping surfaces (walls, beams, slabs, etc.) require a minimum CSP-2 profile to prepare for bonding, achieved by light sandblast, grinding or other approved methods per ICRI 310.2R. Tyfo® Composite Anchors may be incorporated in the designs. FyfeFRP LLC engineering staff will provide the proper specifications and details based on project requirements.

MIXING TYFO® S EPOXY
For pre-measured units in 5-gallon containers, pour the contents of component B into the component A container. Mix thoroughly with a low speed mixer at 400 to 600 RPM until uniformly blended. Ensure epoxy is transferred between the A and B buckets. For 55-gallon drums, mix component A and component B per the appropriate weight or volumetric mix ratio. Resin may be heated to achieve desired viscosity (i.e. radiant heating, drum heaters, water bath). Mixed Tyfo® S Epoxy may be thickened by adding up to 7 percent by weight of fumed silica (such as Cab-o-sil TS-720) or approved filler such as HDPE fibers. DO NOT THIN. Solvents will prevent proper cure.

THICKENED TYFO® S EPOXY
Use Cab-o-sil TS-720 by Cabot Corp. or similar. For horizontal and vertical surfaces, use up to 2.0 lbs. fumed silica per kit or 5.4 percent by weight. For overhead surfaces use up to 2.5 lbs. per kit or 6.7 percent by weight. Site conditions may affect the amount of fumed silica required to achieve desired thickness. Do not exceed 7 percent by weight.

APPLICATION
Tyfo® S Epoxy is applied to the Tyfo® fabric using a saturator machine or by approved manual saturation methods (trowel, roller, or similar). Hand saturation is allowable, provided the epoxy is applied uniformly and meets the required fiber-to-epoxy ratio. Tyfo® S Epoxy is applied as a prime coat by brush or roller. Please refer to FyfeFRP LLC's NSF Listing for the NSF 61-G listed application method (www.NSF.org).

LIMITATIONS
Recommended substrate temperature range is 50°F to 100°F (10°C to 38°C). All coating applications to be performed at a minimum of 5.4°F above the dew point. Maintain conditions for the first 48 hours of cure. Temperatures below 50°F will significantly increase the viscosity of the mixed product. Higher viscosity will reduce fabric penetration, introduce additional air into the system, and extend the cure times beyond 48 hours. DO NOT THIN. Solvents will prevent proper cure.

CAUTION!

CLEANUP
Collect with absorbent material. Dispose in accordance with local disposal regulations. Uncured material can be removed with approved solvent. Cured materials must be mechanically removed.

HAZARDS
Consult the Safety Data Sheets (SDS) for associated hazards. SDS will be supplied upon request.

Consult safety data sheet (SDS) for more information.
For industrial use only.

FyfeCo.com | FyfeInfo@cs-nri.com | +1.855.708.3617

V: 03.06.2022

Appendix I. Crack Maps

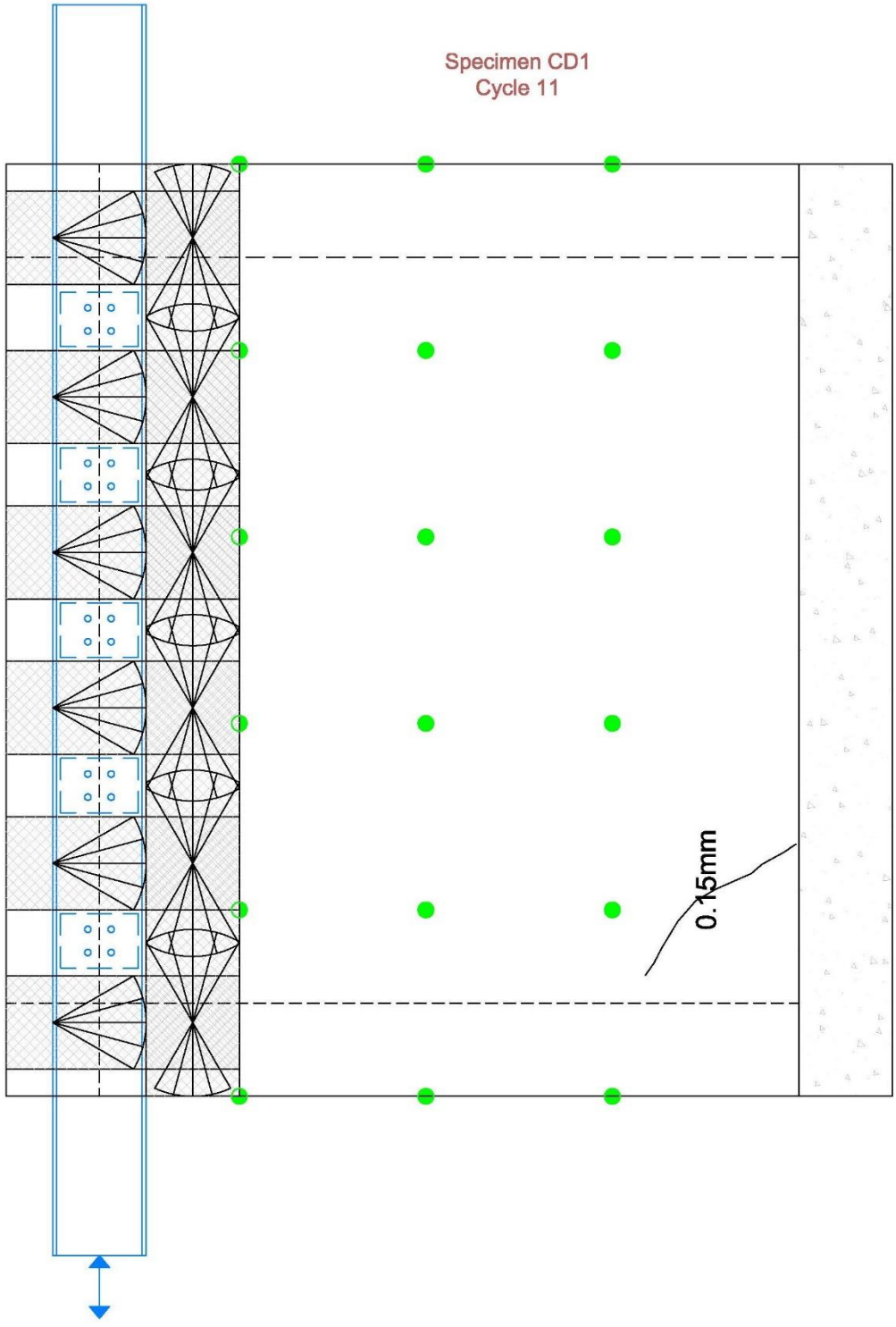

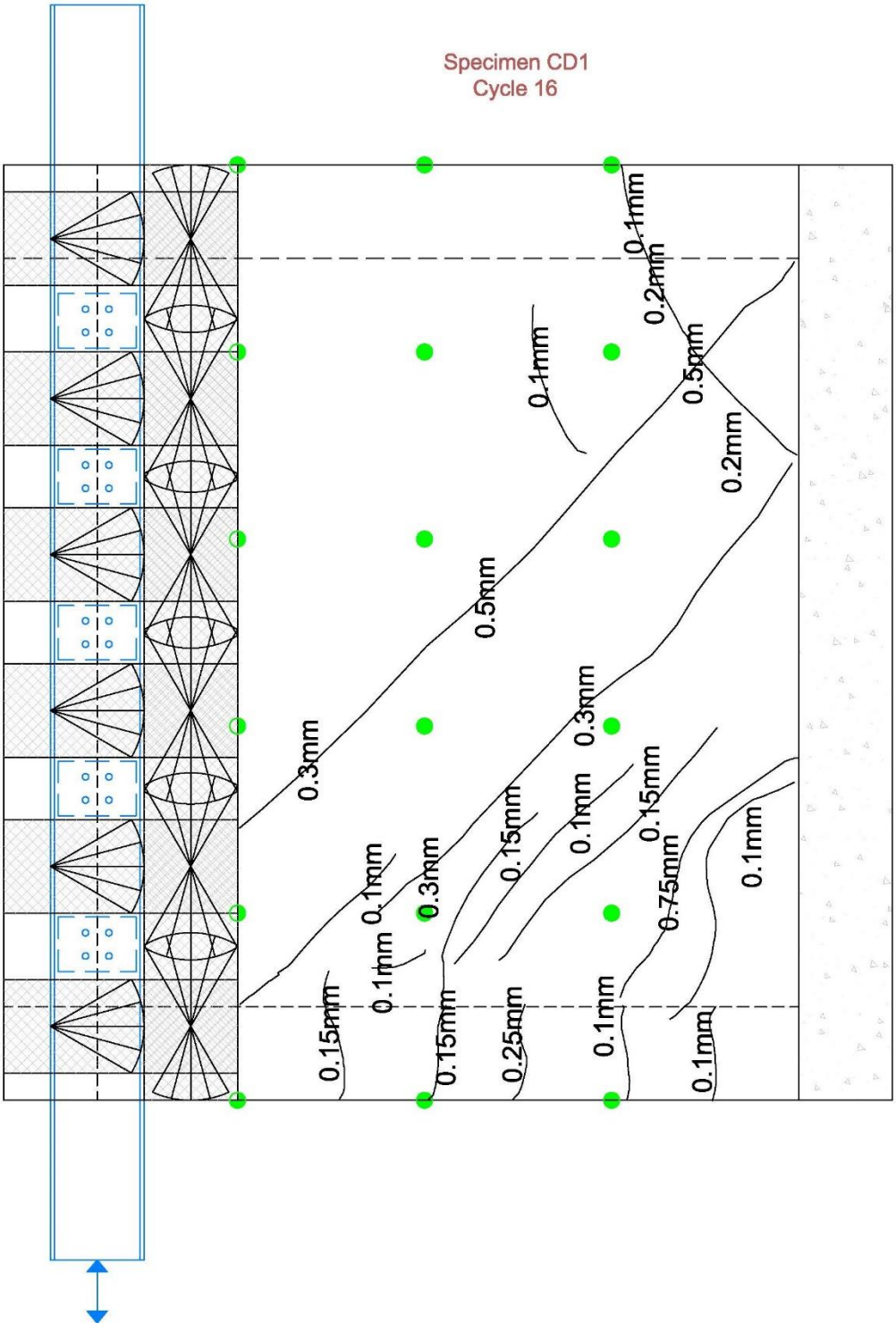
Specimen CD1
Cycle 16
0.1mm
0.2mm
0.5mm
0.1mm
0.2mm
0.5mm
0.3mm
0.3mm
0.3mm
0.15mm
0.1mm
0.15mm
0.1mm
0.3mm
0.1mm
0.75mm
0.1mm
0.15mm
0.25mm
0.1mm
0.1mm

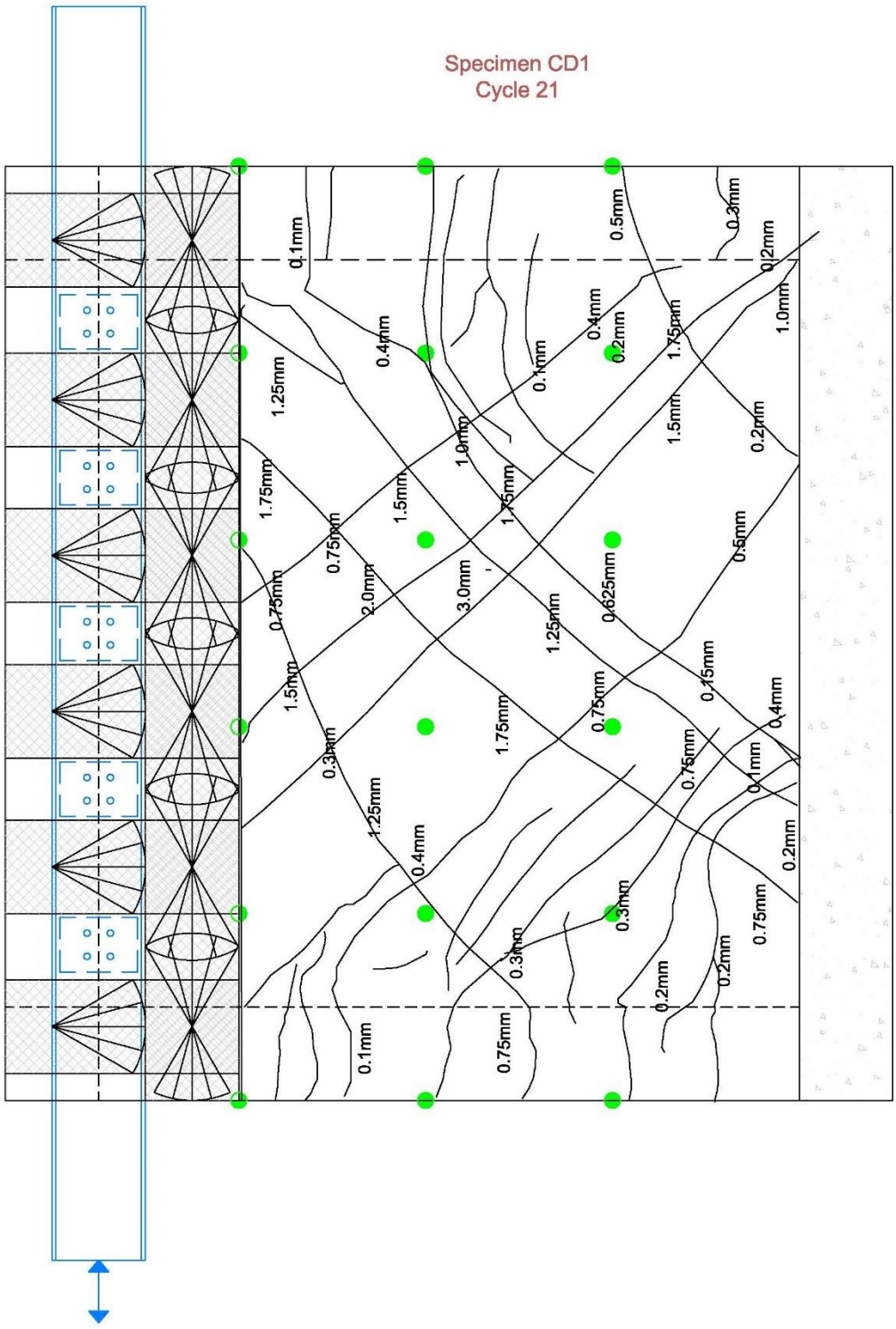
Specimen CD1
Cycle 21
0.1mm
0.5mm
0.3mm
0.2mm
0.4mm
0.2mm
1.75mm
1.0mm
1.25mm
0.1mm
1.5mm
0.2mm
1.0mm
1.75mm
1.75mm
1.5mm
0.75mm
0.5mm
0.75mm
2.0mm
3.0mm
0.625mm
1.25mm
1.5mm
0.15mm
0.75mm
0.4mm
0.3mm
1.75mm
0.75mm
0.1mm
1.25mm
0.4mm
0.2mm
0.3mm
0.75mm
0.3mm
0.2mm
0.2mm
0.2mm
0.75mm
0.1mm
0.75mm

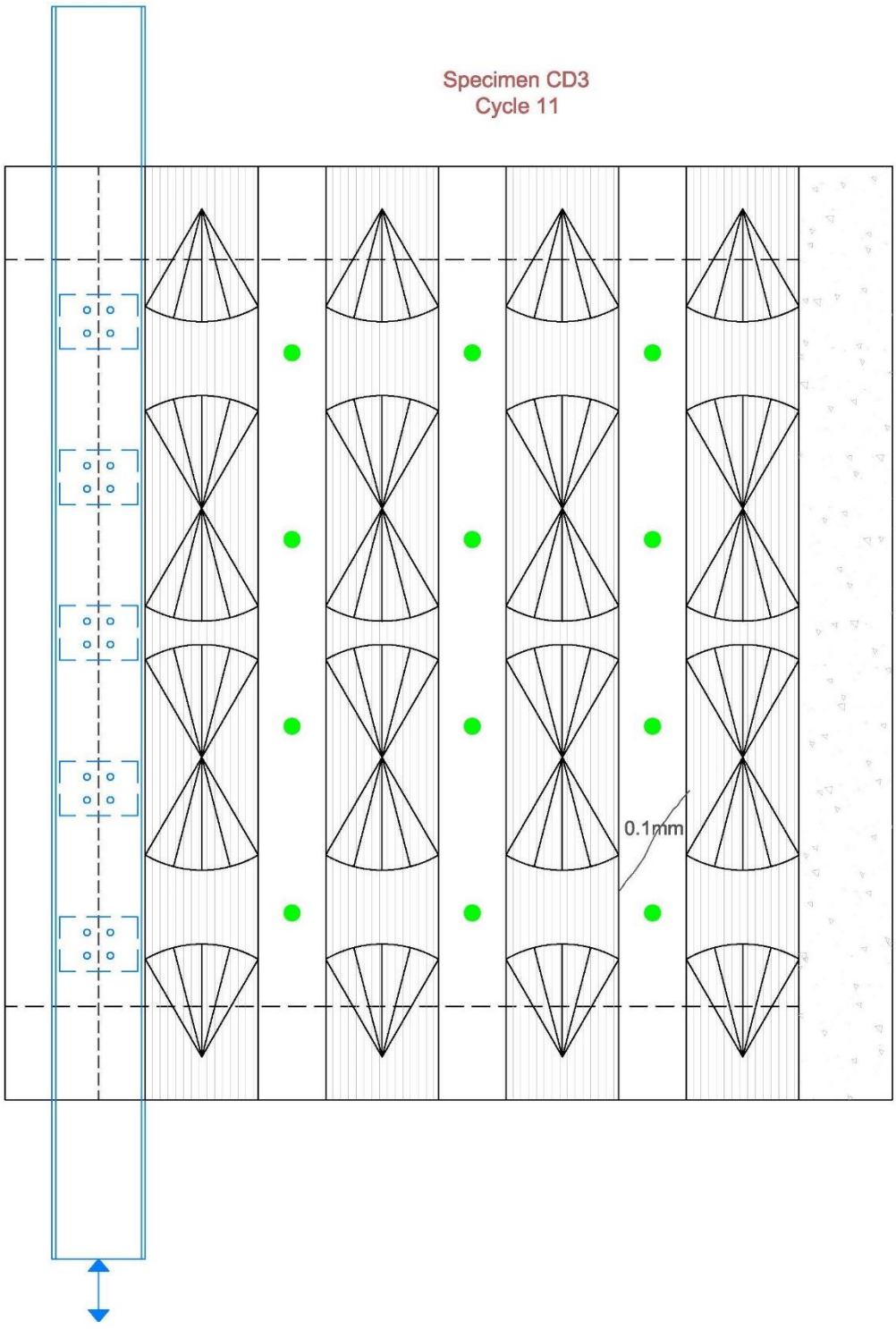
Specimen CD3
Cycle 11
0.1mm

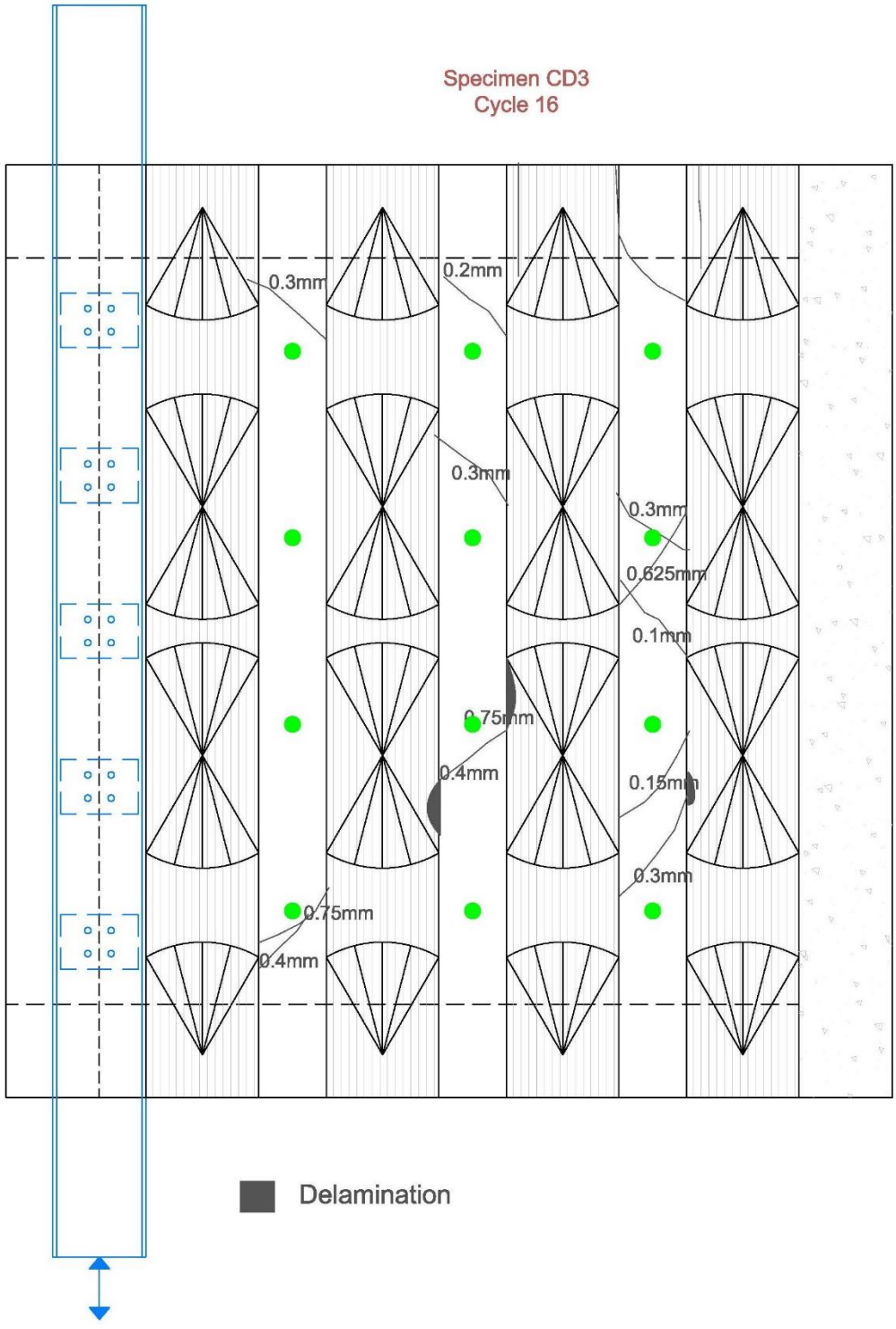
Specimen CD3
Cycle 16
0.3mm
0.2mm
0.3mm
0.3mm
0.625mm
0.1mm
0.75mm
0.4mm
0.15mm
0.3mm
0.75mm
0.4mm
Delamination

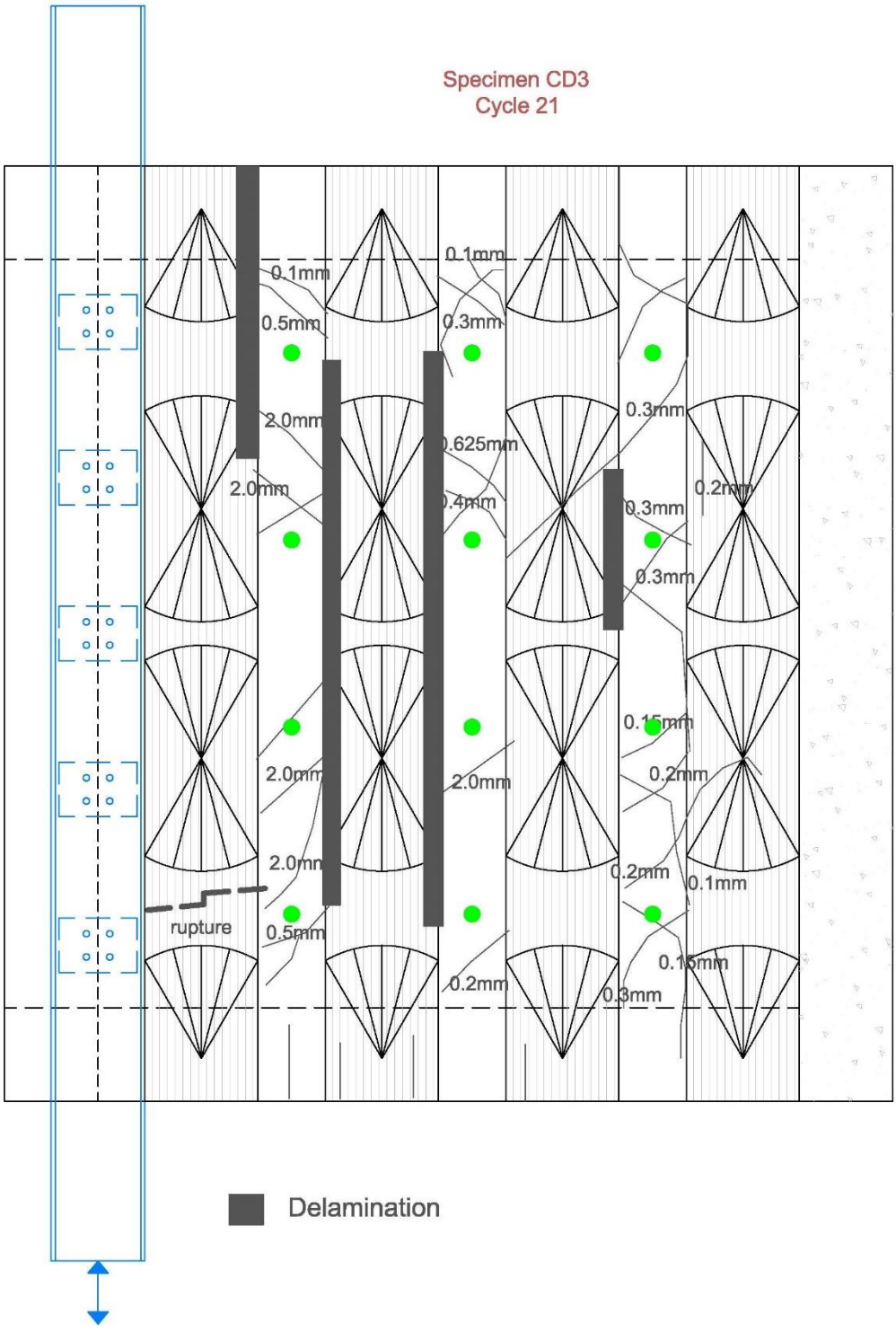
Specimen CD3
Cycle 21
0.1mm
0.5mm
2.0mm
2.0mm
0.1mm
0.3mm
0.625mm
0.4mm
2.0mm
0.3mm
0.3mm
0.2mm
0.3mm
0.3mm
0.15mm
0.2mm
2.0mm
2.0mm
0.2mm
0.1mm
rupture
0.5mm
0.15mm
0.2mm
0.3mm
Delamination

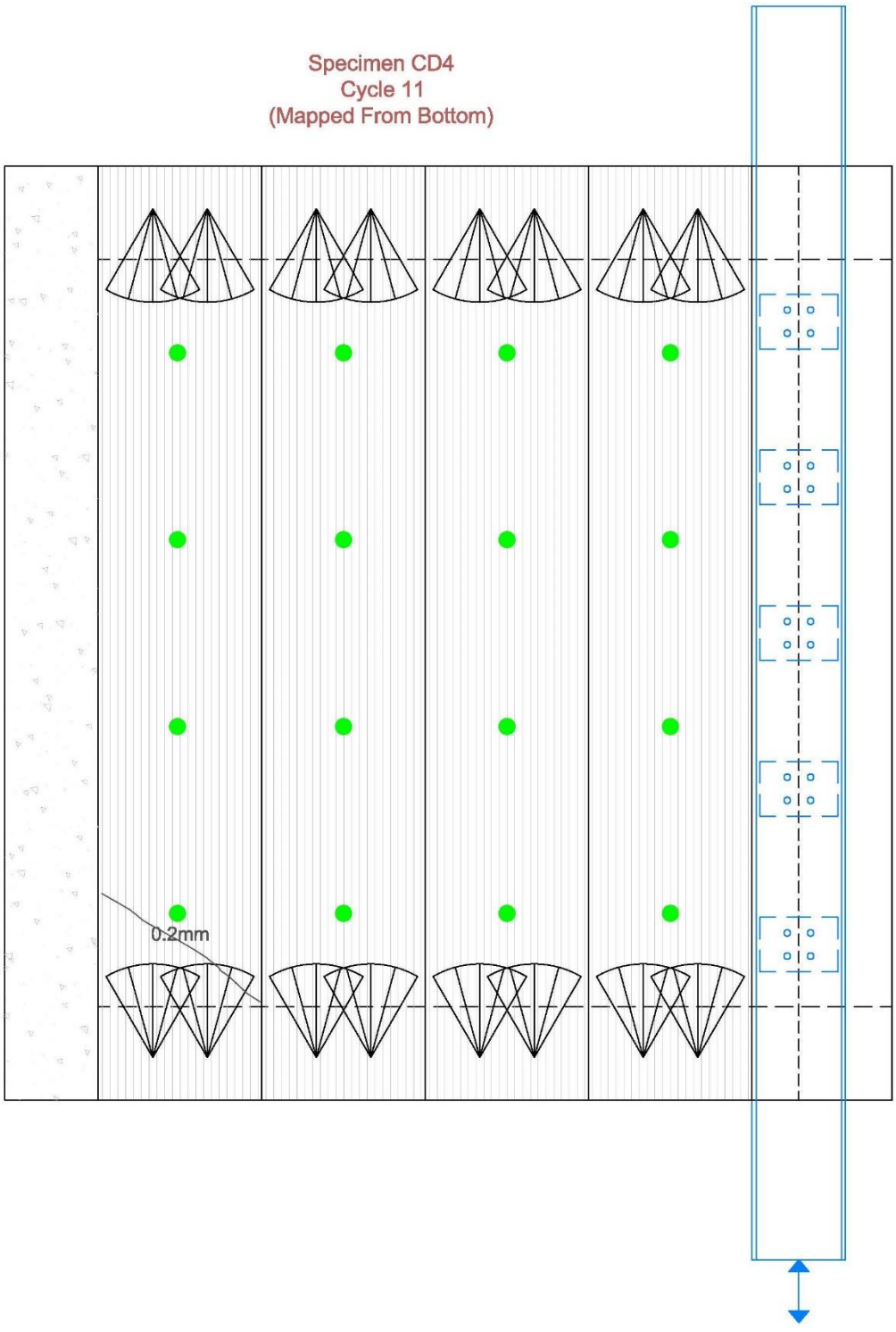
Specimen CD4
Cycle 11
(Mapped From Bottom)
0.2mm

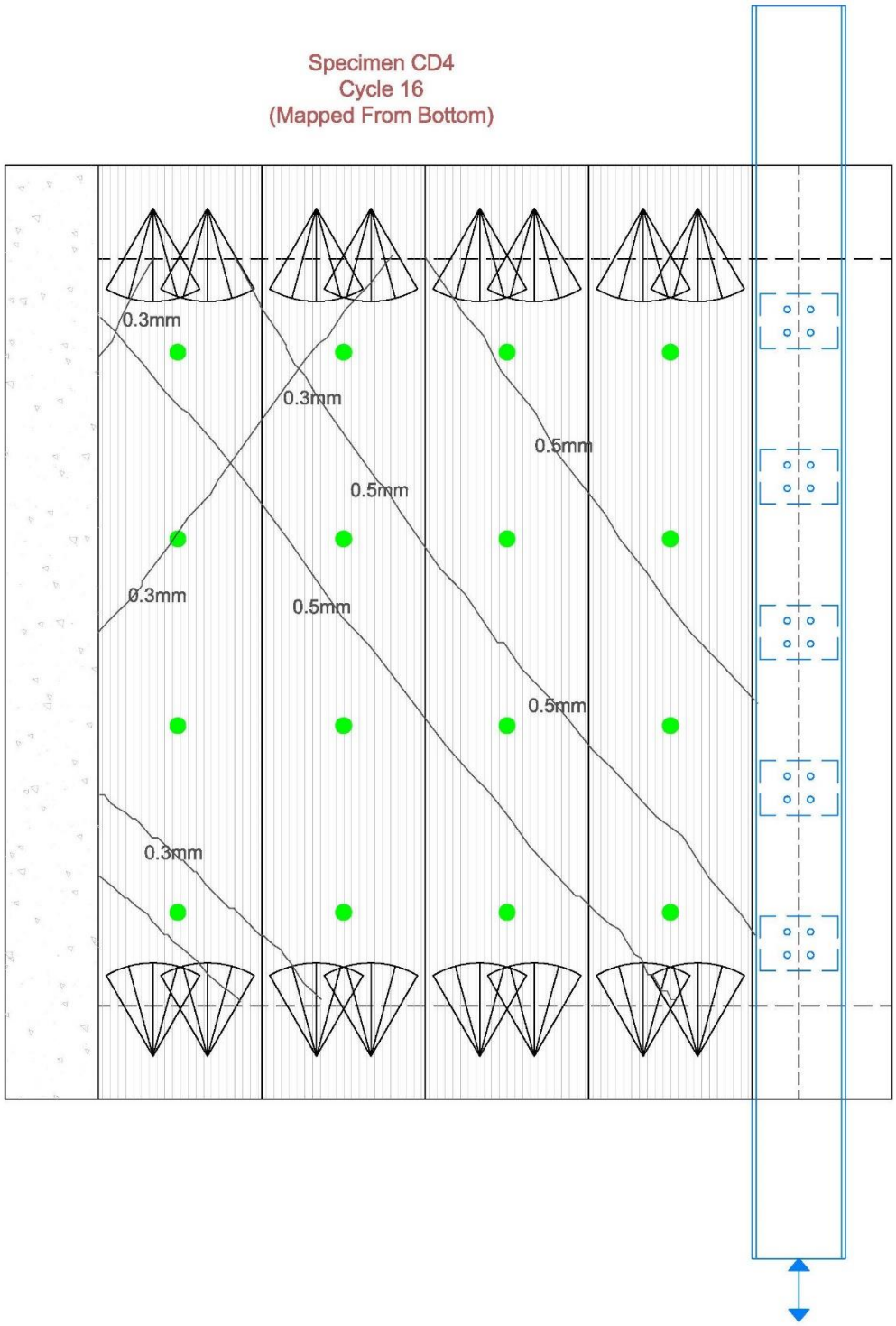
Specimen CD4
Cycle 16
(Mapped From Bottom)
0.3mm
0.3mm
0.5mm
0.5mm
0.3mm
0.5mm
0.5mm
0.3mm

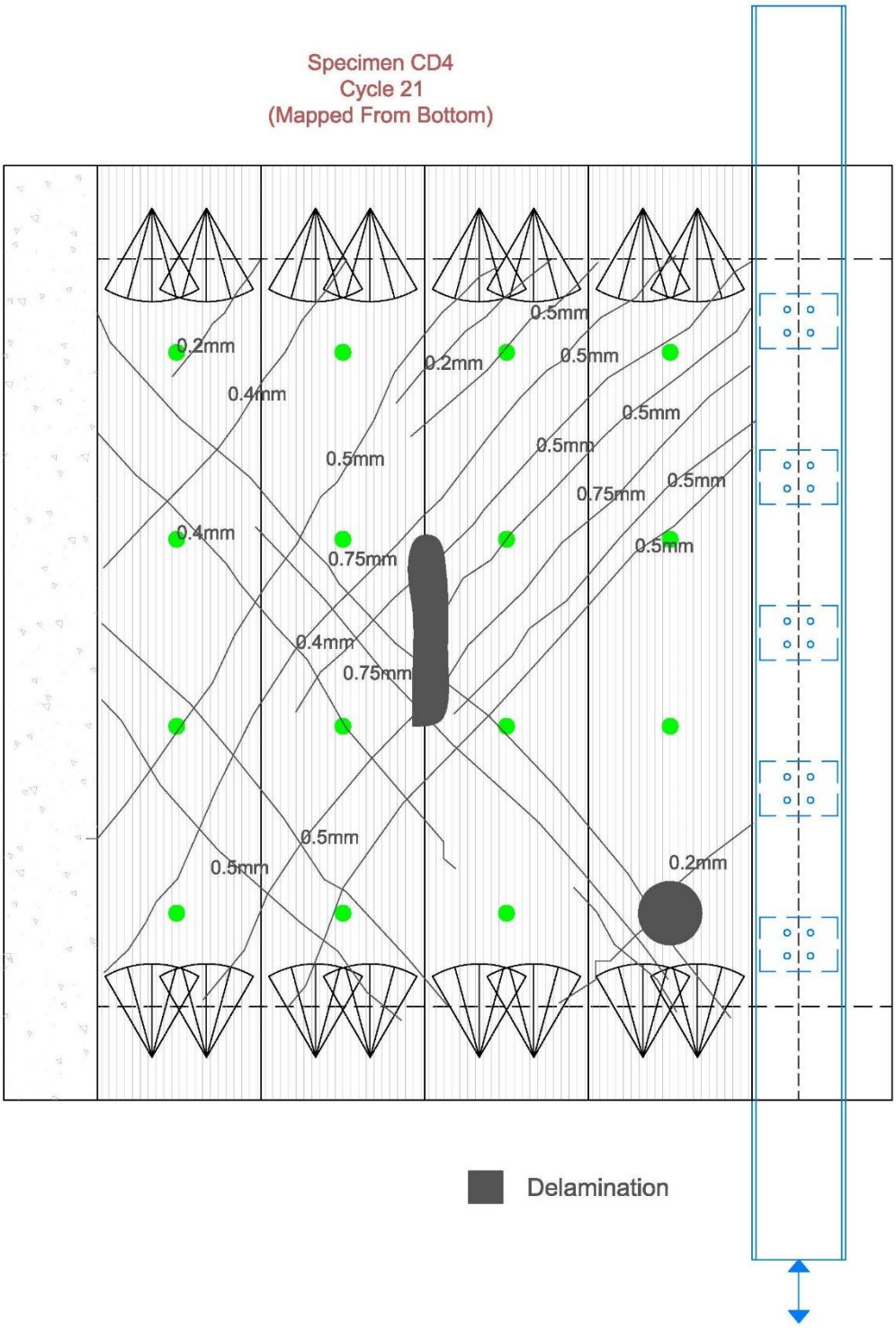
Specimen CD4
Cycle 21
(Mapped From Bottom)
0.2mm
0.4mm
0.5mm
0.4mm
0.75mm
0.4mm
0.75mm
0.5mm
0.5mm
0.2mm
0.5mm
0.5mm
0.5mm
0.75mm
0.5mm
0.5mm
0.5mm
0.2mm
Delamination

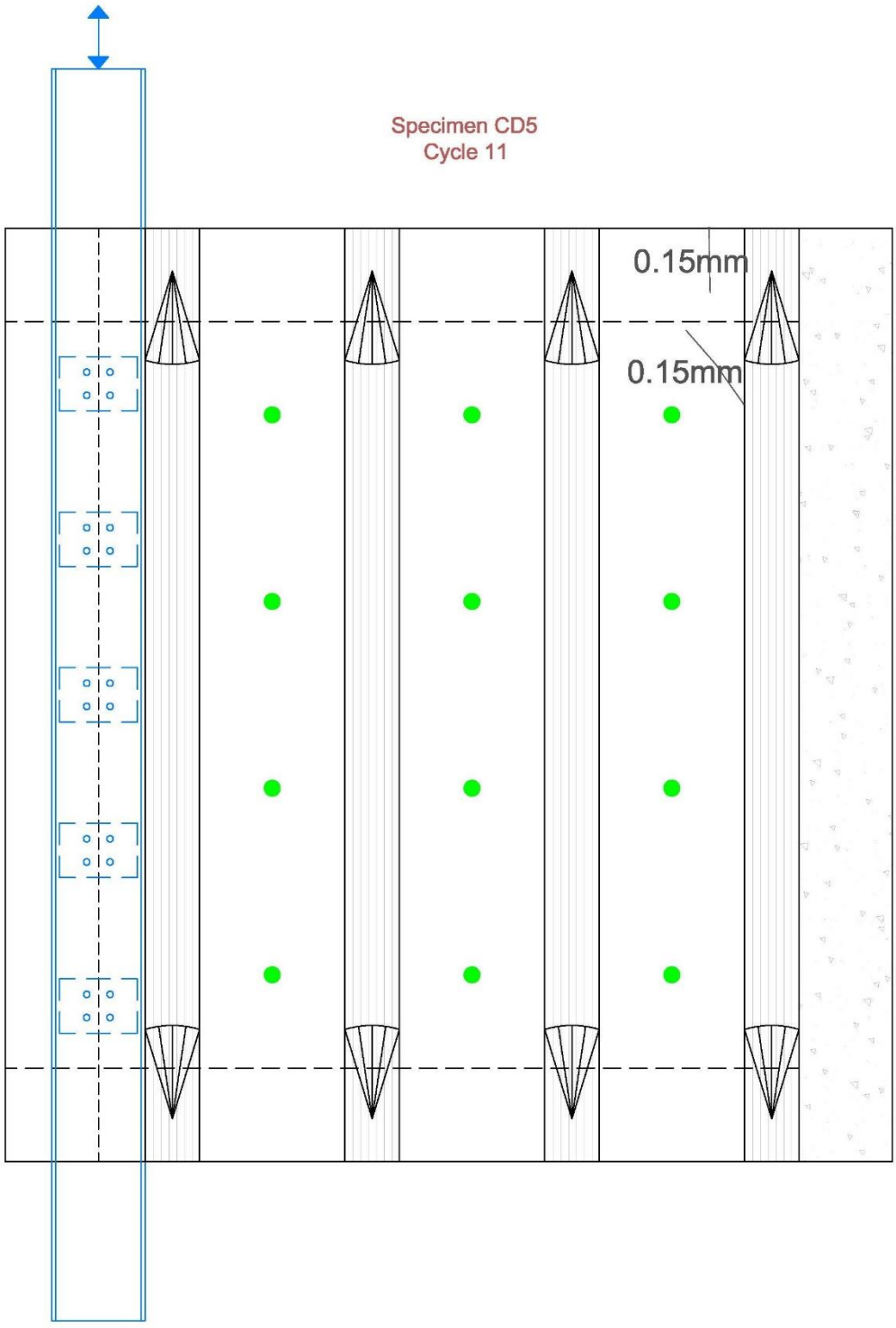
Specimen CD5
Cycle 11
0.15mm
0.15mm

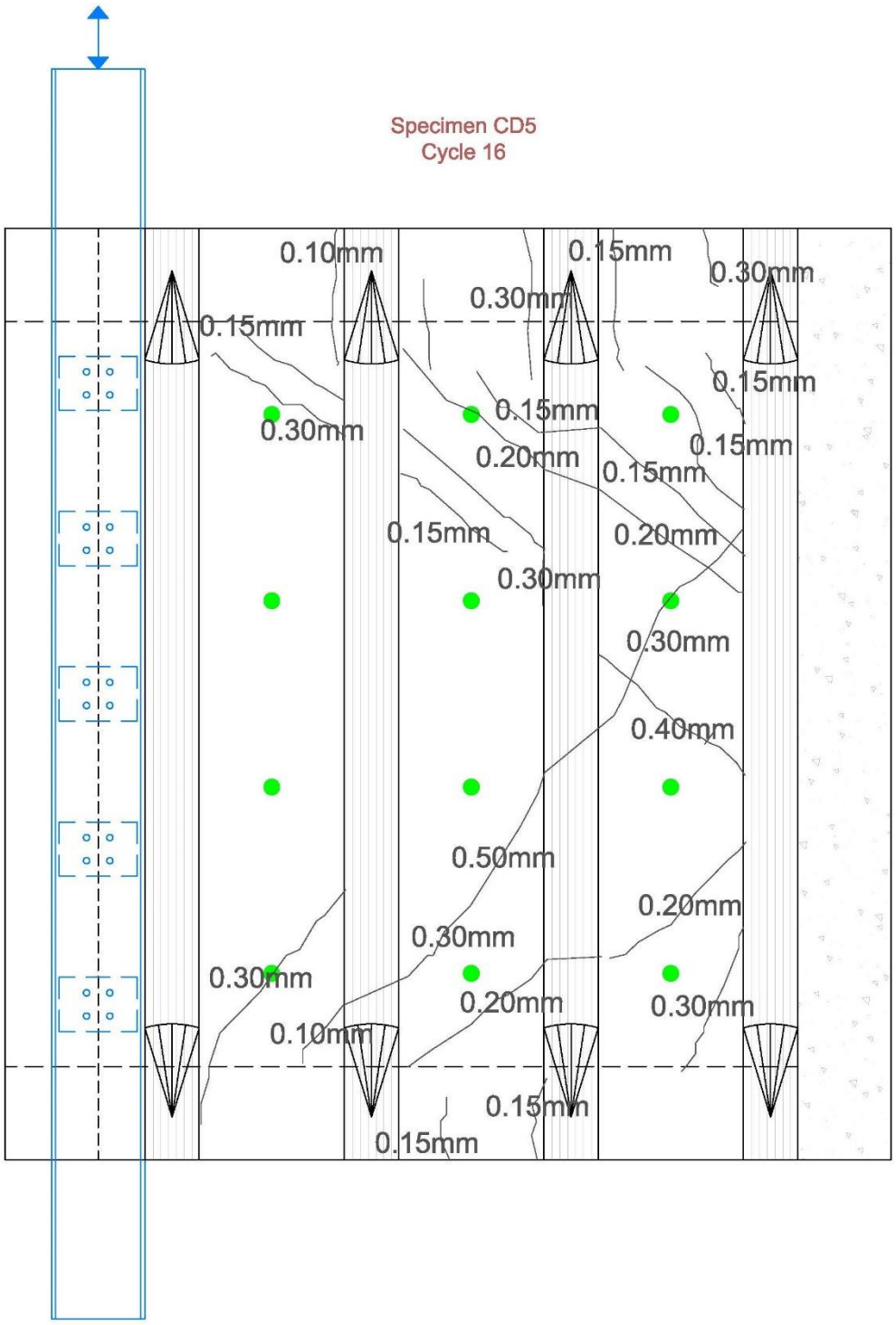
Specimen CD5
Cycle 16
0.10mm
0.15mm
0.30mm
0.30mm
0.15mm
0.15mm
0.30mm
0.15mm
0.20mm
0.15mm
0.15mm
0.20mm
0.30mm
0.30mm
0.40mm
0.50mm
0.20mm
0.30mm
0.30mm
0.20mm
0.30mm
0.10mm
0.15mm
0.15mm

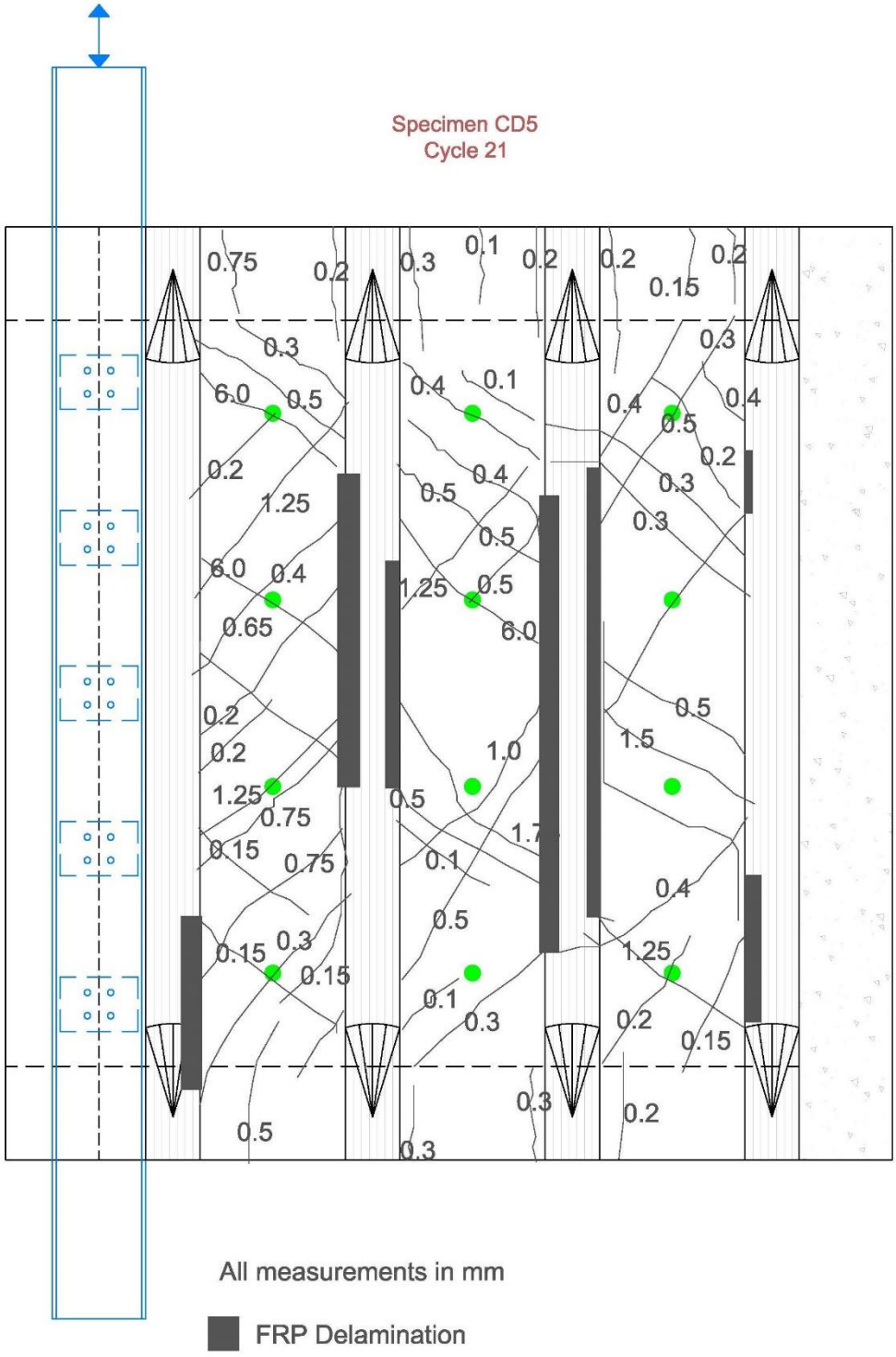
Specimen CD5
Cycle 21
All measurements in mm
FRP Delamination

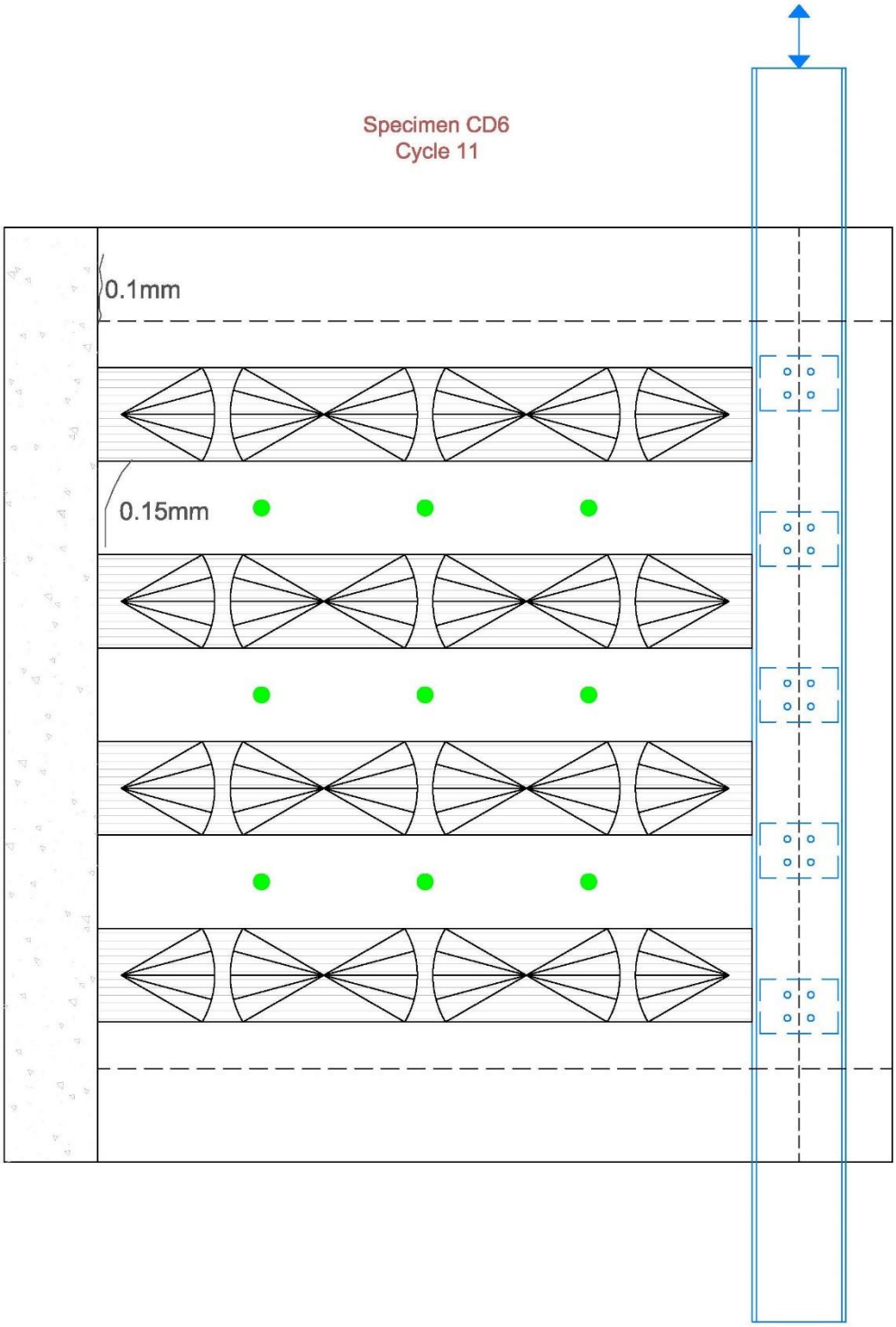
Specimen CD6
Cycle 11
0.1mm
0.15mm

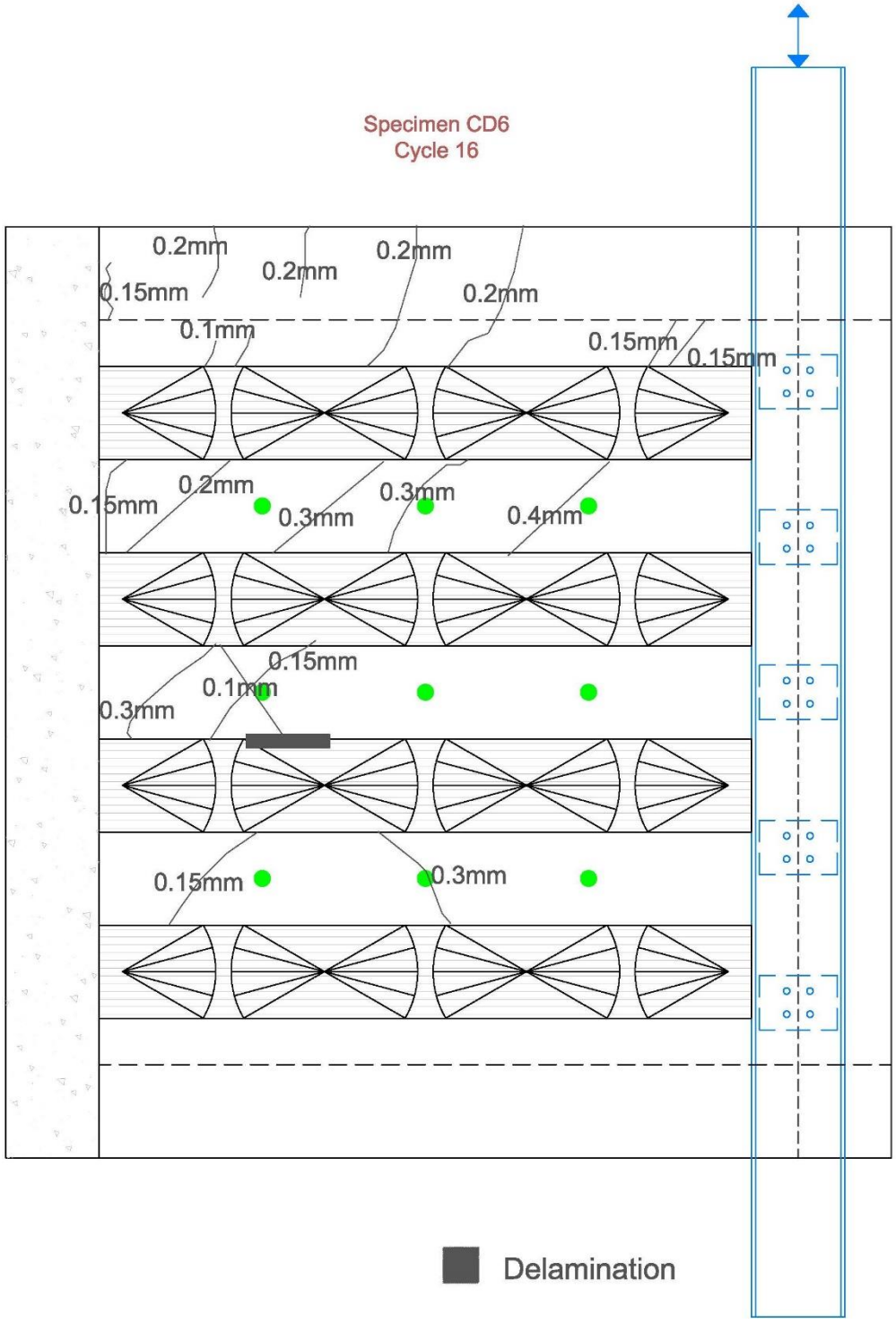
Specimen CD6
Cycle 16
0.2mm
0.2mm
0.2mm
0.15mm
0.2mm
0.1mm
0.15mm
0.15mm
0.15mm
0.2mm
0.3mm
0.3mm
0.4mm
0.15mm
0.1mm
0.3mm
0.15mm
0.3mm
Delamination

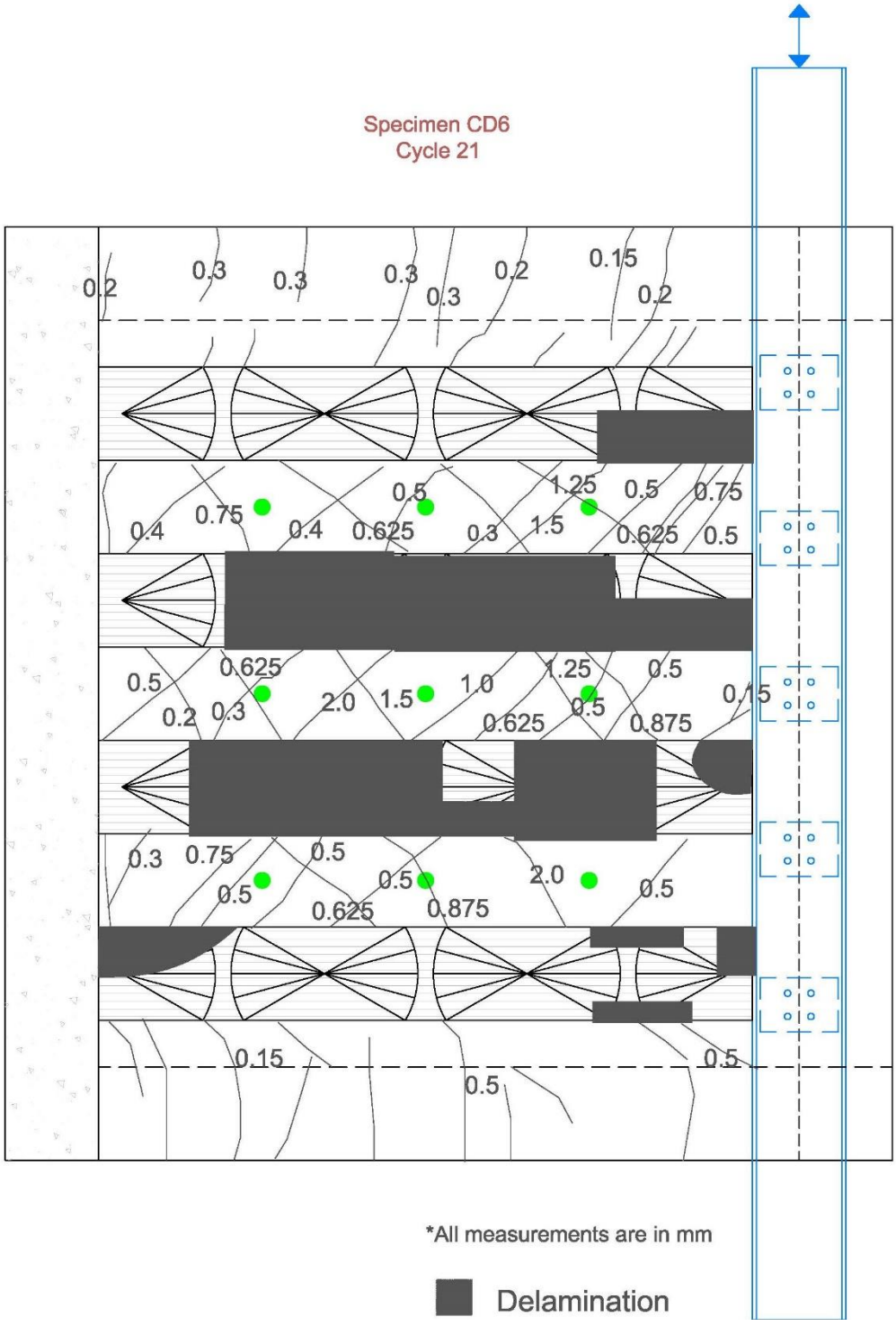
Specimen CD6
Cycle 21
0.2
0.3
0.3
0.3
0.3
0.2
0.15
0.2
0.5
1.25
0.5
0.75
0.4
0.75
0.4
0.625
0.3
1.5
0.625
0.5
0.5
0.625
1.25
0.5
0.5
0.2
0.3
2.0
1.5
1.0
0.5
0.625
0.875
0.15
0.3
0.75
0.5
0.5
0.5
2.0
0.5
0.625
0.875
0.15
0.5
0.5
*All measurements are in mm
Delamination

Appendix J. Shear Angle Corrections

Due to string potentiometers SP-TN and SP-TS being mounted to the reaction truss during the testing of Specimen CD1, the associated displacements of these sensors used to calculate the global shear angle were imperfect. The reaction truss was not perfectly rigid during testing; therefore, the instruments did not capture the entire out-of-plane displacement measurements of the shear wall. To account for this issue, the shear wall rotations of Specimens CD1, CD3, and CD4 were calculated using Eq. (46). These rotations were compared, and a linear line was best fit to each shown in Figure J1(a).

$$\gamma_{wall} = \frac{\Delta TN - \Delta TS}{B} \tag{46}$$

where: γ_{wall} is the rotation of the shear wall; ΔTN is the recorded displacement from sensor SP-TN; ΔTS is the recorded displacement from sensor SP-TS; and B is the distance between sensors SP-TN and SP-TS.

The slope of each best-fit line was then determined and used in Eq. (47) to correct the global shear angle of Specimen CD1. The average slope of the lines corresponding to Specimens CD3 and CD4 were thought to be accurate because SP-TN and SP-TS were fixed to the ground during testing. Figure J1(b) compares the uncorrected and corrected global shear angle measurements for Specimen CD1.

$$\gamma_{CD1\_Cor} = \gamma_{wall} + \frac{V}{k_{avg}} - \frac{V}{k_{CD1}} \tag{47}$$

where: γ_{CD1_Cor} is the corrected global shear angle for Specimen CD1; γ_{wall} is the shear wall rotation of Specimen CD1; V is the recorded actuator force; k_{avg} is the average slope of lines k_3 and k_4 within Figure J1(a); and k_{CD1} is the slope of k_1 in Figure J1(a).

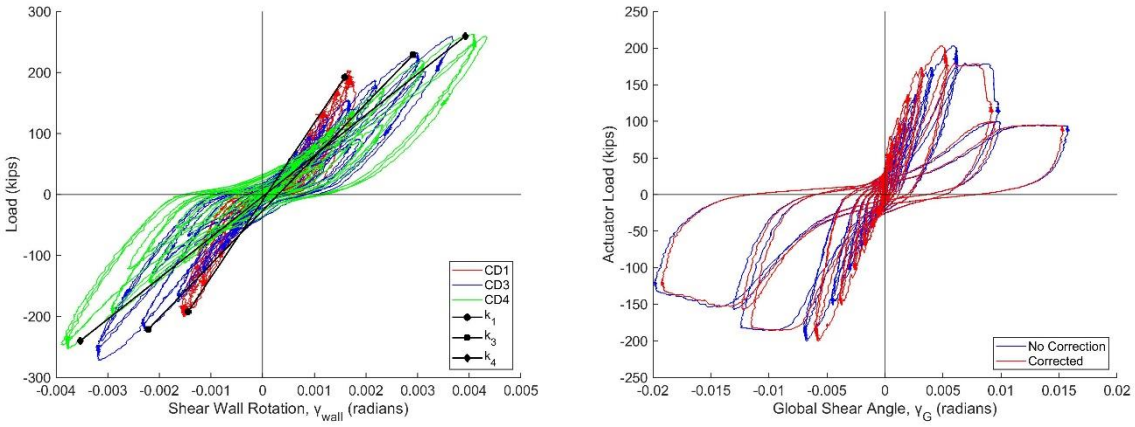

(a) (b)

Figure J1. Global Shear Angle Corrections for Specimen CD1: (a) Shear Wall Rotation Calibration; (b) Uncorrected Versus Corrected Global Shear Angle.

Furthermore, a correction to the global shear angle of Specimen CD2 was required because the mounting location of sensors SP-SW and SP-SE both experienced concrete spalling during testing. To approximate the global shear angle of this specimen, a relationship between the displacement of these sensors and the actuator's displacement and load had to be established. This relationship is shown in Figure J2(a) where a linear line is best fit to the plot. The slope of the best-fit line was then used in Eq. (48) to correct the global shear angle of Specimen CD2. Figure J2(b) compares the uncorrected and corrected global shear angle measurements for Specimen CD2.

$$\gamma_{CD2\_Cor} = \frac{\Delta_{MTS} - (k_{CD2} \cdot V)}{A} - \frac{\Delta TN - \Delta TS}{B} \tag{48}$$

where: γ_{CD2_Cor} is the corrected global shear angle for Specimen CD2; Δ_{MTS} is the actuator's recorded displacement; k_{CD2} is the slope of line k_2 in Figure J2(a); V is the recorded actuator force; ; ΔTN is the recorded displacement from sensor SP-TN; ΔTS is the recorded displacement from sensor SP-TS; A is the distance between sensors SP-SE and SP-SW; and B is the distance between sensors SP-TN and SP-TS.

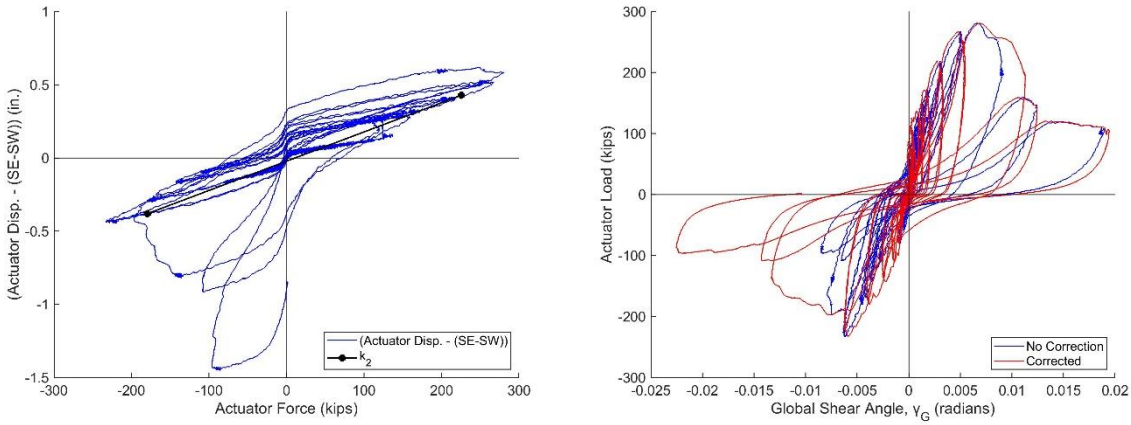

(a) (b)

Figure J2. Global Shear Angle Corrections for Specimen CD2 (a) Actuator Calibration (b) Uncorrected Versus Corrected Global Shear Angle.